UC Berkeley
UC Berkeley Electronic Theses and Dissertations

Title

Physicochemical Modeling of Copper Chemical Mechanical Planarization (CMP) Considering Synergies in Removal Materials

Permalink

https://escholarship.org/uc/item/0zg1b4gm

Author

Choi, Seungchoun

Publication Date

2013

Peer reviewed|Thesis/dissertation

Physicochemical Modeling of Copper Chemical Mechanical Planarization (CMP)
Considering Synergies in Removal Materials

By

Seungchoun Choi

A dissertation submitted in partial satisfaction of the

requirements for the degree of

Doctor of Philosophy

in

Engineering - Mechanical Engineering

in the

Graduate Division

of the

University of California, Berkeley

Committee in charge:

Professor David A. Dornfeld, Co-chair
Professor Fiona M. Doyle, Co-chair
Professor C. K. Hari Dharan
Professor Thomas M. Devine

Fall 2013

Physicochemical Modeling of Copper Chemical Mechanical Planarization (CMP)
Considering Synergies in Removal Materials

Copyright © 2013

by

Seungchoun Choi

Abstract

**Physicochemical Modeling of Copper Chemical Mechanical Planarization (CMP)
Considering Synergies in Removal Materials**

by

Seungchoun Choi

Doctor of Philosophy in Engineering – Mechanical Engineering

University of California, Berkeley

Professor David A. Dornfeld, Co-chair

Professor Fiona M. Doyle, Co-chair

With stringent requirements of copper chemical mechanical planarization (CMP), such as minimized step heights, enhanced uniformity and minimal defects, the CMP process needs to be improved based on a fundamental understanding of the material removal mechanisms. Also, with the stringent requirements, the problems in copper CMP process cannot be resolved solely improving the process itself; rather, systemic understanding of the entire manufacturing processes is necessary, demanding a robust copper CMP model to be implemented to design for manufacturing (DfM) tools. Previous models heavily relied on Preston's equation ($MRR \propto (pressure) \cdot (sliding\ velocity)$), which needs to be calibrated for every new set of processing parameters, slowing down the process development. Previous models focused on limited interactions of the consumables and the workpiece during copper CMP, being insufficient at capturing the synergies between chemical and mechanical aspects of copper CMP.

Therefore, a quantitative and physicochemical model of copper CMP that predicts material removal rate (MRR) was proposed while focusing on the interplay of consumables and copper and the synergies between chemical and mechanical aspects of the process. While considering the synergies, two mechanisms of the material removal during copper CMP were suggested: chemically dominant and mechanically dominant mechanisms. The total MRR during copper CMP was determined by summing those two contributions.

The chemically dominant mechanism attributed the material removal during copper CMP to the removal of the protective material formed on the surface of copper and to the chemical dissolution of copper from the surface both at regions occupied and not occupied by the protective material with different rates. The kinetics of the formation of the protective material at the millisecond scale were studied through electrochemical experiments and theoretical analysis where a governing equation for the adsorption of benzotriazole (BTA) was constructed and solved. It was found that the grown protective material (CuBTA) during copper CMP was only a fraction of a monolayer partly occupying the surface of a wafer. This was because the time allowed for the adsorption of BTA on the surface of copper was limited by the time between consecutive asperity and copper interactions, which was only of the order of one millisecond. The formation and the removal of the protective material were assumed to be balanced during CMP, yielding a constant chemically dominant MRR. The removal of the protective material by abrasion with abrasive particles was investigated by *in situ* electrochemical measurement during polishing. The removal efficiency of a pad asperity

where abrasive particles are embedded was evaluated from the measurements and was compared with the theoretical analysis. It showed a good agreement and suggested that the copper during CMP is mostly deformed elastically by the abrasive particles.

The influence of the concentration of copper ions on the kinetics of the formation of the protective material was also investigated using potential-step chronoamperometry using two types of copper microelectrode, namely a three dimensional and a planar electrode. The amount of copper ion may easily build up to a level that exceeds the solubility product of $Cu(II)BTA_2$. Under these conditions, $Cu(II)BTA_2$ can nucleate, consuming the protective material formed on the surface of copper. This phenomenon is highly undesirable as it increases the dissolution rates at the regions where the protective material is removed, worsening the topography after copper CMP.

The mechanically dominant MRR was determined from the volume of a wafer that is plastically deformed by indentation of abrasives that are squeezed between pad asperities and the wafer. The shear stress induced in copper by the force applied on an abrasive is lower than the ideal shear strength of copper, which is the relevant property for plasticity at this length scale. However, the crystallographic defects in the copper crystal may reduce the hardness of the material, allowing the material to be plastically deformed. Especially the roughness of the surface induced by chemical additives in the slurry greatly reduces the resistance to plastic deformation of copper. Because of the localized spatial distribution of those crystallographic defects the plastic deformation occurs only locally. Also, only a part of the plastically deformed material will be detached from the surface, contributing to the MRR. While applying this mechanism, the discrepancy of the MRR behavior with varying size and concentration of abrasives between the prediction and the experimental observations was resolved by proposing a new mechanism that determines the number of abrasives participating in the abrasion of the material. The transport mechanisms of abrasive particles toward a wafer and the electrostatic interactions between abrasives were considered to affect the number of abrasive particles deposited on the surface of a wafer. If the deposition of abrasives on the surface of a wafer is limited by the diffusion of abrasives, the MRR decreases with the size of the abrasives. In contrast, the MRR increases with the size of abrasives if the deposition of the abrasives is limited by the jamming limit of the deposited abrasives at the surface of the wafer. Also, micrometer sized abrasives increases the MRR when the size is increased because the deposition of abrasives is limited by the interception mechanism of the abrasives.

The proposed model successfully captured the synergies between chemical and mechanical aspects and quantitatively predicted the MRR during copper CMP. In the future, the model will be applied to predict the pattern dependent variability of topography of a wafer after CMP. The proposed model quantitatively predicts the local MRR of copper. Along with a robust model for dielectric and barrier materials, the model can predict the topography after CMP, contributing to the optimization of the CMP process.

2

Table of Contents

List of Tables

List of Figures

vii

viii

List of Symbols

A	$\dfrac{\lambda Z^2 \kappa L_B \exp(2\kappa r_{ab})}{1 + \kappa r_{ab}}$
A_{ab}	Total contact area between abrasives and a wafer
A_i	Cross sectional area of a trench on a wafer generated by the indentation of a sliding abrasive
A_w	Area of the wafer surface
a	Potential-dependent dissolution rate of copper where BTA is not adsorbed
a_{as}	Average contact area of an asperity and copper contacts
$a_{as\text{-}def}$	Contact area between copper and a contacting portion of an asperity that is deformed by the embedded abrasives
b	Potential-dependent dissolution rate of copper where BTA is adsorbed
C_{ab}	Number concentration of the abrasives per unit volume
c	Constant that relates the fractional coverage to the charge density of the oxidized copper that constitutes the Cu(I)BTA on the copper surface
c_{wt}	Bulk weight concentration of abrasives in a slurry
$D_{Cu^{2+}}$	Diffusion coefficient of Cu^{2+}
D_∞	Brownian diffusion coefficient of the particles
d	Distance between the surface of a wafer and the mean plane of asperities after the pad asperities are deformed
d_{ab}	Average diameter of the abrasives in a slurry
d_{as}	Average diameter of the circular contact areas between asperities and a wafer
E	Elastic modulus of a material
E^*	Effective elastic modulus when two materials are in contact
E_0	Elastic modulus of pad asperities
E_p	Elastic modulus of porous CMP pad
E_w	Elastic modulus of a workpiece
e	Elementary charge, 1.602176×10^{-19} C/electron
F	Faraday's constant
f	Ratio of the effective interaction radius of a particle to the radius of the particle
f_{ab}	Force exerted by a trapped abrasive particle on a wafer
$f_{ab\text{-}lb}$	Lower bound of the estimation of f_{ab}
$f_{ab\text{-}ub}$	Upper bound of the estimation of f_{ab}
f_{as}	Average force transmitted through an asperity
f_{ra}	Fraction of the deposited abrasives move with the pad asperity while trapped between the wafer and the asperity
f_{rw}	Fraction of the deposited abrasives left on the surface of the wafer after an interaction with an asperity
f_{tip}	Applied load by an AFM tip
G	Shear modulus for the preferred glide system

H^*	Dimensionless effective interaction range
H_{Cu}	Hardness of copper
H_w	Hardness of the copper samples
h^*	Effective interaction range
h_e	Penetration depth of abrasive particle into elastically deformed copper
h_{max}	Maximum height of the asperities
h_p	Penetration depth of abrasive particle into plastically deformed copper
h_w	Measured depth of scratches on the copper samples using AFM
i_{diss}	Current density responsible for direct dissolution of copper ions into the solution
$\bar{i}_{diss}$	Nearly constant portion of the current density due to direct dissolution of copper
i_m	Current density at t_m
$i_{measured}$	Electrochemically measured oxidation rate of copper
i_{pass}	Current density that contributes to the formation of Cu(I)BTA on the surface
i_{total}	Total oxidation rate of copper
j	Rate of deposition in unfavorable condition
j_0	Rate of deposition in favorable condition
$(j_{ab})_d$	Flux of the abrasives per unit area toward the surface of the wafer by diffusion
$(j_{ab})_i$	Flux of the abrasives per unit area toward the surface of the wafer by interception
K	Parameter that determines the deformation of copper by a hemispherical scratching tip
K_{re}	A factor used to account for partial removal of the dislodged material of a wafer by abrasive particles
$K_{preston}$	Preston's constant
k	Boltzman constant
L_B	Bjerrum length
l	Number of copper CMP steps to fabricate one layer of interconnect
M	Number of layers of a multilevel interconnect
M_{Cu}	Atomic mass of copper
$MRR_{chem.}$	Chemically dominant component of MRR
MRR_{mech}	Mechanically dominant component of MRR
m	Number of dielectric CMP steps to fabricate one layer of interconnect
N	Surface density of Cu(I)BTA on the surface of copper
N_{ab}	Number of the deposited abrasives per unit area during consecutive asperity and wafer interactions t_{as-as}
N_{as}	Number of asperities that contact the surface of a wafer
n_{ab}	Number of abrasives that are situated between pad asperities and a wafer
n_{ab}^*	Number of abrasive particles that are involved in the ploughing or abrasion of a wafer
$\tilde{n}_{ab}$	Number of abrasives that are situated between an asperity and a wafer
n_{dep}	Number of newly deposited abrasives during t_{as-as}

P	Down pressure during CMP
P_{Cu}	Probability that a surface defect or damage cause a wiring failure in a die during one copper CMP Process
P_D	Probability that a surface defect or damage cause a wiring failure in a die during one dielectric CMP Process
P_{pad}	Porosity of a pad
P_{th}	Threshold pressure for material removal to occur
p	Average contact stress or hardness
p_0	Maximum Hertz pressure
q	Charge density of the oxidized copper that constitutes the Cu(I)BTA on the copper surface before abrasion
$\Delta q(t)$	Charge density of the oxidized copper within the Cu(I)BTA removed from the copper surface during an abrasion event at time t
R_0	Static removal rate of a material during CMP
r_{ab}	Average radius of abrasives
r_{ab}^{*}	Equivalent hard sphere radius
$r_{contact}$	Areal ratio of the real contact area between a CMP pad and a wafer
r_{tip}	Radius of an AFM tip
S_e	Geometrical excluded area
$S(t)$	Cumulative amount of copper ions [mol/cm^2] dissolved per unit area from the copper surface during time t after stepping up the potential
T	Temperature of a system
t_0	Characteristic time which dictates the coverage ratio by the protective material on the surface of a wafer during copper CMP
t_m	The time at which a complete monolayer forms
V_{ab}	Indented volume on a wafer by the contacting abrasives
V_{film}	Volume of a slurry film
v	Sliding velocity of a wafer over the CMP pad
w_{as}	Width of a sliding trajectory of an asperity
w_{abs}	Accumulative width of sliding trajectories of the trapped abrasives under an asperity over the surface of copper
$(w_{ab})_i$	Expected width of a sliding trajectory of i-th abrasive
y	Distance from a copper electrode surface
Z	Effective charge of a particle
z	Oxidation state of the oxidized copper
$\tilde{z}/\tilde{x}$	Shape factor of the spheroidal pores which is one for spherical pores
α	Collision efficiency
ζ_{ab}	Zeta potentials of abrasives
ζ_w	Zeta potentials of a wafer
η	Removal efficiency
η_v	Viscosity of a slurry
θ	Fractional coverage by Cu(I)BTA
θ_{ab}	Coverage ratio by deposited abrasive particles
θ_{jam}	Maximum attainable surface coverage ratio for monodispersed hard spheres where the interaction between particles is not considered
θ_{max}	Maximum surface coverage ratio by abrasive particles at the jamming state

θ_{t_0}	Areal coverage ratio by protective materials on the surface of copper right after an interaction with squeezed abrasives
$\theta_{t_0+t_{as-as}}$	Areal coverage ratio by protective materials on the surface of copper right before an interaction with squeezed abrasives
κ^{-1}	Debye length
ν	Poisson's ratio
ν_k	Kinematic viscosity of a slurry
ρ	Density of copper
ρ_{ab}	Density of abrasives
ρ_{slurry}	Density of slurry
Δ	Sum of the amounts of indentation onto a pad asperity and a wafer
σ_{ab}	Standard deviation of the size distribution of abrasives
σ_n	Normal stress exerted on a wafer by the down force
τ_{max}	Maximum shear stress induced in the copper
τ_s	Shear stress applied by slurry flow
τ_{th}	Theoretical shear strength of copper
ϕ	Angle between the rotational axis of the spheroids and the stress direction
χ	Fill factor by abrasives
ω	Rate of rotation of the wafer

Acknowledgements

I would like to express the deepest gratitude to my advisors, Professor Fiona M. Doyle and Prof. David A. Dornfeld for their guidance and encouragement for higher level of achievement throughout my study at University of California, Berkeley. I remember the pleasant moment when Professor Dornfeld called me in spring 2007 to discuss about the possibility of pursuing my PhD at Berkeley in the area of chemical mechanical planarization (CMP). He has been a great mentor and an exceptional role model who guided and supported me on both my research and my personal life. I would like to thank him for leading the fantastic group of students and researchers, Laboratory of Manufacturing and Sustainability (LMAS). I was honored for being a member of such a group. Professor Doyle has also been an outstanding mentor in my graduate study and even for my life. She has always encouraged me with positive feedback and inspired me to pursuit an ambitious goal. Her comments and feedback on my presentations for academic conferences, academic journals and dissertations were always very helpful and urged me to think a topic in a different perspective. My intellectual ability has been framed by her guidance. I would like to thank her for letting me to think deeply and thoroughly to accomplish an ambitious goal. I would never forget the wonderful moments when I and my wife were invited to Professor Dornfeld's graduation parties and Professor Doyle's dinner parties. I also would like to thank again for their financial support throughout my education at Berkeley. I could concentrate on my study because of them.

I would like to thank Professor C. K. Hari Dharan and Professor Thomas M. Devine for being my qualifying exam committees and dissertation committees. I would also like to thank Professor Sara McMains for being my qualifying exam committee chair and Professor Liwei Lin for being my qualifying exam committee.

It has been a great pleasure to be a part of the great research groups: LMAS and Professor Doyle's group. Among others, I would like to thank Moneer, Joshua and Saurabh who started the graduate study in fall 2007 with me and have been great friends. Also, I enjoyed the chat with all my previous and current LMAS lab mates, Daeyoung, Nancy, Stephanie, Joanna, Yifen, Jeff, Miguel, Athulan, Teresa, Kevin, Jennifer, Barbara, Anton, Yuchu, Chris and Sangkee and many others. I would like to thank Professor Doyle group members, Anh, Tom, Allison, Daniel and Yegan for their thought-provoking comments and advice on my research during the meetings. I would enjoyed the discussion with Dr. Boumyoung Park, Dr. Kihyun Park, Shantanu, Adrien and Amaury in the area of CMP and thank them all for such fruitful discussions.

My deepest appreciation goes to my wife Kyungah and my mother and my late father for their patience, sacrifice and support throughout my study at Berkeley. Kyungah has always been my side and sacrificed even at the expense of her career for my accomplishment. I would like to thank my mother and late father for their sacrifice and understanding for my success.

Chapter 1
Introduction

1.1 Background of copper Chemical Mechanical Planarization (CMP)

Chemical mechanical planarization (CMP) was first used in practice to remove the damaged surface layer of a silicon wafer that was freshly cut from a silicon ingot in early 1960s.[1] Then the materials to be polished were extended to include metals by IBM for the fabrication of circuit wiring interconnects in early 1980s. CMP has become a standard fabrication process in the semiconductor industry since 1995.[2] The wiring of the advanced integrated circuits (IC) has been improved through the three dimensional stacking of the interconnect levels, shown in Figure 1.1, allowing high packaging efficiency. Chemical mechanical planarization or polishing (CMP) has been a key enabling technology for the multilevel metallization of the interconnects. Copper is the metal of choice for interconnects because of its high conductivity and high resistance to electromigration.[3,4,5] Since the copper cannot easily be dry etched, CMP of copper was employed to planarize each layer of the interconnects. This planarization step is essential to resolve the depth of focus issues for lithography, which is the manufacturing technique to define features on the wafer substrate, and the topography issues in deposition processes. Copper interconnects are fabricated using the dual damascene process as illustrated in Figure 1.2.

(a)
(b)
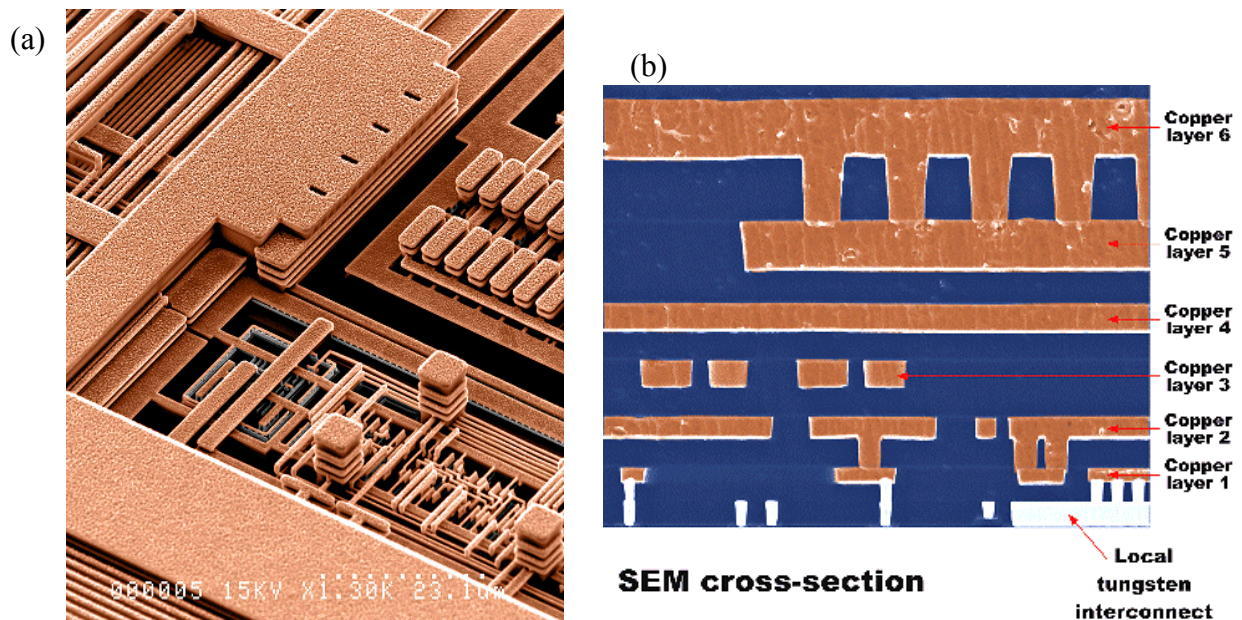
Figure 1.1 (a) Advanced chip with 7 metallization layers by IBM (b) Cross-section on the chip[6]
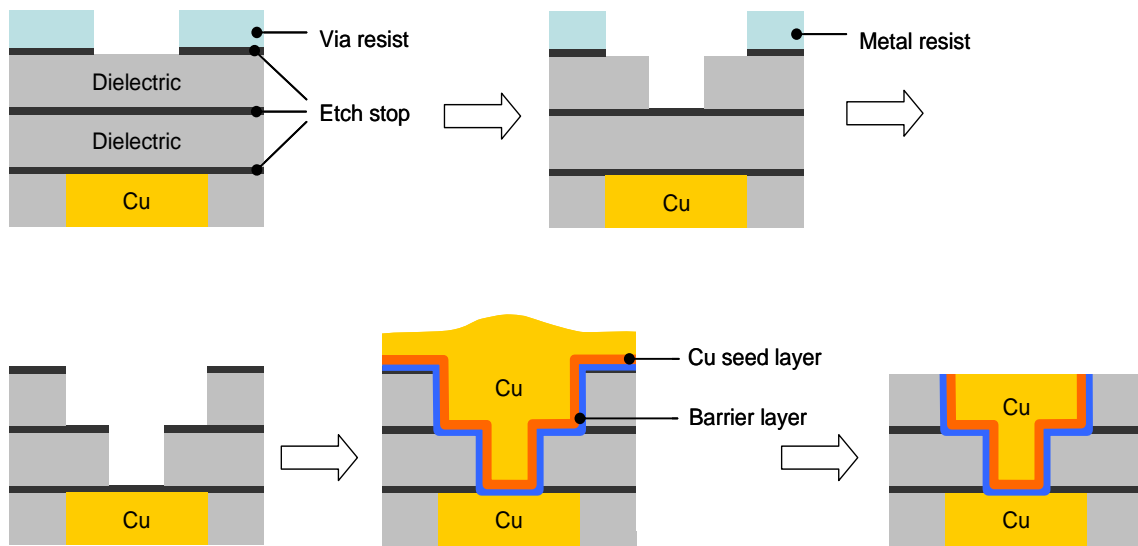
Figure 1.2 Dual damascene process flow.[7]

Two layers of dielectric material are deposited and then vias and metal lines are patterned and etched sequentially. A barrier and a copper seed layer are deposited to prevent interaction with the dielectric and copper and to be used for electrochemical deposition (ECD) of copper, respectively. Then the vias and the metal lines are filled during ECD of copper and finally the excess of the deposited copper is removed and a planar surface is obtained through CMP. Since two metal layers are defined simultaneously during the process, it is called dual damascene process. This process is preferred to the single damascene process because it requires only one deposition of copper and one planarization step whereas the latter requires two deposition and planarization steps. A multi-step CMP process is usually performed to planarize each interconnect layer to remove the excess copper, barrier and dielectric materials.[8] Figure 1.3 shows a multi-step CMP process flow. The as deposited wafer contains topography due to the topography of the underlying dielectric layer (Figure 1.3a). The excess copper is removed in the bulk using a high selective slurry and hard abrasives (alumina) until it stops at the barrier layer (Figure 1.3b). Then the second platen simultaneously removes residual copper, barrier and any hard mask materials with a nonselective slurry and stops when the dielectric material is exposed (Figure 1.3c). The last step is the overpolish step where the copper and dielectric materials are removed until the topography and the thickness are optimized (Figure 1.3d). Each step uses different slurries and polishing pads on different platens to optimize the process.
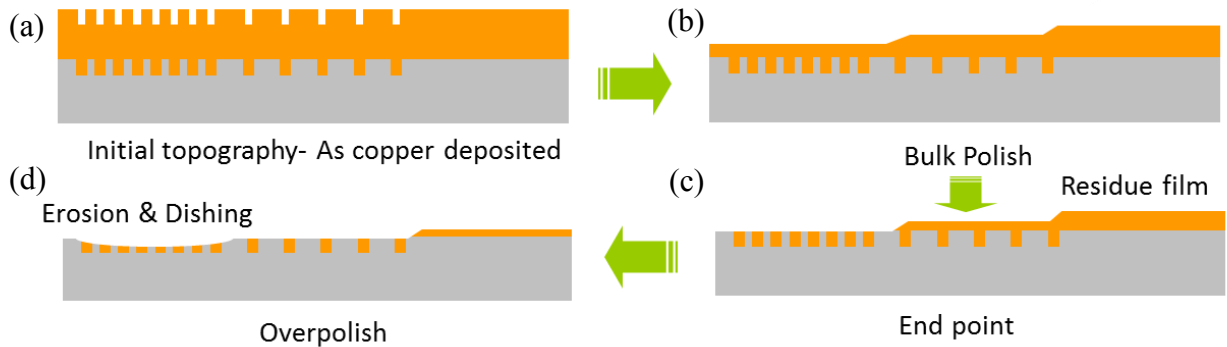
Figure 1.3 A multi-step CMP process flow.

1.2 Requirements and challenges of copper CMP

The process objective of the copper CMP is to obtain a planar surface with minimum topography and defects in a reliable and cost-effective manner while maintaining high throughput.

1.2.1 Process challenges

At the feature level, the resulting surface after copper CMP develops topography resulting from erosion, unintended removal of the dielectric material, or dishing, loss of the metals, as shown in Figure 1.3c because multiple materials are simultaneously polishing using a same pad and slurry and the various incoming topography is introduced to the process. This dishing and erosion issues are attributed to the selectivity of the slurry and are highly dependent on the incoming topography and thus there have been significant efforts to optimize the incoming topography and the CMP process in the same framework through design for manufacturing (DfM) as well as the optimization of the consumables such as the slurry and the polishing pad. Another pattern dependent topography issue includes edge over erosion (EOE) where erosion increases at the edge of pattern arrays.[9] At die and wafer scale, various micro and nano scale defects and contaminations on the surface of the wafer are generated during the CMP and cleaning processes. The contaminants include particulates due to the alumina, silica or metal hydroxide precipitates, debris from the wafer surface film or the pad, metallic ions, and organic substances originated from the chemicals in the slurry.[10] There can also be micro and nano scale scratches, puddling and plug coring. Delamination of the film and the damage to the wafer are another problem during CMP. The adhesion of the deposited film must be strong enough to sustain the stress involved during CMP. Also, the layers of the interconnects must not be damaged by the stress during the CMP. With the introduction of low k, ultra low k dielectric materials and air gap for the dielectric materials, which are porous and mechanically weak, these issues become more stringent.

1.2.2 Cost of ownership

The cost of ownership (COO) of CMP is very high principally due to the use of the pads and the slurries as shown in Figure 1.4.[11] Along with the effects to increase the life time of the pad and to minimize the use of the slurries, the yield and the throughput of the CMP process

must be high to improve the COO. The yield of multiple CMP processes to fabricate a multilevel interconnect with M layers can be calculated using a probability that a surface defect or damage causes a wiring failure in a die during one copper CMP P_{Cu} and that during one dielectric CMP P_D:[12]

$$\text{yield} = [(1 - P_{Cu})^l (1 - P_D)^m]^M \qquad (1.1)$$

where l and m are the number of copper CMP steps and dielectric CMP steps to fabricate one layer of the interconnect. It is evident from equation (1.1) that the yield of the processes can be increased if the number of CMP processes are reduced to fabricate a layer of the interconnects as in the case of the dual damascene process. With increasing number of the interconnect layers for the effective wiring of the ever decreasing size of the devices, the yield of the individual CMP process must be high to ensure an acceptable overall yield of the manufacturing processes. While maintaining high yield the throughput of the CMP process is also critical to reduce the cost. The enhancement of the throughput can be accomplished through process or design improvement such as increasing the material removal rate (MRR) during the process or minimizing the excess copper to be polished and through the optimization of the manufacturing system by reducing the down time and enhancing the utilization.
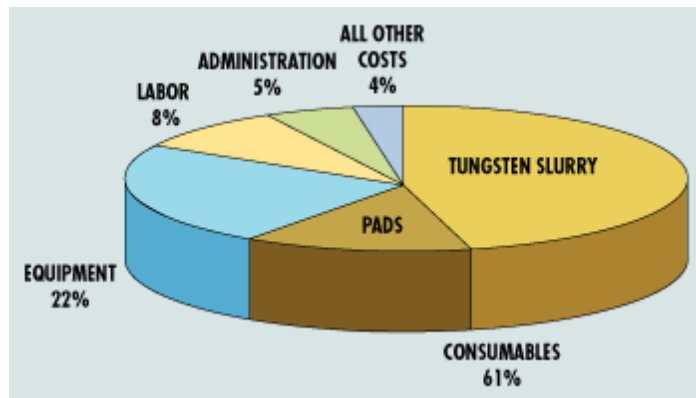
Figure 1.4 Typical cost of ownership breakdown for tungsten plug CMP[11]

1.3 Overview of Copper CMP Process

Figure 1.5 shows the schematic of conventional CMP machines. The wafer carrier which holds the copper wafer is spinning at commanded velocity while pressed onto the CMP pad. The pressure during the process is usually from 1 to 10 psi and the sliding velocity is set to give a linear velocity at the surface of a wafer of about 1 m/s. The pad is attached to the platen which is also spinning in the same direction as the wafer carrier to give constant relative velocity throughout the wafer surface. CMP slurry that contains various chemicals and abrasive particles is constantly supplied during the process to evenly wet the pad surface. For copper CMP, the slurry contains oxidizer (usually H_2O_2) to chemically dissolve the surface of copper, inhibitor (usually benzotriazole, BTA) to prevent active dissolution at recessed regions of copper by forming a protective film on the copper surface, complexing agent (usually glycine) to chemically dissolve mechanically detached copper debris, and

4

abrasive particles to remove the copper on the surface and the protective material formed on the copper surface. The surface of the CMP pad is very rough, comprising numerous asperities, which actually support the pressure applied to the wafer. Since the pad and asperities are made with very soft material (such as polyurethane), the number and the area of asperity and copper contacts change with the applied pressure. In between the asperity and the wafer, there are many abrasive particles trapped to remove copper and the protective material.
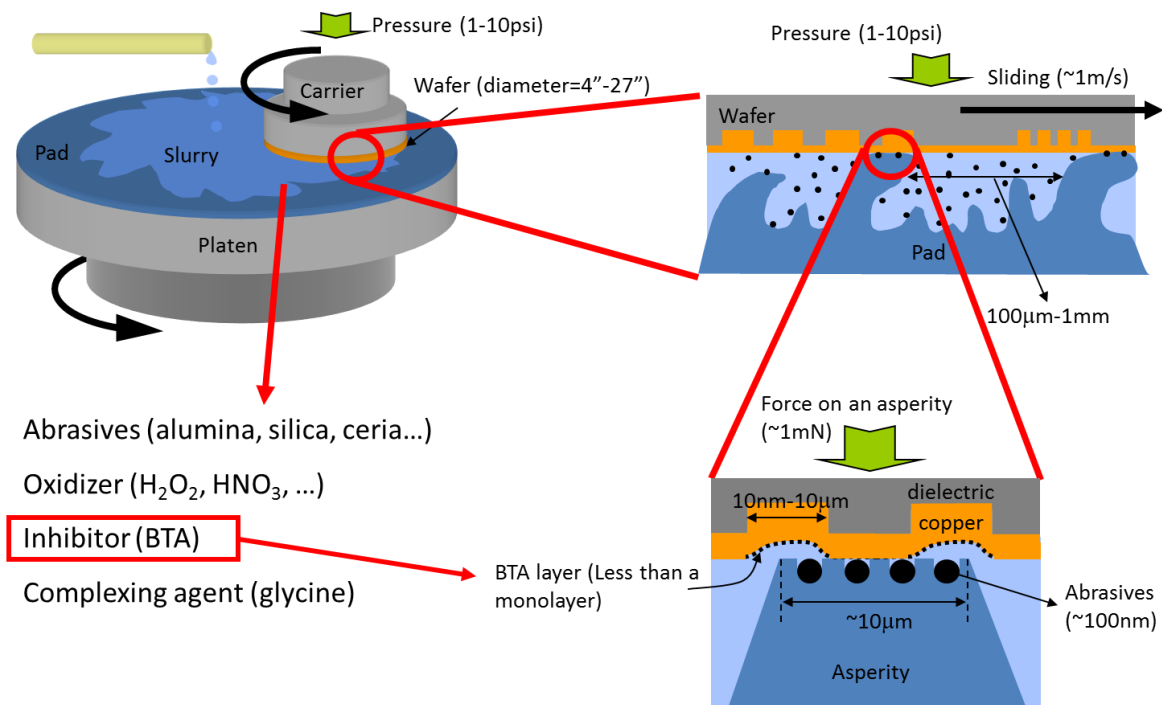
Figure 1.5 Schematic of copper CMP process

1.4 Motivation

With scaling down of the semiconductor devices and interconnect and enlargement of the wafer size, the process requirements for copper CMP have become more challenging (i.e. requiring less variation in height (step height) of the polished surface and less defect level, etc)[13]. Integration of fragile low-k materials and even air gap structure with thinner barrier layers (which have high k value) to reduce the interconnect delay has imposed further challenges to the copper CMP, requiring low stress during the process and very low amount of step heights. Furthermore, introduction of new barrier materials (Ru, Mn and Co) and hard mask materials to the interconnect and the adoption of the CMP in various front end processing and 3D integrated circuit processing operations necessitate understanding of the new materials and the interplay of the new materials with consumables during CMP. It is evident that process development is possible only by understanding the role and interplay of various participants of copper CMP; without fundamental and systemic understanding of the

5

process the improvement should rely on the trial and error with a significant amount of experimental calibration to optimize the process.
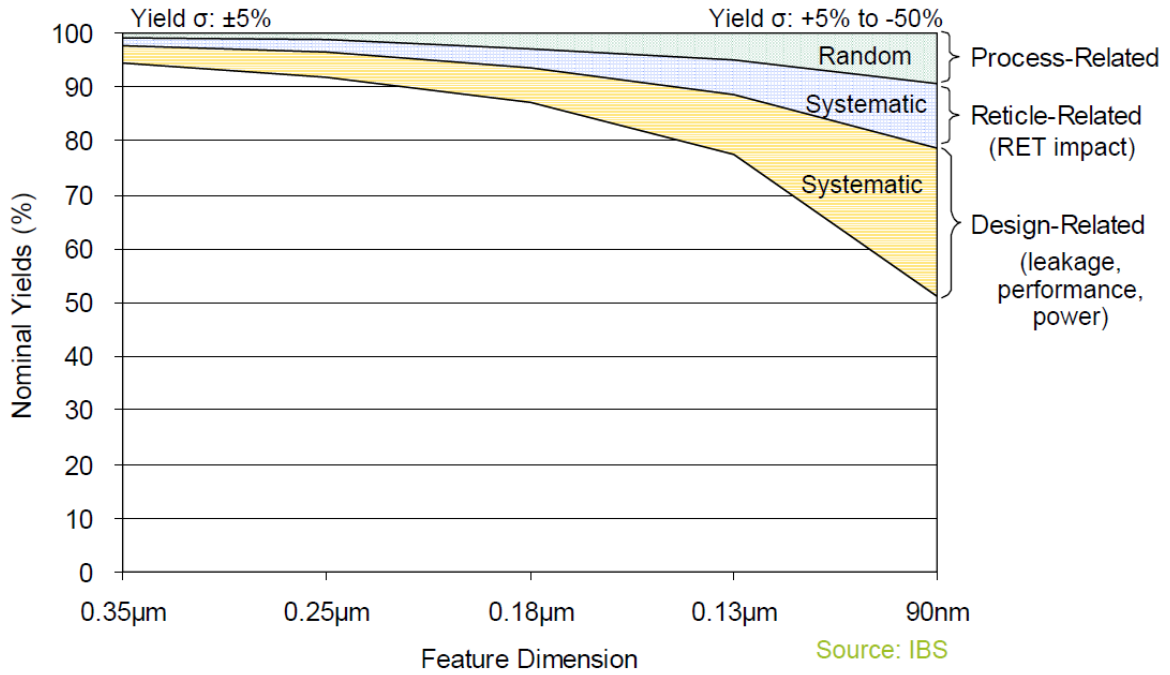
Figure 1.6 Sources of yield loss for semiconductor manufacturing[14]

Moreover, major yield loss during manufacturing of the semiconductor devices is increasingly related to the design of the chips (i.e. systemic errors) rather than the processes themselves (i.e. random errors) as the scaling down of the devices (Figure 1.6)[14]. This systemic error must be addressed by systemic understanding of the manufacturing processes; but CMP is the least understood process although its impact on the systemic error (such as the topography of the interconnect after CMP) is among the largest. DfM has been adopted to address this systemic error of the manufacturing system, but it has been mostly focused on the lithography processes. In a DfM tool, the result of manufacturing process for a proposed design is simulated and expected problems are resolved by adjusting the design before the manufacture. Thus, a robust process model is essential for successful implementation of DfM. Recently, several commercial DfM tools that incorporate copper CMP have been available, but their usefulness is greatly limited by the use of an empirical model that requires a significant amount of calibration through experiment. This is because the commercial DfM tools (e.g. by Cadence and Synopsis) were constructed based on Preston's equation[15] to predict material removal rate (MRR) during copper CMP. Preston's equation is an empirical model that predicts the MRR during CMP to be proportional to the applied pressure and the sliding velocity of work piece over the polishing pad. All other participants of the process are lumped in the proportionality constant $K_{preston}$ as shown in equation (1.2).

$$MRR = K_{preston}Pv \tag{1.2}$$

where $K_{preston}$ is a Preston's constant, P is the applied pressure and v is the sliding velocity.

Since the input parameters of Preston's equation are oversimplified lumping all other parameters than the pressure and the velocity in the Preston's constant, the model needs to be calibrated whenever any of the input parameters is changed. The need for the experimental calibration limits the adjustment of the input parameters during the manufacturing process (or during the design stage of the manufacturing processes), thus limiting the usefulness of the DfM tools. Therefore, a new CMP model that reduces the burden of the calibration is required. A mechanistic model based on the fundamental understanding of the process will contribute to an increase in the yield of the manufacturing process by optimizing the design and manufacturing system as well as the CMP process itself, which can contribute to the yield increase up to 40% (i.e. sum of the proportions for design related and process related defects) based on the data in Figure 1.6.

In addition, research in the CMP area has been conducted over the last two decades but there has hardly been a holistic study that relates various areas of research regarding CMP. Mechanical engineers have concentrated on the removal of the material via mechanical interactions and tribological phenomena between the pad, wafer and the abrasives while minimizing the electrochemical contribution. Research in the electrochemistry has usually focused on the role of the individual chemical additives in the slurry to the removal of the material. Researchers focused on the colloidal behavior of the abrasives have studied the agglomeration of the abrasives by the slurry chemistry and the influence of the slurry chemistry on the zeta potential of the abrasives or the surface of the pad or the wafer. Connection between these areas of research has hardly been studied and thus it has limited our understanding of the copper CMP in which interplay of the consumables and the wafer is critical to the removal of the material.

1.5 Outline of the dissertation

The objective of this study is to develop a quantitative and physicochemical model of copper CMP that predicts material removal rate based on the fundamental understanding of the material removal mechanisms and the synergies between various consumables and the copper during the process. While developing a quantitative and physicochemical model of copper CMP, well established knowledge from various areas of interest other than CMP were adopted to explain the behavior of materials during copper CMP. The theories from traditional colloidal science and from the research about the incipient plasticity of a material were employed to explain the behavior of the colloidal abrasive particles in the slurry and the mechanical response of copper during CMP.

In Chapter 1 general background of copper CMP is introduced. Also, motivation of this study is presented based on the challenges and requirements of the copper CMP processes in the fabrication of the multilevel metallization of the interconnects.

In Chapter 2 previous research, especially by University of California, Berkeley researchers, regarding the modeling of the CMP and the study of the copper CMP are reviewed. Recognizing the limitations of the previous studies, a new quantitative and physicochemical model of copper CMP that predicts the MRR is developed. In the proposed model two

mechanisms of the material removal during copper CMP are proposed: one is the chemically dominant mechanism and the other is the mechanically dominant mechanism. Important parameters of the model are studied in the following chapters.

In Chapter 3 Millisecond scale benzotriazole (BTA) adsorption kinetics in acidic aqueous solution containing 0.01 M glycine and 0.01 M BTA are investigated. This is a part of work to investigate the chemically dominant material removal mechanism. This study is required to understand the adsorption of BTA on the surface of copper during CMP that protects the surface from active chemical dissolution. Based on the data obtained from chronoamperometry of copper at the acidic aqueous solution an equation that governs the adsorption of BTA is constructed and solved to determine the initial kinetics of BTA adsorption.

In Chapter 4 the influence of copper ions on the formation of protective layers in an acidic electrolyte containing BTA and glycine is investigated using potential-step chronoamperometry using two types of copper microelectrode, namely a three dimensional and a planar electrode. This chapter emphasizes the importance of controlling the amount of dissolved copper ions in the slurry during electrochemical mechanical planarization (ECMP) process.

In Chapter 5 the efficiency of a pad asperity on which abrasive particles are embedded in removing the protective materials on the surface of copper, which was defined as "removal efficiency", during copper CMP is experimentally obtained. The removal efficiency is a crucial parameter that determines the average amount of the remaining protective material on the surface of copper during the process. A good agreement was found between the experimentally resolved removal efficiencies for various concentrations of the abrasives in the slurry and the ones obtained by analytical methods. This evaluated removal efficiency determines the amount of copper that was removed by the chemically dominant removal mechanism.

In Chapter 6 the mechanism where the copper is removed by the mechanical interactions is proposed based on the material behavior at nano-scale. This chapter is devoted to explaining the mechanically dominant material removal mechanism during copper CMP.

In Chapter 7 previous studies regarding the relationship between the size and the concentration of abrasive particles in a slurry and the MRR during CMP are extensively reviewed to find general dependencies of those parameters and the MRR, and to recognize the limitation of the previous studies. A novel approach to explain the observed dependencies is proposed in Chapter 8.

In Chapter 8 the dependencies of MRR during CMP on the size and the concentration of the abrasive particles are explained by considering the number of the abrasives that are deposited on the surface of a wafer during the process. The deposition of the abrasives is dominated by three different mechanisms, namely diffusion or interception of the abrasives, or the saturation limit of the abrasives on the surface of a wafer, depending on the number concentration and the size of the abrasives and the chemical constituents in the slurry.

In Chapter 9 the proposed model is summarized and the mechanisms of the material removal during copper CMP are detailed. Some areas of research that may benefit from the proposed material removal mechanisms are proposed as a future work.

References

[1] J.-Y. Lai, PhD dissertation, Massachusetts Institute of Technology (2001).

[2] G. Banerjee and R. L. Rhoades, *ECS Trans.*, **13**(4), 1, (2008).

[3] C. Y. Mak, B. I. Miller, L. C. Feldman, B. E. Weir, G. S. Hifashi, E. A. Fitzgerald, T. Boone, C. J. Doherty and R. B. van Dover, *Appl. Phys. Lett.*, **26**, 3449 (1991).

[4] P. L. Pai and C. H. Ting, *IEEE Electron Device Lett.*, **10**(9), 423 (1989).

[5] J. Tao, N. W. Cheung and C. Hu, *IEEE Electron Device Lett.*, **14**(5), 249 (1993).

[6] *http://www.tf.uni-kiel.de/matwis/amat/elmat_en/kap_5/backbone/r5_1_3.html*, accessed in June 2013.

[7] R. C. Jaeger, *Introduction to microelectronic fabrication, 2nd Ed.*, p.170, Prentice Hall, New Jersey (2002).

[8] K. Wijekoon, S. Mishra, S. Tsai, K. Puntambekar, M. Chandrachood, F. Redeker, R. Tooles, B. Sun, L. Chen, T. Pan, P. Li, S. Nanjangud, G. Amico, J. Hawkins, T. Myers, R. Kistler, V. Brusic, S. Wang, I. Cherian, L. Knowles, C. Schmidt, and C. Baker, *Proceedings of the Advanced-Semiconductor Manufacturing Conference and Workshop*, p.354, IEEE/SEMI, Boston, MA (1998).

[9] *International Technology Roadmap for Semiconductors (ITRS) 2011 Edition*.

[10] L. Zhang, S. Raghavan and M. Weling, *J. Vac. Sci. Technol. B*, **17**(5), 2248 (1999).

[11] K. Holland, A. Hurst, H. Pinder, *Micro Magazine*, April 2002.

[12] T. A. Ring, P. Feeney, D. Boldridge, J. Kasthurirangan, S. Li and J. A. Dirksen, *J. Electrochem. Soc.*, **154**(3), H239 (2007).

[13] *International Technology Roadmap for Semiconductors (ITRS) 2009 Edition*

[14] *IBS May 2004 Newsletter (Design for Manufacturability).*

[15] F. W. Preston, *J. Soc. Glass Technol.*, **11**, 247 (1927).

Chapter 2
Quantitative and Physicochemical Modeling of Copper CMP

2.1 Previous studies on the modeling of CMP

There have been a wide range of models to explain the material removal mechanism and thus to predict the MRR during CMP. However, the most widely used models are still based on Preston's equation[1], which was originally developed for glass polishing. As discussed in Chapter 1, Preston's equation is an empirical model that predicts that the MRR is proportional to the product of the sliding velocity and the down pressure during CMP processes. All other parameters are lumped in the Preston's constant.

2.1.1 Mechanical models
Earlier modeling studies of copper CMP heavily relied on the modeling of oxide CMP; thus modeling of oxide CMP is also reviewed for initial copper CMP modeling studies.

2.1.1.1 Modification of Preston's equation
Many researchers investigated the validity of Preston's equation and proposed other models that have different dependencies of the MRR on the sliding velocity and the down pressure during the process. Runnel et al.[2] proposed a model based on tribological consideration of the interface between a pad and a wafer that the MRR during CMP is proportional to the shear stress τ_s applied by the slurry flow between a wafer and a pad and the normal stress σ_n on the wafer exerted by the pad:

$$MRR \propto \sigma_n \tau_s \tag{2.1}$$

Tseng et al.[3] rephrased Runnel et al.'s model using principles of elasticity and fluid mechanics to express it with the down pressure and the sliding velocity as follows:

$$MRR \propto P^{5/6} v^{1/2} \tag{2.2}$$

where P is the applied pressure and v is the sliding velocity. Zhang et al.[4] also rephrased Runnel et al.'s model by considering the adhesive force between asperities and a wafer when evaluating the normal stress component as follows:

$$MRR \propto P^{1/2} v^{1/2} \tag{2.3}$$

Shi et al.[5] proposed a modified Preston's model for processes using a soft pad where the MRR is proportional to the 2/3 power of the down pressure:

$$MRR \propto P^{2/3}v \tag{2.4}$$

Zhao et al.[6] modified Shi et al.'s model by introducing a threshold pressure P_{th} for material removal to occur:

$$MRR \propto (P^{2/3} - P_{th}{}^{2/3})v \tag{2.5}$$

Maury et al.[7] considered the static removal of a material even without any applied pressure or sliding velocity by modifying Preston's equation:

$$MRR = K_{preston}Pv + R_0 \tag{2.6}$$

where $K_{preston}$ is a Preston's constant and R_0 is the static removal rate of a material.

2.1.1.2 *Material removal by abrasion of a material*

There have been studies that attributed material removal during CMP to the abrasion of a material on the surface by abrasive particles or pad asperities. Brown et al.[8] developed a model for optical polishing of metals. They argued that the material removal rate is determined by the volume of a workpiece that is gouged by abrasives as the abrasives move on the surface of the workpiece. The deformation of a material by the abrasives was assumed to be elastic to give the following expression:

$$MRR = \frac{1}{2E_w}Pv \tag{2.7}$$

where E_w is the elastic modulus of a workpiece. This model has the same dependencies on the down pressure and the sliding velocity as Preston's equation with a Preston's constant of $1/2E$. The same argument, except that the material is regarded to be plastically deformed, was accepted by many researchers, who suggested that the material removal during CMP is expressed as the sum of the material abraded by the abrasive particles squeezed between pad asperities and a wafer. General expression for this argument can be given as:

$$MRR = K_{re}\frac{n_{ab}{}^{*}A_i v}{A_w} \tag{2.8}$$

where K_{re} is a factor used to account for partial removal of the material dislodged from a wafer by the abrasive particles, $n_{ab}{}^{*}$ is the number of the abrasive particles participating in the material removal, A_i is the cross sectional area of a trench on a wafer generated by the indentation of a sliding abrasive, v is the sliding velocity of a wafer over the polishing pad and A_w is the area of the wafer surface. Detailed review of this argument is given in Chapter 7. One of the most extensive models was developed by Luo and Dornfeld.[9] They argued that the material removal during CMP is attributed to the abrasion of the material on the surface of a wafer by the squeezed abrasive particles of specific sizes, called "active abrasives", between pad asperities and a wafer. Only abrasives larger than the gap distance between the

tip of a pad asperity and a wafer can be squeezed between asperities and a wafer to become active abrasives. Specifically, they assumed a large separation gap between the asperities and the wafer; thus only very large abrasives of sizes from $d_{ab}+3\sigma_{ab}-\Delta$ to $d_{ab}+3\sigma_{ab}$ can be squeezed in the gap. Here, d_{ab} is the average diameter of the abrasives in a slurry, σ_{ab} is the standard deviation of the size distribution of the abrasives and Δ is the sum of the amounts of indentation onto a pad asperity and a wafer. The portion of the active abrasives is illustrated in Figure 2.1. They assumed plastic deformation of a material by the indentation of the abrasives. They evaluated the number of abrasives to be present at the gap between asperities and abrasives using the bulk concentration of abrasives assuming that the local concentration of abrasives is equivalent to that in the bulk. Similar to Maury et $al.$[7], they considered the contribution of the static chemical etching for metal CMP by adding a term for that in equation (2.8):

$$MRR = K\frac{n_{ab}^{*}A_{i}v}{A_{w}} + R_{0} \qquad (2.9)$$
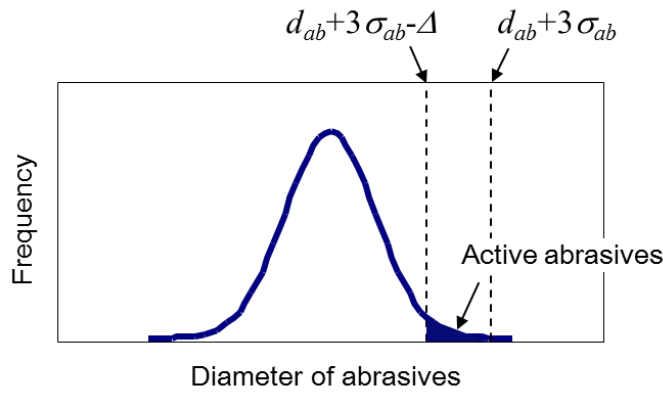
Figure 2.1 Schematic showing the range of the sizes of abrasives to be considered as active abrasives.

2.1.1.3 *Models considering the removal of a material by slurry flow*

There have been some researchers[10,11] who argued that the material removal during CMP is due to the shear stress by the slurry film between the CMP pad and a wafer. Runnels[10] assumed the presence of a thin layer of slurry film between a flat pad and wafer and solved Navier-Stokes equation to evaluate the shear stress applied on the surface of a wafer. Runnels then used the stress to estimate the amount of erosion of the material at the surface, which results in the removal of the material. Xin et $al.$[11] also argued the removal of a material by the shear stress induced by the slurry flow but the role of abrasives was emphasized. The shear stress makes the abrasive particles impact the surface of a wafer, which was weakened by the chemicals in the slurry, and then the impacted material is pulled off by the applied shear stress.

2.1.1.4 *Limitation of the mechanical models*

The proposed mechanical models recognized the importance of abrasive particles and the

flow of a slurry during CMP on the removal of a material. The forces applied on a single abrasive and on a pad asperity were estimated and the behaviors of a material by the force were hypothesized. They also contributed to the mathematical representation of the surface topography of CMP pads and evaluated the real contact area between a pad and a wafer during CMP.

However, there are several limitations of the proposed models as they apply to metal CMP. Most importantly, the proposed models underestimated the influence of chemical additives in a slurry. The role of the chemicals was limited to softening or weakening the material on the surface to be easily removed by the slurry flow or the abrasion by the abrasive particles. However, the chemical additives are known to actively dissolve the material on the surface to result in MRR even without mechanical abrasion. Also, the chemical dissolution may be enhanced by the mechanical abrasion[12], which calls for a synergistic mechanism. Moreover, the chemical additives may influence the colloidal motion of the abrasive particles by affecting the zeta potential and the Debye length of the particles. Second, the material behavior was speculated to be at a macro and continuum scale, whereas the length scale of abrasives and a wafer contact is only of the order of nanometers. Because of this treatment, the proposed model predicted unrealistic MRR during copper CMP, which called for special treatments to scale down the predicted MRR, such as the "active abrasives" concept.

2.1.2 Chemical or electrochemical aspects of copper CMP

Chemical phenomena during copper CMP are electrochemical in nature; thus electrochemical studies including construction of potential-pH diagrams, various electrochemical experiments with or without polishing, corrosion rate evaluation and use of electrochemical quartz crystal microbalance (EQCM) for kinetics studies were conducted to investigate the role of various chemical additives in a slurry during copper CMP. Aksu and Doyle investigated the role of glycine during copper CMP by constructing a potential-pH diagram for copper-water-glycine system for various activities of copper and glycine in the system.[13] The potential-pH diagram shows the thermodynamically stable species of copper at various pH values and potentials. Glycine greatly extended the solubility regions of copper to lower potentials and higher pH. Polarization of copper was conducted for wide range of potentials using a rotating copper electrode and confirmed the validity of the constructed potential-pH diagram. *In situ* polarization tests with polishing of copper electrode showed that glycine in a slurry curtailed the formation of oxide films on the surface of copper.[14] Also, the abrasion of copper in a slurry with a polishing pad and abrasives hindered the formation of a passive film especially at pH 12 as shown in Figure 2.3. It was concluded that the role of glycine in a slurry was to enhance the dissolution of copper especially at protruding regions easily abraded by a polishing pad and abrasives.

Aksu, Wang and Doyle also investigated the effect of hydrogen peroxide in a slurry containing glycine for copper CMP on the oxidation of copper.[15] Passivation of copper was compared when the potential of the system was electrochemically controlled using a potentiostat and when the potential was adjusted with hydrogen peroxide. The copper was passivated only at high pH when the potential was electrochemically controlled as predicted by the potential-pH diagram. However, the copper was passivated, which was observed by measuring dissolution rate shown in Figure 2.4, at neutral pH values such as at 4 and 9 when

13

the added hydrogen peroxide was more than some threshold value as shown in Figure 2.5.
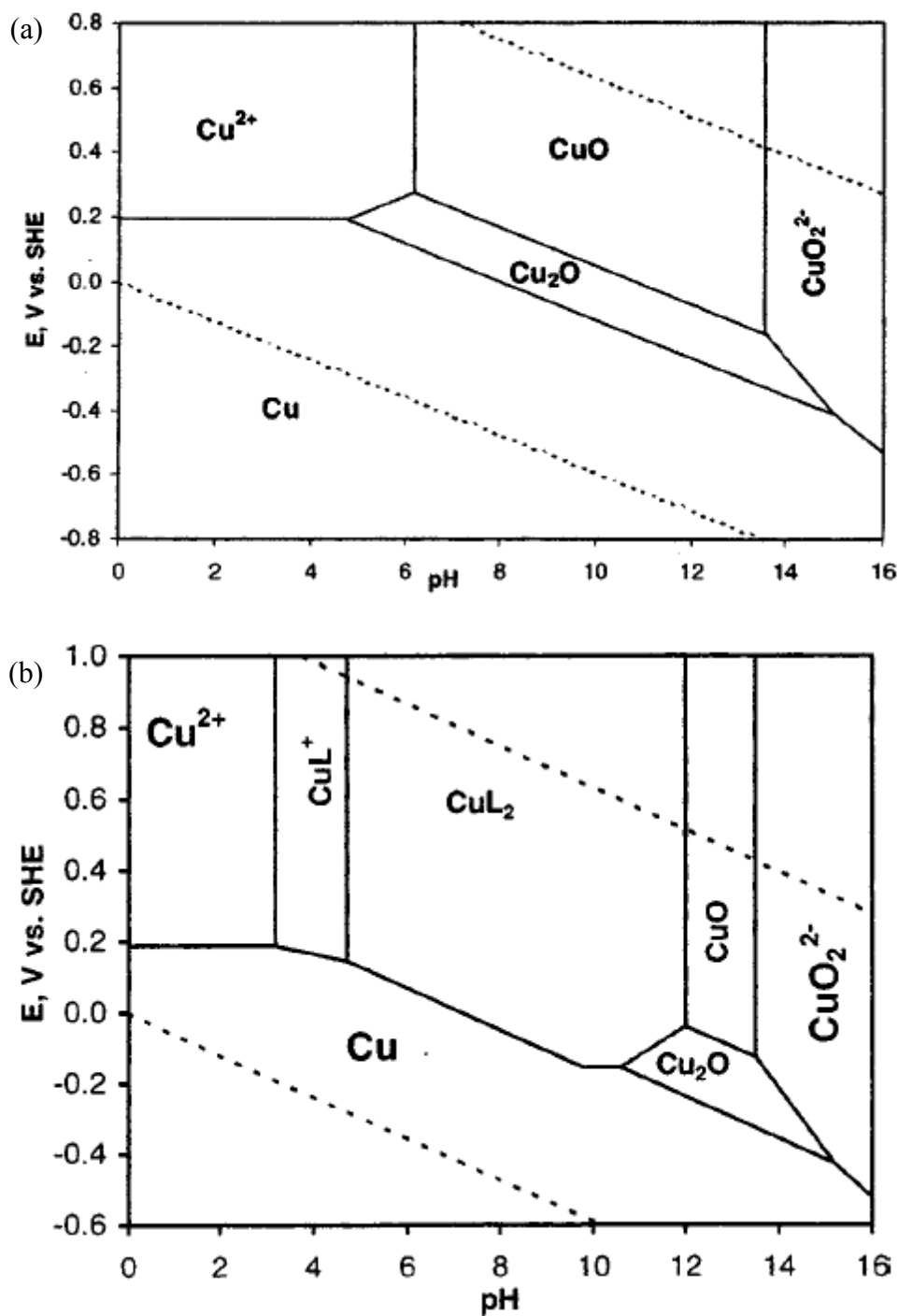
Figure 2.2 Potential-pH diagram for (a) copper-water system with 10^{-5} of the activity of copper and (b) copper-water-glycine system with the activity of copper of 10^{-5} and the activity of glycine of 10^{-2}.[15]
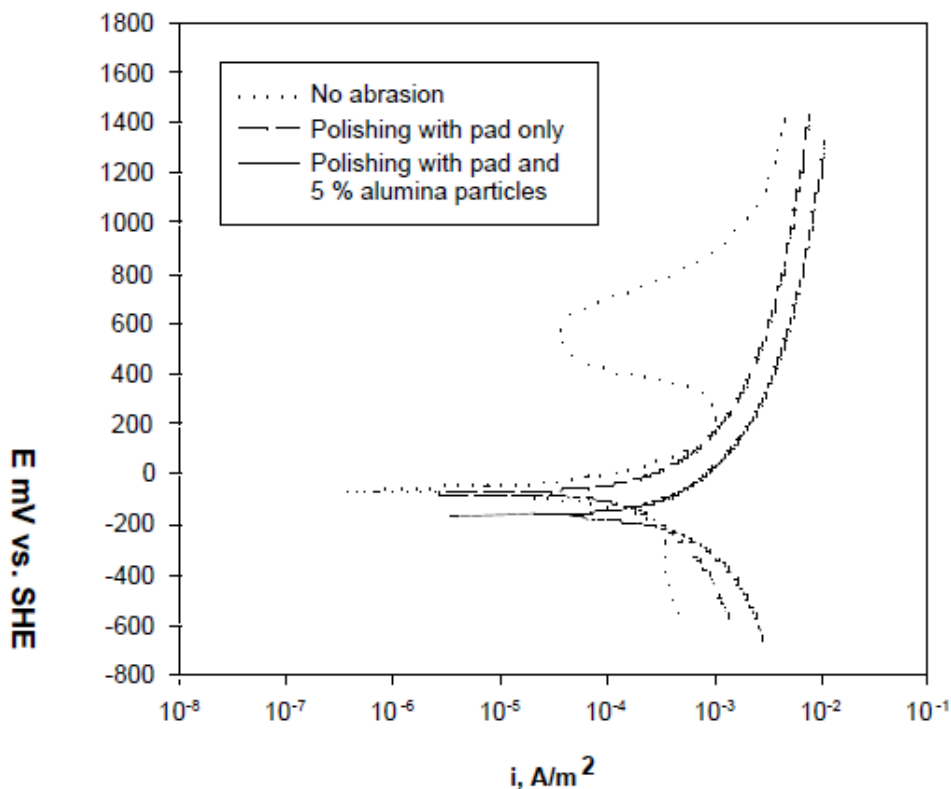
Figure 2.3 Effect of abrasion on in-situ polarization behavior of copper in 10^{-2} glycine at pH 12. Scan rate was 2mV/sec, down pressure was 27.6 kPa and the rotating velocity of the copper electrode was 200 rpm.[16]
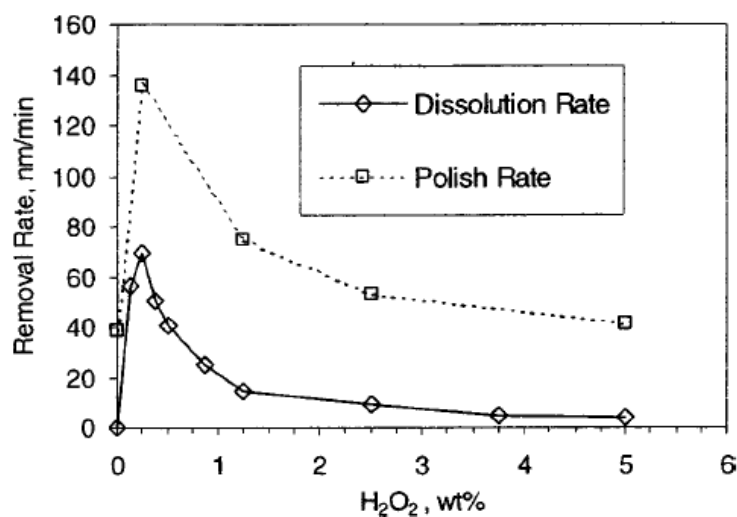
Figure 2.4 Dissolution and polish rates (at 27.6 kPa of down pressure and 200 rpm of rotational velocity of a copper electrode) in aqueous 10^{-2} glycine at pH 4 at different H_2O_2 concentrations.[15]
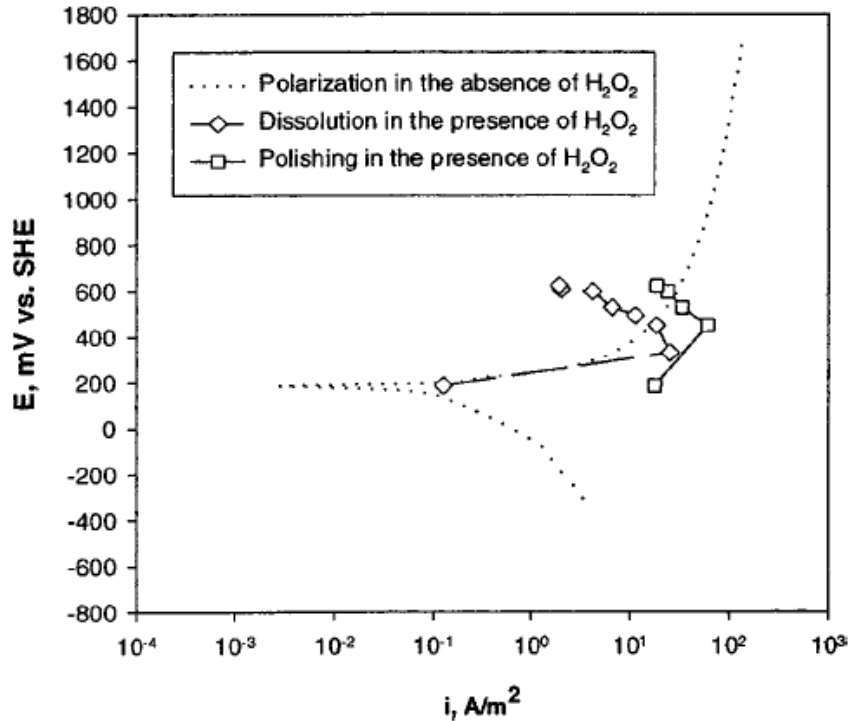
Figure 2.5 Equivalent polarization curves for copper dissolution and polishing in aqueous 10^{-2} M glycine solutions containing different amounts of H_2O_2 at pH 4.[15]

Wang and Doyle confirmed that the unexpected passivation of copper by hydrogen peroxide was due to the adsorption of species on the surface of copper by measuring the change of mass of copper using EQCM.[17] The experiments with EQCM also showed that the copper lost weight, indicating dissolution, when the concentration of hydrogen peroxide was low.

2.1.3 Models considering synergies between chemical and mechanical aspects

Kaufman *et al*. proposed a material removal mechanism for tungsten CMP that considers some interplay of chemical and mechanical effects[18]. They argued that a thin passivation layer is formed on the tungsten surface by chemical additives in a slurry and mechanical abrasion of the passivation layer by abrasives will expose fresh surface that is subsequently etched by the slurry chemistry. This cycle is repeated during CMP and the material removal is due to the wet etching at the exposed fresh tungsten surface and the removal of the passivation layer. However, this model did not provide quantitative evaluation processes of MRR and assumed that the mechanical actions of abrasives only remove the passivation layer not the work piece material itself. A similar model, but one that is quantitative, was proposed by Tripathi, Doyle and Dornfeld for copper CMP[19]. They assumed that the passivation layer on copper is thick enough that the abrasives or asperities remove only some fraction of the passivation layer at the top. They also neglected the direct removal of copper by the action of abrasives or asperities. However, it is evident from experimental data[20,21,22] that mechanical action alone (without any chemicals) can remove some copper. Also, the time between consecutive asperity and copper interactions is too short for forming a thick layer of the protective (passivation) material.

16

To overcome the limitation of the previous models and mechanisms, both mechanical and chemical aspects and their synergies must be considered.

2.2 A proposed model of copper CMP

A quantitative and physicochemical model of copper CMP was proposed partly based on the model by Tripathi, Doyle and Dornfeld[19]. The electrochemical aspects of copper CMP emphasized by Tripathi, Doyle and Dornfeld were further developed to quantitatively predict the electrochemical contribution of the material removal during copper CMP. To overcome the limitation of the previous models, a wide range of input parameters were considered focusing on the behavior of individual consumable at the scale of abrasive particles. The model focused on the interactions between consumables such as pad and a slurry containing abrasives and various chemical additives and the surface of copper during CMP as illustrated in Figure 2.6. Specifically, the following interactions were considered:

- The reaction between a slurry and the surface of copper to both dissolve copper and form a protective layer on the surface (Chapter 3 and 4)
- Deposition of abrasive particles on the surface of copper leading to the removal of material from the surface of a wafer (Chapter 8)
- Sliding of abrasive particles across the protective material on the surface of copper leading to removal of the protective material (Chapter 5)
- Deformation and abrasion of copper on the surface of a wafer by the abrasive particles (Chapter 6)
- Contact between pad asperities and copper on the surface of a wafer resulting in a certain ratio of the area of the wafer being contacted by the pad asperities (Chapter 3)
- Squeezing of abrasive particles between pad asperities and a wafer, which in turn determines the force applied on a single abrasive particle (Chapter 3, 7 and 8)

When considering these different interactions, the synergies between chemical and mechanical aspects were highlighted. A fraction of the surface of copper is occupied by protective materials that develop through the interaction of slurry chemicals and the copper; these inhibit the copper from active chemical dissolution. Abrasive particles dispersed in the slurry are squeezed at the interface of pad asperities and a wafer and move with the pad asperities as they slide across the surface of a wafer. While sliding across the surface of the copper, abrasive particles remove a fraction of the protective material from the surface, which will expose unprotected copper to the chemical environment. Active chemical dissolution occurs at the exposed areas as well as at the protected areas with much lower rates until the region is protected again by the re-grown protective material. The duration in which the protective material can grow is limited by the interval between consecutive interactions between asperities and a given position on the wafer surface. The removal of copper by chemical dissolution and the removal of the protective material by the sliding abrasives are referred to as chemically dominant material removal. Note that the protective materials grow on the surface of copper by consuming copper atoms, and thus the rate of removal of the protective material is assumed to be balanced by the rate of growth of the protective materials. The growth and the removal of the protective materials are balanced

during copper CMP, giving a constant fraction of the area on the wafer that is occupied by the protective materials and thus eventually resulting in a constant dissolution rate of copper. This quasi-steady state assumption is further discussed in Chapter 3.

Moreover, the force applied on abrasives trapped between pad asperities and a wafer will result in plastic deformation of copper if the shear stress induced in the copper by the abrasives overcomes the shear strength of the material. However, the deformation of copper is restricted to regions where crystallographic defects such as voids, vacancies, impurities, dislocations, surface steps and grain boundaries in or on the copper crystal are accumulated. The plastically deformed material is piled up along the path of the sliding abrasives. Also, some material on the surface of copper can be directly detached from the surface through a mechanism similar to cutting. The dislodged and the detached material contain a very high density of defects and thus are preferentially oxidized by the complexing agents or the oxidizing agents in a slurry. The oxidized material may also be removed by abrasion by another abrasive during the successive interactions. This type of material removal is referred to as mechanically dominant material removal. The MRR during copper CMP is estimated by adding those chemically (MRR_{chem}) and mechanically dominant (MRR_{mech}) components:

$$MRR_{total} = MRR_{mech} + MRR_{chem} \qquad (2.10)$$

A detailed description of the proposed model is given in the following sections.
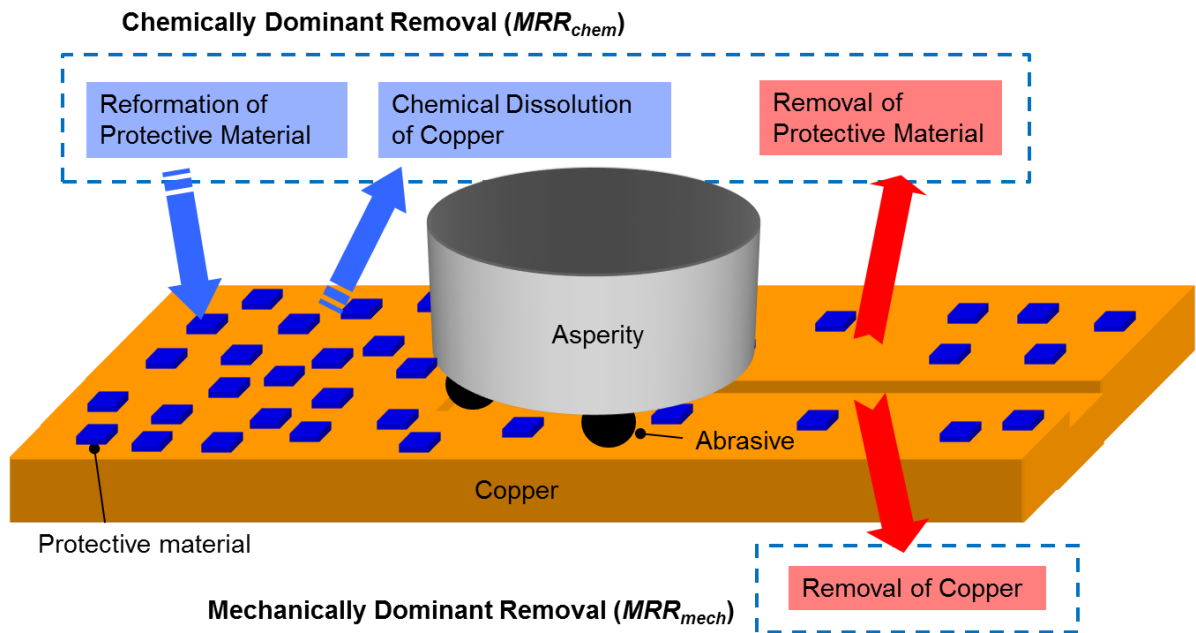
Figure 2.6 Schematic of the interactions between abrasives, a slurry, a pad asperity and copper during CMP. The red and blue text boxes show the removal of materials on the surface of a wafer during the interaction with the abrasives, and the interaction between the slurry chemistry and copper, respectively. Dashed text boxes categorize the chemically dominant and mechanically dominant portions of the material removal.

2.2.1 Chemically Dominant Material Removal Mechanism

The procedure to calculate the material removal rate by a chemically dominant mechanism can be illustrated as shown in Figure 2.7.
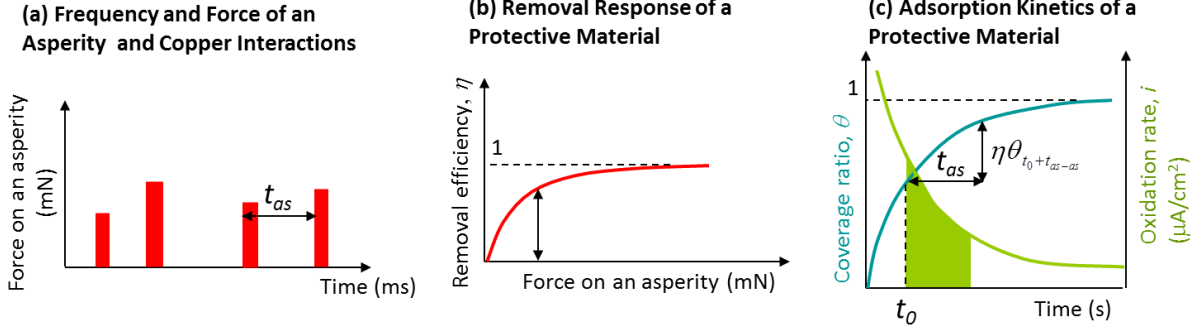
Figure 2.7: Modeling framework for the chemically dominant material removal mechanism.

2.2.1.1 *Frequencies of a pad asperity and a wafer interactions*

The surface of a polishing pad used for copper CMP comprises of numerous peaks called asperities as shown in Figure 2.8. As pad asperities slide on the surface of a wafer, the asperities intermittently exert a force on a spot on the wafer. The magnitude of such force determines the contact area between an asperity and a wafer. The contact pressure is maintained constant because of the compliant pad. The interval between such interactions is determined by knowing the distance between the peaks of the asperities and the velocity that the asperities slide on the surface of a wafer. The distance between the asperities has been obtained by characterizing the surface of a polishing pad using confocal reflectance interference contrast microscopy (C-RICM) as shown in Figure 2.9[23] or dual emission laser induced fluorescence (DELIF)[24]. Based on these data, the interval between consecutive an asperity and copper contacts (t_{as-as}) was determined to be 1-10 ms and the duration of each contact (t_{con}) was 10 µs using equation (2.11) and (2.12), assuming a circular contact area between asperities and a wafer.[19]

$$t_{as-as} = \frac{\pi d_{as}}{4 v r_{contact}} \tag{2.11}$$

$$t_{con} = \frac{d_{as}}{v} \tag{2.12}$$

where $r_{contact}$ is the areal ratio of the real contact area between a CMP pad and a wafer, and d_{as} is the average diameter of the circular contact areas between asperities and a wafer.
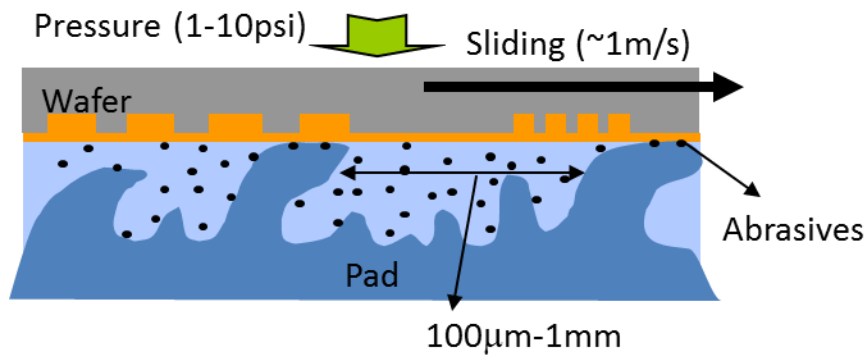
Figure 2.8 Interface of pad asperities and a wafer during copper CMP.
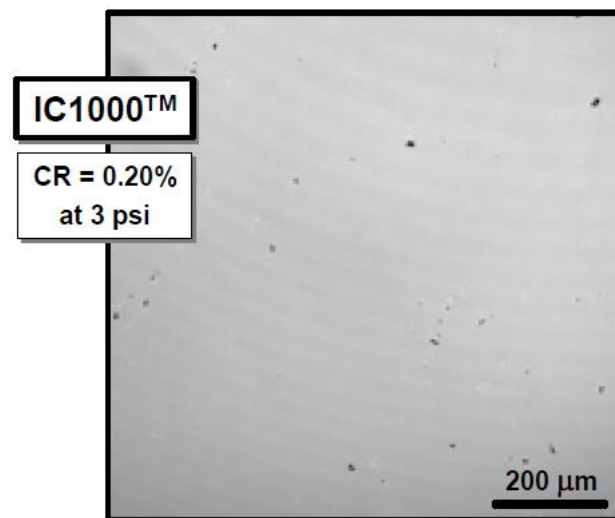
Figure 2.9 Contact interface between IC1000[TM] CMP polishing pad and a glass slide characterized by confocal microscopy.[23] Dark spots are the contact between asperities and the glass slide.

2.2.1.2 Removal response of a protective material

During the interval between consecutive asperity-wafer interactions, chemical additives in a slurry react with the surface of copper to generate protective material on the surface of a wafer. The protective material occupies only a fraction of the surface of a wafer because of very short time, t_{as-as}, available for growth. This will be further explained in Chapter 3. This protective material is removed during the interaction with the abrasive particles that are squeezed between pad asperities and a wafer. The number of abrasive particles squeezed between a pad asperity and a wafer is determined by the surface density of the attached abrasive particles on the surface of a wafer and the contact area between an asperity and a wafer. As the force applied on a pad asperity increases the contact area between the asperity and a wafer increases, forcing more abrasives onto the surface of the wafer. As the squeezed abrasives slide across the surface of the wafer, they remove the protective material formed on the surface. The fraction of the protective material on the trajectory of a sliding asperity

20

removed during an interaction with the abrasives squeezed between an asperity and a wafer is defined as the removal efficiency η:

$$\eta = 1 - \frac{\theta_{t_0}}{\theta_{t_0+t_{as-as}}}$$ (2.13)

where θ_{t_0} and $\theta_{t_0+t_{as-as}}$ are the areal coverage ratio by protective materials on the surface of copper after and before an interaction with the squeezed abrasives. With increasing force applied on an asperity, the contact area between the asperity and a wafer increases. Then, the number of squeezed abrasives between an asperity and a wafer also increases. Therefore, as the force applied on an asperity and thus number of the squeezed abrasives increase the removal efficiency increases as shown in Figure 2.7b. The removal efficiency approaches unity as the squeezed abrasives between an asperity and a wafer saturate the surface of a wafer. Note that the changes of the coverage ratio by the protective material between consecutive abrasive-wafer interactions was neglected because such a moment is only a fraction of the duration of an asperity and a wafer contact t_{con} which is of the order of 1 μs. The evaluation of the removal efficiency is explained in detail in Chapter 5.

2.2.1.3 *Adsorption kinetics of protective material*

The protective material progressively grows on the surface of copper as shown with a blue curve in Figure 2.7c. Note that the growth of the protective material is represented as the areal coverage ratio because the short time scale is not enough for complete growth of a monolayer. Copper dissolves at different rates at the areas occupied by the protective material and the areas free of the protective materials. As the protective material grows the overall dissolution rate at the surface of copper decreases as shown by the green curve in Figure 2.7c. As the squeezed abrasives remove the protective material, the coverage by protective material decreases by an amount determined by the removal efficiency ($\eta\theta_{t_0+t_{as-as}}$). The frequency of asperity- copper interactions t_{as-as} and the removal efficiency determine the characteristic time t_0 in Figure 2.7c which dictates the coverage ratio by the protective material on the surface of a wafer during copper CMP. The coverage ratio right after and right before an interaction with an asperity is the value at t_0 and at t_0+t_{as}, respectively. During copper CMP the coverage ratio changes cyclically between these two values and the amount of copper oxidized through chemical dissolution and through forming the protective material can be calculated by evaluating the area under the current density curve between t_0 and t_0+t_{as} (shaded area in Figure 2.7c). It was assumed that the amount of protective material removed during an interaction with squeezed abrasives is equivalent to that grown on the surface during t_{as-as}. Thus, the chemically dominant removal of copper can be calculated using Faraday's law as follows:

$$MRR_{chem} = \frac{M_{Cu}}{\rho z F t_{as-as}} \int_{t_0}^{t_0+t_{as-as}} i_{total}(t)dt$$ (2.14)

where M_{Cu} is the atomic mass of copper, ρ is the density of copper, z is the oxidation state of

the oxidized copper, F is Faraday's constant and i_{total} is the oxidation rate of copper. The evaluation of the kinetics of the adsorption of a protective material on the surface of copper during CMP is further discussed in Chapter 3. The influence of copper ions in a slurry on the kinetics of the protective material formation is discussed in Chapter 4.

2.2.2 Mechanically Dominant Material Removal Mechanism

Figure 2.10 shows the interaction of an abrasive and copper during copper CMP. The force exerted on copper by an abrasive was evaluated to be 0.1-1 µN for typical copper CMP processes. Because of the small force exerted on an abrasive and the small contact area between an abrasive and copper, the material behavior at this length scale might be very different from that occurring at the macro-scale. It is proposed that plastic deformation of copper only occurs at regions where the density of crystallographic defects is high. Also, the sliding motion of abrasives across the surface of a wafer mostly ploughs on the surface rather than removing the material. The dislodged material is removed by preferential oxidization of the highly defective material or a process similar to cutting by the sliding abrasives. The material removed from the surface of a wafer is proportional to the amount of the dislodged material. Therefore, the material removal rate by this mechanically dominant mechanism is expressed as:

$$MRR_{mech} = K_1 K_2 \frac{n_{ab}^* A_c v}{A_w} \tag{2.15}$$

where K_1 is a correction factor accounting for partial removal of oxidized pile up copper and K_2 is a correction factor accounting for the plastic deformation of copper only at highly defective regions. The success of this proposed mechanism is dependent on the evaluation of the number of abrasives participating in the abrasion of copper and the volume of the trenches generated by the abrasion as illustrated in Figure 2.10. The limitations and achievements of previous approaches are reviewed in Chapter 7 and n_{ab}^* is evaluated by considering the transportation mechanisms of the abrasives and the interactions between abrasives in Chapter 8. The mechanically dominant removal mechanism that evaluates K_1, K_2 and A_c is discussed in detail in Chapter 6.
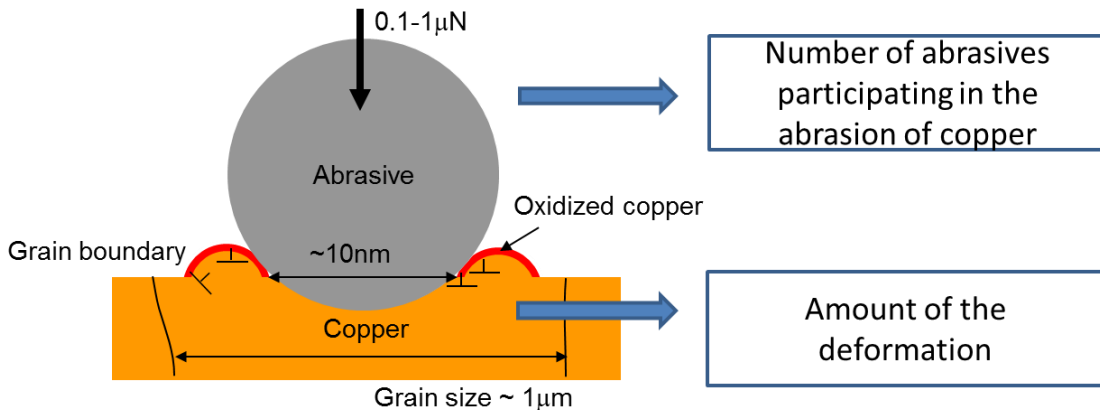
Figure 2.10 Indentation of an abrasive onto copper at nano-scale during copper CMP.

References

[1] F.W. Preston, *Nature*, **119**, 13 (1927).

[2] S. R. Runnels and L. M. Eyman, *J. Electrochem. Soc.*, **141**, 1698 (1994).

[3] W.-T. Tseng and Y.-L. Wang, *J. Electrochem. Soc.*, **144**, L15 (1997).

[4] F. Zhang and A. Busnaina, *Electrochem. Solid-State Lett.*, **1**, 184 (1998).

[5] F. G. Shi and B. Zhao, *Appl. Phys. A*, **67**, 249 (1998).

[6] B. Zhao and F. G. Shi, in *Proceedings of the Fourth International Chemical Mechanical Planarization for ULSI Multilevel Interconnection Conference*, Santa Clara, CA, pp. 13-22 (1999).

[7] A. Maury, D. Ouma, D. Boning and J. Chung, *Advanced Metalization and Interconnect Systems for ULSI Applications*, San Diego, CA, October 1997.

[8] N. J. Brown, P. C. Baker and R. T. Maney, *Proc. SPIE*, **306**, 42 (1981).

[9] J. Luo and D. A. Dornfeld, IEEE Trans. Semicond. Manuf., 14, 112 (2001).

[10] S.R. Runnels, *J. Electrochem. Soc.*, **141**(7), 1900 (1994).

[11] J. Xin, W. Cai and J. A. Tichy, *Wear*, **268**, 837 (2010).

[12] W. Che, A. Bastawros and A. Chandra, *Mater. Res. Soc. Symp. Proc.*, **867**, W5.8.1 (2005).

[13] S. Aksu and F. M. Doyle, *J. Electrochem. Soc.*, **148**(1), B51 (2001).

[14] S. Aksu and F. M. Doyle, *J. Electrochem. Soc.*, **149**(6), G352 (2002).

[15] S. Aksu, L. Wang and F. M. Doyle, *J. Electrochem. Soc.*, **150**(11), G718 (2003).

[16] S. Aksu and F. M. Doyle, Proceedings *VMIC 2001 (Eighteenth International VLSI Multilevel Interconnection Conference)*, Santa Clara, CA, November 2001.

[17] Ling Wang and Fiona M. Doyle, Proceedings *Tenth International Conference on Chemical-Mechanical Polish (CMP) Planarization for ULSI Multilevel Interconnections*, Fremont, California, February 22-25, 2005, IMIC Headquarters, Tampa, FL, pp. 200-209.

[18] F. B. Kaufman, D. B. Thompson, R. E. Broadie, M. A. Jaso, W. L. Guthrie, D. J. Pearson, and M. B. Small, *J. Electrochem. Soc.*, **138**, 3460 (1991).

[19] S. Tripathi, S. Choi, F. M. Doyle, and D. A. Dornfeld, *Mater. Res. Soc. Symp. Proc.*, **1157**, E02 (2009).

[20] K.-W. Chen and Y. L. Wang, *J. Electrochem. Sci.*, **154**, H41 (2007).

[21] S. Balakumar, T. Haque, A. S. Jumar, M. Rahman, and R. Kumar, *J. Electrochem. Sci.*, **152**, G867 (2005).

[22] T.-H. Tsai, S.-C. Yen, *Appl. Surf. Sci.*, **210**, 190 (2003).

[23] C. L. Elmufdi and G. P. Muldowney, *Mater. Res. Soc. Symp. Proc.*, **991**, C01-02 (2007).

[24] C. Gray, C. Rogers, V. P. Manno, R. White, M. Moinpour and S. Anjur, *Mater. Res. Soc. Symp. Proc.*, **991**, 0991-C01-04 (2007).

Chapter 3
Millisecond Scale Adsorption Kinetics of Benzotriazole (BTA) in Glycine-Containing Solutions at pH4

3.1 Introduction

Chemical mechanical planarization (CMP) is used widely for local and global planarization of wafers in the manufacture of integrated circuits (IC). Copper is the metal of choice for interconnects because of its high conductivity and high resistance to electromigration. Copper interconnects are fabricated using the dual damascene process, in which CMP plays a crucial role for removing excess copper and planarizing damascene structures. As the semiconductor industry ramps to 14 nm feature size[1] there is an increasing need for a robust copper CMP model for successful implementation of design for manufacturability (DfM). Although Preston's equation[2] has been widely accepted for wafer-scale CMP modeling, its treatment of CMP as an exclusively mechanical process is overly simplistic. Hence it has limited applicability to CMP processes where chemical or electrochemical mechanisms are known to be at play, such as copper CMP. This limitation has been an impetus for developing many CMP models,[3,4,5,6,7,8] but despite various degrees of success, most of these models fail to fully capture the synergy between mechanical and chemical phenomena.

Recently, Tripathi *et al*. recognized this synergy in their mechanistic tribochemical model of copper CMP.[9] They argued that during copper CMP material is primarily removed by wear-induced corrosion. Under typical CMP conditions, where the slurry chemistry allows inhibitor layers or passive films to form on copper, the oxidation rate of copper decreases as the protective surface films progressively grow. At a given site on the copper there will be periodic removal of the protective film during polishing (for example by interaction with abrasive particles and pad asperities), causing a sudden increase in oxidation rate, followed by formation and progressive growth of new passive film, with a concurrent decrease in oxidation kinetics. Copper oxidizes throughout the intervals between these interactions. Some of the oxidized copper forms the passive film and is subsequently removed mechanically, and some dissolves directly into solution, but both processes contribute to the removal of copper. The amount of protective film generated between successive asperity-pad interactions and then removed will depend on the interval between the interactions, determined by the pad geometry and rotational velocity relative to the wafer; the chemical conditions, which determine the passivation kinetics; and the amount of passive film remaining after the preceding asperity-copper interaction, which depends on how the protective film interacts (both mechanically and chemically) with abrasive particles and/or

pad asperities. The total amount of copper removed at a specific point is given by the cumulative amount of protective film removed plus all direct dissolution from the copper (which is influenced by the amount of remaining protective material on the copper surface). Since it is difficult to characterize the transient surface condition of copper at every asperity or abrasive contact during CMP (i.e. how thick the film is, or what fraction of reactive surface sites are covered by protective species), Tripathi *et al*. postulated a quasi-steady state for a more computationally efficient numerical implementation of the model.[9] The details of this are discussed below. To explore the model, the passivation kinetics of copper in both acidic and alkaline slurries were studied by potential-step chronoamperometry with a copper microelectrode, using electrochemical impedance spectroscopy data to distinguish capacitive charging from Faradaic currents.[10]

However, as noted above, the current density measured during potential-step chronoamperometry measures the total rate of copper oxidation. To numerically implement the CMP model, one needs to know the portion of the overall current density attributable to direct dissolution and the portion due to formation of the protective film. Here we analyze the current densities measured during potential-step chronopotentiometry in an acidic (pH 4) solution, containing benzotriazole (BTA) as a corrosion inhibitor, and glycine as a complexing agent for copper. We deduce the millisecond scale kinetics of adsorption of BTA onto copper surfaces, the current due to formation of the protective BTA layer, the current due to direct dissolution, and the fractional coverage of copper by BTA during typical CMP operations. This gives significant insight into the molecular scale mechanism of copper CMP in acidic slurries containing inhibitors.

3.2 Chronoamperometry Experiments

Using potential step chronoamperometry, we have measured the current decay of a bare copper microelectrode exposed to two different aqueous solutions buffered at pH 4 using acetic acid/sodium acetate, containing either 0.01 M glycine, which complexes copper ions, or 0.01 M glycine and 0.01 M benzotriazole (BTA). Full details of the experimental setup and procedures are provided elsewhere[10] but in brief, a copper microelectrode was conditioned at a cathodic potential between -1.5 and -1 V for 30 s to reductively remove any oxidized surface films, then stepped up to an oxidizing potential, recording the current as a function of time over short time periods relevant to the intervals between the interaction of pad asperities with the wafer surface in copper CMP. All potentials are reported with respect to the saturated calomel electrode (SCE), unless otherwise stated. Figure 3.1 shows the current measured experimentally after stepping up to different potentials from -1.2 V (SCE) in pH 4 aqueous solution containing both 0.01 M glycine and 0.01 M BTA. The current decay is very similar for all potentials. EIS data for these conditions, reported elsewhere[11], predict that capacitive charging should be over in less than a millisecond, since the maximum $R_U C_{DL}$ is 0.3 ms. After this time, Figure 3.1 shows that at most final potentials the current decays at a remarkably constant and similar rate of 0.5 orders of magnitude per decade of time, that is the current density varies as the inverse of the square root of time. The behavior is very different in the absence of BTA (Figure 3.2). At first sight this suggests a Cottrell type decay behavior in the presence of BTA (Figure 3.1), with current densities determined by

25

diffusion of BTA to the copper surface. However, given the fact that the current is strongly affected by the fraction of sites occupied by BTA, as discussed below, there is not compelling evidence for diffusion control. At lower potentials (< -0.2 V) in Figure 3.1, the anodic currents eventually became lower in magnitude than the cathodic current due to hydrogen evolution, causing the net current to become cathodic.
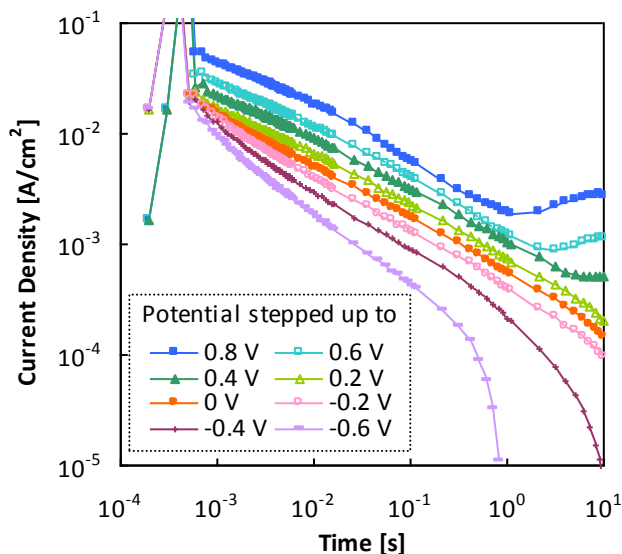
Figure 3.1 Current decay after stepping step from -1.2V to different potentials, copper in pH 4 aqueous solution containing 0.01 M glycine and 0.01 M BTA.
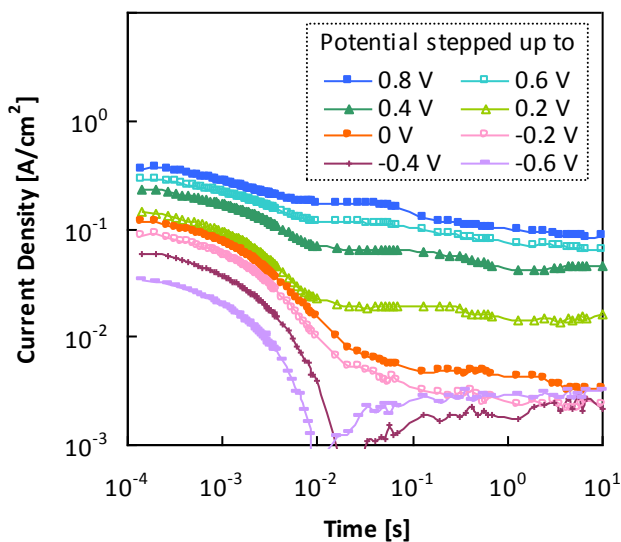
Figure 3.2 Current decay after stepping up to different potentials from -0.9V (using fixed range data acquisition), copper in pH 4 aqueous solution containing 0.01 M glycine.

Several researchers have examined the interaction of BTA with copper substrates, both adsorption[12,13,14] and the formation of polymeric CuBTA films[15,16,17,18,19], albeit over much

26

longer time scales than those studied here. A 1:1 stoichiometric association of Cu with BTA[-] in adsorbed layers indicates the formation of a Cu(I) species[19,20,21,22,23,24]. BTA has been reported to adsorb on copper at low pH, lower potentials and low adsorption densities, while polymerized Cu(I)BTA multilayers appear at high pH, higher potentials, and higher adsorption densities[14,20,25,26,27,28,29,30,31]. Adsorption has been reported on both oxide-free copper surfaces and Cu_2O[21,32,33,34,35]. Youda *et al.*[25] and Tromans[26,36] presented Eh-pH diagrams that show Cu(I)BTA predominating at pH 4 aqueous solutions at oxidizing potentials, but these are equilibrium diagrams and may not reflect the dynamic condition during active polishing of copper, where any adsorbed BTA is regularly disturbed by pad asperities and copper is continuously oxidized. Nevertheless, it is evident that the copper on the surface is oxidized to form a protective layer of BTA.

At some of the higher potentials in Figure 3.1 (>0.4 V), the current densities leveled off after a few seconds. This suggests that either there is no more adsorption of BTA, or that any subsequent adsorption of BTA provides no further passivity. Although at first sight the transition could be associated with a change in behavior for either a monolayer or a Cu(I)BTA multilayer, it is unlikely that a multilayer could have developed to the point of establishing a limiting current in just a few seconds. Furthermore, since the formation of a monolayer involves diffusion of BTA through the boundary layer at the copper-solution interface, whereas the formation of a Cu(I)BTA multilayer involves transport of species through layers that had already formed, which is much slower than boundary layer diffusion, one would expect a change in gradient when monolayer formation changed to multilayer formation. As discussed above, the change in gradient in Figure 3.1 below 1 ms has been correlated with the cessation of capacitive charging, and there are no further changes in gradient until those seen at a few seconds. Hence, this point can reasonably be assumed to correspond to complete occupation by BTA of all available anodic sites on the copper surface, i.e. the formation of a protective monolayer on the copper surface. The time at which the monolayer first forms is designated t_m. Any subsequent uptake of BTA is assumed to correspond to the precipitation of polymerized multilayers by the interaction of copper ions that had previously dissolved into the aqueous solution with BTA species diffusing to the surface region from the bulk. If this is the case, the removal of the precipitated layers would not contribute to the material removal during copper CMP, regardless of the amount of copper within them, because this copper will have already have been accounted for as direct dissolution from the copper surface.

3.3 Quasi-steady State Assumption

As noted above, for computational efficiency Tripathi *et al.* postulated a quasi-steady state during copper CMP such that on average the amount of protective film removed at each asperity-copper interaction is equal to the amount of film that reforms before the next interaction.[9] In principle, the estimation could have considered successive abrasive particle-copper interactions, rather than asperity-copper interactions. However, the interval between sequential abrasive particle–copper interactions under an asperity was estimated at less than 10 μs, which is 2 or 3 orders of magnitude smaller than the interval between asperity-copper interactions (1~10 ms).[9] Hence the electrochemical changes on copper between sequential

abrasive contacts under the same asperity would be minor compared to the electrochemical changes occurring between two asperity contacts. Indeed, assuming that the abrasive particles are relatively uniformly distributed under each asperity, they can be considered part of the asperity itself, and most likely provide the "chemical tooth"[3] that preferentially interacts with CuBTA complexes. Therefore, only the interval between two consecutive asperity-copper interactions was considered in the concept of a quasi-steady state.

The oxidation rates shown in Figure 3.1 decrease from about 0.05 A/cm^2 immediately after capacitive charging has ceased to about 0.003 A/cm^2 or less at t_m, equivalent to material removal rates declining from about 1100 to 66 nm/min or less (assuming that Cu(II) is formed). For copper CMP in slurries containing BTA and glycine, typical material removal rates are 130~600 nm/min[37]. Since these rates lie between the rates corresponding to the extreme currents seen in Figure 3.1, it appears that during most copper CMP operations there is less than a monolayer of BTA on the copper.

Figure 3.3 schematically illustrates the establishment of the quasi-steady state when the copper surface is partially covered by Cu(I)BTA between pad asperity-copper interactions. The upper curve shows the fraction of the copper surface sites occupied by Cu(I)BTA at any time. It is assumed that an asperity moving across the surface will remove a constant fraction of all the Cu(I)BTA present (it is implicit in this assumption that the mechanism for removing Cu(I)BTA species is preferential adsorption onto abrasive particles held under the asperity, and that the abrasive particles themselves will already have some sites occupied by Cu(I)BTA, because of either previous interactions with copper or through having adsorbed dissolved copper and BTA in the slurry). Figure 3.3 was constructed assuming (arbitrarily, to illustrate the principle involved) that 20 percent of the Cu(I)BTA species present on the copper surface at any time are removed by a given interaction with a pad asperity, regardless of the absolute concentration of the species on the surface (shown as the dashed line). It is assumed that when abrasion starts there is a monolayer of Cu(I)BTA present (at least a monolayer is reasonable, given that the time taken to move a copper-covered wafer into position above a polishing pad exceeds the values for t_m seen in Figure 3.1) and that the fraction of surface sites occupied by Cu(I)BTA after the first interaction corresponds to the state at $t_1{}^*$ (indicated by the downward arrow and horizontal dashed line). More Cu(I)BTA forms on the copper surface before the next asperity-copper interaction (indicated by the upward arrow), but the time, t_{as-as}, until the next interaction is not long enough to reform a monolayer. Accordingly, the next abrasion (again assuming that it removes 20 percent of all Cu(I)BTA on the surface) will further reduce the coverage of the surface by Cu(I)BTA beyond that achieved in the first interaction, to one corresponding to a different state at $t_2{}^*$. This process is repeated n times until a quasi-steady state is reached where exactly as much Cu(I)BTA is removed during an asperity-copper interaction as reforms in the interval before the next interaction, t_{as-as} (at $t_n{}^*$). Note that the duration of the asperity-copper interaction is very short compared to the interval between asperity-copper contacts and no significant electrochemical reaction occurs during the interaction itself (the electrochemical state at the beginning of a single interaction is almost the same as that at the end of the interaction). Hence the asperity-copper interactions are denoted by vertical lines, while the reformation of Cu(I)BTA is relatively gradual, and is shown as diagonal lines.
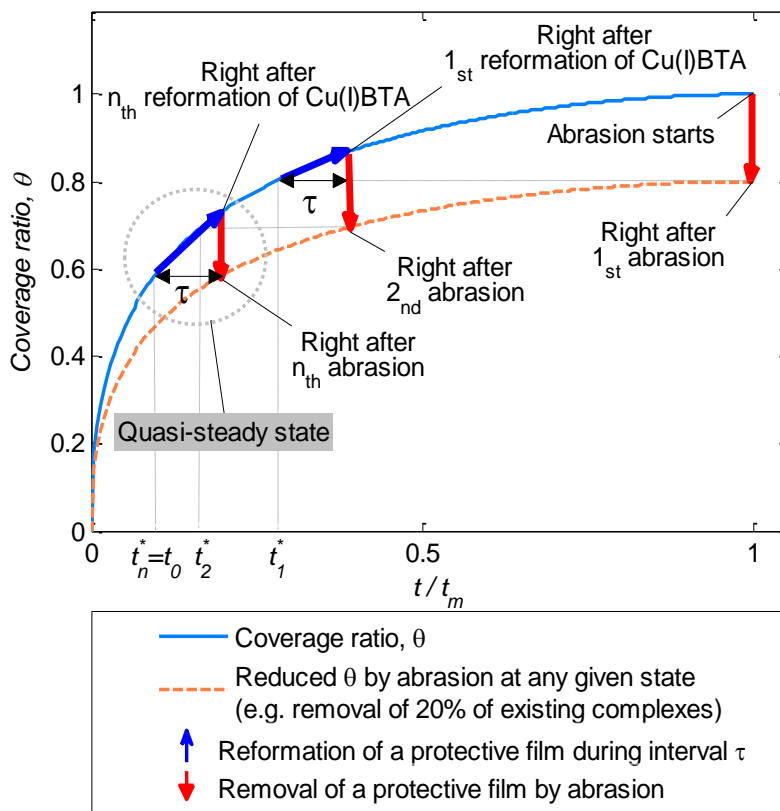
Figure 3.3 Establishment of the quasi-steady state when there is less than a monolayer of protective material on copper surface.

Although Figure 3.3 was constructed for an initial condition of monolayer coverage of copper by Cu(I)BTA, the same principles would be applicable to an initial state with thicker polymeric Cu(I)BTA multilayers. Conversely, if there is bare copper when abrasion starts (less likely), a quasi-steady state is eventually reached because of net growth of the protective layer resulting from repetitive abrasion and BTA adsorption.

Regardless of the initial condition, since the reduction of coverage upon abrasion and the gain in the coverage during t_{as-as} is always equal once the quasi-steady state has been reached, the red and blue arrows in Figure 3.3 cycle inside of the dashed circle (i.e. the fractional coverage immediately after the nth abrasion is the same as that immediately after the n+1th abrasion). This introduces the time parameter t_0, defined by:

$$t_n^* = t_{n+1}^* = t_{n+2}^* = ... \equiv t_0 \qquad (3.1)$$

Faraday's law can be invoked to express the balance between the amount of Cu(I)BTA formed at the surface and the amount removed:

$$\int_{t_0}^{t_0+t_{as-as}} i_{pass}(t)dt = \Delta q(t_0 + t_{as-as}) \qquad (3.2)$$

where $\Delta q(t)$ is the charge density of the oxidized copper within the Cu(I)BTA removed from the copper surface during an abrasion event at time t, $i_{pass}(t)$ is the current density that contributes to the formation of Cu(I)BTA on the surface at time t and $t_{as\text{-}as}$ is the interval between abrasion events when a quasi-steady state is reached.

The chemically dominant material removal rate (which becomes constant once the quasi-steady state has been reached) is given by:

$$MRR_{chem} = \frac{M_{Cu}}{\rho z F t_{as-as}} \int_{t_0}^{t_0+t_{as-as}} i_{total}(t)dt \qquad (3.3)$$

where i_{total} is the total oxidation rate, including both the current density responsible for forming the first layer of Cu(I)BTA on the surface (i_{pass}) and the current density responsible for direct dissolution of copper ions into the solution (i_{diss}) (which will eventually form soluble copper complexes with glycine[38,39] or the acetate buffer, or as mentioned above, may reprecipitate with BTA). M_{Cu} is the atomic mass of copper, ρ is the density of copper, z is the oxidation state of the oxidized copper and F is Faraday's constant. However, before the integral in equation (3.3) can be evaluated using the kinetics of current decay shown in Figure 3.1, it is necessary to determine where t_o lies.

3.4 Theoretical Analysis

Given that the intervals between two asperity-copper contacts for typical operating parameters during CMP are around 1 to 10 ms,[9] the thickness of copper that is removed between each interaction (due to both dissolution between the two interactions and removal of oxidized copper film by the interaction) is equivalent to about 0.1 to 1 Å. This is less than the atomic radius of copper, 1.4 Å. Since it is clearly impossible to remove a fraction of a copper atom, this low average means that the likelihood that a given surface copper species is removed in any given interaction is well below unity. The "mechanical" phenomena during copper CMP, which have hitherto been envisaged as mechanical damage to a passive film (as first proposed by Kaufman[8]) are evidently more akin to the plucking of certain atoms or molecules from an incompletely covered surface during each abrasive interaction. This appears completely consistent with Cook's "chemical tooth" model[3], but suggests far less mechanical action in chemical *mechanical* planarization than is considered in most models.

The small amount of material removed with each asperity-copper interaction, in conjunction with the establishment of a quasi-steady state in the sub-monolayer regime, implies that Cu(I)BTA only covers a fraction of the copper surface between asperity-copper interactions, and each interaction only removes a portion of this oxidized material. This situation is illustrated schematically in Figure 3.4. Figure 3.4 (a) shows the surface condition right before abrasion (i.e. at $t_0 + t_{as\text{-}as}$) and Figure 3.4 (b) shows the surface immediately after an abrasion event that removed 20 percent of the total adsorbed Cu(I)BTA (i.e. at t_0). It is assumed that the Cu(I)BTA species are randomly distributed on the surface, and that abrasion will remove a constant fraction of the total number of Cu(I)BTA species present on the surface. The arbitrary percentage chosen (20 percent) was selected for consistency with Figure 3.3. The

removal efficiency, η, can be expressed as:

$$\Delta q = \eta q \qquad (0 \le \eta \le 1) \tag{3.4}$$

where q is the charge density of the oxidized copper that constitutes the Cu(I)BTA on the copper surface before abrasion.
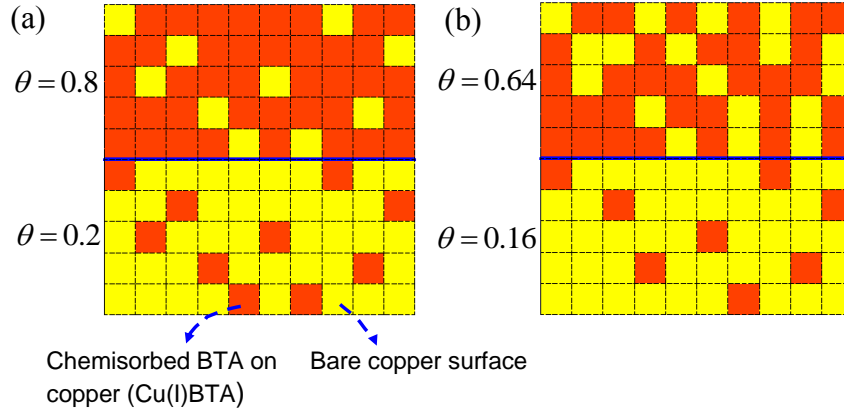
Figure 3.4 Coverage ratio change before (a) and after (b) asperity contact during copper CMP. The removal efficiency η is assumed to be 0.2.

To the best of our knowledge the kinetics for forming a monolayer of protective film in a pH 4 aqueous solution containing glycine and BTA have not been studied to date, and it would be challenging to investigate the kinetics in this regime by direct experimental measurement. The electrochemical quartz crystal microbalance (EQCM) technique has been employed to study the kinetics of forming multilayers of BTA over time scales of the order of hours.[40,41] Unfortunately, the resolvable time scale of the EQCM, about 0.1 s[42], limits the usefulness of this technique for studying the millisecond time scale. Hence, we employed a theoretical approach, using our experimental chronoamperometric data to determine the rates of dissolution of copper from bare copper sites and from the sites that are occupied by BTA, and then used these data to calculate the kinetics of adsorption of BTA onto copper.

The experimentally measured current densities in Figure 3.1 and Figure 3.2 include current that leads to the formation of the protective film and current that leads to direct dissolution of the copper. As noted above, the total current was inversely proportional to the square root of time:

$$i_{total} = i_{pass} + i_{diss} = i_m \left(\frac{t}{t_m} \right)^{-0.5} \quad \text{for } t \le t_m \tag{3.5}$$

where i_m is the current density at t_m.

The current density responsible for forming adsorbed Cu(I)BTA can be written as:

$$i_{pass}(t) = \frac{dq}{dt} = c\frac{d\theta}{dt} \tag{3.6}$$

where θ is the fractional coverage and c is a constant that relates the fractional coverage to the charge density of the oxidized copper that constitutes the Cu(I)BTA on the copper surface.

The constant c is easily evaluated. When a complete Cu(I)BTA monolayer has formed (i.e. $\theta=1$), q is equal to c (by $q=c\theta$). Hence c is given by:

$$c = zeN \tag{3.7}$$

where z is unity for Cu(I), e is the elementary charge, 1.602176×10^{-19} C/electron and N is the surface density of Cu(I)BTA on the surface.

Assuming that copper dissolves directly into the solution from both bare sites and those on which BTA is adsorbed, but with different, potential-dependent rate constants denoted by a and b respectively, and that these rate constants are independent of the fractional coverage, θ, the current density for the direct dissolution of copper can be written as:

$$i_{diss} = a(1-\theta)+b\theta \tag{3.8}$$

Combining equations (3.5), (3.6) and (3.8) gives the following linear differential equation that governs the kinetics of BTA adsorption for $t \leq t_m$:

$$a(1-\theta)+b\theta+c\frac{d\theta}{dt} = i_m\left(\frac{t}{t_m}\right)^{-0.5} \text{ or } \frac{d\theta}{dt} = \frac{i_m}{c}\left(\frac{t}{t_m}\right)^{-0.5}+\frac{a-b}{c}\theta-\frac{a}{c} \tag{3.9}$$

Solving the first order differential equation using the boundary condition $\theta_{t=0}=0$ yields:

$$\theta(t) = \left[\frac{i_m\sqrt{t_m}\sqrt{\pi}}{\sqrt{c(a-b)}}erf\left(\sqrt{\frac{a-b}{c}}t\right)+\frac{a}{a-b}e^{-\left(\frac{a-b}{c}t\right)}-\frac{a}{a-b}\right]e^{\frac{a-b}{c}t} \tag{3.10}$$

From equation (3.9) and the definition of t_m, it is apparent that at t_m, $\theta=1$ and $d\theta/dt=0$, hence:

$$b = i_m \tag{3.11}$$

This is consistent with the oxidation rate at t_m being due exclusively to dissolution of copper from BTA adsorbed sites. The coefficient a can be determined from the oxidation rate at t_m in a solution that does not contain BTA, which is given by Figure 3.2. The coefficient c can be calculated from equation (3.10) using the determined coefficients a and b and the condition at t_m ($\theta=1$). The adsorption density of BTA at monolayer coverage can then be determined from equation (3.7) and the kinetics of adsorption evaluated from equation (3.10).

For pH 4 aqueous solution containing glycine and BTA, one can use material removal rates reported in the literature to estimate the position of quasi-steady state under typical conditions, assuming that the kinetics of BTA adsorption would be similar under polishing conditions to those for the microelectrode. Substituting equations (3.5) and (3.11) into equation (3.3) gives:

$$MRR_{chem} = \frac{M_{Cu}}{\rho z F t_{as-as}} \int_{t_0}^{t_0+t_{as-as}} b \left(\frac{t}{t_m} \right)^{-0.5} dt \tag{3.12}$$

$$= \frac{M_{Cu} b \sqrt{t_m}}{\rho z F t_{as-as}} \int_{t_0}^{t_0+t_{as-as}} \frac{1}{t^{0.5}} dt \tag{3.13}$$

$$= \frac{2 M_{Cu} b \sqrt{t_m}}{\rho z F t_{as-as}} \left[(t_0 + t_{as-as})^{0.5} - t_0^{0.5} \right] \tag{3.14}$$

Thus, knowing the parameters b and t_m for given conditions, one can determine the characteristic time t_o corresponding to the beginning of quasi-steady state for a given MRR and value of t_{as-as}.

3.5 Results and Discussion

The kinetics of adsorption of BTA onto a copper microelectrode at 0.6 and 0.4 V (SCE) in a pH 4 aqueous solution containing 0.01 M glycine and 0.01 M BTA (the second and third highest lines in Figure 3.1) were modeled using the equations derived. The evaluated coefficients and constants are listed in Table 3.1. Note that the ratio of coefficients a and b (a/b) and the coefficient c are similar at both potentials, which is physically reasonable. The current density at unoccupied sites (coefficient a) is nearly two orders of magnitude higher than that at sites occupied by BTA (coefficient b), which demonstrates the efficacy of BTA as a corrosion inhibitor.

Table 3.1 Derived values for a governing equation of the kinetics of BTA adsorption in a pH 4 aqueous solution containing 0.01 M glycine and 0.01 M BTA

Potential (V (SCE))	t_m (sec)	a (A/cm^2)	b (A/cm^2)	c (C/cm^2)
0.6	2	7.0×10^{-2}	8.4×10^{-4}	6.26×10^{-5}
0.4	4	4.4×10^{-2}	4.7×10^{-4}	6.24×10^{-5}

To further assess the validity of the derived values, the coefficient c was converted into the adsorption density of BTA on copper and compared with values in the literature. An upper limit for the adsorption density of Cu(I)BTA on copper surfaces can be estimated from the

surface density of the most closely packed copper surface, namely the (111) surface, 1.77×10^{15} atoms/cm^2.[43] The surface density can also be estimated from the area that each BTA molecule occupies on the copper surface. Xu *et al.* used the molecular structure of adsorbed BTA reported by Tomas *et al.*[44] to estimate that each BTA molecule occupies about 35 Å^2 if adsorbed with its molecular plane parallel to the surface, corresponding to a saturation limit of 2.8×10^{14} molecules/cm^2 and about 12 Å^2 if adsorbed with its molecular plane normal to the surface, corresponding to a saturation limit of 8.4×10^{14} molecules/cm^2.[24] Xu *et al.* also reported the surface density of a monolayer of BTA$^-$ on Cu$_2$O equilibrated with a neutral pH aqueous BTA solution to be 6.3×10^{14} cm^{-2}.[45] Bastidas reported the projected area of a vertically oriented adsorbed BTA molecule to be about 20 Å^2 (the projected area of a rectangle surrounding the molecule), as compared with 38 Å^2 for the horizontal orientation of BTA,[46] corresponding to surface densities of 5.0×10^{14} molecules/cm^2 and 2.6×10^{14} molecules/cm^2, respectively. Thus, the adsorption density of BTA on copper surface is between 2.6×10^{14} and 8.4×10^{14} molecules/cm^2.

The experimentally evaluated coefficient c in Table 3.1 corresponds to BTA adsorption densities of 3.91×10^{14} (at 0.6 V) and 3.89×10^{14} molecules/cm^2 (at 0.4 V) on copper, intermediate between the saturation limits for BTA molecular planes parallel to the surface and normal to the surface. This implies either a range of orientations of BTA molecules in a monolayer, or that each BTA molecule is adsorbed onto the surface with its molecular plane tilted with respect to the surface normal. This consistency with independently obtained data affirms the validity of the approach adopted here for determining the adsorption behavior of BTA in pH 4 aqueous solution containing BTA and glycine.

The resulting millisecond scale kinetics of adsorption of BTA onto copper surfaces from acidic aqueous solution are shown in Figure 3.5, which shows rapid initial adsorption of BTA onto the copper surface. Within 30 ms (at 0.6 V), more than 90 percent of the copper surface is occupied by adsorbed BTA. The adsorption kinetics of BTA at 0.4 V are very similar to those at 0.6 V when plotted as a function of normalized time (i.e. t/t_m), despite the differences in the coefficients a, b, and c (inset of Figure 3.5).

Substituting the coefficients a, b, and c, along with the adsorption kinetics shown in Figure 3.5, into equations (3.5), (3.8) and (3.9) yields Figure 3.6, which shows the current density responsible for passivation and the current density for direct dissolution of copper as a function of time during the formation of a monolayer of BTA on copper. It is evident that initially the vast majority of the current is due to the formation of the passive layer, albeit at a steadily declining magnitude (it should also be recognized that this portion of Figure 3.6 is extrapolated, since capacitive charging dominated the current observed in the experimental potential step chronoamperometry experiments). At around 0.1 ms the current due to direct dissolution of copper becomes comparable to that due to the formation of the passive layer, and by 1 ms the majority of the current is due to direct dissolution of copper.
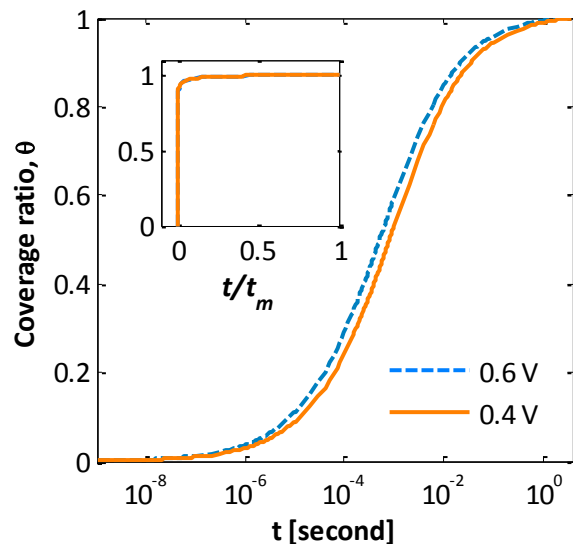
Figure 3.5 Millisecond scale adsorption kinetics of BTA in pH 4 aqueous solution containing 0.01 M glycine and 0.01 M BTA (inset: adsorption kinetics over the normalized time in linear scale)
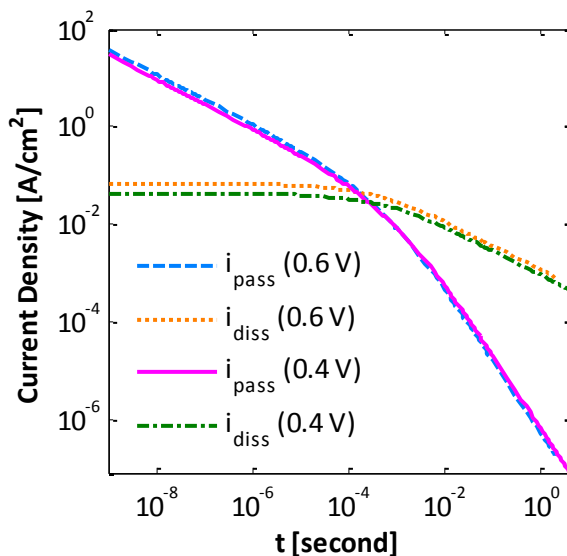
Figure 3.6 Current density for forming Cu(I)BTA and the current density for direct dissolution as a function of time during the formation of a monolayer of BTA on copper

Equation (3.14) was solved numerically for the different parameters of b and t_m corresponding to potentials of 0.6 V and 0.4 V, using the atomic weight of copper (63.54 g/mole) and density (8.96 g/cm^3). The value of n was taken as 2, because although copper is in the +1 oxidation state in adsorbed Cu-BTA complexes, it enters solution in the +2 oxidation state. Two extreme values of material removal rates taken from the literature were considered, namely 130nm/min and 600 nm/min. Two extreme values of τ were also considered, namely 1 and 10 ms, values representative of typical pads and rotational

velocities. The resulting values of t_o are reported in Table 3.2, along with the values of θ corresponding to these times, and the values of θ at $t_o + \tau$. There was no physically realistic solution to equation (3.14) for the higher value of τ in conjunction with the higher material removal rate. Physically it is reasonable that high material removal rates would not be seen with slow rotational speeds in CMP. It is seen that for the lowest material removal rates typically encountered in copper CMP, the surface is almost completely covered by BTA throughout the polishing process. The fractional coverage is about 93 % at 0.6 V (SCE), and 88 % at 0.4 V(SCE), and only a miniscule amount of BTA is removed with each asperity-copper interaction. Under such conditions, essentially all material is removed by direct electrochemical dissolution of copper. Conversely, at the highest material removal rates typically encountered in copper CMP, the copper surface undergoing active polishing is only partially covered by BTA (of course recessed areas on the copper surface that do not interact with the pad would be fully protected by thick BTA layers). Immediately after an asperity-copper interaction, about 64 and 49 % of the sites on copper would be occupied by BTA at 0.6 and 0.4 V, respectively. These occupancies would have increased to 71 and 61 % after just 1 ms. These conditions correspond to values of t_o of around 1 ms, which from Figure 3.6 is the time at which material removal involves both direct dissolution and formation of passive layers. Regardless of the precise material removal rate, it is clear that dissolution is an important material removal mechanism.

Table 3.2 Time corresponding to beginning of quasi-steady state, corresponding fractional coverage, and fractional coverage at next asperity-copper interaction, for MRRs and operating conditions typical of copper CMP processes

Potential (V (SCE))	t_m (sec)	b (A/cm^2)	t_{as-as} (ms)	MRR (nm/min)	t_o (sec)	θ (t_o)	$\theta(t_o + t_{as-as})$
0.6	2	8.4×10^{-4}	1	130	4.01068×10^{-2}	0.9273	0.9283
0.6	2	8.4×10^{-4}	10	130	3.57592×10^{-2}	0.9224	0.9326
0.6	2	8.4×10^{-4}	1	600	1.43898×10^{-3}	0.6422	0.7087
0.6	2	8.4×10^{-4}	10	600	N/A	N/A	N/A
0.4	4	4.7×10^{-4}	1	130	2.49268×10^{-2}	0.8777	0.8801
0.4	4	4.7×10^{-4}	10	130	2.06701×10^{-2}	0.8653	0.8902
0.4	4	4.7×10^{-4}	1	600	7.45896×10^{-4}	0.4875	0.6056
0.4	4	4.7×10^{-4}	10	600	N/A	N/A	N/A

3.6 Conclusions

The millisecond scale adsorption kinetics of BTA onto copper surfaces in pH 4 aqueous solution containing 0.01 M glycine and 0.01 M BTA have been determined from analysis of potential step chronoamperometry data. These kinetics show that BTA rapidly adsorbs onto copper surfaces, forming a monolayer of Cu(I)BTA within a second or so. Building on this analysis, we have shown that under typical CMP conditions, with typical material removal rates, copper surfaces undergoing active polishing in acidic slurries containing BTA have less than a monolayer of BTA on the surface. Further, only a small proportion of the adsorbed BTA is removed with any given asperity-copper interaction; most material removal is due to direct dissolution of Cu^{2+} ions (which may subsequently form complexes with other slurry

components) into the slurry. This mechanistic picture of copper CMP differs from the commonly accepted model first depicted schematically by Kaufmann et al.[8] involving thick passive layers that are completely removed with each interaction. We have also confirmed that, as proposed earlier[9] CMP is a wear-induced corrosion process, rather than a corrosion-enhanced wear process.

References

[1] *International Technology Roadmap for Semiconductors (ITRS) 2009 Edition* (http://www.itrs.net/Links/2009ITRS/Home2009.htm)

[2] F. W. Preston, *J. Soc. Glass Technol.*, **11**, 247 (1927).

[3] L. M. Cook, *Journal of Non-crystalline Solids*, **120**, 152 (1990).

[4] C. W. Liu, B. T. Dai, W. T. Tseng and C. F. Yeh, *J. Electrochem. Soc.*, **143**, 716 (1996).

[5] S. R. Runnels, *J. Electrochem. Soc.*, **141**, 1900 (1994).

[6] F. Zhang and A. Busnaina, *Electrochem. Solid-State Lett.*, **1**, 184 (1998).

[7] J. Luo and D. A. Dornfeld, *IEEE Transaction: Semiconductor Manufacturing*, **16**, 45 (2003).

[8] F. B. Kaufman, D. B. Thompson, R. E. Broadie, M. A. Jaso, W. L. Guthrie, D. J. Pearson and M. B. Small, *J. Electrochem. Soc.*, **138**, 3460 (1991).

[9] S. Tripathi, S. Choi, F. M. Doyle and D. A. Dornfeld, *Mater. Res. Soc. Symp. Proc.*, **1157,** E02-03 (2009).

[10] S. Tripathi, F. M. Doyle and D. A. Dornfeld, *Mater. Res. Soc. Symp. Proc.*, **1157,** E06-02 (2009).

[11] S. Tripathi, Ph.D. Thesis, University of California, Berkeley, Berkeley, CA (2008).

[12] F. Mansfeld, T. Smith and E. P. Parry, *Corrosion*, **27**, 289 (1971).

[13] G. Lewis, *Br. Corros. J.*, **16**, 169 (1981).

[14] D. Thierry and C. Leygraf, *J. Electrochem. Soc.*, **132**, 1009 (1985).

[15] N. Morito and W. Suetaka, *J. Japan Inst. Metals*, **35**,1165 (1971).

[16] J. J. Kester, T. E. Furtak and A. J. Bevolo, *J. Electrochem. Soc.*, **129**, 1716 (1982).

[17] M. Fleischmann, I. R. Hill, G. Mongoli and M. M. Musiani, *Electrochim Acta*, **28**, 1325 (1983).

[18] C. Tornkvist, D. Thierry, J. Bergman, B. Liedberg and C. Leygraf, *J. Electrochem. Soc.*, **136**, 58 (1989).

[19] G. W. Poling, *Corros. Sci.*, **10**, 359 (1970).

[20] T. Notoya and G. W. Poling, *Corrosion*, **32,** 216 (1976).

[21] D. Chadwick and T. Hashemi, *Corros. Sci.*, **18**, 39 (1978).

[22] F. El-Taib Heakal and S. Haruyama, *Corros. Sci.*, **20**, 887 (1980).

[23] J. Rubim, I. G. R. Gutz, O. Sala and W. J. Orville-Thomas, *J. Mol. Struct.*, **100**, 571 (1983).

[24] Z. Xu, S. Lau, and P. W. Bohn, *Langmuir*, **9**, 993 (1993).

[25] R. Youda, H. Nishihara, K. Aramaki, *Electrochim. Acta*, **35**, 1011 (1990).

[26] D. Tromans, *J. Electrochem. Soc.*, **145,** L42 (1998).

[27] F. Mansfeld, T. Smith, *Corrosion*, **29**, 105 (1973).

[28] M. Metikos-Hukovic, R. Babic, A. Marinovic, *J. Electrochem. Soc.*, **145**, 4045 (1998).

[29] R. Babic, M. Metikos-Hukovic, M. Loncar, *Electrochim. Acta*, **44**, 2413 (1999).

[30] V. Brusic, M. A. Frisch, B. N. Eldridge, F. P. Novak, F. B. Kaufman, B. M. Rush, and G. S. Frankel, *J. Electrochem. Soc.*, **138**, 2253 (1991).

[31] M. R. Vogt, W. Polewska, O. M. Magnussen, and R. J. Behm, *J. Electrochem. Soc.*, **144**, L113 (1997).

[32] B.-S. Fang, C. G. Olson and D. W. Lynch, *Surf. Sci.*, **176**, 476 (1986).

[33] K. Cho, J. Kishimoto, T. Hashizume and T. Sakurai, *Jpn. J. Appl. Phys.*, **33**, 125 (1994).

[34] S. L. Cohen, V. A. Brusic, F. B. Kaufman, G. S. Frankel, S. Motakef and B. Rush, *J. Vac. Sci. Technol.*, **A 8**, 2417 (1990).

[35] J.-O. Nilsson, C. Tornkvist, and B. Liedberg, *App. Surf. Sci.*, **37**, 306 (1989).

[36] D. Tromans and R. Sun, *J. Electrochem. Soc.*, **138**, 3235 (1991).

[37] Q. Luo, S. Ramarajan, and S. V. Babu, *Thin Solid Films*, **335**, 160 (1998).

[38] S. Aksu and F.M. Doyle, *.J Electrochemical Soc.,* **148** B51-B57 (2001).

[39] S. Aksu and F.M. Doyle, *.J Electrochemical Soc.,* **149** G352-G361 (2002).

[40] F. M. Bayoumi, A. M. Abdullah, and B. Attia, *Mater. Corros.*, **59**, 691 (2008).

[41] A. Frignani, M. Fonsati, C. Monticelli and G. Brunoro, *Corros. Sci.*, **41**, 1217 (1999).

[42] M.D. Ward and D.A. Buttry, *Science*, **249**, 1000 (1990).

[43] M. W. Roberts and C. S. Mckee, *Chemistry of the Metal-Gas Interface*, p. 82, Clarendon Press, Oxford (1978).

[44] F. Tomas, J. –L. M. Abboud, J. Laynez, R. Notario, L. Santos, S. O. Nilsson, J. Catalan, R. Ma. Claramunt, and J. Elguero, *J. Am. Chem. Soc.*, **111**, 7348 (1989).

[45] Z. Xu, S. Lau, and P. W. Bohn, *Surf. Sci.*, **296**, 57 (1993).

[46] D. M. Bastidas, *Surf. Interface Anal.*, **38**, 1146 (2006).

Chapter 4
Influence of Copper Ion Concentration on the Kinetics of Formation of a Protective Layer on Copper in an Acidic CMP Solution Containing BTA and Glycine

4.1 Introduction

With the adoption of porous ultra-low-k dielectrics in integrated circuits, the planarization processes used in manufacturing multi-level metallic interconnects have been modified to maintain low down pressures, in order to avoid damaging the dielectric. Chemical mechanical planarization (CMP) only yields low material removal rates when low down pressures are applied, although these low rates can be acceptable if the copper films are very thin. Electrochemical mechanical planarization (ECMP) [1] was developed to achieve reasonable material removal rates with low down pressures, although it is not widely used. In ECMP copper is oxidized with an applied voltage instead of the chemical oxidizing agents used in conventional CMP. During ECMP mechanical abrasion with a polishing pad and abrasives removes the thin passive layer formed on the copper surface at the applied voltage. At the same time, the copper at these unprotected protruding regions is dissolved by applied voltages of up to 2 V. A very low down pressure (< 0.5 psi) provides removal rates similar to those in conventional CMP.

In either CMP or ECMP, in order to achieve a planar surface, the solution must form a protective layer on the copper surface, thereby preventing unwanted dissolution of copper at recessed regions. Inhibitors such as benzotriazole (BTA) and ammonium dodecyl sulfate (ADS) usually perform this protective function. The role of other additives in the CMP slurry or ECMP electrolyte, such as complexing agents, inhibitors and oxidizers, has been investigated [2,3,4] and new formulations have been developed. [5,6] If the slurry or electrolyte is only replenished slowly, or transport of chemical species is impaired by features on the wafer, high concentrations of copper ions may develop in the solution, particularly near the wafer. The role of copper ions in the slurry during CMP has been investigated. Steigerwald *et al*. found that copper ions in the slurry dramatically increase the polish rate of titanium. [7] Hariharaputhiran *et al*. argued that Cu^{2+} ions complexed by amino acids such as glycine promote the generation of hydroxyl radicals from hydrogen peroxide. [8] Copper ions are also known to affect the agglomeration behavior of abrasive particles in the slurry. [9] However, little work has probed the effect of copper ions on the kinetics of formation of the passive layer on the copper surface. Given that passivating BTA films contain copper ions, the

buildup of dissolved copper ions in a CMP slurry or ECMP electrolyte with time might be expected to alter the passivation kinetics.

The importance of passivation kinetics for ensuring protection of recessed regions of the wafer surface undergoing CMP or ECMP is obvious. In addition, however, passivation is typically rapid enough to affect the material removal rate at protruding regions that are actively interacting with abrasive particles or pad asperities. Tripathi *et al*. developed a tribo-chemical model that considers CMP to be a wear enhanced corrosion process, where intermittent asperity/abrasive action removes some of the passivating film, thereby temporarily enhancing the local oxidation rate, followed by time-dependent passivation of copper.[10] This model allows determination of the material removal rate if the passivation kinetics, frequency of interaction, and amount of passive film removed per interaction are known and remain unchanged during the process. Tripathi *et al*. postulated that the stochastic processes across the entire wafer could be simplified by assuming that a given site on the wafer operates in a quasi-steady-state (the oxidation rate returns to the same value after each interaction). The kinetics of passivation were then examined by potential step chronoamperometry using copper microelectrodes, to provide data to use in the tribo-chemical model.[11,12] However, the earlier studies of passivation kinetics used solutions that contained no added copper salts. Accordingly, the current study followed the methodology of the earlier work to investigate the influence of copper ions in an acidic electrolyte containing BTA and glycine on the passivation kinetics. Chronoamperometry was used to allow measurement of the oxidation rate of copper at very short time scales. However, it must be emphasized that the kinetics of passivation would be similar if the copper were being oxidized chemically rather than electrochemically.

4.2 Experimental Details

4.2.1 Copper microelectrodes

Two types of copper microelectrode were fabricated from a 160 μm diameter copper wire (99.95% purity, MWS wire industries) insulated by enamel coating: 1) a microelectrode with a three dimensional exposed area was cut with a fine blade to expose a fresh copper surface (Figure 4.1a). The tip of the cut wire can be accessed by species present in a spherical region of electrolyte around the tip, as shown in Figure 4.1a (recognizing that the figure is a two-dimensional section) 2) A planar microelectrode was fabricated by embedding the copper wire in uncured epoxy within a 10 mm diameter plastic tube, then cutting the cured assembly perpendicular to the axis of the wire. The cut assembly was subsequently polished with P320, P800, P2400 and P4000 sandpaper (Buehler). Then CMP was conducted to finish the electrode surface using an IC1010 pad (Rohm and Haas Electronic Materials) and a slurry containing 10 wt% alumina particles, 0.01M BTA, 0.01M glycine, 0.1 mM $Cu(NO_3)_2$ and 1 wt% H_2O_2. The final shape of the microelectrode was a flat, circular copper disk, 160 μm in diameter, embedded in cured epoxy (Figure 4.1b).
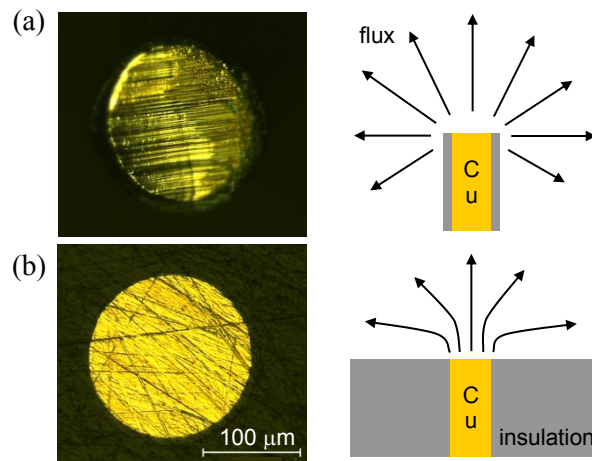
Figure 4.1 Exposed tip of a copper microelectrode and flux lines around a copper microelectrode: a) three dimensional and b) planar electrode.

4.2.2 Chronoamperometry

A three electrode electrochemical cell, housed in a glass beaker, was used for all experiments. The microelectrode was suspended at the center of the beaker facing downwards. A saturated calomel reference electrode (SCE) was placed in a Luggin capillary 5 mm from the copper microelectrode. A platinum mesh was used as a counter electrode. The pH 4 aqueous electrolyte contained 0.01 M BTA, 0.01 M glycine and different concentrations of $Cu(NO_3)_2$. The pH of the electrolyte was adjusted using acetate buffer. The solution was not aerated before the tests. All potentials are reported with respect to the SCE (+0.2444 V vs. SHE at 25 °C).

Chronoamperometry was conducted using a Gamry G300 potentiostat. The copper microelectrode was freshly cut (for the three dimensional electrode) or polished (for the planar electrode) before each experiment. After immersion in the electrolyte, the microelectrode was conditioned at -1.5 V for 20 seconds to reduce any surface oxides, and then stepped up to an intermediate potential of -1.2 V for 10 seconds. The potential was then stepped up to 0.6 V and the current was measured at time intervals of 0.1 ms minimum for 10 seconds. Each experiment was repeated several times to check for reproducibility. Experiments were conducted either with or without agitation of the solution. The measured currents are reported in this work rather than current densities because the precise surface area of the three dimensional electrode was not easily determined.

4.3 Results

Figure 4.2-4.4 show chronoamperometry curves for copper after the potential had been stepped up to 0.6 V in a pH 4 electrolyte containing 0.01 M BTA, 0.01 M glycine and 0.0, 0.1 and 0.6 mM $Cu(NO_3)_2$, respectively. The current decayed with time due to the progressive formation of a protective layer of adsorbed BTA on the surface of the copper.[11] Initially, at any given time, the current passing at the three dimensional electrode exceeded that for the

planar electrode by a factor of 1.5 (with no $Cu(NO_3)_2$) to 3.5 (with $Cu(NO_3)_2$). This is most likely due to the real surface area of the three dimensional electrode being larger than that of the planar electrode because of roughness induced by cutting (Figure 4.1). Agitation did not, in general, have much effect on the current at a given time. However, the current decayed very differently for the planar and three dimensional electrodes, especially after 0.1 seconds; the current passed by the planar electrode decayed more rapidly than that of the three dimensional electrode. This appears to be due to a difference in the transport of dissolved species. Copper ions that dissolve from the three dimensional electrode were able to be transported in three dimensions into the spherical volume surrounding the microelectrode, whereas copper ions released by the planar electrode were transported into a smaller, predominantly hemispherical volume adjacent to the electrode (Figure 4.1). Thus, for a given current, the concentration of copper ions near the surface of the three dimensional electrode at a given time would be expected to be lower than that near the planar electrode. To maintain charge neutrality, more BTA^- would be expected to migrate to the surface of the planar electrode, thereby providing better protection of the planar electrode against dissolution at a given time. The insensitivity of the current to agitation is, at first sight, surprising. This is thought to be due to agitation increasing transport of both copper ions away from the electrode, which might increase the current, and BTA ions to the electrode, which would be expected to decrease the current. The interactions of these ions are discussed further below.
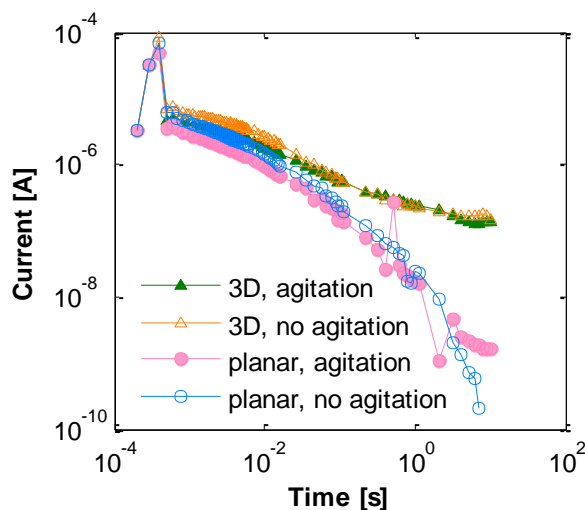
Figure 4.2 Measured current of copper microelectrodes (nominal surface area=2.01×10^{-4} cm^2) in a pH 4 solution containing 0.01 M BTA and 0.01 M glycine (no Cu(NO$_3$)$_2$).

42
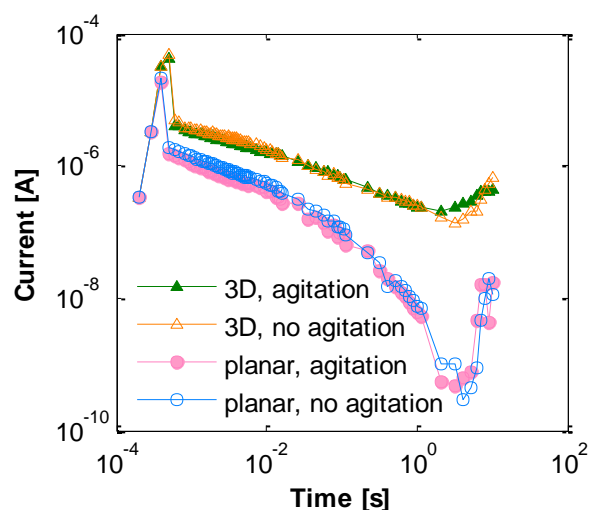
Figure 4.3 Measured current of copper microelectrodes (nominal surface area=2.01×10^{-4} cm^2) in a pH 4 solution containing 0.01 M BTA, 0.01M glycine and 0.1 mM Cu(NO$_3$)$_2$.
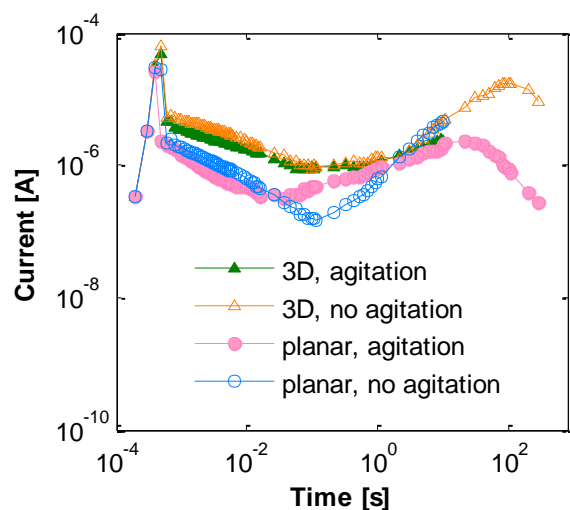
Figure 4.4 Measured current of copper microelectrodes (nominal surface area=2.01×10^{-4} cm^2) in a pH 4 solution containing 0.01 M BTA, 0.01M glycine and 0.6 mM Cu(NO$_3$)$_2$.

Comparing Figure 4.2-4.4, the most obvious result is that the current stopped decreasing and then began to increase when Cu(NO$_3$)$_2$ was present. The current reached a minimum sooner at the higher Cu(NO$_3$)$_2$ concentration. This is attributed to the initial formation of protective Cu(II)BTA$_2$ films on the surface of copper, followed by nucleation and growth of bulk, non-protective Cu(II)BTA$_2$ precipitates. The mechanism of precipitation and nucleation of bulk Cu(II)BTA$_2$ is further investigated in the following section.

Two experiments shown in Figure 4.4 were conducted for a longer period, 300 s, than the others, which were stopped at 10 s. For both cases, the current reached a maximum at about 100 s and then began decreasing again. This implies that a protective layer eventually formed again on the copper. This is analyzed below.

43

4.4 Discussion

Although complexation with glycine affects the stability region of Cu^{2+} ions,[13] at the pH and BTA concentrations used in this work, copper dissolves as Cu^{2+}.[14] Cu^{2+} ions react with two BTA$^-$ ions to precipitate Cu(II)BTA$_2$ when the solution pH exceeds 3.[15] In addition, Cu(II) and BTA form films on oxidized copper that have been reported to be as effective in inhibiting corrosion as Cu(I)BTA.[16,17]

The solubility product of Cu(II)BTA$_2$ was estimated as follows. The pK_a for acid dissociation of BTA has been reported as 8.2[18]). A solution containing 10^{-4} M Cu^{2+} and 5×10^{-3} M BTA at pH 3 was reported to be just saturated on the basis of such a solution becoming turbid after a few hours.[15] The concentration of the BTA$^-$ anion at pH 3 in a solution containing a total of 5 $\times 10^{-3}$ M BTA would be 3×10^{-8} M, assuming that the activity coefficient of H$^+$ is unity. Thus the solubility product for Cu(II)BTA$_2$ is estimated to be 9×10^{-20} mol^3/L^3.

In the chronoamperometry experiments, Cu^{2+} and BTA$^-$ ions are transported across the boundary layer by both diffusion and migration. At elevated potentials (or in the presence of a chemical oxidizing agent), Cu^{2+} ions are continuously generated at the copper surface, and are transported into the bulk, while BTA$^-$ ions are transported toward the copper surface, where adsorption and complexation of dissolved copper ions lowers their activity. Here we consider diffusion to be the primary transport mechanism, which would be the case for conventional CMP, where copper is oxidized by a chemical oxidizing agent. In ECMP, where the wafer is held at a high potential, migration would further enhance the transport of Cu^{2+} into the bulk and BTA$^-$ toward the electrode surface. The concentration of BTA$^-$ and Cu^{2+} at different positions relative to the copper surface could be obtained by solving Fick's second law with appropriate boundary conditions. However, an analytical solution to the differential equation is difficult to obtain, because the concentrations of free Cu^{2+} and BTA$^-$ ions at the copper surface are affected by the time-dependent adsorption of BTA$^-$, the dissolution rate of Cu and complex formation, as well as by diffusion.

Recognizing these challenges, the Cu^{2+} concentration profile near the copper electrode, $C_{Cu^{2+}}(y,t)$, was estimated by assuming: 1) that the concentration of copper ions is a function of the distance from the electrode, governed by one dimensional diffusion of copper ions from the electrode surface; and 2) the Cu^{2+} ions dissolved from the surface of the electrode into the electrolyte remain in the diffusion layer after stepping up the potential, giving the following concentration profile:

$$C_{Cu^{2+}}(y,t) = \frac{S}{\sqrt{\pi D_{Cu^{2+}} t}} \exp\left(\frac{-y^2}{4 D_{Cu^{2+}} t}\right) \tag{4.1}$$

where $S(t)$ is the cumulative amount of copper ions [mol/cm^2] dissolved per unit area from the copper surface during time t after stepping up the potential, expressed as

$$S(t) = \frac{\int_0^t i_{diss}(\tau)d\tau}{zF}$$, y is the distance from the electrode surface, $D_{Cu^{2+}}$ is the diffusion coefficient of Cu^{2+}, t is the time elapsed since the potential of copper was stepped up to an anodic value, i_{diss} is the current density responsible for direct dissolution of copper ions into the solution, $d\tau$ is an infinitesimal time increment, z is the oxidation state of the oxidized copper and F is Faraday's constant. If copper ions are present before stepping up the potential, they are assumed to be uniformly dispersed. Assuming that the bulk concentration of copper ions does not change the copper ion activity coefficient, and that there is no complexation or precipitation, the bulk concentration of copper ions does not affect diffusion behavior and thus can be added as a constant to equation (4.1).

As shown in Figure 4.5,[12] the current density attributable to dissolution of copper is nearly constant for the first 0.1 ms after stepping up the potential, and then decays following $t^{-0.5}$. The data in Figure 4.5 were obtained from current densities measured on copper at 0.6 V, similar to those shown in Figure 4.2, using theoretical analysis to determine the kinetics of adsorption of BTA onto the surface of copper from a pH 4 aqueous solution containing 0.01 M BTA and 0.01 M glycine. The current densities were measured using the same three dimensional copper electrode and experimental setup as this work. In this analysis, the total measured current densities were attributed to both the direct dissolution of copper into the solution and the oxidization of copper on the surface to form a complex with the adsorbed BTA, yielding the following governing equation:

$$a(1-\theta) + b\theta + c\frac{d\theta}{dt} = i_m\left(\frac{t}{t_m}\right)^{-0.5} \tag{4.2}$$

where t_m is the time at which a complete monolayer is formed, i_m is the current density at t_m, θ is the fraction of surface sites covered by adsorbed BTA, a and b are the dissolution rates of copper ions from bare sites and those on which BTA is adsorbed, respectively (expressed in terms of current densities), and c is a constant that relates the fractional coverage with the charge density of the oxidized copper that constitutes the Cu(I)BTA on the copper surface. The coefficients a, b and c were obtained by solving equation (4.2) using the boundary conditions: $\theta=0$ at $t=0$; and $\theta=1$ and $d\theta/dt=0$ at $t = t_m$. After solving equation (4.2) to evaluate θ as a function of time, the portion of the current density attributable to the direct dissolution of copper, $a(1-\theta)+b\theta$, could be determined using equation (4.2).
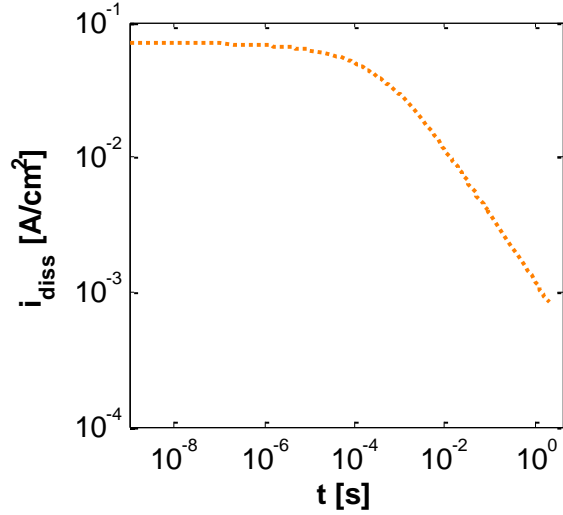
Figure 4.5 Current density for direct dissolution of copper, i_{diss}, as a function of time during the formation of a monolayer of BTA on copper[12].

Thus, considering the current density up to 0.1 ms to be constant, the cumulative amount of copper ions dissolved from the electrode surface can be simplified to:

$$S(t) = \left[\begin{array}{ll} \dfrac{\bar{i}_{diss}}{zF} t & (for\, t \leq 0.1ms) \\[3mm] 2\dfrac{\bar{i}_{diss}}{zF}\sqrt{0.0001}\sqrt{t} - \dfrac{\bar{i}_{diss}}{zF}(0.0001) & (for\, t > 0.1ms) \end{array} \right] \tag{4.3}$$

where $\bar{i}_{diss}$ is the nearly constant portion of the current density due to direct dissolution of copper shown in Figure 4.5 and t is expressed in seconds.

The concentration of copper ions is highest at the electrode surface and changes with time. From equation (4.1):

$$C_{Cu^{2+}}(0,t) = \frac{S}{\sqrt{\pi D_{Cu^{2+}} t}} \tag{4.4}$$

It is also useful to consider a diffusion layer "boundary", $2\sqrt{D_{Cu^{2+}} t}$, at which the concentration of copper ions is given by:

$$C_{Cu^{2+}}(2\sqrt{D_{Cu^{2+}} t}, t) = \frac{S}{e\sqrt{\pi D_{Cu^{2+}} t}} = \frac{C_{Cu^{2+}}(0,t)}{e} \tag{4.5}$$

The limits on the concentration of copper ions at the electrode surface at a given time, t^*, can be estimated as follows. The highest concentrations can be estimated by dividing time t^* into n increments and only considering the diffusion behavior of copper ions dissolved during

46

each t^*/n time increment. The copper ions dissolved during the first of these increments, $0 \leq t < t^*/n$, will have diffused into the electrolyte for t^*, leaving only a fraction of the dissolved copper ions remaining at the surface of copper, as given by equation (4.3) and (4.4). The copper ions dissolved during the next t^*/n time increment ($t^*/n < t < 2\,t^*/n$) will have diffused for ($t^* - t^*/n$). Repeating until the nth time segment gives the concentration of copper ions at the surface of copper shown in equation (4.6). Here the cumulative amount of copper ions dissolved for the first 0.1 ms was used, so that i_{diss} can be approximated as being constant, designated as $\bar{i}_{diss}$.

$$C_{Cu^{2+}}(0,t^*) = \frac{\dfrac{\bar{i}_{diss}}{zF}(t^*/n)}{\sqrt{\pi D_{Cu^{2+}} t^*}} + \frac{\dfrac{\bar{i}_{diss}}{zF}(t^*/n)}{\sqrt{\pi D_{Cu^{2+}} (\dfrac{n-1}{n})t^*}} + \frac{\dfrac{\bar{i}_{diss}}{zF}(t^*/n)}{\sqrt{\pi D_{Cu^{2+}} (\dfrac{n-2}{n})t^*}} +$$

$$\ldots + \frac{\dfrac{\bar{i}_{diss}}{zF}(t^*/n)}{\sqrt{\pi D_{Cu^{2+}} \dfrac{1}{n}t^*}} = \sum_{k=1}^{n} \frac{\dfrac{\bar{i}_{diss}}{zF}(t^*/n)}{\sqrt{\pi D_{Cu^{2+}} \dfrac{k}{n}t^*}}$$

(4.6)

For infinitesimal time increments, t^*/n ($n \rightarrow \infty$), equation (4.6) can be rewritten as:

$$C_{Cu^{2+}}(0,t^*) = \int_0^{t^*} \frac{\dfrac{\bar{i}_{diss}}{zF}}{\sqrt{\pi D_{Cu^{2+}} t}} dt = \frac{2\bar{i}_{diss}\sqrt{t^*}}{zF\sqrt{\pi D_{Cu^{2+}}}} \quad \text{for } t^* \leq 0.1 ms$$

(4.7)

This analysis assumes that the concentration profile of copper ions follows the diffusion profile created by a constant total amount of solute during each infinitesimal time increment, and ignores the concentration gradients that already existed because of copper ions that had already diffused into the electrolyte during earlier time increments. Had these been considered, the concentration gradients would have been steeper, resulting in faster diffusion. Hence this simplified approach overestimates the concentration of Cu^{2+} near the electrode surface and underestimates the bulk concentration of Cu^{2+} away from the surface. The corresponding concentrations of Cu^{2+} at the diffusion layer boundary can be obtained from equation (4.5).

Substituting the constant value of $\bar{i}_{diss}$ from Figure 4.5 up to 0.1 ms, $0.06 A/cm^2$, into equation (4.7) and taking the diffusion coefficient of Cu^{2+}, $D_{Cu^{2+}}$, as $7.13 \times 10^{-6} cm^2 s^{-1}$ (from Marcinkowsky and Philips[19]), gives a concentration of Cu^{2+} at the electrode surface at 0.1 ms of approximately 1.3 mM. The upper bound of estimated $[Cu^{2+}]$ at the diffusion layer boundary is 0.48 mM. Those estimates are listed in Table 4.1 along with the estimates in the following calculations.

Table 4.1. Concentrations of Cu^{2+} [mM] at the limit of diffusion layer boundary at various times during anodic polarization

Duration of anodic polarization [s]		10^{-4}	0.1	3
[Cu^{2+}] at the electrode surface	dissolved from the electrode	0.66-1.3	1.3	1.3
[Cu^{2+}] at the diffusion layer boundary	dissolved from the electrode	0.24-0.48	0.48	0.48
	not complexed with glycine	0.21	0.41	0.41
	total concentration when current increases in presence of added Cu^{2+}	-	0.93 for 0.6 mM [Cu^{2+}]	0.50 for 0.1 mM [Cu^{2+}]

Conversely, a lower bound for the concentration of Cu^{2+} at the electrode surface can be estimated by assuming that the total amount of Cu^{2+} dissolved from the surface during time t^{*} was introduced at $t = 0$ and diffused into the electrolyte for t^{*}. For t^{*} less than 0.1 ms, the concentration of copper ions at the electrode surface would be:

$$C_{Cu^{2+}}(0,t) = \frac{S(t=t^{*})}{\sqrt{\pi D_{Cu^{2+}}t^{*}}} = \frac{\dfrac{\bar{i}_{diss}t^{*}}{zF}}{\sqrt{\pi D_{Cu^{2+}}t^{*}}} = \frac{\bar{i}_{diss}\sqrt{t^{*}}}{zF\sqrt{\pi D_{Cu^{2+}}}} \tag{4.8}$$

This lower bound (for $0 < t^{*} \leq 0.1 ms$) gives a concentration of Cu^{2+} at the electrode surface of 0.66 mM, half of the upper bound value. The concentration falls to 0.24mM at the diffusion layer boundary. Because the purpose of the following analysis is to determine whether or not there could have been homogeneous precipitation of Cu(II)BTA$_2$ in the boundary layer, for the sake of simplicity, we consider only the lower bound values. This provides a conservative assessment of the likely behavior. When t^{*} exceeds 0.1 ms, the lower bound estimation of [Cu^{2+}] becomes:

$$C_{Cu^{2+}}(0,t^{*}) = \frac{2\sqrt{0.0001}\,\bar{i}_{diss}}{zF\sqrt{\pi D_{Cu^{2+}}}} - \frac{\bar{i}_{diss}(0.0001)}{zF\sqrt{\pi D_{Cu^{2+}}t^{*}}} \tag{4.9}$$

This equation suggests that the concentration of Cu^{2+} at the surface of the copper electrode increases, albeit gradually, with time for times exceeding 0.1 ms. However, the numerical values of the constants are such that the increases are imperceptible; the lower bound concentration at the surface is 1.3 mM at both 0.1 s and 3 s (the times at which the current densities began to increase in Figure 4.3 and Figure 4.4. The concentrations at the boundary of the diffusion layer are 0.48 mM at both times. Therefore, the concentration of Cu^{2+} in the diffusion layer after 0.1 ms, 0.1 s and 3 s of anodic polarization can conservatively be assumed to be at least 0.24 mM, 0.48 mM and 0.48 mM, respectively (Table 4.1).

All of the discussion above considers total copper concentrations. However, the proportion

of Cu^{2+} available to interact with BTA^- depends upon how much is already complexed by glycine in the electrolyte. At pH 4, glycine exists mostly as a zwitterion, $^+H_3NCH_2COO^-$.[20] $^+H_3NCH_2COO^-$ reacts with Cu^{2+} to generate $Cu(H_2NCH_2COO)^+$:[13]

$$Cu^{2+} + {}^+H_3NCH_2COO^- \rightarrow Cu(H_2NCH_2COO)^+ + H^+ \tag{4.10}$$

Aksu and Doyle calculated the equilibrium for reaction (4.10) to be:

$$pH = 1.219 - \log\{{}^+H_3NCH_2COO^-\} + \log(\{Cu(H_2NCH_2COO)^+\}/\{Cu^{2+}\}) \tag{4.11}$$

Assuming that all species in the electrolyte are ideal, with activity coefficients of $1\ M^{-1}$, the concentration of copper glycine complexes can be calculated. Setting this value to x, for a pH 4 electrolyte that contains 0.01 M glycine, in which the only copper ions at the diffusion layer boundary are those that have dissolved from the electrode (0.24 mM at 0.1 ms after first raising the potential), equation (4.11) can be rewritten as

$$4 = 1.219 - \log(10^{-2} - x) + \log x - \log(2.4 \times 10^{-4} - x) \tag{4.12}$$

The minimum concentration of Cu^{2+} in the diffusion layer boundary shown in Table 4.1 is used in the calculation. Solving equation (4.12) gives that $\{Cu(H_2NCH_2COO)^+\}$ is 3.3×10^{-5}. Similarly, the amount of Cu^{2+} complexed by glycine at 0.1 and 3 s after first raising the potential is 6.6×10^{-5} M for both cases, based on the minimum concentration of Cu^{2+} at the boundary of the diffusion layer shown in Table 4.1. Given the large excess of glycine, it is reasonable to assume that it is readily available, allowing rapid attainment of the equilibrium. Thus the concentration of free Cu^{2+} at the diffusion layer boundary at 10^{-4}, 0.1 and 3 s after anodic polarization is 0.21, 0.41 and 0.41 mM, respectively. For solutions that contained 0.1 mM and 0.6 mM copper salts initially, the free Cu^{2+} concentrations would be 0.50 mM and 0.93 mM, respectively, at the times when the measured currents were first observed to increase. These values are tabulated in Table 4.1.

The concentration of BTA^- at the surface of copper is much lower than that in the bulk because the adsorption of BTA on the surface of copper at this condition is very rapid,[12] resulting in depletion of the BTA^- near the surface of the copper. The resulting concentration profile is shown conceptually in Figure 4.6. Referring back to the solubility product for $Cu(II)BTA_2$ of $9 \times 10^{-20}\ mol^3/L^3$, it should be noted that the participating species are free Cu^{2+} cations and BTA^- anions. The bulk concentration of the BTA^- anion in the pH 4 electrolyte, 6.3×10^{-7} M for 0.01 M of total BTA, is obtained from the acid dissociation constant[18] (equation (4.13)):

$$BTA \rightarrow BTA^- + H^+ \qquad pK_a = 8.2 \tag{4.13}$$
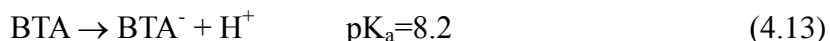
This exceeds the concentration of BTA^- anions required to exceed the solubility product of $Cu(II)BTA_2$ in the boundary layer after 10 s of anodic polarization, which was the longest duration for the data in Figure 4.2-4, which would have provided the highest concentration of copper ions dissolved from the electrode, 1.5×10^{-8} M, even when the electrolyte contained

49

no added Cu^{2+}. However, supersaturation would be needed for homogeneous precipitation of $Cu(II)BTA_2$, and this was achieved much sooner in electrolytes that contained added copper ions. Figure 4.6a depicts schematic concentration profiles for Cu^{2+} and BTA^- across the diffusion layer. It is clear that the product of the concentrations of Cu^{2+} and BTA^- reaches a maximum within the boundary layer, but at a distance y_0 from the copper surface because of the convex profile of the curves and more weight on $[BTA^-]$. This, then, is likely to be the location where solid $Cu(II)BTA_2$ would nucleate, at a time t_n. Once $Cu(II)BTA_2$ has nucleated, the concentrations of free Cu^{2+} and BTA^- would drop locally, because these species have been removed from solution, as depicted in Figure 4.6b. This perturbs the concentration profile, creating localized concentration gradients for both Cu^{2+} and BTA^- that would drive further flow of these ions to the precipitation site, allowing the nuclei of $Cu(II)BTA_2$ to grow (Figure 4.6c).
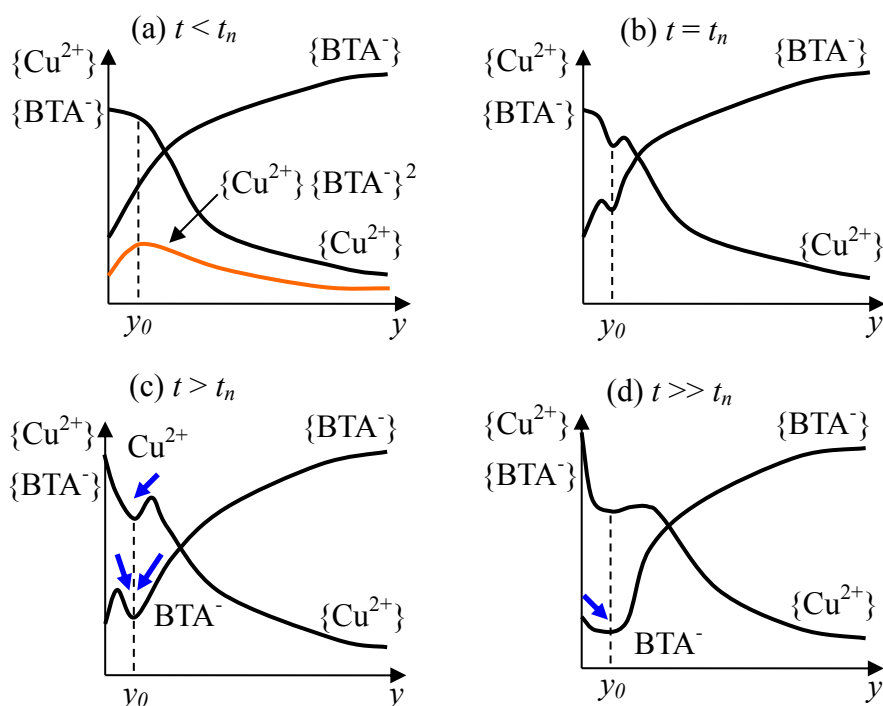
Figure 4.6 Schematic depiction of activity profiles of Cu^{2+} and BTA^- near the surface of a copper electrode at different times after raising the potential.

The $Cu(II)BTA_2$ nuclei would grow as more Cu^{2+} and BTA^- diffuse toward the precipitate, with a concurrent broadening of the perturbed region of the concentration profiles. Because copper ions continue to dissolve at the copper surface, there will be an ongoing supply of copper ions to the growing $Cu(II)BTA_2$ precipitates. These will only form $Cu(II)BTA_2$ if there is a stoichiometric supply of BTA^- ions. Some of these will come from the bulk, but others would be expected to desorb from the copper surface, because the solid $Cu(II)BTA_2$ precipitates are more thermodynamically stable than adsorbed $Cu(I)BTA$ complexes, yielding the situation conceptualized in Figure 4.6d. This removal of protective species would result in an increase in the current density at the copper electrode, as indeed is seen in Figure 4.3 and 4.4. Note that the onset of this increase in current occurs earlier for higher dissolved Cu^{2+}

concentrations, which is consistent with earlier nucleation of Cu(II)BTA$_2$.

Eventually, however, the bulk Cu(II)BTA$_2$ precipitates would be expected to grow toward the copper ion source, namely the copper surface, and may repassivate it. This is seen experimentally; Figure 4.4 shows that at longer durations repassivation does, indeed, occur.

This conceptual understanding of the disruptive influence of Cu(II)BTA$_2$ on passivation has important ramifications for CMP and ECMP, where the topography of the wafer surface is smoothed by preferential removal of materials at protruding regions, ideally without dissolution of materials from recessed regions. The dissolution rate of copper, along with the removal rate of the protective layer, determines the material removal rate. As discussed in the introduction, for protruding regions, the protective material would be partly removed by interaction with the pad asperities and any abrasives; and the area contacted by the asperity and abrasives will again become protected by adsorbing BTA until the next interaction. If the interval between the interactions is uniform enough, the removal and reformation of the protective material will occur in a quasi-steady manner.[10] The interval between consecutive interactions of asperities with copper is much shorter for the protruding areas than for the recessed areas because only the longer, narrower asperities can reach the recessed areas, whereas all asperities can contact protruding regions.[21] For typical CMP and ECMP conditions, the time period between interactions for protruding regions is too short for significant depassivation, and any Cu(II)BTA$_2$ nucleated in the boundary layer would be removed by the motion of the asperities. In addition, the hydrodynamic conditions at these protruding regions being swept regularly by pad asperities would differ from those assumed in the analysis above. Given both considerations, the overall material removal rates would not be expected to be strongly affected by dissolved copper in the slurry or electrolyte.

In contrast, at recessed regions there would be less agitation, and BTA has enough time to be adsorbed onto the copper surface and form protective layers or multilayers. If the electrolyte contains a sufficiently high concentration of Cu^{2+} ions and BTA, however, the adlayer formed on the surface may be destroyed as depicted conceptually in Figure 4.6, which could account for the transient elimination of passivity seen in Figure 4.3 and 4.4. This situation is not unlikely; in conventional copper CMP processes, the concentration of Cu^{2+} ions can exceed 20 mM, which is much higher than the concentrations used in this study, if the material removal rate is 1000 nm/min.[22] With elimination of passivity, the recessed regions of the wafer would not be protected, which could lead to roughened topography, or at least longer times needed to achieve planarization. Even for low concentrations of copper ions in the bulk, high concentrations of copper ions may develop if mass transport of dissolved Cu^{2+} into the bulk is hindered. This suggests that the influence of copper ions on the kinetics of formation of the protective layer must be considered when formulating new electrolytes or slurries for ECMP or CMP of copper. Also, the concentration of copper ions in the electrolyte must be controlled below a certain level to ensure the integrity of the protective material during the process. This might be achieved with lower residence times for slurries, and passage of the withdrawn slurry through a bed of a cation exchange resin that could replace Cu^{2+} by H$^+$ ions.

4.5 Conclusions

The influence of copper ions on the performance of CMP and ECMP using an acidic electrolyte containing BTA and glycine was investigated. Even modest additions of copper ions to the electrolyte impacted the kinetics of formation of the protective layer on the copper surface. We propose that this is due to Cu^{2+} ions complexing with BTA^{-} in the boundary layer, and eventually nucleating and precipitating $Cu(II)BTA_2$. The higher the concentration of Cu^{2+} in the electrolyte, the more easily $Cu(II)BTA_2$ nucleates. Nucleation and growth of $Cu(II)BTA_2$ in the boundary layer causes desorption of BTA species from the adsorbed protective layer. This nucleation of $Cu(II)BTA_2$ followed by desorption of BTA could be particularly problematic at recessed regions on the wafer surface because the interaction of asperities is less frequent in those areas. Therefore, the influence of copper ions on the stability of the protective layer must be considered when developing new electrolytes and slurries. It is also suggested that it is important to control the concentration of copper ions in the electrolyte during CMP and ECMP processes.

Reference

[1] L. Economikos, X. Wang, A. Sakamoto, P. Ong, M. Naujok, R. Knarr, L. Chen, Y. Moon, S. Neo, J. Salfelder, A. Duboust, A. Manens, W. Lu, S. Shrauti, F. Liu, S. Tsai, and W. Swart, p.233, *IITC Proceedings Series* (2004).

[2] P.C. Goonetilleke and D. Roy, *Appl. Surf. Sci.*, **254**, 2696 (2008).

[3] P.C. Goonetilleke and D. Roy, *Mater. Chem. Phys.*, **94**, 388 (2005).

[4] B. K. Klug, C. M. Pettit, S. Pandija, S. V. Babu and D. Roy, *J. Appl. Electrochem.*, **38**, 1347 (2008).

[5] K. G. Shattuck, J. -Y. Lina, P. Cojocaru and A. C. West, *Electrochim. Acta*, **53**, 8211 (2008).

[6] A. Tripathi, C. Burkhard, I. I. Suni, Y. Li, F. Doniat, A. Barajas and J. McAndrew, *J. Electrochem. Soc.*, **155**, H918 (2008).

[7] J. M. Steigerwald, S. P. Murarka, R. J. Gutmann and D. J. Duquette, *J. Electrochem. Soc.*, **141**, 3512 (1994).

[8] H. Hariharaputhiran, J. Zhang, S. Ramarajan, J. J. Keleher, Y. Li, and S. V. Babu, *J. Electrochem. Soc.*, **147**, 3820 (2000).

[9] R. Ihnfeldt and J. B. Talbot, J. Electrochem. Soc., **154**, H1018 (2007).

[10] S. Tripathi, S. Choi, F. M. Doyle and D. A. Dornfeld, *Mater. Res. Soc. Symp. Proc.*, **1157,** E02-03 (2009).

[11] S. Tripathi, F. M. Doyle and D. A. Dornfeld, *Mater. Res. Soc. Symp. Proc.*, **1157,** E06-02 (2009).

[12] S. Choi, S. Tripathi and D. A. Dornfeld, F. M. Doyle, *J. Electrochem. Soc.*, **157**, H1153 (2010).

[13] S. Aksu and F. M. Doyle, *J. Electrochem. Soc.*, **148**, B51 (2001).

[14] D. Tromans, *J. Electrochem. Soc.*, **145,** L42 (1998).

[15] F. Pergola, M. R. Moncelli and R. Guidelli, *J. Electroanal. Chem.*, **107**, 295 (1980).

[16] V. S. Sastri and R. H. Packwood, *Mater. Corros.*, **38**, 77 (1987).

[17] P. G. Fox, G. Lewis and P. J. Boden, *Corros. Sci.*, **19**, 457 (1979).

[18] D. D. Perrin, *Dissociation Constants of Organic Bases in Aqueous Solutions*, Butterworths, London (1965).

[19] A. E. Marcinkowsky, H. O. Philips, *J. Chem. Soc. A.*, **1**, 101 (1971).

[20] R. M. Smith and A. E. Martell, *Critical Solubility Constants*, Vol. 6, Plenum Press, New York (1977).

[21] S. Choi, A. de Closset, F. M. Doyle and D. A. Dornfeld, p. 239, in *Proceedings of International Conference on Planarization/CMP Technology 2010*, Phoenix, AZ (2010).

[22] A. Nennemann, M. Voetz, G. Hey, L. Puppe and S. Kirchmeyer, *Progr. Colloid. Polym. Sci.*, **133**, 159 (2006).

Chapter 5
Evaluation of the Efficiency of a CMP Pad in Removing Protective Materials from Copper during CMP

5.1 Introduction

The surface of porous polishing pads used in chemical mechanical planarization (CMP) application is rough, comprising numerous asperities formed by the pores. The rough surface is constantly regenerated through conditioning between the runs or during the process. The pad is wet by applying a polishing slurry that contains various chemicals such as oxidizing agent, inhibitor and complexing agent, and abrasive particles to remove the material on the surface of the wafer through the interplay between the chemical and mechanical actions. The mechanisms of the material removal during copper CMP have been studied but few studies have investigated the true synergy between the chemical and mechanical components. Tripathi *et al.* postulated a quasi-steady state during the CMP process where the removal rate of the protective layer by a pad asperity is balanced by the rate of formation of the protective layer until the next interaction by another asperity.[1,2] Based on this assumption, they predicted the material removal rates during copper CMP as a sum of the dissolution rates of the copper and the removal rates of the protective layer, which can be measured by the oxidation rates during the process. Choi *et al.* further developed the Tripathi's model so that the quasi-steady state assumption can be applied even when less than a monolayer of the protective material is present on the surface of copper.[3] The kinetics of the protective material formation on the surface of copper at acidic solution containing BTA and glycine were determined based on the quasi-steady state assumption. It was found that only a fraction of a monolayer of the protective material is present during copper CMP and a portion of the existing protective materials is removed by the interaction with the asperities. It was also proposed that the interaction with the pad asperity where abrasive particles are embedded caused the material to be removed by occasional plastic deformation of the material and subsequent removal of the piled up copper that was preferentially oxidized by the oxidizing agents in the slurry.[4] However, the exact interaction between the embedded abrasive particles and copper has not been understood although most researchers have envisaged that the interaction between these two materials is critical for understanding the material removal mechanisms during copper CMP. Traditionally it has been considered that the embedded abrasive particles plough the surface of copper to dislodge materials.[5,6,7] The chemical contribution to the material removal has also been considered by assuming that the chemical additives in the slurry change the hardness of the copper or the abrasive size distribution, although these approaches have not successfully predicted the material removal rates during

copper CMP.[5] In this work, the interaction between the embedded abrasives and the copper on which a protective film has are formed was investigated based on the work of Choi *et al.*[3]. Specifically the efficiency of a pad asperity in removing protective material from the surface of copper, which was defined as the removal efficiency, was determined for various experimental conditions. The removal efficiency is essential for completing the mechanistic model that predicts the material removal rates during CMP proposed by Choi *et al.*[4].

5.2 Experimental Detail

In situ electrochemical measurements during polishing were conducted using the apparatus shown in Figure 5.1 connected to Gamry G300 Potentiostat. A three electrode electrochemical cell, housed in a plastic beaker, was constructed on the table of a vertical machining center tool (Matsuura MC-510VSS). The working electrode was a copper tube (99.99 % purity from McMaster-Carr) with a 1 mm difference between the outer and inner diameters, so as to minimize the variation of sliding velocities relative to the CMP pad across the annulus. The copper tube was embedded in insulating epoxy, exposing an annulus at the bottom of the electrode, with a cross sectional area of 0.46 cm^2. The surfaces of the copper electrode were insulated by epoxy except the bottom with cross sectional area of 0.46cm^2 where electrochemical reactions occurred and corresponding current density was measured. A platinum mesh was used as a counter electrode and was placed under the polishing pad. A saturated calomel reference electrode (SCE) was placed in a Luggin capillary, and the tip of the capillary was located between the polishing pad and the counter electrode. IC1010^{TM} (Rohm and Haas) CMP pad, on which four through holes (4.76mm diameter) were machined along the trajectory of the contact by the copper electrode (Figure 5.2), was fixed to the bottom of the beaker. Note that the through holes on the CMP pad reduced the uncompensated resistance between the working electrode and the counter electrode and facilitated the delivery of the slurry to the interface of the working electrode and the pad. The pad was maintained parallel to the open surface of the copper electrode to ensure uniform pressure distribution throughout the copper during polishing. The polishing slurry contained 5 wt% alumina particles (primary diameter of 20nm and a median aggregate diameter of 150nm, from Cabot Corporation) and 0.01 M glycine in deionized water (DI water) with or without 0.01 M benzotriazole (BTA). The pH of the slurry was adjusted to 4 by adding acetate buffer. All potentials are reported with respect to the SCE.
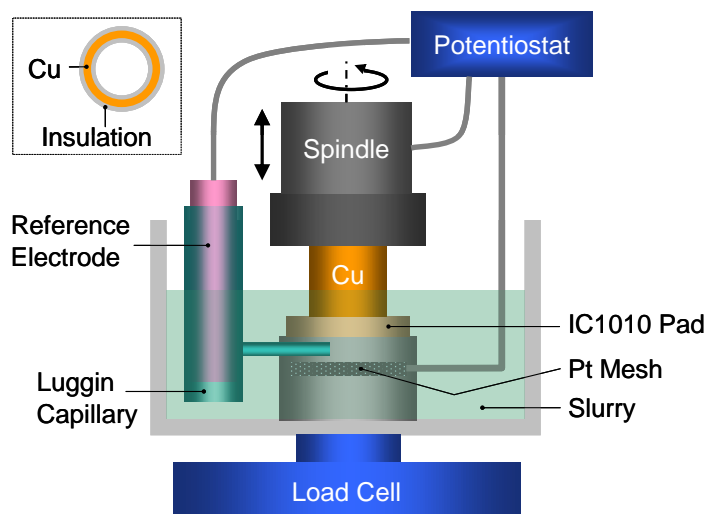
Figure 5.1 *In situ* **electrochemical measurement apparatus constructed on the table of a vertical machining center tool (Matsuura MC-510VSS). Shown in upper left is the cross-section of the copper working electrode.**

The pressure applied on the copper surface was adjusted by moving the axis of the machine tool vertically; this position was numerically controlled as precisely as one micrometer. The load applied during polishing was measured by a load cell (TUF-010-025-S from Loadstar Sensors) placed under the electrochemical cell. The sliding velocity of the copper surface over the polishing pad was adjusted by varying the rotational speed of the working electrode.

Potentiodynamic polarization was performed from -0.8 V to 0.8 V with a scan rate of 5 mV/s. The copper electrode was conditioned at -0.8 V for 30 seconds before each scan to remove any oxides on the surface. Slurries contained 0.01 M glycine, 5 wt% alumina abrasives with or without 0.01 M BTA at pH 4. *In situ* IR compensation was not applied because of the noise in the output data. Scans were obtained while rotating or not rotating the copper electrode. Reproducibility of the data was ensured by conducting several scans for each condition.

The CMP pad was conditioned using a diamond conditioner supplied from GNP Technology while supplying DI water onto it before each experiment. The open surface of the copper working electrode was polished before each experiment with an IC1010^{TM} CMP pad using the same slurry specified above for 30 seconds to flatten the entire surface including the epoxy insulating layer, followed by additional polishing using commercial CMP slurry for 30 seconds to reduce the topography of the copper surface. The electrode was then immediately rinsed with DI water. Any remaining oxides on the copper surface were reduced by applying a cathodic potential of -1.5 V for 5 seconds followed by -1.2V for 10 seconds while abrading the working electrode on the pad. The potential was then stepped up to 0.6 V and the current was measured for 10 seconds during polishing. *In situ* IR compensation was applied using an integrated function of the potentiostat. Since the experimental results were highly dependent on the surface of the copper electrode and the top surface of the pad being parallel, this was ensured throughout the measurements. Figure 5.2 shows the pad after CMP when the bottom of the copper was well aligned with the top surface of the pad. The uniform annular trajectory

of the copper electrode demonstrates that the pad interacted with all points of the electrode. Polishing was conducted with different down pressures and sliding velocities while maintaining the potential of copper at 0.6 V. The same experiments were repeated, exerting a down pressure but holding the electrode stationary, to compare with the data for the rotating electrode. Experiments were repeated at least three times for each condition.
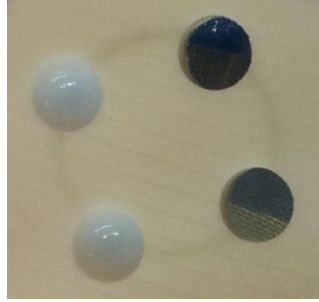
Figure 5.2 IC1010^{TM} CMP pad with four machined holes after CMP of copper. Oxidized copper remained on the surface of the pad leaving an annular trajectory corresponding to the electrode.

5.3 Results

Figure 5.3 shows the efficacy of BTA at protecting the surface of copper over the entire range of the scan. At anodic potentials the oxidation rates of the copper were nearly two orders of magnitude lower than when the slurry contains BTA. Complying with the experimental results of Tripathi *et al.*[1], BTA also suppresses the reduction of oxygen at cathodic potentials. When the copper electrode sled over the CMP pad at 0.5 m/s under 3.6 psi of down pressure in the presence of BTA, the current densities increased about two orders of magnitude at anodic region approaching the oxidation rates in the absence of BTA, showing the efficacy of the abrading actions in removing the protective layer on the surface of the copper. Note that the current densities at cathodic regions also increased when the copper was polished in the presence of BTA. This implies that the inhibition by BTA at cathodic potentials was induced by physical adsorption of BTA and the abrading actions by pad asperities and abrasives easily remove the weakly bonded layer of BTA from the surface.
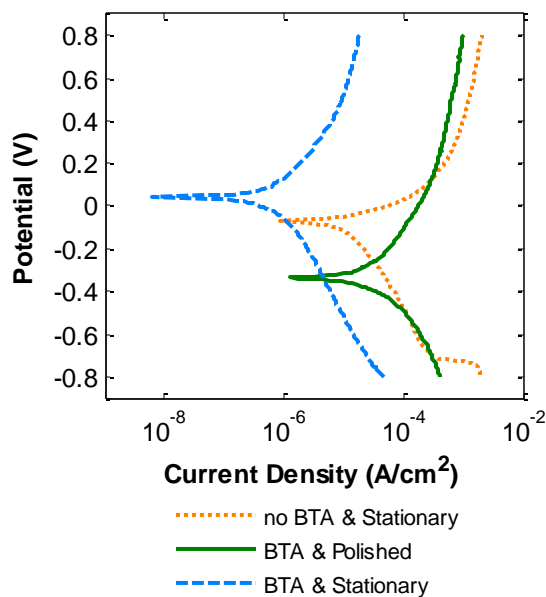
Figure 5.3 Potentiodynamic polarization scan of copper electrode in a pH 4 slurry containing 0.01 M glycine, 5 wt% alumina abrasives with or without 0.01 M BTA. Scanned from -0.8 V to 0.8 V with the rate at 5 mV/s. Polishing, when used, was done with a sliding velocity of 0.5 m/s and 3.6 psi of down pressure.

Figure 5.4 shows a typical chronoamperometry curve when the potential of copper was stepped up to an anodic potential, 0.6 V. The current density decreased rapidly before stabilizing at a quasi-steady state[2] after two seconds; thus the values for the first two seconds were excluded when evaluating the average current densities for each experimental condition. The initial decay of the current density (see the inset of Figure 5.4) was attributed to adsorption of BTA on the oxide-free surface of copper. Capacitive charging for the macroelectrode used to give Figure 5.4 was not considered because it was finished by 0.05 seconds in the absence of BTA (see filled circles in Figure 5.5) and the protective layer on the surface of copper would further reduce the time for the capacitive charging in the presence of BTA.[1] After the initial decay of the current, a quasi-steady state was reached where the current densities were nearly constant, implying that the overall fraction of sites occupied by BTA remained constant, although the exact location of the occupancy would change as the asperities swept the surface of the copper. The noise of the measured current densities was due to the rotation of the copper electrode; the frequency of the noise corresponded to that of rotation.
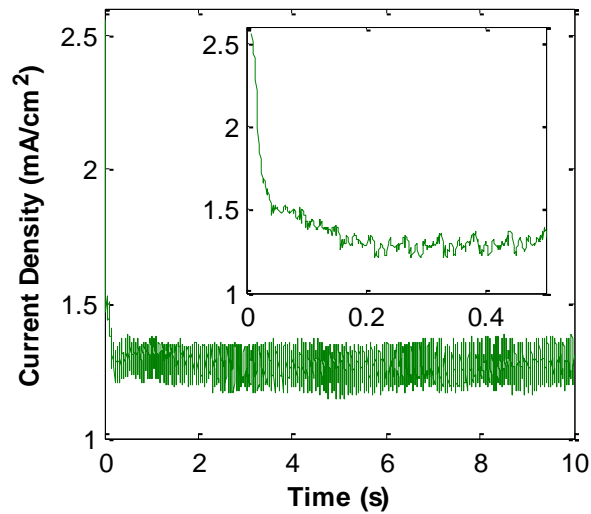
Figure 5.4 Chronoamperometry curve during polishing when the potential of copper was stepped up to 0.6 V. Inset shows the current density in the first 0.5 seconds. Sliding velocity and down pressure were 0.75 m/s and 3.6 psi, respectively.
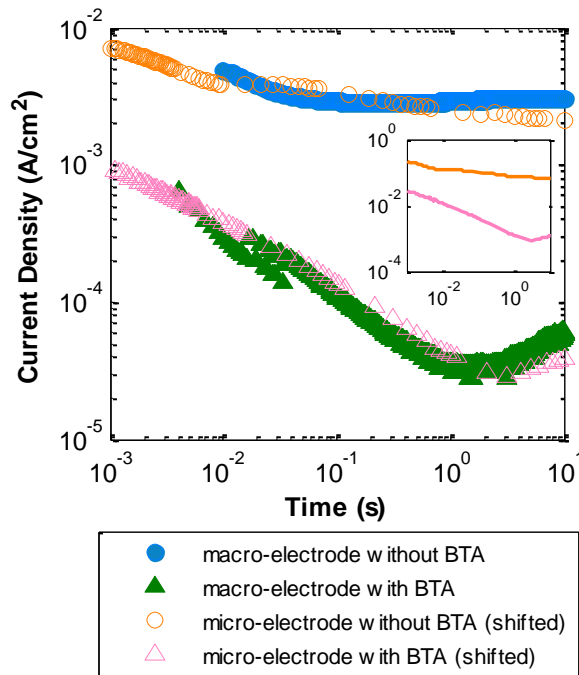
Figure 5.5 Comparison of the current decaying characteristics using a micro-electrode [from reference 1] and a macro-electrode. The current densities were measured after stepping up the potential to 0.6 V after polarizing at -1.2 V in a pH 4 electrolyte containing 0.01 M glycine with or without 0.01 M BTA for a micro-electrode and additional 5 wt% alumina abrasives for a macro-electrode. A macro-electrode was in contact with the polishing pad. Inset shows the original data for a micro-electrode before shifting.

59

Figure 5.6 shows the average steady-state current densities of copper during polishing (between two and ten seconds) with different down pressures or sliding velocities. It is clear that the current densities in the absence of BTA, where protective material was not expected to form, were insensitive to the down pressure and sliding velocity. In contrast, the current densities in the presence of BTA, where some surface sites on the copper were expected to be protected, increased with increasing down pressure and sliding velocity. This suggests that increasing pressure and velocity increased the amount of protective material removed from the surface of copper by the pad asperities and the abrasives embedded between the asperity and the copper, leaving more unprotected surface sites.
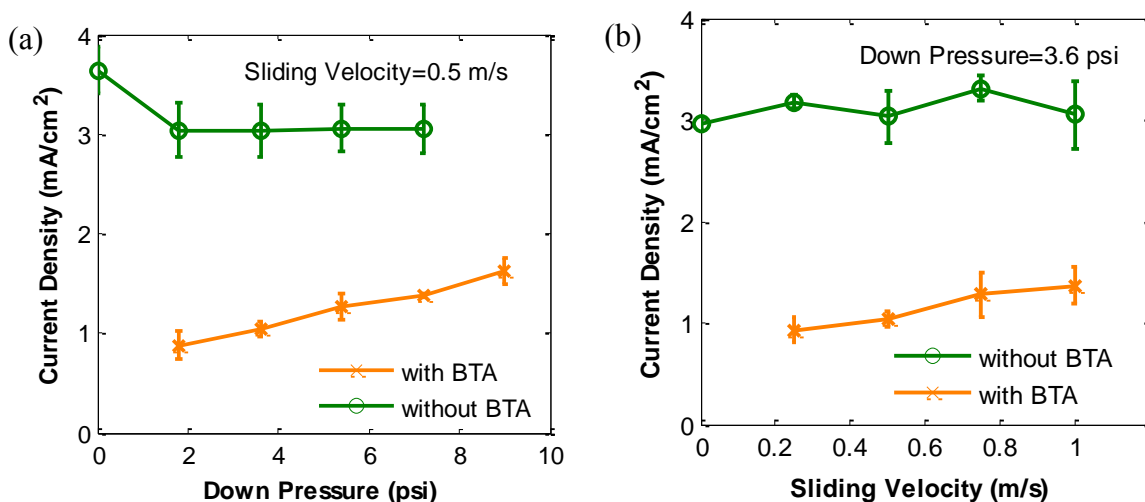
Figure 5.6 Average current density of copper during polishing when the potential was stepped up to 0.6 V for different down pressures (a) and for different sliding velocities (b). The slurry is at pH 4 and contains 0.01 M glycine and 5 wt% alumina abrasives with or without 0.01 M BTA. Error bars denote one standard deviation of the measurements.

Figure 5.5 compares the decrease in the current densities over time for micro- and macro-electrodes, both of which were stationary, in a pH 4 aqueous solution containing BTA and glycine. It also shows the nearly constant current densities when there was no BTA in the solution. 5 wt% of alumina abrasives were added to the solution only when macro-electrode was used. The macro-electrode was in contact with the perforated CMP pad without rotation during the measurements to allow comparison with the currents during polishing. It was of interest to compare the data obtained using a macro-electrode in the polishing slurry used in this work with the data obtained by Choi *et al.*[3] using a micro-electrode in the same aqueous solution, but with added alumina particles, because the adsorption kinetics of BTA for this case were known. The current densities for the micro-electrode at any given time were about 22.7 times larger than those for the macro-electrode (see inset of Figure 5.5). To aid the comparison the data for the micro-electrode were shifted by a factor of 22.7 in the main plot of Figure 5.5. It is clear that, with this correction, the relative magnitudes of the current densities in the absence and the presence of BTA were the same for the macro and microelectrodes.

This discrepancy between the micro and macro electrodes reflects better mass transport for the microelectrode, which is surrounded by a spherical region of electrolyte. Copper ions dissolving from the macro electrode are restricted to two dimensional transport, and the presence of the CMP pad between the macro-electrode and the counter electrode blocked and changed the electric field, further lowering the oxidation rates. Despite the discrepancy in the magnitude of the oxidation rates for the two different electrodes, the intrinsic mechanism for passivation would be unchanged. Therefore, the approach used by Choi *et al.*[3] of considering the fractional coverage of the copper by Cu(I)BTA complexes as a function of time was adopted to examine the material removal efficiencies from the measured current densities.

5.4 Discussion

5.4.1 Evaluation of the removal efficiencies from the experimental results

Recalling the concept of a quasi-steady state, it is reasonable to assume that the steady current seen during polishing corresponds to a state where the rate of removal of the protective material on copper is balanced by the rate of the formation of new protective material. The removal of the protective material by an asperity is nearly instantaneous, whereas the protective material, Cu(I)BTA, forms again comparatively gradually, until the next interaction with an asperity. The average duration of the contact between a given point on the copper and a pad asperity, t_{as}, was estimated assuming circular asperity and copper contacts:

$$t_{as} \leq \frac{d_{as}}{v}$$

(5.1)

where d_{as} is the average diameter of the circular contacts between the asperities and copper and v is the sliding velocity of the wafer over the pad. Equation (5.1) gives a maximum because the duration of the contact varies with the wear distances[1] across the circular contact, as shown in Figure 5.7.
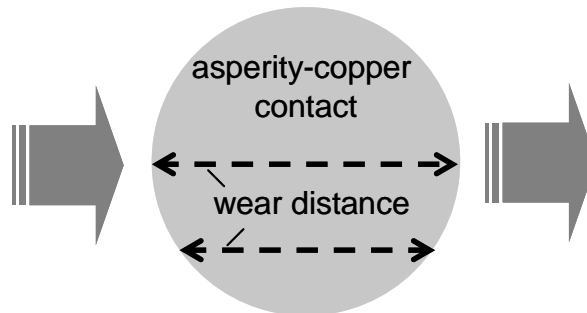
Figure 5.7 Wear distances of an asperity sliding over the surface of copper from left to right.

The growth of the protective material on the copper surface is dependent on the fraction of

occupied sites at the moment, characterized as θ_{t_0} in Figure 5.8, and the duration until the subsequent contact by another asperity, defined as $t_{as\text{-}as}$ in Figure 5.8.
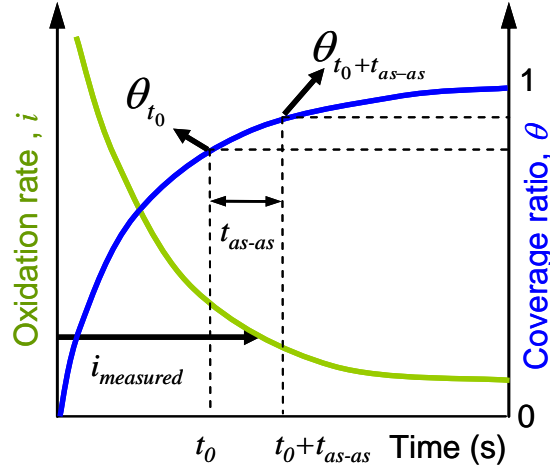
Figure 5.8 Evaluation of t_0 by knowing the average oxidation rate, $t_{as\text{-}as}$ and the curve of the coverage ratio.

The time for a point on the surface of copper that has just interacted with an asperity to interact with the next asperity, $t_{as\text{-}as}$, can be determined by equating it with the time required to completely sweep the surface of the copper wafer by the asperities:

$$N_{as}d_{as}vt_{as-as} = A_w \text{ or } t_{as-as} = \frac{A_w}{N_{as}d_{as}v} \tag{5.2}$$

where N_{as} is the number of asperities that contact the surface of a wafer, d_{as} is the average diameter of the circular contact areas between asperities and copper and A_w is the surface area of a wafer. Note that the influence of the sliding velocity on N_{as} and d_{as} is not considered. The number of asperities that contact the surface of a wafer (N_{as}) is calculated by the following expression:

$$N_{as} = \frac{r_{contact}A_w}{a_{as}} \tag{5.3}$$

where $r_{contact}$ is the ratio of real area of contact between a CMP pad and a wafer to the nominal contact area and a_{as} is the average contact area of an asperity contacting the copper. Thus, assuming a circular contact area between an asperity and a wafer the time interval between consecutive contacts by asperities at a point on the surface of copper is determined as:

$$t_{as-as} = \frac{\pi d_{as}}{4vr_{contact}} \tag{5.4}$$

where $r_{contact}$ is an increasing function of the down pressure[8,9] and d_{as} can either increase or stay constant with the down pressure. Both can be experimentally characterized using confocal reflectance interference contrast microscopy (C-RICM)[8] or dual emission laser induced fluorescence (DELIF)[10].

t_0 and t_{as-as} can be determined from a plot of the oxidation rate of copper as a function of time since a bare surface of copper is raised to an anodic potential, knowing the experimentally observed average oxidation rate of copper, as illustrated in Figure 5.8. Since the measured oxidation rate, $i_{measured}$, is the sum of the currents from the entire surface of the copper where some points have just been abraded by an asperity while others are waiting to be abraded, the exact location of t_0 can be determined using the following expression:

$$i_{measured} = \frac{\int_{t_0}^{t_0+t_{as-as}} i \, dt}{t_{as-as}} \tag{5.5}$$

When a spot on the surface is abraded by an asperity, the oxidation rate at that point will increase immediately because the fraction of sites occupied by protective materials, θ_{t_0} will decrease. As time elapses until the interaction with another asperity, the protective material progressively accumulates, finally giving a coverage ratio of $\theta_{t_0+t_{as-as}}$.

Using these coverage ratios at a given point on the surface immediately before and after abrasion, the removal efficiency, η, can be defined as:

$$\eta = 1 - \frac{\theta_{t_0}}{\theta_{t_0+t_{as-as}}} \tag{5.6}$$

This is the efficiency of an asperity and abrasives embedded between the asperity and copper in removing protective materials on the surface of copper.

t_0 was evaluated for different experimental conditions using the measured average current densities and the kinetics for adsorption of BTA onto the surface of copper (coverage ratio by Cu(I)BTA with time) reported by Choi et al.[3], shifted by a factor of 22.7 times lower, as previously discussed. Table 5.1 shows these data, along with the intervals between consecutive asperity-copper interactions, the corresponding coverage ratios and the removal efficiencies. When estimating t_{as-as}, the average area of the contact of an individual asperity with copper was assumed to be constant regardless of the applied pressure or the sliding velocity. However, the real contact area ratio was considered to increase with increasing down pressure, due to the increase in the number of asperities that contact the wafer.[11] Data for the average area of the individual asperity and copper contacts and the real contact area ratio, which was linearly proportional to the down pressure, were not measured for the conditioned CMP pad used in this work; instead, these data were adopted from experimental measurements made by Elmufdi et al. who used an IC1010[TM] pad conditioned with SPD-01 or CG-181060 conditioner.[8] It was assumed that t_{as-as} and a_{as} values for the pad used in this work are not very different from the values in the literature. The estimated intervals between

consecutive asperity interactions with a given point on the copper surface were of the same order as the periodicity of the protective material formation and removal on the surface of copper derived by DeNardis *et al.* from spectral analysis of the coefficient of friction[12].

Figure 5.9 further illustrates the changes in the removal efficiencies with the down pressure or the sliding velocity when $t_{as\text{-}as}$ and a_{as} values for SPD-01 or CG-181060 conditioners determined by Elmufdi *et al*. were used to evaluate the removal efficiencies from the measured current densities in Figure 5.6. Error bars indicate one standard deviation. No error bar is shown where a current density smaller than one standard deviation than the mean current density corresponds to a removal efficiency of unity. The CG-181060 and SPD-01 conditioners yielded asperity-copper contact areas of 22 μm^2 and 11 μm^2, respectively, with the real area of contact being 0.100% and 0.135% of the total for a 3.6 psi down pressure. The removal efficiencies evaluated using those parameters were insenstive to the down pressure or the sliding velocity considering the large error bars. The removal efficiency was very sensitive to the precision of the measured current density especially when $t_{as\text{-}as}$ was large, due to the very rapid adsorption of BTA onto copper in a very short time after the copper was anodically polarized (the curve for the coverage ratio by Cu(I)BTA with time appears to be almost a step function[3]; this curve is schematically shown as a blue line in Figure 5.8). When $t_{as\text{-}as}$ is large the positions of t_0 and $t_0 + t_{as\text{-}as}$ are distant, leading to a large difference in the coverage ratios by the protective material at those moments. Any slight increase in the measured current density, oxidation rate curve shown as a green line in Figure 5.8, would shift the location of t_0 towards smaller values, leading to a huge difference in the coverae ratios at t_0 and $t_0 + t_{as\text{-}as}$ and thus an increase in the coverage ratio for a given $t_{as\text{-}as}$.
Since $t_{as\text{-}as}$ and a_{as} are highly dependent on the choice of the conditioner and the duration of the conditioning, the actual removal efficiencies shown in Table 5.1 and Figure 5.9 may not be representative of the experimental conditions used in this work. However, this analysis indicates that the removal efficiencies are insensitive to the down pressures or the sliding velocities regardless of the use of different $t_{as\text{-}as}$ and a_{as} values (Figure 5.9).

Table 5.1 Removal efficiency and BTA coverage ratio on the surface of copper during CMP under different experimental conditions. The real contact area ratio and the average area of individual asperity and copper contacts were taken from reference 8, using data obtained using an SPD-01 conditioner.

Condition	Down Pressure (psi)	Sliding Velocity (m/s)	$t_{as\text{-}as}$ (ms)	t_0 (ms)	θ_{t_0}	$\theta_{t_0+t_{as}}$	η
1	1.8	0.5	8.71	0.530	0.505	0.841	0.400
2	3.6	0.25	8.71	0.298	0.426	0.839	0.492
3	3.6	0.5	4.35	0.820	0.566	0.790	0.284
4	3.6	0.75	2.90	0.532	0.505	0.748	0.325
5	3.6	1	2.18	0.566	0.514	0.723	0.289
6	5.4	0.5	2.90	0.575	0.516	0.749	0.311
7	7.2	0.5	2.18	0.545	0.509	0.722	0.295
8	9	0.5	1.74	0.340	0.443	0.689	0.357

64
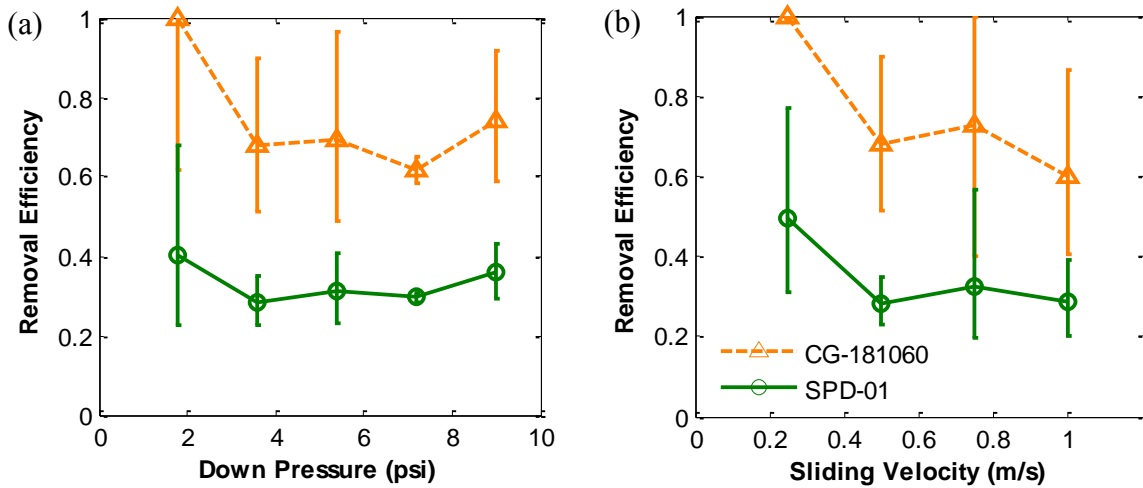
Figure 5.9 Removal efficiency under various down pressures at 0.5 m/s of sliding velocity (a) and sliding velocities under 3.6 psi of down pressure (b). Error bars correspond to the standard deviation of the experimental data in Figure 5.6.

5.4.2 Analytical evaluation of the removal efficiency

The removal efficiency was evaluated analytically to assess whether the removal efficiencies evaluated from experimental data were reasonable. The response of the protective material on the surface of copper, Cu(I)BTA, to the sliding motion of abrasive particles embedded between an asperity and the copper was considered. It was assumed that the embedded abrasive particles remove all the adsorbed Cu(I)BTA in their paths as they slide over the surface. Removal of the protective material by asperities in direct contact with the copper was neglected because prior studies on polishing rates in the absence of abrasives indicate that pad asperities alone are ineffective in removing the protective material.[13] Thus, one can estimate the fraction of the Cu(I)BTA on the surface that was removed by interaction with a pad asperity where abrasives are embedded by comparing the areas swept by the asperity and by the embedded abrasives during the interaction:

$$\eta = \frac{w_{abs}}{w_{as}} \tag{5.7}$$

where w_{abs} is the cumulative width of sliding trajectories on the copper of all abrasive particles trapped under an asperity and w_{as} is the width of the sliding trajectory of an asperity. It was assumed that all the embedded abrasives and the asperity slide in the same direction by the same distance. It is necessary to account for overlapping paths because once protective material has been removed by an abrasive particle, there is no time for any more protective material to form before the next abrasive particle embedded in the same asperity interacts at that site on the copper. The total width of the resultant sliding trajectories of the embedded abrasives under an asperity was calculated by summing the expected widths of the sliding trajectories of the individual abrasives:

65

$$w_{abs} = (w_{ab})_1 + (w_{ab})_2 + (w_{ab})_3 + ... + (w_{ab})_{n_{ab}}$$

$$= (w_{ab})_1 \left[1 + (1 - \frac{(w_{ab})_1}{w_{as}}) + (1 - \frac{(w_{ab})_1 + (w_{ab})_2}{w_{as}}) + ... + (1 - \frac{(w_{ab})_1 + (w_{ab})_2 + ... + (w_{ab})_{n_{ab}-1}}{w_{as}}) \right] \quad (5.8)$$

where $(w_{ab})_i$ is the expected width of a sliding trajectory of i-th abrasive. The expected width of the sliding trajectory of the second abrasive is reduced by the probability which it overlaps the trajectory of the first abrasive. Figure 5.10 shows that the second abrasive can leave a trajectory only when it slides area not overlapping with the trajectory by the first abrasive, giving a probability that the second abrasive removes the protective material to $1 - \frac{(w_{ab})_1}{w_{as}}$.

The same argument is applied to the remaining abrasives to determine the cumulative width of the sliding trajectories of all embedded abrasives.
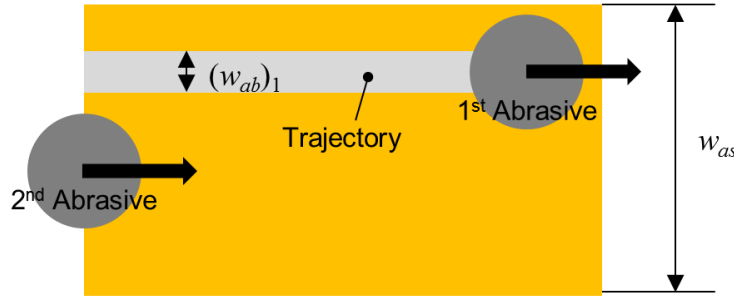
Figure 5.10 Trajectories by embedded abrasives during an interaction of a pad asperity with the surface of copper.

It is assumed that the removed protective material does not redeposit on the surface of the copper, if did, this would lower the removal efficiency. Any change in the ability of an abrasive particle to remove protective material due to protective material already accumulated on its surface was neglected. The embedded abrasives were also not considered to be rolling. If rolling were considered, it might reduce the evaluated removal efficiency, because of the shorter moving distance than during sliding as illustrated in Figure 5.11. Any interaction between the down pressure and the tangential frictional force between the abrasives and copper was neglected; thus the pressure distribution in the copper transmitted by the abrasive particle, and the shape of the contact area, were obtained from the Hertz contact theory, assuming elastic deformation of copper.[14] The same assumption could be made if the embedded abrasives rolled on the surface of copper. The width of the sliding trajectory of the first abrasive particle was estimated using Hertz contact theory[14] as follow:

$$(w_{ab})_1 = 2\sqrt{r_{ab}h_e} \quad (5.9)$$

where h_e is the penetration depth of an abrasive particle into elastically deformed copper, which is also determined using Hertz contact theory:

$$h_e = \left(\frac{3 f_{ab}}{4 E^* r_{ab}^{1/2}} \right)^{2/3} \tag{5.10}$$

where f_{ab} is the force transmitted by an abrasive to a wafer, $E^* = \left(\frac{1-v_1^2}{E_1} + \frac{1-v_2^2}{E_2} \right)^{-1}$, E and

v are the elastic modulus and Poisson's ratio, respectively, and subscripts 1 and 2 denote the contacting materials; in this case copper and the abrasive, respectively. It was assumed that the presence of protective material on the surface of copper does not affect the indentation depth or the area of contact between the abrasive and copper because it is very soft and thin.
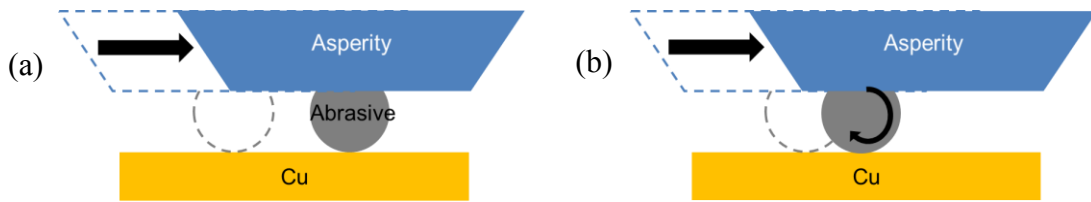
Figure 5.11 Sliding (a) and rolling (b) of an abrasive embedded on a pad asperity on the surface of copper. Shapes with dotted lines show the original position before the movement.

If the copper is plastically deformed by the force applied on an embedded abrasive, the width of the contact and indentation depth are:

$$(w_{ab})_1 = 2\sqrt{2 r_{ab} h_p} \tag{5.11}$$

where the indentation depth of plastically deformed copper, h_p, is given by:

$$h_p = \frac{f_{ab}}{\pi r_{ab} H_{Cu}} \tag{5.12}$$

where H_{Cu} is the hardness of copper. Note that in this case, only the leading edge of the area contacted by the abrasive particle supports the load applied by the abrasive while the abrasive ploughs on the surface of the copper.

To calculate the indentation depth by the embedded abrasives, the force applied on the abrasive f_{ab} was estimated, starting from calculating of the force applied on a pad asperity.

5.4.2.1 *Force applied on a pad asperity*

The observation in the section 5.4.1 that the removal efficiencies were insensitive to the down pressure and sliding velocity could be explained if the average area of an asperity-copper contact is independent of those parameters. This is an appropriate approximation to assume because the number of asperities contacting a wafer during copper CMP is a small

portion of the total number of asperities and thus the Gaussian distribution of the asperity heights[15] can be approximated to the exponential distribution, which results in the number of contacts being proportional to the applied load.[11] The exponential distribution of pad asperities contacting the wafer was experimentally observed by Sun *et al.*[16] Using this assumption and the experimental observation that the real overall contact area was linearly proportional to the down pressure,[8,9] the average area of each asperity-copper contact should be independent of applied pressure, and hence the force transmitted through an asperity (f_{as}) should be constant for a given pad with given conditioning specifications:

$$f_{as} = \frac{P a_{as}}{r_{contact}}$$

(5.13)

where P is the nominal down pressure applied on a wafer. Using the values used in this work, the average force per asperity was 0.2 mN or 0.5 mN when conditioning by an SPD-01 conditioner or CG-181060, respectively.

5.4.2.2 *Number of abrasive particles embedded between an asperity and copper*

Alumina abrasives may agglomerate when the pH of a slurry, the concentration of copper ions or additives in a slurry lower the zeta potential sufficiently to eliminate the electrostatic repulsion between particles.[17,18] Ihnfeldt *et al.*[5] estimated the force required to break up the agglomerate using the equations developed by Brown *et al.* to calculate the shear strength of a powder.[19] Using their analysis, the lower and upper bounds of the force required to break up an agglomerate 20 nm in diameter were only 70 pN and 0.9 – 4 nN (discussed below). These forces are nearly three orders of magnitude lower than the force transmitted to an embedded abrasive, suggesting that any agglomerates are broken up when squeezed between an asperity and copper. Therefore, it was assumed in the following analysis that only individual abrasive particles are present in the squeezed areas.

Slurry containing abrasive particles wets the CMP pad and is squeezed between the pad and the wafer as the wafer is contacted with the pad to begin the CMP process. Neglecting any forces that could influence the spatial distribution of abrasives around the pad asperities such as electrostatic and van der Waals forces between the abrasives and asperities, the local concentration of abrasive particles in the slurry squeezed between the pad and the copper is assumed to be identical to that in the bulk slurry, c_{wt}, which is expressed as a ratio of the weight of abrasives to the total weight of the slurry. Further, assuming that the abrasive particles are rigid spheres with uniform radius, r_{ab}, the number of abrasive particles that are embedded between an asperity and the copper, $\tilde{n}_{ab}$, is determined as:

$$\tilde{n}_{ab} = \frac{3 c_{wt} a_{as} \rho_{slurry}}{2 \pi r_{ab}^{2} \rho_{ab}}$$

(5.14)

where ρ_{slurry} and ρ_{ab} are the density of slurry and abrasives, respectively. It was assumed that the number of embedded abrasives is in steady state in which abrasives in the slurry are

continuously drawn into and discharged from the gap between the asperities and the copper as the wafer slides over the pad. The assumptions employed in this analysis are similar to those in the work of Che *et al.*[20], Zhao *et al.*[21] and Bastawros *et al.*[22]. The estimated number of abrasives embedded on an asperity is listed in Table 5.2 for various concentrations of the abrasives in the slurry.

5.4.2.3 *Force applied on an abrasive*

The force applied on an abrasive particle that is embedded between an asperity and copper was estimated by investigating the upper and lower bounds of the situation where pad asperities are deformed by the embedded abrasive particles as shown in Figure 5.12. Note that pad asperities will be deformed by the applied force in preference over the abrasives and copper because the pad material has a much lower elastic modulus and hardness than copper and abrasives. The upper bound of the estimated force is obtained when the pad asperity is not deflected enough to contact the surface of the copper (Figure 5.12 (a)). Thus the force applied to the asperity is supported only by the embedded abrasives. The upper bound of the estimated force on an abrasive, $f_{ab\text{-}ub}$, is then:

$$f_{ab-ub} = f_{as} / \tilde{n}_{ab} \qquad (5.15)$$

The lower bound of the estimated force, $f_{ab\text{-}lb}$, would occur when a pad asperity is deformed enough to encapsulate the abrasive particles and to contact the surface of the copper completely; so the force applied to the asperity is evenly distributed across all abrasive particles and the deformed asperity contacting the copper (Figure 5.12 (c)). Then the force on an individual abrasive particle is independent of the number of embedded abrasives, and dependent only on the cross-sectional area of the particle:

$$f_{ab-lb} = \pi r_{ab}^{2} (f_{as} / a_{as}) \qquad (5.16)$$

If the pad asperities are deflected enough to contact the surface of the copper only partly, as shown in Figure 5.12 (b), the force applied on an abrasive will be intermediate between those two extremes, and will be inversely proportional to the area of the contact between the deflected asperity and the copper. Thus the force applied on an embedded abrasive, in general, can be written as:

$$f_{ab} = f_{as} \left(\frac{\pi w_{ab}^{2}}{\pi w_{ab}^{2} \tilde{n}_{ab} + 4a_{as-def}} \right) \qquad (5.17)$$

where $a_{as\text{-}def}$ is the contact area between copper and the asperity that is deformed by the embedded abrasives.
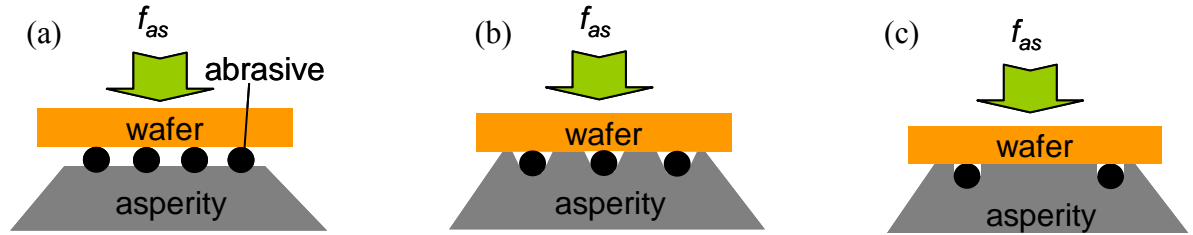
Figure 5.12 Contact between a pad asperity and a copper wafer in the presence of abrasive particles in the slurry: (a) An asperity is not deformed much, and does not itself contact the wafer (b) An asperity is deformed to partly contact the surface of a wafer and (c) An asperity is deformed enough to encapsulate the abrasives and to contact the wafer.

The estimated upper and lower bounds on the force applied to an abrasive for the varied concentrations of abrasives is tabulated in Table 5.2. The parameters for an SPD-01 conditioner were used. The upper bound of the estimated force transmitted to each embedded abrasive particles decreases with increasing concentration of the abrasives, from 3.06 µN for 0.5 wt% of abrasives to 0.304 µN for 5 wt% of abrasives. In contrast, the lower bound of the estimated force applied to an abrasive is 5.78 nN, regardless of the concentrations of the abrasives.

Table 5.2 Number of abrasive particles embedded between an asperity and the wafer, force on an embedded abrasive particle, shear stress and penetration depth induced by the applied force for different concentrations of abrasives. The down pressure, the sliding velocity and the diameter of abrasives were 3.6 psi, 0.5 m/s and 20 nm, respectively. $a_{ab} = \pi r_{ab}^2$

c_{wt} (wt%)	$\tilde{n}_{ab}$	f_{ab} (upper) (µN)	f_{ab} (lower) (nN)	τ_{max} (upper) (GPa)	τ_{max} (lower) (GPa)	h_e (upper) (nm)	h_e (lower) (nm)	$a_{ab} \tilde{n}_{ab}/a_{as}$ (%)
0.5	66	3.06	5.78	12.3	1.51	3.6	0.06	0.188
1	133	1.52	5.78	9.71	1.51	2.2	0.06	0.380
3	399	0.507	5.78	6.73	1.51	1.1	0.06	1.14
5	665	0.304	5.78	5.68	1.51	0.77	0.06	1.90

5.4.2.4 *Prediction of the removal efficiency*

Applying this analysis to predict the removal efficiencies using equation (5.7) and (5.8) for the experimental conditions 1 to 8, removal efficiencies of 0.208 and 0.582 were obtained for the lower and upper bounds of the estimated forces, respectively when conditioning the pad with an SPD-01 conditioner, assuming that the copper underwent elastic deformation only. If copper was considered to undergo plastic deformation, a removal efficiency of 0.678 was predicted for the upper bound of the estimated force. For a pad conditioned with a CG-181060 conditioner, the predicted removal efficiencies were 0.280 and 0.709 at the lower and upper bounds of the estimated forces, respectively when the copper was elastically deformed. If plastic deformation of the copper was considered, the predicted removal efficiency was 0.844 for the upper bound of the estimated force. Note that all the experimental conditions 1

to 8, other than conditions 1 and 2 for the CG-181060 conditioner, yielded the same removal efficiencies for each conditioning specification because the average area of the asperities and copper contacts was assumed to be invariable. Referring back to the evaluated removal efficiencies shown in Table 5.1, these can be seen to be intermediate between the upper and lower bounds calculated here, which provides some confirmation of the validity of the analysis.

To further examine the validity of the analysis, chronoamperometry measurements were made during polishing with various concentrations of abrasives in the slurry, with other conditions unchanged. Four different concentrations were used, namely 0.5, 0.1, 3 and 5 wt% of alumina abrasives in the slurry. The experimental data, analyzed by equation (5.7) and (5.8), for either an SPD-01 or CG-181060 conditioner, yielded the removal efficiencies shown in Figure 5.13. The analytical prediction using equation (5.8) yielded the removal efficiencies shown as continuous curves in Figure 5.13. The upper bound of the estimated force on an abrasive gave two different curves, one for the condition where the copper underwent plastic deformation, and the other for the condition where copper only deformed elastically. However, the lower bound of the estimated force gave only a single curve for elastic deformation of copper, because the indentation depth resulting from the force was only a fraction of the diameter of a copper atom, 0.6 Å, which is too small to initiate dislocations in the crystal lattice, and hence plastic deformation. This is discussed further below.

The widths of the sliding trajectories for plastic deformation of the copper were calculated using nanohardness values obtained from molecular dynamic (MD) simulations of nanoindentation. Mechanical properties obtained at larger scales, which have been used to model the material removal during CMP, have limited relevance to copper CMP because the mechanical properties of materials are known to exhibit a significant size effect as the volume decreases. For hardnesses measured by nanoindentation, the hardness of the materials increases as the indenter tip radius or the indentation depth decreases.[23,24,25,26,27] The hardness of copper at the nano-scale, determined through molecular dynamic (MD) simulations of nanoindentation of copper by Ziegenhain *et al.*[28] and Saraev *et al.*[29], was about 15 GPa, which is nearly one order of magnitude larger than the hardness measured by nanoindentation with higher loads on the order of Newtons, with deeper depths of tens of to hundreds of nanometers[30,31,32,33,34]. Although the MD simulations considered a defect-free crystal, the surface of the copper that is in contact with a single abrasive particle can also be assumed nearly defect-free because of the small area of the contacts. The penetration depths caused by the force applied on an abrasive particle, used to determine the widths of the trajectories for different concentrations of abrasives in the slurry, are listed in Table 5.2. The upper bound estimate of the force on an abrasive gave a penetration depth of the order of 1 nm for both elastic and plastic deformation, which is of the same order as the roughness after copper CMP.[35,36]
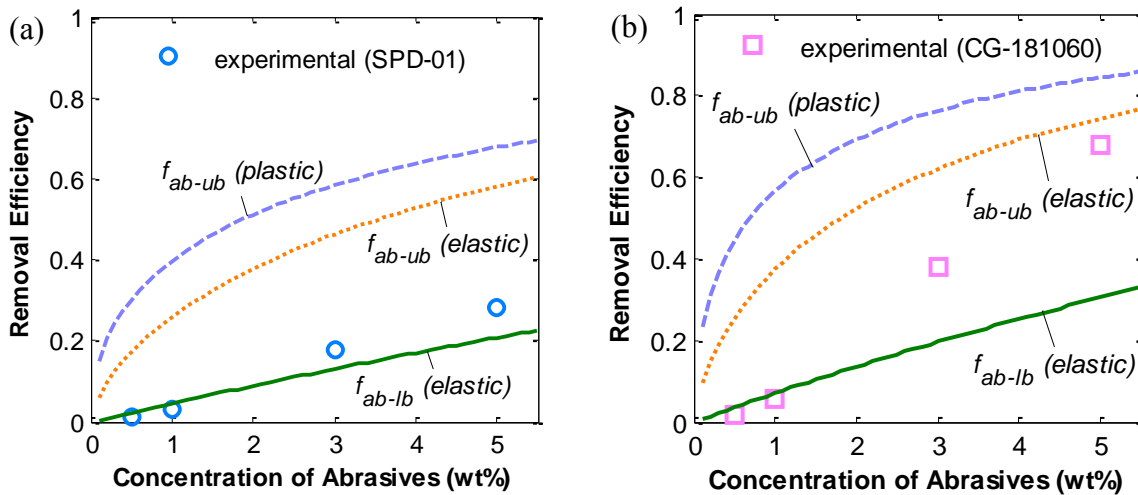
Figure 5.13 Removal efficiencies evaluated from analysis using equation (5.8) and obtained from experimental data assuming either a (a) SPD-01 conditioner or (b) CG-181060 conditioner.

For lower concentrations of the abrasives, the experimentally evaluated removal efficiencies approximated the analytically predicted removal efficiencies for the lower bound of the estimated force when copper was elastically deformed, regardless of the assumed conditioning specifications. This implies that the pad asperities supported by the abrasives were deformed enough to contact the copper, such that the force applied to the embedded abrasive particles approached the lower bound of the estimate. In contrast, for higher abrasive concentrations the experimentally evaluated removal efficiencies were intermediate between the lower and upper bound predictions for elastically deformation. This suggests that the pad asperities supported by the embedded abrasives were deflected to partly contact the surface of the copper. As the concentration of the abrasive particles increases, the portion of the asperity ($a_{as\text{-}def}$) contacting the wafer decreases, so that a higher force is borne by the abrasives. This was evidenced by the experimentally evaluated removal efficiency being higher than the lower bound predicted values for 3 and 5 wt% abrasives, particularly for 5 wt%. These trends would be expected, as the distance between the embedded abrasive particles decreases with increasing concentration of the abrasives. However, the separation remains much larger than the size of the abrasives, because as shown in Table 5.2, only 1.90 % of the total contact area between an asperity and the copper is occupied by embedded abrasives when 5 wt% abrasives is used. Thus the pad asperities will be deflected enough to contact the copper, although the contact area by the deflected portion would decrease with increasing abrasive concentration. These inferences that deflected asperities completely or partly contact the copper are consistent with the work of DeNardis et al.[12] and Li et al.[37] who deduced a contact mode during copper CMP from the slopes of experimentally obtained Stribeck curves. The contact mode during copper CMP using slurry containing abrasive particles and oxidizing agent was "partial lubrication" where abrasive particles and slurry separate the pad asperities and the copper in part or "boundary lubrication" where the asperities, abrasives and copper are in direct contact. Both the analysis in this work and the work of DeNardis et al.[12] and Li et al.[37] suggested that copper CMP does not operate in hydrodynamic lubrication mode.

72

However, it is challenging to predict the amount of the deformation of the pad asperities supported by the embedded abrasives precisely. This is because mechanical properties such as hardness, elastic modulus and Poisson's ratio measured for a porous pad in the bulk[38,39] are not representative of the local properties during an interaction. The pad asperities themselves are solid material, whereas the elastic modulus of the bulk, porous material is lower, following the expression:[40,41]

$$E_0 = E_p (1 - P_{pad}^{2/3})^{-s}$$ (5.18)

where E_0 and E_p are the elastic moduli of the asperities and porous CMP pad, respectively, P_{pad} is the porosity of the pad and

$$s = 1.21 \left(\frac{\tilde{z}}{\tilde{x}} \right)^{1/3} \sqrt{1 + \left\{ \left(\frac{\tilde{z}}{\tilde{x}} \right)^{-2} - 1 \right\} \cos^2 \phi}$$ (5.19)

where $\tilde{z}/\tilde{x}$ is the shape factor of the spheroidal pores (unity for spherical pores), and ϕ is the angle between the rotational axis of the spheroids and the stress direction. $\cos^2 \phi$ for isotropic materials is 1/3. Using the porosity of IC1000 pads, 0.56,[42,43] and the elastic modulus of a porous IC1000[TM] pad at 25°C measured by Lu et al.[38], 380 MPa, the local elastic modulus of the asperities was estimated to be 1.5 GPa, nearly four times larger than the bulk modulus. The estimated local elastic modulus is similar to the value used by Che et al.[20]. In addition, the elastic modulus of the pad is strain rate dependent. The pad asperities in contact with the embedded abrasives are much stiffer during CMP than during typical measurements of the elastic modulus because the strain rate is more than five orders of magnitude higher than that used in typical measurements. Moreover, Hertz contact theory and other models such as the Johnson-Kendall-Roberts (JKR) theory[44] cannot give a realistic prediction of the deformation of the asperities, which would be expected to be of the order of the size of the abrasives, because these models were constructed for small deformations of the contacting materials. Therefore, the exact deformation of the asperities was not sought.

5.4.3 Material behavior of copper at nano-scale

To confirm that the copper was elastically deformed by interaction with the embedded abrasives, as Figure 5.13 implies, the mechanical response of copper at the nano-scale was investigated. The maximum shear stress induced in the copper (v_{Cu}=0.33 and E_{Cu}=132 GPa)[45] by an abrasive particle (v_{ab}=0.16 and E_{ab}=380 GPa)[45] indenting the surface was calculated from the following expression derived from Hertz contact theory and the Tresca yield criterion:[14]

$$\tau_{max} = 0.30 p_0$$ (5.20)

where p_0 is the maximum Hertz pressure, given by:

$$p_0 = \left(\frac{6 f_{ab} E^{*2}}{\pi^3 r_{ab}{}^2} \right)^{1/3} \tag{5.21}$$

The maximum shear stress is observed below the contact surface. The determined maximum shear stress in the copper, τ_{max}, for the upper bound of the estimated force ranged from 5.68 GPa to 12.3 GPa, depending on the concentrations of the abrasives, whilst the lower bound of the estimate gave a constant maximum shear stress of 1.51 GPa. Note that the shear stresses in Table 5.2 were evaluated assuming indentation of copper by embedded abrasive particles, which is equivalent to frictionless sliding or rolling in terms of the induced shear stress. If friction between the abrasives and copper during the sliding or rolling of the particles is considered, the shear stress for incipient plasticity of the copper will be lowered, due to the additional tangential force component, and will decrease as the coefficient of friction increases. The maximum Hertz pressure that induces the first yield of copper decreases to approximately 1.5 times of the shear strength of copper for a coefficient of friction of 0.6 compared to 3.3 times for frictionless sliding.[14] In addition, the first yield occurs at the contact surface when the coefficient of friction exceeds 0.3 whilst subsurface yield is observed for smaller coefficients of friction. The maximum Hertz pressure does not deviate much from that for frictionless sliding when the coefficient of friction is smaller than 0.3.[14] If rolling of the abrasive particles with tangential traction is assumed, the required maximum Hertz pressure will be intermediate between the values for frictionless sliding and sliding with friction.[14]

The addition of abrasive particles into an abrasive free electrolyte increases the overall coefficient of friction between the pad and the copper during copper CMP[46,47]; thus it is appropriate to assume the presence of friction between the surfaces, although their magnitude cannot be resolved at present. Some information about the coefficient of friction can be found in the literature. Molecular dynamic simulation of the scratching of the surface of copper by a cutting tool gave estimated coefficients of friction between the tool and copper. When the (001) plane of copper was scratched or machined at 18 m/s with a tool that has -45° rake angle, MD simulation predicted a coefficient of friction of 0.64.[48] When the (001) plane of copper was scratched at 1 m/s with a hemispherical diamond tool of 2.3nm radius with MD simulation, the coefficient of friction was 0.57.[49] Note that the scratching was deep enough compared to the size of the tool that the copper was plastically deformed in the simulations. Deep scratching (~100 nm) of electroplated copper with a diamond Berkovich nano-indenter of 100 nm radius at 333nm/s resulted in a coefficient of friction of approximately 0.5.[50] Those values, ranging from 0.5 to 0.64, were obtained based on dry contact of a tool or tip with copper. However, the coefficient of friction during copper CMP may be different because fluid may be present between the surfaces of the abrasives and copper, and protective materials may be present on the surfaces. Moreover, the small indentation depth and the very low negative rake angle presented by spherical abrasive particles would further reduce the friction coefficient during the interaction. Nevertheless, a coefficient of friction of 0.6 gives a very conservative estimation of the maximum shear stress required to initiate plasticity in the copper during CMP. Then, the maximum Hertz contact stress would have to be at least 1.5 times the shear strength of copper to initiate plastic deformation of copper, as described in equation (5.22). At the nano-scale the maximum shear stress in the copper at the

onset of plasticity is approximately the same as the theoretical shear strength of copper (τ_{th}).[28,29,51,52] Therefore, the maximum Hertz contact pressure to plastically deform the copper can be written as:

$$p_0 \geq 1.5\tau_{th} \qquad (5.22)$$

Substituting equation (5.20) into equation (5.22) gives a lower limit for the maximum shear stress induced in copper required to induce plasticity in the presence of strong frictional forces:

$$\tau_{max} \geq 0.45\tau_{th} \qquad (5.23)$$

The theoretical shear strength of copper can be approximated as

$$\tau_{th} = \frac{G}{2\sqrt{2}\pi} \qquad (5.24)$$

where G is the shear modulus for the preferred glide system.[53] The theoretical shear strength of copper calculated using *ab initio* density functional theory (DFT) by Ogata *et al.*[54] and Krenn *et al.*[55] was 2.16 GPa for relaxed shear and 3.42 GPa for unrelaxed shear, and 2.65 GPa for relaxed shear and 4.0 GPa for unrelaxed shear, respectively. The theoretical shear strength obtained from MD simulations of nanoindentation by Zhu *et al.*[56] and by Ziegenhain *et al.*[28] were 4.56 GPa and 3.46 GPa – 5.90 GPa, respectively. The discrepancy between the values obtained by DFT calculations and nanoindentation simulations was attributed to the triaxial stress at the critical site under the indenter where dislocations nucleate.[56,57] As briefly mentioned above, the maximum shear stress in the copper during load controlling nanoindentation at the onset of the plasticity was approximately the same as the theoretical shear strength of the material,[28,29,51,52] suggesting that plastic deformation is due to homogeneous nucleation of dislocations in the subsurface below the indented area. Nanoindentation into copper, either by experiments or simulations has been widely employed to study the onset of plasticity. Suresh *et al.*[51] performed nanoindentation into polycrystalline copper with an average grain size of 500 nm, where most of the surface had (111) texture, using a diamond Berkovich indenter with a tip radius of 50 nm. They observed displacement bursts at certain discrete loads as the indenting load was increased. The first burst is generally accepted to be the onset of plasticity.[45] The maximum shear stress in the copper at the first displacement burst, calculated using Hertz theory, was 10.7 GPa, which is similar to the ideal shear strength of copper. Chen *et al.*[52] conducted similar nanoindentation tests on a coarse grained copper with a 60 μm grain size using a diamond indenter with a tip radius of 50 nm; the calculated maximum shear stress in the copper at the onset of the plasticity was 8.5 GPa. Ziegenhain *et al.*[28] performed molecular dynamic (MD) simulations of the nanoindentation test using an indenter with an 8 nm tip radius, and found that the maximum shear stress in the copper at the yield point was 7.8 GPa – 11.2 GPa for the (100) plane and 10.3 GPa – 13.1 GPa for the (111) plane. MD simulations of nanoindentation with a 3 nm radius tip indenter by Saraev *et al.*[29] predicted a maximum shear stress of 8.5 GPa underneath the indenter at the onset of plasticity for (001) surfaces of single crystal copper. Note that all the maximum

shear stresses at the onset of plasticity were larger than the theoretical shear strengths obtained by DFT calculations. This is due to the use of the Hertz contact theory to evaluate the maximum shear stress underneath the indenter. This approximates a linear relationship between the strain and stress. However, at the strain at the onset of the plasticity during indentation the relationship is nonlinear; thus the Hertz theory overestimated the maximum shear stresses.[57] Nevertheless, the maximum shear stresses obtained by the indentation experiments were adopted to compare with the shear stresses in Table 5.2 since the shear stresses in the table were also obtained using the Hertz theory. Also note that the shear strength values obtained through the nanoindentation experiments on a polycrystalline copper sample were comparable to simulations for single crystal copper. This was due to the area contacted by the indenter being very small compared to the grain size of the copper, and far away from the grain boundaries that can be sources for the heterogeneous nucleation of dislocations. Thus it is reasonable to use the shear strengths obtained from the nanoindentation tests or simulations to predict the mechanical response of copper by interaction with abrasive particles embedded in pad asperities during CMP.

Applying 8.5 GPa as the theoretical shear strength of copper for nano-scale interactions, equation (5.23) predicts that copper would be plastically deformed if the maximum shear stress in the copper exceeds 3.8 GPa. The lower bounds of the estimated forces in Table 5.2 were below this level, while the upper bounds of the estimated forces exceeded it. Recalling that the pad asperities were fully deflected by the embedded abrasives to contact the copper (Figure 5.12a) for lower concentrations of the abrasives, the lower bound of the estimated force was applied by the abrasives. Since the shear stress induced by this lower bound of the force was lower than the threshold for the copper to be plastically deformed the copper was elastically deformed during the process. For higher concentrations of the abrasives, the deflected asperities would only partially contact the copper. Thus the maximum shear stress in the copper induced by the embedded abrasives would be intermediate between the upper and lower bounds, which can be either higher or lower than the threshold value. Noticing that both the width of the sliding trajectory (and thus approximately the analytically predicted removal efficiency, especially when the concentrations of the abrasives are low) and the induced maximum shear stress are proportional to the power of 1/3 of the applied force on an abrasive, they can be approximated to be linearly proportional each other, provided that the elastic modulus and the radius of the abrasive are invariant. Therefore, the maximum shear stress in the copper can be interpolated for a given concentration of the abrasives using the corresponding experimentally evaluated removal efficiency and the predicted removal efficiencies for the upper and lower bounds of the estimated forces. When parameters for an SPD-01 conditioner were used, the maximum shear stresses in the copper during the process were approximately 2.2 GPa and 2.4 GPa for 3 wt% and 5 wt% of the abrasives, respectively, indicating that the deformation of the copper was elastic. For the parameters for a CG-181060 conditioner, the maximum shear stresses were 3.7 GPa and 5.0 GPa for 3 wt% and 5 wt% of the abrasives, respectively, suggesting that the copper might be plastically deformed for 5 wt % of the abrasives. In fact, the experimentally determined removal efficiency for this condition in Figure 5.13b was close to the curve predicted by assuming plastic deformation of copper, although it was still a little lower than that predicted by assuming elastic deformation of the material for the upper bound of the estimated force. Moreover, the 5.0 GPa maximum shear stress may still be lower than the threshold stress for plasticity if the

coefficient of friction between the abrasives and copper is lower than the assumed value, 0.6.

In summary, the copper appears to be elastically deformed by the force exerted through the embedded abrasives for most of the abrasive concentrations used in this study, with plastic deformation only possible when high concentrations of the abrasives were used, agreeing well with the results shown in Figure 5.13.

5.5 Conclusion

The removal efficiencies for abrasive particles that are embedded on a pad asperity removing protective material from the surface of copper during CMP were experimentally determined and were compared with analytically predicted values. The predicted removal efficiencies agreed well with the experimentally evaluated efficiencies. Also, the removal efficiencies were found to be insensitive to the down pressure and sliding velocity during the CMP process. Comparison of the analytically resolved removal efficiencies for various concentrations of the abrasives in the slurry with the experimentally evaluated values suggested that the pad asperities encapsulated the embedded abrasive particles and themselves contacted the surface of the copper at low abrasive concentrations, while at higher abrasive concentrations the asperities were only partially deflected. Most of the load was borne by the abrasive particles, and less by asperities that were only partially contacted the copper. The maximum shear stresses calculated assuming these different asperity-copper contact modes implied that the copper was elastically deformed for most of the abrasive concentrations used in this study, although some plastic deformation may have occurred at the highest abrasive concentrations. In conclusion, an increase in the concentration of abrasives in the slurry not only gradually increases the efficiency of removal of the protective film on the copper surface, but also increases the possibility of the copper being plastically deformed by the embedded abrasives, both of which contribute to increased material removal rates during copper CMP.

References

[1] S. Tripathi, Ph.D. Thesis, University of California, Berkeley, Berkeley, CA (2008).

[2] S. Tripathi, S. Choi, F. M. Doyle and D. A. Dornfeld, *Mater. Res. Soc. Symp. Proc.*, **1157,** E02-03 (2009).

[3] S. Choi, S. Tripathi, D. A. Dornfeld, F. M. Doyle, *J. Electrochem. Soc.*, **157**, H1153-9 (2010).

[4] S. Choi, F. M. Doyle and D. Dornfeld, *Procedia Eng.*, **19**, 73 (2011).

[5] R. Ihnfeldt and J. B. Talbot, *J. Electrochem. Soc.*, **154**, H1018 (2007).

[6] J. Luo and D. A. Dornfeld, *IEEE Trans. Semicond. Manuf.*, **16**, 45 (2003).

[7] M. Bastaninejad and G. Ahmadi, *J. Electrochem. Soc.*, **152**, G720 (2005).

[8] C. L. Elmufdi, and G. P. Muldowney, *Mater. Res. Soc. Symp. Proc.*, **991**, 0991-C01-02 (2007).

[9] T. Sun, Y. Zhuang, L. Borucki and A. Philipossian, *Jpn. J. Appl. Phys.*, **49**, 066501-1

(2010).

[10] C. Gray, C. Rogers, V. P. Manno, R. White, M. Moinpour and S. Anjur, *Mater. Res. Soc. Symp. Proc.*, **991**, 0991-C01-04 (2007).

[11] J. A. Greenwood and J. B. P. Williamson, *Proc. R. Soc. Lond. A*, **295**, 300 (1966).

[12] D. DeNardis, J. Sorooshian, M. Habiro, C. Rogers, and A. Philipossian, *Jpn. J. Appl. Phys.*, **42**, 6809 (2003).

[13] S. Aksu and F. M. Doyle, *J. Electrochem. Soc.*, **149**, G352 (2002).

[14] K. L. Johnson, *Contact Mechanics*, p. 90-95, p. 208, Cambridge University Press, Cambridge, UK (1985).

[15] T.Yu, C.Yu, M. Orlowski, Proceedings of the 1993 International Electron Devices Meetings, IEEE, Washington DC, December, p.35 (1993).

[16] T. Sun, L. Borucki, Y. Zhuang and A. Philipossian, *Microelectron. Eng.*, **87**, 553 (2010).

[17] R. Ihnfeldt and J. B. Talbot, *J. Electrochem. Soc.*, **153**, G948 (2006).

[18] R. Ihnfeldt and J. B. Talbot, *ECS Trans.*, **3**, 21 (2007).

[19] R. L. Brown and J. C. Richards, *Principles of Powder Mechanics*, Pergamon, Elmsford, NY (1970).

[20] W. Che, Y. Guo, A. Chandra and A. Bastawros, *J. Manuf. Sci. Eng.*, **127**, 545 (2005).

[21] Y. Zhao, L. Chang, *Wear*, **252**, 220 (2002).

[22] A. Bastawros, A. Chandra, Y. Guo and B. Yan, *J. Electron. Mater.*, **31**, 1022 (2002).

[23] J. G. Swadener, E. P. George and G. M. Pharr, *J. Mech. Phys. Solids*, **50**, 681 (2002).

[24] S. Qu, Y. Huang, W. D. Nix, H. Jiang, F. Zhang and K. C. Hwang, *J. Mater. Res.*, **19**, 3423 (2004).

[25] W. D. Nix and H. Gao, *J. Mech. Phys. Solids*, **46**, 411 (1998).

[26] Y. Huang, F. Zhang, K. C. Hwang, W. D. Nix, G. M. Pharr and G. Feng, *J. Mech. Phys. Solids*, **54**, 1668 (2006).

[27] G. Feng, A. S. Budiman, W. D. Nix, N. Tamura and J. R. Patel, *J. Appl. Phys.*, **104**, 043501 (2008).

[28] G. Ziegenhain, A. Hartmaier and H. M. Urbassek, *J. Mech. Phys. Solids*, **57**, 1514 (2009).

[29] D. Saraev and R. E. Miller, *Modell. Simul. Mater. Sci. Eng.*, **13**, 1089 (2005).

[30] S. Chang, T. Chang and Y. Lee, *J. Electrochem. Soc.*, **152**, C657 (2005).

[31] D. Beegan, S. Chowdhury and M. T. Laugier, *Surf. Coat. Technol.*, **201**, 5804 (2007).

[32] Y. M. Soifer, A. Verdyan, M. Kazakevich and E. Rabkin, *Scr. Mater.*, **47**, 799 (2002).

[33] R. Ihnfeldt and J. B. Talbot, J. Electrochem. Soc., **155(6)**, *H412* (2008).

[34] C. Liao, D. Guo, S. Wen and J. Luo, Tribol. Lett., **45**, *309* (2011).

[35] N. Chandrasekaran, S. Ramarajan, W. Lee, G. M. Sabde and S. Meikle, *J. Electrochem. Soc.*, **151**, G882 (2004).

[36] M. T. Wang, M. S. Tsai, C. Liu, W. T. Tseng, T. C. Chang, L. J. Chen and M. C. Chen, *Thin Solid Films*, **308**, 518 (1997).

[37] Z. Li, K. Ina, P. Lefevre, I. Koshiyama and A. Philipossian, *J. Electrochem. Soc.*, **152**, G299 (2005).

[38] H. Lu, Y. Obeng and K. A. Richardson, *Mater. Charact.*, **49**, 177 (2003).

[39] L. Borucki, *J. Eng. Math.*, **43**, 105 (2002).

[40] P. Mazilu and G. Ondracek, in Thermal Effects in *Fracture of Multiphase Materials, Proc. Euromech Colloquium 255, October 31-November 2, 1989, Paderborn, FRG*, K. P. Herrmann and Z. S. Olesiak, Editors, p. 214, Springer-Verlag, Berlin (1990).

78

[41] A. R. Boccaccini, G. Ondracek, P. Mazilu and D. Windelberg, *J. Mech. Behav. Mater.*, **4**, 119 (1993).

[42] H. Gao and J. X. Su, *Adv. Mat. Res.*, **102-104**, 724 (2010).

[43] M. J. Kulp and T. T. Crkvenac, U.S. Patent 2010/0035529 (2010).

[44] K. L. Johnson, K. Kendall and A. D. Roberts, *Proc. R. Soc. London*, **A 324**, 301 (1971).

[45] A. Gouldstone, H.-J. Koh, K.-Y. Zeng, A. E. Giannakopoulos and S. Suresh, *Acta Mater.*, **48**, 2277 (2000).

[46] D. Ng, M. Kulkarni, J. Johnson, A. Zinovev, D. Yang and H. Liang, *Wear*, **263**, 1477 (2007).

[47] H. Liang, J.-M. Martin and R. Lee, *J. Electron. Mater.*, **30**, 391 (2001).

[48] Y. Y. Ye, R. Biswas, J. R. Morris, A. Bastawros and A. Chandra, *Nanotechnol.*, **14**, 390 (2003).

[49] J. Zhang, T. Sun, Y. Yan and Y. Liang, *Mater. Sci. Eng., A*, **505**, 65 (2009).

[50] S. Islam and R. N. Ibrahim, *Tribol. Lett.*, **42**, 275 (2011).

[51] S. Suresh, T.-G. Nieh and B. W. Choi, *Scr. Mater.*, **41**, 951 (1999).

[52] J. Chen, W. Wang, L. H. Qian and K. Lu, *Scr. Mater.*, **49**, 645 (2003).

[53] A. Kelly, N. H. Macmillan, *Strong Solids, third ed.*, Clarendon Press, Oxford (1986).

[54] S. Ogata, J. Li and S. Yip, *Science*, **298**, 807 (2002).

[55] C. R. Krenn, D. Roundy, J. W. Morris Jr. and M. L. Cohen, *Mater. Sci. Eng.*, **A317**, 44 (2001).

[56] T. Zhu, J. Li, K. J. Van Vliet, S. Ogata, S. Yip and S. Suresh, *J. Mech. Phys. Solids*, **52**, 691 (2004).

[57] C. R. Krenn, D. Roundy, M. L. Cohen, D. C. Chrzan and J. W. Morris Jr., *Phys. Rev. B*, **65**, 134111 (2002).

Chapter 6
Material Removal Mechanism During Copper CMP Based on Nano-Scale Material Behavior

6.1 Introduction

Earlier modeling studies for copper CMP have relied on models developed for oxide CMP.[1,2,3,4,5,6] Material was considered to be removed by abrasion by abrasive particles that are trapped between a wafer and pad asperities while sliding on the surface being polished. The chemical additives in the slurry were considered to function by reacting with the surface of a wafer, to soften the material[2,3,6,7,8], or by dissolving physically dislodged material[4]. However, much earlier, Kaufmann *et al*. proposed a synergistic model for metal CMP that attributes material removal during CMP of metals to the cyclic removal of the passivation layer on the surface of a metal through mechanical abrasion with the abrasives and the pad asperities, and subsequent active oxidative dissolution of the metal from the resulting exposed regions, until the passivation layer has regenerated.[9] This model assumed that the passivation layer was thick enough that the abrasive particles did not indent the unoxidized metal beneath the passivation layer. Tripathi, Doyle and Dornfeld proposed a quantitative model similar to Kaufmann's model by postulating a quasi-steady state where the overall rate of removal of passivation material and the overall rate of growth of passivation material are balanced, giving an overall constant removal rate during copper CMP.[10] In this model the abrasives and asperities served only to remove the passivation material from the surface, thereby exposing copper to undergo oxidative dissolution by the slurry. Choi, Doyle and Dornfeld suggested that at steady state the passivation film formed on copper during CMP using an acidic slurry containing BTA and glycine (Cu(I)BTA and Cu(II)BTA$_2$) is only a fraction of a monolayer, partly protecting the surface of a wafer from dissolution.[11] Removal of the passivation layer is only a small portion of the the electrochemically measured material removal rate; most of the electrochemically measured material removal rate is due to active dissolution of copper. Both Tripathi *et al*. and Choi *et al*. considered the material removal during copper CMP to be mostly due to the electrochemical oxidation of the copper while the protective material is repetitively removed by the abrasives, and copper is dissolved from exposed regions (although they recognized the role of the mechanical interactions between abrasives and copper in removing the passivated material). However, measurable amount of copper are removed even when the slurry contains no chemical additives other than deionized water and abrasive particles, implying that copper can be removed directly from the surface through mechanical interactions with the abrasive particles, even when there only oxidizing agent in the slurry is dissolved oxygen.[12,13,14] Quantitative approaches to modelling the material

removal behavior during copper CMP have not been successful to date because the relative contributions of each mechanism have not been unambiguously determined. In this study, the relative contribution of each mechanism is determined by comparing material removal rate (MRR) and corrosion rate during copper CMP. A model is proposed to elucidate the mechanism for removing copper by mechanical abrasion based on the material properties of copper at the nano-scale.

6.2 Experimental Procedure

6.2.1 In situ Electrochemical Measurement

The electrochemical material removal (corrosion rate) of copper was evaluated by measuring the current density at a copper electrode while polishing using the apparatus shown in Figure 6.1. A three electrode electrochemical cell, housed in a glass beaker, was assembled on the table bed of a high precision machine tool (Matsuura MC-510VSS), which rotated the working electrode at high speed with high precision. The working electrode was a copper tube (99.99 % purity from McMaster-Carr) with a 1 mm difference between the outer and inner diameters, so as to minimize the variation of sliding velocities relative to the CMP pad across the annulus. The copper tube was embedded in insulating epoxy, exposing an annulus at the bottom of the electrode, with a cross sectional area of 0.46 cm^2. A saturated calomel reference electrode (SCE) was placed in a Luggin capillary 5 mm from the copper electrode. The counter electrode was platinum mesh. The slurry contained 2 wt% alumina particles (primary diameter 20nm, median aggregate diameter 150nm), 0.01 M glycine, 0.01 M BTA, 0.1 mM $Cu(NO_3)_2$ and 0.5 wt% H_2O_2 in deionized (DI) water at pH 4. Only during the potentiodynamic scans a slurry containing 4 wt% alumina particles, 0.01 M glycine, 0.01 M BTA, 0.1 mM $Cu(NO_3)_2$ and 1wt% H_2O_2 in DI water at pH 4 was used. A piece of IC10101 pad was fixed horizontally on the bottom of the beaker. The pressure applied to the copper surface was measured with a load cell (TUF-010-025-S from Loadstar Sensors) placed under the beaker. Before each run the electrode was polished using the apparatus, to maintain a consistent surface roughness. It was then washed with DI water and any remaining oxides on the copper surface were reduced by holding at -1.2 V (SCE) for 60 seconds while polishing the working electrode. Potentiodynamic polarization was conducted by scanning the potential from -0.8 V (vs. SCE) to 0.8 V (or 1.0 V) at a rate of 5mV/s, to estimate the corrosion rate of copper during CMP. The corrosion rate was evaluated from the measured potentiodynamic curves using the linear polarization resistance technique[16] and Faraday's law.

6.2.2 Copper CMP

A 4 inch blanket copper wafer underwent CMP using a POLI-500 CMP machine (GNP Technology). The blanket copper wafer has a 1000 nm thick layer of copper electrochemically deposited on a thin Ta and Cu seed layer. The CMP pad (IC1010) pad was broken-in initially, and then conditioned for 30 seconds using a diamond condidtioner (supplied from GNP Technology) between each run. During conditioning deionized water was passed at 300 ml/min; the slurry (composition as above) was supplied at 100 ml/min during CMP of copper. The applied pressure and sliding velocity of a wafer over the CMP pad were varied from 2 psi to 6 psi, and 0.5 m/s to 1.25 m/s, respectively. CMP was

performed for three minutes for each test, and the material removal rate (MRR) was evaluated by measuring the sheet resistance of the remaining copper at 21 points.

CMP of the copper blanket wafer was also performed using a slurry containing only 4 wt% of alumina abrasives and 0.3 mM sodium oleate in DI water. The surfactant sodium oleate was added to prevent excessive frictional force between the wafer and the pad during the process.[15] It did not affect the measured material removal rates. The pH of the slurry was not controlled; the natural pH of the alumina suspension was about pH 4. The sliding velocity was 0.75 m/s and the applied down pressure 4 psi. The wafer was weighted before and after two minute CMP five times using an electronic balance (Sartorius A200S) to evaluate the material removal rate. The MRR was evaluated by averaging the MRRs from three runs of CMP.
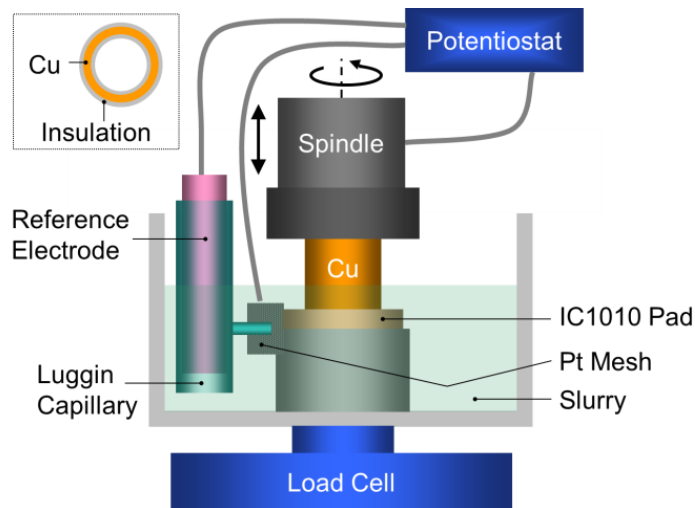
Figure 6.1 Apparatus used for *in situ* electrochemical measurement during polishing of copper.

6.3 Results

Figure 6.2 shows the influence of polishing on the electrochemical behavior of copper. Abrasion had little impact on the cathodic current, but significantly increased the oxidation rate at anodic potentials, resulting in both a lower corrosion potential and a corrosion rate (evaluated using the linear polarization resistance technique[16]) that was about an order of magnitude higher than that observed under static conditions. This demonstrates the efficacy of BTA as a corrosion inhibitor. It also shows that abrasion by the abrasives removed the protective material on the copper surface, thereby allowing more rapid oxidation at the exposed surfaces.
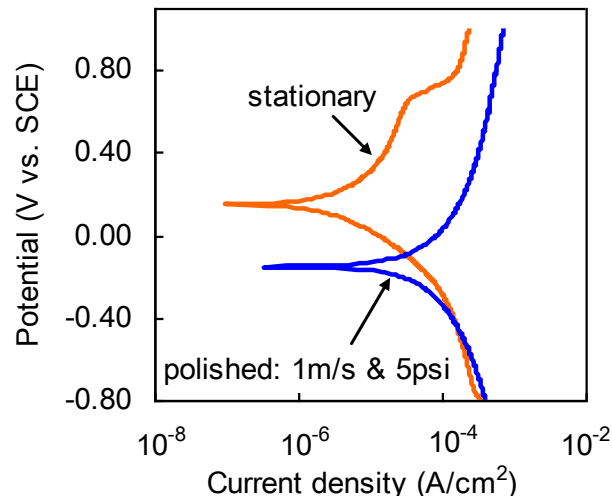
Figure 6.2 Influence of polishing on the polarization behavior of copper in a slurry containing 4 wt% alumina particles, 0.01 M BTA, 0,01 M glycine, 0.1 mM Cu(NO$_3$)$_2$, and 1 wt% H$_2$O$_2$ at pH4 with the scan rate at 5mV/s.

Figure 6.3 compares the MRR measured from CMP experiments and the corrosion rates evaluated from potentiodynamic curves during polishing. The electrochemically measured corrosion rates are the sum of the rate of removal of the protective material and the overall dissolution rate at the surface (because copper must be oxidized before it interacts with BTA to form protective material). The corrosion rates was less than 1 % of the total MRR measured in CMP experiments for all conditions shown in Fig. 6.3. Similar results were observed by Jindal *et al.* comparing the polish rate and dissolution rate of copper using a slurry containing hydrogen peroxide, glycine and abrasives.[17] This implies that during CMP almost all of the copper is removed by direct mechanical action, rather than by electrochemical dissolution. It is possible that the evaluated corrosion rate underestimates the total oxidation rate of copper if hydrogen peroxide acts via a Fenton-type mechanism that yields hydroxyl radicals, which are strong oxidizers. The MRR measured from the CMP experiments using a slurry containing only alumina abrasives and sodium oleate was 9 nm/min, which is lower than the MRR for the slurry containing H$_2$O$_2$, glycine, BTA and Cu(NO$_3$)$_2$ but not insignificant compared to the corrosion rate. Other researchers observed similar or higher MRR when copper was polished with DI water containing only abrasive particles.[12,13,14] Given that some MRR is observed when copper is polished with DI water containing only abrasives, it is apparent that most of the total MRR during copper CMP must be due to the mechanical removal of copper.

Removal of the material by the CMP pad material itself was not considered because CMP without abrasive particles showed negligible MRR.[13] The linear increase in total MRR with applied pressure and sliding velocity seen in Figure 6.3 contrasts with the near constant corrosion rate of about 0.2 nm/min, providing further support for mechanical removal of some of the copper; down pressure and sliding velocity would be expected to affect the indentation depth of abrasives into the surface of copper, the number of abrasives contacting the copper at a given asperity, and the sliding velocity of the abrasives. It should be noted that the chemical additives used in the slurry enhanced the overall MRR, as observed from

the significant difference in the MRRs obtained using the slurry containing chemicals, 23 nm/min, and that using the slurry with only abrasives and a small amount of surfactant, 9 nm/min with a sliding velocity of 0.75 m/s and 3.6 psi of pressure. The probable mechanism for this increase in the MRR is discussed in detail below.
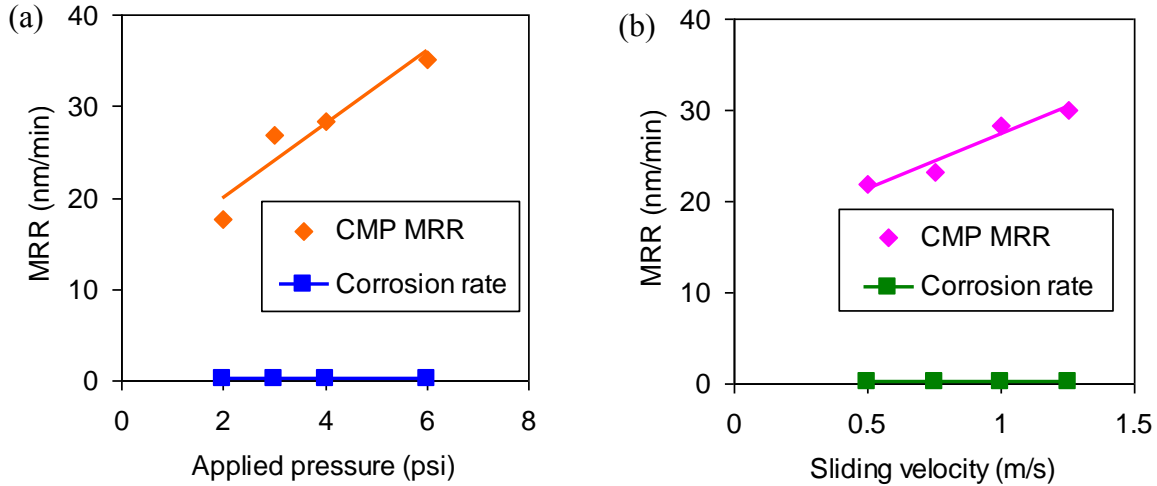
Figure 6.3 Influence of (a) applied pressure and (b) sliding velocity on the material removal rate (MRR) during CMP and the corrosion rate measured by potentiodynamic testing during polishing. The sliding velocity was maintained at 1m/s for (a) and the pressure was 4 psi for (b) for both CMP and potentiodynamic testing. pH 4 slurry containing 0.01M BTA, 0.01M glycine, 0.1 mM Cu(NO₃)₂, 2wt% alumina and 0.5 wt% H₂O₂ was used.

6.4 Discussion

6.4.1 Model for material removal by abrasion

Applying the material removal mechanism for oxide CMP, some researchers have considered that material is removed mechanically from the surface of a wafer during copper CMP by abrasive particles trapped between the wafer and pad asperities. The abrasive particles are considered to slide on the surface while plastically deforming the surface, piling up dislodged material along the trajectory of the sliding abrasives to form shallow trenches. This dislodged material is then removed by chemical additives in the slurry[4] or by another abrasion[2]. Some researchers have also argued that material is cut from the surface by sliding abrasive particles, with detached material becoming debris[1]. Regardless of whether the dislodged material becomes debris or piles up on the surface, plastic deformation of copper has generally been assumed. Although there are some variations in the representation of the number of abrasive particles that are involved in the ploughing or abrasion of the wafer, n_{ab}^{*}, estimation of the forces exerted by the abrasives, f_{ab}, calculation of the depth of the trenches, h_w, and the portion of the deformed wafer that contributes to the material removal rate K_{re}, the material removal rate predicted by this mechanism is generally be expressed as:

$$MRR = K_{re} \frac{n_{ab}^* A_i v}{A_w} \tag{6.1}$$

where A_i is the cross sectional area of the trench generated on the wafer by the indentation of the sliding abrasive, v is the sliding velocity of the wafer over the pad and A_w is the area of the wafer surface. The equation gives the MRR as a unit of thickness reduction per unit processing time. The cross sectional area of a trench generated on the wafer surface by a sliding abrasive can be expressed as:

$$A_i \propto h_w w_{ab} \propto \frac{f_{ab}^{3/2}}{r_{ab} H_w^{3/2}} \tag{6.2}$$

where r_{ab} is the average radius of the abrasive particles, H_w is the hardness of a wafer, h_w the depth of the indentation, $h_w = \frac{f_{ab}}{\pi r_{ab} H_w}$, and w_{ab} is the width of the trench $w_{ab} = 2\sqrt{2 r_{ab} h_w}$.

Then equations (6.1) and (6.2) give that the MRR during CMP is:

$$MRR \propto K_{re} \frac{n_{ab}^* f_{ab}^{3/2} v}{r_{ab} H_w^{3/2} A_w} \tag{6.3}$$

Note that n_{ab}^* depends on the concentration and the size of the abrasive particles in the slurry, the ionic strength of the slurry, the zeta potential of the abrasive particles (which determines the degree of agglomeration), the zeta potential of the wafer surface and pad asperities, and the interval between consecutive interactions of a given site on the copper surface with pad asperities, which in turn depends on the surface topography of the pad, down pressure and the sliding velocity. f_{ab} depends on n_{ab}^*, the amount to which trapped abrasive particles deflect the pad asperities, the surface topography of the pad and the down pressure. The hardness of the wafer, H_w, depends on the processing and consumable parameters, as discussed below.

This model has not been successful when applied to copper CMP, yielding MRR values that are two or three orders of magnitude higher than those experimentally observed when the bulk hardness of copper was used. Numerous hypotheses have been proposed to address this discrepancy. Luo and Dornfeld adopted the concept of "active abrasives", particles that are large enough to be squeezed between the pad asperities and the wafer to reduce the number of abrasives participating in the material removal.[18] Other researchers[1,3,19,20] used similar criteria to filter out the size of the abrasive particles participating in the material removal. It has also been argued that only a portion of the material dislodged by the sliding abrasives is actually removed. Xie et al.[1] suggested that only a portion becomes loose debris that contributes to material removal. On the basis of experimental observations of material removal by micro-scale scratches, Che et al. asserted that the material dislodged by a scratching event is removed only when it is involved in another scratching event.[2] Hardness values measured by nano- or micro-indentation, which are a few orders of magnitude higher than hardnesses measured at the macro-scale, have also been adopted to estimate the

deformation of copper.[13,21,22,23] However, it is well known that indentation hardnesses show a size effect, with larger indenter size or indentation depth yielding lower apparent indentation hardnesses.[24,25,26,27,28,29,30] As the size of the indented volume decreases the probability of crystallographic defects being present under the indenter decreases, leading to enhanced resistance to plastic deformation. The indentation experiments that measured the surface hardness during copper CMP were conducted with indentation loads ranging from hundreds of micro-Newtons to milli-Newtons, and indentation depths of the order of tens or hundreds of nanometers. These indentation depths are one or two orders of magnitude larger than the values when abrasive particles interact with a wafer (Figure 6.4)[31]. Therefore the material properties at more relevant length scale are required to understand the deformation of copper induced by interaction with abrasive particles.
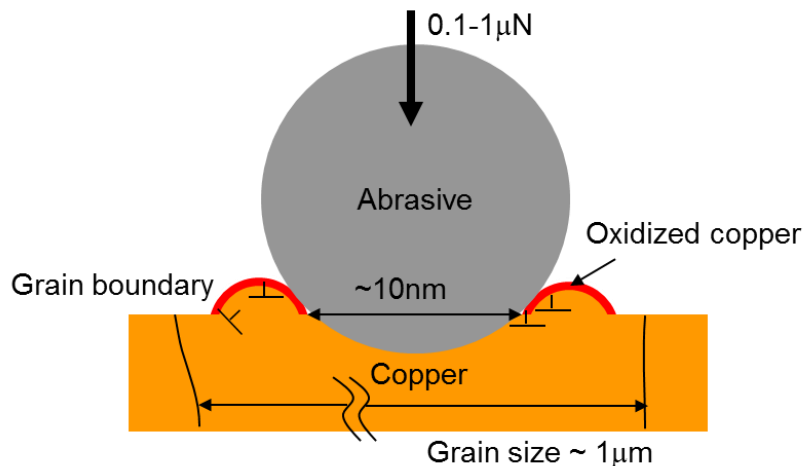
Figure 6.4 Length scales during the interaction between an abrasive particle and the copper during CMP.

6.4.2 Material properties of copper at the nano-scale

Hardness at more relevant length scales can be obtained from atomistic simulations of nanoindentation where the indentation depth is of the order of nanometers and the load is of the order of tens or hundreds of nano-Newtons. The maximum shear stress in the copper during load controlled nanoindentation at the onset of the plasticity was approximated as the theoretical shear strength of the material,[32,33,34,35] suggesting that plastic deformation is due to homogeneous nucleation of dislocations at the subsurface of the indented area. Nanoindentation into copper has been studied extensively, both experimentally and in simulations, to examine the onset of plasticity. Suresh *et al.*[34] performed nanoindentation into polycrystalline copper with average grain size of 500 nm and most of the surface with a (111) texture, using a diamond Berkovich indenter with a tip radius of 50 nm. They observed displacement bursts at certain discrete loads as the indenting load was increased. The first burst is generally considered to be the onset of the plasticity.[36] The maximum shear stress in the copper at the first displacement burst was 10.7 GPa, which is similar to the ideal shear strength of copper. The maximum shear stress induced in the material was calculated using Hertz theory. Note that polycrystalline copper started deforming plastically at about the same load as the single crystalline material. This is attributed to the grain boundaries of the copper

used in the experiments being far from the region undergoing indentation, because the copper grains are much, much larger than the volume undergoing nanoindentation, as shown in Figure 6.4. Chen *et al.*[35] conducted similar nanoindentation tests on coarse grained copper with 60 μm grains using a diamond indenter with a 50 nm tip radius; the calculated maximum shear stress in the copper at the onset of the plasticity was 8.5 GPa. Ziegenhain *et al.*[32] performed molecular dynamic (MD) simulations of nanoindentation using an indenter with 8 nm of a tip radius, and found that the maximum shear stress in the copper at the yield point was 7.8 GPa – 11.2 GPa for the (100) plane and 10.3 GPa – 13.1 GPa for the (111) plane. MD simulations of nanoindentation with a 3 nm radius tip indenter by Saraev *et al.*[33] identified a 8.5 GPa maximum shear stress underneath the indenter at the onset of plasticity for the (001) surface of single crystalline copper. Thus the maximum shear stress in the copper at the onset of the plasticity can be considered to be at least 7.8 GPa.

The theoretical shear strength of copper can be approximated as

$$\tau_{th} = \frac{G}{2\sqrt{2}\pi} \qquad\qquad (6.4)$$

where G is the shear modulus for the preferred glide system.[37] The theoretical shear strength of copper calculated using ab initio density functional theory (DFT) by Ogata *et al.*[38] was 2.16 GPa for relaxed shear and 3.42 GPa for unrelaxed shear, while Krenn *et al.*[39] calculated strengths of 2.65 GPa for relaxed shear and 4.0 GPa for unrelaxed shear. The theoretical shear strengths obtained from MD simulations of nanoindentation by Zhu *et al.*[40] and by Ziegenhain *et al.*[32] were 4.56 GPa and 3.46 GPa – 5.90 GPa, respectively. The discrepancy between the strengths predicted by DFT calculations and nanoindentation simulations was attributed to the triaxial stress at the critical site under the indenter where dislocations nucleate.[38,41] Also note that all the maximum shear stresses at the onset of plasticity during nanoindentation experiments or simulations were larger than the theoretical shear strengths predicted by DFT calculations. This is due to the use of the Hertz contact theory to evaluate the maximum shear stress underneath the indenter. This approximates a linear relationship between the strain and stress. However, at the strain corresponding to the onset of plasticity during indentation, the relationship is nonlinear; thus the Hertz theory overestimated the maximum shear stresses.[39] Nevertheless, the use of the maximum shear stress at the onset of plasticity during nanoindentation experiments for comparison is justified because the estimated maximum shear stress is also obtained using the Hertz contact theory.

6.4.3 Material behavior of copper during CMP at nano-scale
The maximum shear stress induced in the copper by indentation by abrasives during CMP was estimated to be of the order of a few GPa[31,42], which is similar to the ideal shear strength of copper. Since the ideal shear strength is only the threshold shear stress to initiate plasticity of a material, higher loads, as high as the ideal strength, would be required for plastic flow. This implies that the load exerted by the trapped abrasive particles during CMP may not be enough to plastically deform the copper. However, there are notable differences between the conditions for nanoindentation simulations or experiments and the condition of copper during CMP. Some regions of a copper film on a wafer during CMP may have a high dislocation

density resulted from the previous deposition and etching processes. Those regions of high dislocation density may undergo plastic deformation by the abrasive particles sliding on the surface of the wafer, leaving a high dislocation density in the copper. MD simulation of the nano-scale machining of copper showed that dislocations left in the copper after machining were not relieved[43] and the plastic zone was large[44] at slow cutting velocities where the temperature rise was small, which is the situation during copper CMP. MD simulation of repetitive scratching events on copper predicted an increased number of defects in the crystal compared to non-scratched regions.[45] In addition, the copper may contain voids, vacancies, impurities and grain boundaries created during the deposition processes.

6.4.3.1 *Influence of crystallographic defects*

The crystallographic defects lower the shear strength of copper because they facilitate activation of the dislocation source[25,46,47] or function as heterogeneous nucleation sites for dislocations[47]. MD simulations predicted that vacancies in otherwise perfect Fe crystals[48] and Ni cyrstals[26,49] reduced the stress required for the onset of plasticity. Dislocations did not nucleate at the vacancies but interacted with them during subsequent motion so as to reduce the shear strength of the materials. Static atomistic simulations of nanoindentation on (111) Cu crystal planes[50] and MD simulations of nanoindentation on Ni[51] showed that the hardness was also reduced by voids in the crystal. The cutting and thrust forces during nanomachining of single crystalline copper were also reduced by voids.[52] Nanoindentation experiments on a single crystal of tungsten using a Berkovich indenter with a tip radius of 390 nm showed that the load for plasticity decreased as the dislocation density in the crystal increased.[46] Simulations of nanomachining of copper showed that dislocations nucleate near the surface of the workpiece and emit into the crystal.[45] When machining was conducted at previously scratched regions with high defect densities, the cutting load was decreased.[45] Also, atomistic simulation of nanoindentation of Cu[53,54,55], Ni[56] and Mo[57] at grain boundaries predicted that lower contact stresses were required for plasticity than required for perfect crystals.

6.4.3.2 *Influence of roughness on the surface of a wafer*

The chemical additives used in CMP slurries have been reported to change the topography of the copper so that it contains surface peaks and valleys.[58] In addition, the nano-scale scratches or trenches generated by sliding abrasive particles further roughen the surface. Crystallographic defects such as vacancies, dislocations, impurities and grain boundaries make copper more susceptible to chemical attack[59], which exacerbates the roughness on the surface. Surface roughness that is smaller than the size of an indenter has been observed to induce plasticity by facilitating the nucleation of dislocations near the surface.[60] Since the abrasive particles used in CMP, on the order of tens of nanometers in size, are larger than the scale of roughness of the wafer after CMP, on the order of less than a nanometer, dislocations would be expected to nucleate at the surface roughness when the wafer interacts with sliding abrasive particles. Simulations and experiments of nanoindentation have shown the influence of surface roughness on the shear strength of various materials, including copper. Atomistic simulations of nanoindentation of Cu showed that the load needed to nucleate dislocations decreased significantly when indented near surface steps.[61] Similar behavior was predicted for the (111) faces of Au.[62] Nanoindentation experiments on Au using 25, 72, 100 and 230 nm radius tungsten tips showed a 45% reduction in yield stress when indented near surface

steps.[63]

6.4.3.3 AFM scratching experiments

The influence of the surface roughness caused by chemical additives on the shear strength of copper has also been studied by scratching copper that was previously treated with chemicals using an AFM tip. Liao *et al*.[58] exposed copper samples to solutions containing: only 5 wt% H_2O_2; 5 wt% H_2O_2 and 1 wt% glycine; and 5 wt% H_2O_2, 1 wt% glycine and 0.1 wt% BTA for 8 minutes and then measured the surface roughness and hardness by SEM and nanoindentation, respectively. The nanoindentation experiments used a load of 100 to 2500 μN with a 100 nm diameter Berkovich indenter, yielding an indentation depth exceeding 50 nm. Deep indentation was performed to avoid measuring the hardness at the surface layer, which was presumed to be oxides of copper. The chemically treated copper samples were also scratched using an AFM tip with a diameter of 20 nm under a load of 2.48 μN and the depth of the scratches were measured. The depths of scratches by the AFM tip were summarized in Table 6.1. Increased depths were observed when the copper samples were treated with various chemicals. In addition, each copper sample showed increased roughness after exposure to the chemicals, but the measured nanohardness values evaluated from the indentation experiments were only slightly changed; either increased or decreased. The insensitiveness of the nanohardness to the chemical treatment has also been reported by other researchers.[13,21] This change of the hardness was attributed to the oxide layer on the surface by Ihnfeldt and Talbot[21] and Liao *et al*.[58] However, there appears to be no correlation between the measured hardness of the chemically treated copper, which was presumed to be the hardness of copper oxides, and the MRR during CMP[13,21], suggesting that the measured hardness is not the material property governing the interaction between abrasives and copper during CMP. This is presumably due to a size effect not recognized by the authors. As discussed above, material properties at very small length scales differ from those at larger length scales. When an AFM tip was used for scratching, the applied load was two or three orders of magnitude smaller than that used for the nanoindentation experiments. Also, the tip radius was nearly an order of magnitude smaller than that for indentation. Thus the plastic zone created by the AFM tip was very small, and would have contained few dislocations. At this length scale where only small number of dislocations are contained around the AFM tip during the indentation the nucleation of dislocations, which has been believed to initiate the plasticity at the small length scale, may be homogeneous requiring a shear stress as high as the ideal shear strength of the material. The copper sample that was not exposed to the chemicals can be assumed to have behaved this way. When an AFM tip scratched the surface, the scratches became deeper with increasing surface roughness as shown in Table 6.1. Liao *et al*.[58] attributed the deeper scratches to weaker adhesion of the roughened surface material to the substrate. However, the increase in the scratching depth clearly showed that the increased surface roughness reduced the hardness of the surface material. The plasticity may have been initiated by heterogeneous nucleation of the dislocations or the activation of the dislocations source at the surface steps, voids, vacancies or impurities, reducing the required contact force for plasticity. Moreover, since a given copper sample was scratched repeatedly by the AFM tip to give $2 \times 2 \mu m^2$ of scratched area the region may contain additional defects from the deformation that facilitate heterogeneous nucleation of the dislocations. Therefore, depth of the scratches increased due to the reduction of the resistance to the plasticity, i.e. reduced hardness, at the very small length scale when the surface roughness was high. Oxide of

copper might have been formed on the surface of the copper which was exposed to various chemicals, and the change in the depth of the scratches may be considered to be due to the scratching on those oxides. However, the hardness of the copper oxide such as CuO, which have been suggested to be formed upon exposure to H_2O_2[64] is much higher than that of pure copper[21,65], contradicting to the observed depth of the scratches. Thus the size effect rather than the identity of the scratched material itself was more relevant to explain the enhanced depth of the scratches by the AFM tip.

To confirm that the deformation of the untreated copper sample was due to the homogeneous nucleation of dislocations, and that the reduction of the hardness of the chemically treated samples might be attributed to heterogeneous nucleation of dislocations, the maximum shear stress induced in the copper was evaluated. Since the bulk hardness of CuO or Cu_2O is higher than pure copper the hardness of the copper oxide at the very small length scale was also assumed to have the same trend. Thus the maxim shear stress in the copper instead of copper oxide was investigated in this work. Using the measured depth of scratches on the copper samples h_w and the radius of the AFM tip r_{tip} the contact area between the AFM tip and the copper sample was expressed as $\pi r_{tip} h_w$. Then the hardness of the copper samples that had been exposed to different chemicals H_w was estimated by:

$$H_w = \frac{f_{tip}}{\pi r_{tip} h_w}$$
(6.5)

where f_{tip} is the applied load by the AFM tip. Note that the hardness evaluated by this equation differs from the hardness measured by nanoindentation originally given by Liao *et al.*[58] because of the discrepancy in the length scales at which the hardness was measured. Assuming indentation by the AFM tip and the Tresca yield criterion the maximum shear stress induced in the copper by this scratching was evaluated using

$$\tau_{max} = 0.30 p_0$$
(6.6)

where p_0 is the maximum Hertz pressure, given by[66]:

$$p_0 = \left(\frac{6 f_{tip} E^{*2}}{\pi^3 r_{tip}^2} \right)^{1/3}$$
(6.7)

where $E^* = \left(\frac{1-v_1^2}{E_1} + \frac{1-v_2^2}{E_2} \right)^{-1}$, E and v are the elastic modulus and Poisson's ratio, respectively and subscript 1 and 2 denote the contacting materials; in this case copper and a silicon AFM tip, respectively. The evaluated hardness of copper and the maximum shear stress in copper are summarized in Table 6.1. These values show that the maximum shear stress in the copper sample that had not been treated with chemicals is of the same order as the ideal shear strength of copper and slightly smaller than the maximum shear stress values obtained from nanoindentation simulations, which provides some validation for the analysis.

The evaluated maximum shear stress values for copper samples that had previously been exposed to solutions containing various chemicals were considerably smaller than the ideal shear strength of copper, suggesting heterogeneous nucleation of dislocations. The reduction of the hardness and the maximum shear stress were more pronounced when the surface roughness was larger, e.g. when the copper sample was pre-exposed to aqueous solution at pH 4 or 10 containing 5 wt% H_2O_2 and 1wt% glycine.

Table 6.1 Surface roughness of the copper samples exposed to aqueous solutions containing different chemicals.[58] Hardness and maximum shear stress values were estimated from the depth of scratches by AFM tip.

	Not treated	5 wt% H_2O_2		5 wt% H_2O_2 and 1 wt % glycine		5 wt% H_2O_2, 1 wt% glycine and 0.1 wt% BTA	
		pH 4	pH 10	pH 4	pH 10	pH 4	pH 10
Depth of scratches by AFM [nm]	6.61	12.89	11.78	37.57	29.05	9.35	15.2
Surface roughness [nm]	10	17.9	12	85.5	185.3	12.3	20.3
Hardness [GPa]	11.9	6.12	6.70	2.10	2.72	8.44	5.19
Maximum shear stress [GPa]	5.37	2.76	3.02	0.95	1.22	3.80	2.34

The MRRs during copper CMP using a slurry at pH 4 containing 5 wt% H_2O_2 and 3 wt% of alumina abrasives and the same slurry containing an additional 1 wt% glycine were predicted from equation (6.3) and the hardness values in Table 6.1, and compared with the experimental results of Jindal et al.[13] as shown in Figure 6.5. The MRRs for the same slurry at pH 10 were also predicted and compared. It was assumed that the number of abrasives participating in the abrasion is unaffected by the presence of glycine at a given pH whereas it is influenced by the pH of the slurry. The electrochemical portion of the MRR was also neglected. Equation 6.3 predicts that the MRRs during copper CMP are inversely proportional to the 3/2 power of the hardness at the surface of copper for the same size of abrasives, sliding velocities and down pressures. The prediction was made by least squares fitting the experimental data of Jindal et al.[13] at pH 4 and pH 10, respectively using the hardness values in Table 6.1 at each pH. The predictions based on the hardness values obtained from the AFM tip scratching tests agreed well with the experimental observations while those based on the nanohardness obtained from deep indentation tests were poorly correlated with the experimental values, even in the trends[21].
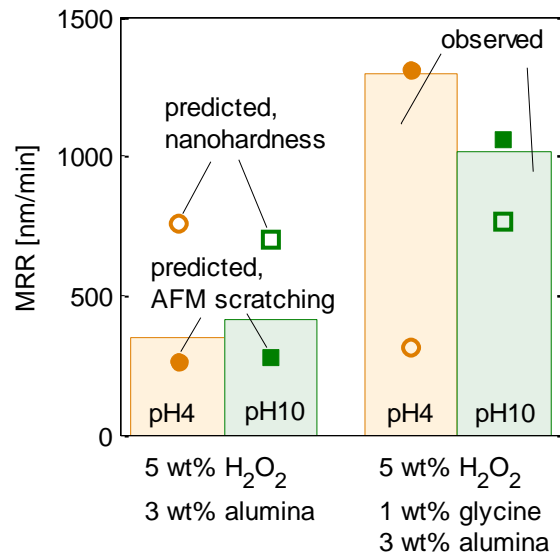
Figure 6.5 Comparison of MRRs due to mechanical action predicted using the hardness values obtained from AFM tip scratching tests by Liao *et al*.[58] (filled) or using the nanohardness by Liao *et al*.[58] (unfilled) and MRRs measured experimentally by Jindal *et al*.[13].

6.4.3.4 *Material removal mechanisms at abrasive scale*

The probability that a given location on a wafer is contacted by squeezed abrasives under an asperity during interaction with the asperity and the wafer was defined as the removal efficiency. In Chapter 5 the removal efficiency during CMP was determined to be smaller than unity, meaning that a point on a wafer during CMP is contacted fewer than once during the contact between a pad asperity and a wafer. Then, the period over which a given location on the surface of copper is exposed to the slurry between successive contacts with abrasive particles is of the same order as the time interval between consecutive asperity and wafer interactions, about 1 ms. Note that this time scale is several order smaller than the time for which the copper sample has been exposed to the chemicals or the aqueous solutions, 8 minutes, before the depth of scratches induced by the AFM tip was measured.. Therefore, the chemical additives in the slurry will result in less roughness during this short time period during CMP than observed by Liao *et al*.'s experiments[58]. On the other hand, the surface of copper during CMP contains numerous nano-scale topography originated from previous etching and deposition processes. The combined effects will roughen the surface so that the hardness of copper at the nano-scale is lowered than the ideal value. Then, the copper can be plastically deformed by the force exerted through the abrasives to result in removal of the material.

The exact mechanism by which the plastically deformed material is removed from the surface is unclear. The material dislodged by indentation by the abrasives and the material in the plastic zone during indentation contain a higher density of crystallographic defects than the material that has not interacted with the abrasives. The material in these defect-rich

regions would be expected to undergo preferential oxidation by the oxidizing agent in the slurry, having a higher thermodynamic activity. As mentioned earlier in this chapter, the mechanism of the oxidation may also be Fenton-type, producing hydroxyl radicals. MD simulation of nano-scale machining showed that dislodged materials generated during nano-machining were removed by chemical dissolution.[67] Also, the material on the surface can be detached directly as debris by sliding abrasives, similar to cutting processes. Yan *et al*. argued, based on MD simulation of scratching, that the deformation of copper by a hemispherical scratching tip can be divided into four categories, depending on a parameter K that is a function of the radius of the tip and the penetration depth into copper[68]. The parameter K was defined as:

$$K = \frac{h_w - 0.07 r_{tip}}{0.07(r_{tip} - h_w)}$$ (6.8)

As the penetration depth increases, the state of deformation of copper changes from a no-wear state, through a ploughing state, and ploughing dominant cutting state, to a cutting dominant cutting state. The scratching depth data reported by Liao *et al*. yielded a value of K ranging from 9.35 to 37.6 and 6.61, when the copper samples were exposed and were not exposed to the chemicals, respectively. For K values between 2 and 8, the copper is mostly ploughed with some material being removed by cutting, while for K values larger than 8 cutting is dominant with some ploughing. This implies that the copper can directly be removed from the surface by cutting, especially when the hardness of the material has been reduced by roughening. Earlier studies of the influence of the attack angle of an indenter on the wear process also showed that only a small fraction of the material dislodged during the wear process become detached debris when the attack angle is sufficiently small[69,70,71] to be comparable to the geometry during CMP, where the indentation depth of abrasives is small compared to the size of the abrasives. The free copper debris may then react with the oxidizing and complexing agents in the slurry and dissolve[72]. Removal of copper by this mechanism is not measured by the electrochemical method used in the work, because electron transfer does not happen when the copper debris particles are in electrical contact with the wafer. Also, not all of the copper deformed by a sliding abrasive particle would be removed, making the coefficient K_{re} in equation (6.3) lower than one. Note that the local density of the crystallographic defects on the surface of copper is not uniform throughout the wafer and that the deformation of the surface by the sliding abrasives occurs only at the regions of high defect density. Therefore, not every scratching event induced by the sliding abrasives will induce plastic deformation of copper; the copper will plastically be deformed to contribute to the material removal only where there are sufficient defects in the copper crystal. This effect will further lower the value of K_{re} to give a much more realistic prediction of the MRR during copper CMP using equation (6.3). For example, for the consumables and processing parameters during copper CMP listed in Table 6.2, the equation (6.1) predicts the MRR of 500nm/min if only one percent of the surface of the copper contains enough defects to initiate plasticity by the force applied by squeezed abrasive particles. The hardness of copper was taken from Table 6.1 for the case where 5 wt% H_2O_2 and 1 wt % glycine were added to the slurry at pH4. If no K_{re} is used, the prediction by equation (6.1) will be 50 μm/min, which is unrealistic.

Table 6.2 Typical consumables and processing parameters during copper CMP

$r_{contact}$	a_{as}	r_{ab}	H_w	$\tilde{n}_{ab}$	f_{ab}
0.1 %	10 μm^2	10 nm	2.1 GPa	1000	100 nN

6.5 Conclusion and Future work

Copper can plastically be deformed by mechanical abrasion with the abrasive particles squeezed between pad asperities and a wafer during CMP even though the shear stress induced in the copper by this interaction may be smaller than the ideal shear strength of the material. This is enabled by the activation of dislocation sources or by the heterogeneous nucleation of dislocations from surface steps generated on the surface of copper by the chemical additives in a slurry and abrasions by the abrasive particles, and from other crystallographic defects including voids, vacancies, impurities and grain boundaries. Note that the local density of those defects and the roughness on the surface is not uniform, making the deformation by the sliding abrasives only at regions of high defect density and roughness. Therefore, not every interaction with the abrasives will induce plastic deformation of copper. Furthermore, only a part of the deformed portion of the material can be detached from the surface through a process similar to cutting by abrasives or by preferential chemical oxidation where there are enough defects to enhance the chemical reactivity.

The size effect of indentation can be applied to explain the micro-scratches generated during copper CMP. While the interactions with the abrasives generate very shallow scratches of the order of the roughness on a wafer after CMP, some large particles can generate deep scratches on the surface. Plastic deformation by the large abrasive is possible because the plastic zone near the interacted region contains a large number of crystallographic defects that may allow heterogeneous nucleation of dislocations, greatly reducing the hardness of the material. The hardness of the material decreases as the contact area increases. Therefore, scratching by large abrasive particles, which may have been generated by agglomeration of the small abrasives or poor filtration of the slurry, generates deep scratches.

Another application of the proposed model would be to explain the relationship between the friction coefficient during CMP and the MRR. These two are believed to be related by some researchers, but no universal relationship has been found[15,73,74,75]. The frictional force could be evaluated, knowing the number of abrasives that are squeezed between pad asperities and a wafer and the mode of the deformation of a material during the interaction with the abrasives, i.e. either elastic or plastic, and the coefficient of friction for each mode of deformation. To evaluate the friction between the pad and the wafer, one needs to know exactly what fraction of the abrasives cause plastic deformation of a material. As discussed in this chapter, the local hardness of copper during CMP is greatly affected by the chemical additives in the slurry. Thus the friction will be closely related to the chemical additives in the slurry that roughen the surface of a wafer, as well as to the number of the squeezed abrasives, which is also influenced by the chemical additives as discussed in Chapter 8.

References

[1] Y. Xie and B. Bhushan, *Wear*, **200**, 281 (1996).

[2] W. Che, Y. Guo, A. Chandra and A. Bastawros, *J. Manuf. Sci. Eng.*, **127**, 545 (2005).

[3] J.-Z. Jiang, Y.-W. Zhao, Y.-G. Wang and J.-B. Luo, *Wear*, **265**, 992 (2008).

[4] A. Bastawros, A. Chandra, Y. Guo and B. Yan, *J. Electron. Mater.*, **31**, 1022 (2002).

[5] M. Bastaninejad and G. Ahmadi, *J. Electrochem. Soc.*, **152**, G720 (2005).

[6] J. Luo and D. A. Dornfeld, *IEEE Trans. Semicond. Manuf.*, **16**, 45 (2003).

[7] K. Qin, B. Moudgil and C.-W. Park, *Thin Solid Films*, **446**(2), 277 (2004).

[8] Y. Zhao, L. Chang and S. H. Kim, *Wear*, **254**, 332 (2003).

[9] F. B. Kaufman, D. B. Thompson, R. E. Broadie, M. A. Jaso, W. L. Guthrie, D. J. Pearson and M. B. Small, *J. Electrochem. Soc.*, **138**, 3460 (1991).

[10] S. Tripathi, S. Choi, F. M. Doyle and D. A. Dornfeld, *Mater. Res. Soc. Symp. Proc.*, **1157,** E02-03 (2009).

[11] S. Choi, S. Tripathi, D. A. Dornfeld, F. M. Doyle, *J. Electrochem. Soc.*, **157**, H1153-9 (2010).

[12] T.-H. Tsai, S.-C. Yen, *Appl. Surf. Sci.*, **210**, 190 (2003).

[13] A. Jindal and S. V. Babu, *J. Electrochem. Soc.*, **151**, G709 (2004).

[14] R. Sato, Y. Ichida, Y. Morimoto and K. Shimuzu, *J. Adv. Mech. Des. Syst. Manuf.*, **2**(4), 685 (2008).

[15] Z. Li, K. Ina, P. Lefevre, I. Koshiyama and A. Philipossian, *J. Electrochem. Soc.*, **152**, G299 (2005).

[16] M. Stern and A. L. Geary, *J. Electrochem. Soc.*, **104**, 56 (1957).

[17] A. Jindal, Y. Li and S. V. Babu, *Mat. Res. Soc. Symp. Proc.*, **671**, M6.8.1 (2001).

[18] J. Luo and D. A. Dornfeld, *IEEE Trans. Semicond. Manuf.*, **14**, 112 (2001).

[19] T. Zeng and T. Sun, *IEEE Trans. Semicond. Manuf.*, **18**, 655 (2005).

[20] D. Bozkaya and S. Muftu, *J. Electrochem. Soc.*, **156**, H890 (2009).

[21] R. Ihnfeldt and J. B. Talbot, *J. Electrochem. Soc.*, **155**, H412 (2008).

[22] Y. Li, M. Hariharaputhiran and S. V. Babu, *J. Mater. Res.*, **16**, 1066 (2001).

[23] D. Ng, M. Kulkarni, J. Johnson, A. Zinovev, D. Yang and H. Liang, *Wear*, **263**, 1477 (2007).

[24] W. D. Nix and H. Gao, *J. Mech. Phys. Solids*, **46**, 411 (1998).

[25] S. Shim, H. Bei, E. P. George and G. M. Pharr, *Scr. Mater.*, **59**, 1095 (2008).

[26] I. Salehinia, V. Perez and D. F. Bahr, *Philos. Mag.*, **92**(5), 550 (2012).

[27] J. G. Swadener, E. P. George and G. M. Pharr, *J. Mech. Phys. Solids*, **50**, 681 (2002).

[28] S. Qu, Y. Huang, W. D. Nix, H. Jiang, F. Zhang and K. C. Hwang, *J. Mater. Res.*, **19**, 3423 (2004).

[29] Y. Huang, F. Zhang, K. C. Hwang, W. D. Nix, G. M. Pharr and G. Feng, *J. Mech. Phys. Solids*, **54**, 1668 (2006).

[30] G. Feng, A. S. Budiman, W. D. Nix, N. Tamura and J. R. Patel, *J. Appl. Phys.*, **104**, 043501 (2008).

[31] S. Choi, F. M. Doyle and D. A. Dornfeld, *Procedia Eng.*, **19**, 73 (2011).

[32] G. Ziegenhain, A. Hartmaier and H. M. Urbassek, *J. Mech. Phys. Solids*, **57**, 1514 (2009).

[33] D. Saraev and R. E. Miller, *Modell. Simul. Mater. Sci. Eng.*, **13**, 1089 (2005).

[34] S. Suresh, T.-G. Nieh and B. W. Choi, *Scr. Mater.*, **41**, 951 (1999).

[35] J. Chen, W. Wang, L. H. Qian and K. Lu, *Scr. Mater.*, **49**, 645 (2003).

[36] A. Gouldstone, H.-J. Koh, K.-Y. Zeng, A. E. Giannakopoulos and S. Suresh, *Acta Mater.*, **48**, 2277 (2000).

[37] A. Kelly, N. H. Macmillan, *Strong Solids, third ed.*, Clarendon Press, Oxford (1986).

[38] S. Ogata, J. Li and S. Yip, *Science*, **298**, 807 (2002).

[39] C. R. Krenn, D. Roundy, J. W. Morris Jr. and M. L. Cohen, *Mater. Sci. Eng.*, **A317**, 44 (2001).

[40] T. Zhu, J. Li, K. J. Van Vliet, S. Ogata, S. Yip and S. Suresh, *J. Mech. Phys. Solids*, **52**, 691 (2004).

[41] C. R. Krenn, D. Roundy, M. L. Cohen, D. C. Chrzan and J. W. Morris Jr., *Phys. Rev. B*, **65**, 134111 (2002).

[42] S. Choi, F. M. Doyle and D. A. Dornfeld, in *Proceedings of International Conference on Planarization/CMP Technology*, J.-G. Park, T. Kim and H. Jeong, Editors, p. 412, ComeBook, Seoul, Korea (2011).

[43] Y. Y. Ye, R. Biswas, J. R. Morris, A. Bastawros and A. Chandra, *Nanotechnol.*, **14**, 390 (2003).

[44] J. Zhang, T. Sun, Y. Yan and Y. Liang, *Mater. Sci. Eng., A*, **505**, 65 (2009).

[45] Y.-C. Liang, J.-X. Chen, M.-J. Chen, D.-P. Song and Q.-S. Bai, *J. Vac. Sci. Technol. B*, **27**(3), 1536 (2009)

[46] A. A. Zbib and D. F. Bahr, *Metall. Mater. Trans. A*, **38A**, 2249 (2007).

[47] C. A. Schuh, J. K. Mason and A. C. Lund, *Nat. Mater.*, **4**, 617 (2005)

[48] E. K. Njeim and D. F. Bahr, *Scr. Mater.*, **62**, 598 (2010).

[49] I. Salehinia and S. N. Medyanik, *Metall. Mater. Trans. A*, **42A**, 3868 (2011).

[50] C.-M. Tan and Y.-R. Jeng, *Int. J. Solids Struct.*, **46**, 1884 (2009).

[51] P. Zhu, Y. Hu and H. Wang, *Sci. China Phys. Mech. Astron.*, **53**(9), 1716 (2010).

[52] S. V. Hosseini, M. Vahdati and A. Shokuhfar, *Adv. Struct. Mater.*, **16**, 661 (2012).

[53] T. Tsuru, Y. Kaji, D. Matsunaka and Y. Shibutani, *Phys. Rev. B*, **82**, 024101 (2010).

[54] X.-L. Ma and W. Yang, *Nanotechnol.*, **14**, 1208 (2003).

[55] J. Sun, L. Fang, K. Sun and J. Han, *Scr. Mater.*, **65**, 501 (2011).

[56] A. K. Nair, E. Parker, P. Gaudreau, D. Farkas and R. D. Kriz, *Int. J. Plast.*, **24**, 2016 (2008).

[57] W. A. Soer, K. E. Aifantis and J. Th. M. De Hosson, *Acta Mater.*, **53**, 4665 (2005).

[58] C. Liao, D. Guo, S. Wen and J. Luo, *Tribol. Lett.*, **45**, 309 (2012).

[59] H.-P. Feng, J.-Y. Lin, M.-Y. Cheng, Y.-Y. Wang and C.-C. Wan, *J. Electrochem. Soc.*, **155**(1), H21 (2008).

[60] A. Gouldstone, K. J. Van Vliet and S. Suresh, *Nature*, **411**, 656 (2001).

[61] D. Shan, L. Yuan and B. Guo, *Mater. Sci. Eng., A*, **412**, 264 (2005).

[62] J. A. Zimmerman, C. L. Kelchner, P. A. Klein, J. C. Hamilton and S. M. Foiles, *Phys. Rev. Lett.*, **87**, 165507-1 (2001).

[63] J. D. Kiely, R. Q. Hwang and J. E. Houston, *Phys. Rev. Lett.*, **81**, 4424 (1998).

[64] J. Hernandez, P. Wrschka, and G. S. Oehlein, *J. Electrochem. Soc.*, **148**, G389 (2001).

[65] A. Szymanski and J. M. Szymanski, *Hardness Estimation of Minerals Rocks and Ceramic Materials*, Elsevier Science Publishers B. V, New York (1989).

[66] K. L. Johnson, *Contact Mechanics*, p. 90-95, p. 208, Cambridge University Press, Cambridge, UK (1985).

[67] Y. Y. Ye, R. Biswas, A. Bastawros and A. Chandra, *Mat. Res. Soc. Symp. Proc.*, **767**, F1.8.1 (2003).

[68] Y. D. Yan, T. Sun, S. Dong, X. C. Luo and Y. C. Liang, *Appl. Surf. Sci.*, **252**, 7523 (2006).

[69] Y. Xie, J. A. Williams, *Wear*, **162-164**, 864 (1993).

[70] Y. Xie, J. A. Williams, *Wear*, **196**, 21 (1996).

[71] E. Rabinowicz, *Friction and Wear of Materials*, 2nd ed., Wiley, New York (1995).

[72] J. M. Steigerwald, S. P. Murarka, and R. J. Gutmann, *Chemical Mechanical Planarization of Microelectronic Materials*, Wiley, New York (1997).

[73] U. Mahajan, M. Bielmann and R. K. Singh, *Electrochem. Solid State Lett.*, **2**, 80 (1999).

[74] A. Philipossian and S. Olsen, *Jpn. J. Appl. Phys.*, **42**, 6371 (2003).

[75] B. Park, H. Lee, Y. Kim, H. Kim and H. Jeong, Jpn. *J. Appl. Phys.*, **47**, 8771 (2008).

Chapter 7
Literature Review of the Dependencies of MRR on the Size and the Concentration of Abrasives

7.1 Introduction

In Chapter 6, the material removal mechanism during copper CMP was suggested to be related to the plastic deformation of the copper by sliding abrasives. If such a mechanism were at play, the MRR during copper CMP would be expected to be proportional to the number of abrasive particles squeezed between pad asperities and a wafer. This chapter reviews previous studies that investigated the relationship between the size and the weight concentration of abrasives in a slurry, and the MRR during CMP. General trends of the MRR during CMP of various materials with the size and the concentration of abrasives are evaluated based on an extensive review of the previous experimental observations of various researchers. Proposed mechanisms for the experimental trends are also reviewed and the limitations of the proposed models are also discussed. Recognizing the limitations of the previously proposed mechanisms for explaining MRR trends during CMP, a novel explanation for the observed MRR behavior during CMP is then proposed in Chapter 8.

7.2 Experimentally observed impact ofthe size and the concentration of abrasives on MRR

Table 7.1 summarizes experimental observations of the impact of size and concentration of abrasive particles on MRR reported by various researchers. Note that the number of abrasive particles decreases with increasing abrasive size for a fixed weight concentration of the abrasives. Also, although studies typically report the average size of the abrasive particles, slurries usually containly polydisperse particles.

For the metal CMP results reported in Table 7.1, the experimental details were as follows: alumina[1,11,12,14] or silica[1,4,13,15] abrasive particles ranging from 12 nm[13] to 880 nm[12] were used with weight concentrations from less than 1%[4] to 15%[12]. The slurries contained an oxidizing agent[1,15] such as $K_3Fe(CN)_6$[12], $Fe(NO_3)_3$[11] and H_2O_2[13], an inhibitor[15] like BTA[11], a complexing agent[15], a surfactant[15], or a combination of these chemicals. A slurry with no chemical additives[14] or a proprietary slurry[4] was also used in some studies. Acidic slurries were used [4,12,13,14] or no data is given for the pH of the slurry. A compressible felt pad, SUBA500[13] or a less compressible porous polyurethane pad, stacked IC1000[11,12,14] or IC1400[15], was used for the experiments.

Table 7.1 Impact of the size or weight concentration of abrasive particles in the slurry on experimentally observed material removal rates during CMP of various materials

Experimental change	Changes in MRR	Silicon Oxide or Silicon CMP	Metal CMP
Increasing weight concentration	Increasing	Jairath et al.[1], Mahajan et al.[2], Zhou et al.[3], Cooper et al.[4], Philipossian et al.[5], Choi et al.[6,7], Park et al.[8,9*], Zhang et al.[10]	Jairath et al.[1†], Luo et al.[11‡], Bielmann et al.[12†], Li et al.[13§‡], Cooper et al.[4‡], Guo et al.[14‡], Lee et al.[15‡]
	Increasing then decreasing	Mahajan et al.[2], Philipossian et al.[5], Choi et al.[6], Yoshida et al.[16*]	-
	Decreasing	Mahajan et al.[2]	-
Increasing size	Increasing	Choi et al.[6], Oh et al.[17]	Xie et al.[18‡], Armini et al.[19‡]
	Increasing then decreasing	Zhou et al.[3], Zhang et al.[20]	Xie et al.[18‡]
	Decreasing	Choi et al.[6,7]	Bielmann et al.[12†], Li et al.[13§‡], Lu et al.[21§]

For silicon oxide or silicon CMP, the experimental details were as follows: silica abrasive was used except by Jairath et al.[1]. Most of the slurries used in the literature did not contain any chemical additives other than deionized water.[2,3,6,8,10] The slurry used by Philipossian et al. was a commercial one whose chemical constituents were not disclosed.[5] Note that the pattern of grooves on a polishing pad also influenced the effect of the weight concentration of the abrasives on MRR using a commercial.[5] All slurries whose pH was reported were alkaline.[1,2,3,4,6,7,8,10,16] The pads were porous polyurethane pads such as IC1000[2,3,5,6,7] or IC1400[8], or a cerium oxide filled polyurethane pad, LP66[10].

7.2.1 Influence of the weight concentration of abrasives

As seen in Table 7.1, the MRR during CMP increased withincreasing weight concentration of the abrasives. The experimental data of Luo et al.[11] demonstrate typical trends in MRR during metal CMP. This was true for tungsten, copper or tantalum, regardless of the chemical additives in the polishing slurries, the polishing pads, or the types, the size ranges and the concentrations of the abrasives. Increasing concentration of abrasives did not have a universal impact on the MRR for oxide CMP. Unlike metal CMP, the impact of weight concentration of abrasives on MRR during oxide CMP depended on the size of the abrasives. This behavior is best represented by the experimental observations by Mahajan et al. as

---

* Silicon
† Tungsten
‡ Copper
§ Tantalum

shown in Figure 7.2.[2] The MRR increased with the weight concentration of the abrasives for relatively small particles, ranging from 7 nm[1] to 200 nm[2,6], but decreased with increasing concentration for micrometer sized particles.   The MRR peaked as the concentration increased from 0.2 to 2 wt% for intermediate sized abrasives. The MRR was independent of the abrasive concentration for concentrations between 0.5[6] to 30 wt%[3,6,10]. CMP of silicon resulted in rather different behavior; as the abrasive size increased, the MRR reached a maximum with 46.2 nm silica abrasives in the presence of ammonia and organic compounds in the slurry[16] and the MRR increased as the concentration increased from 0.5 to 7 wt% in ammoniacal slurries using a felt type pad [9].
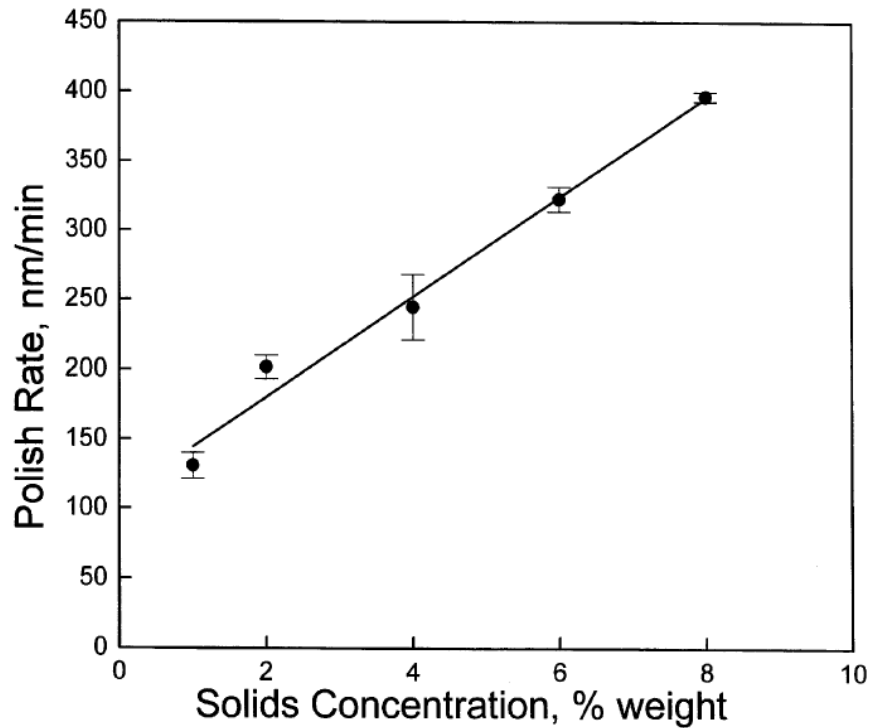
Figure 7.1 Effect of abrasive concentration on measured MRR during CMP of copper using alumina abrasives.[11] 0.005 M BTA and 0.1 M Fe(NO₃)₃ were added to the slurry.
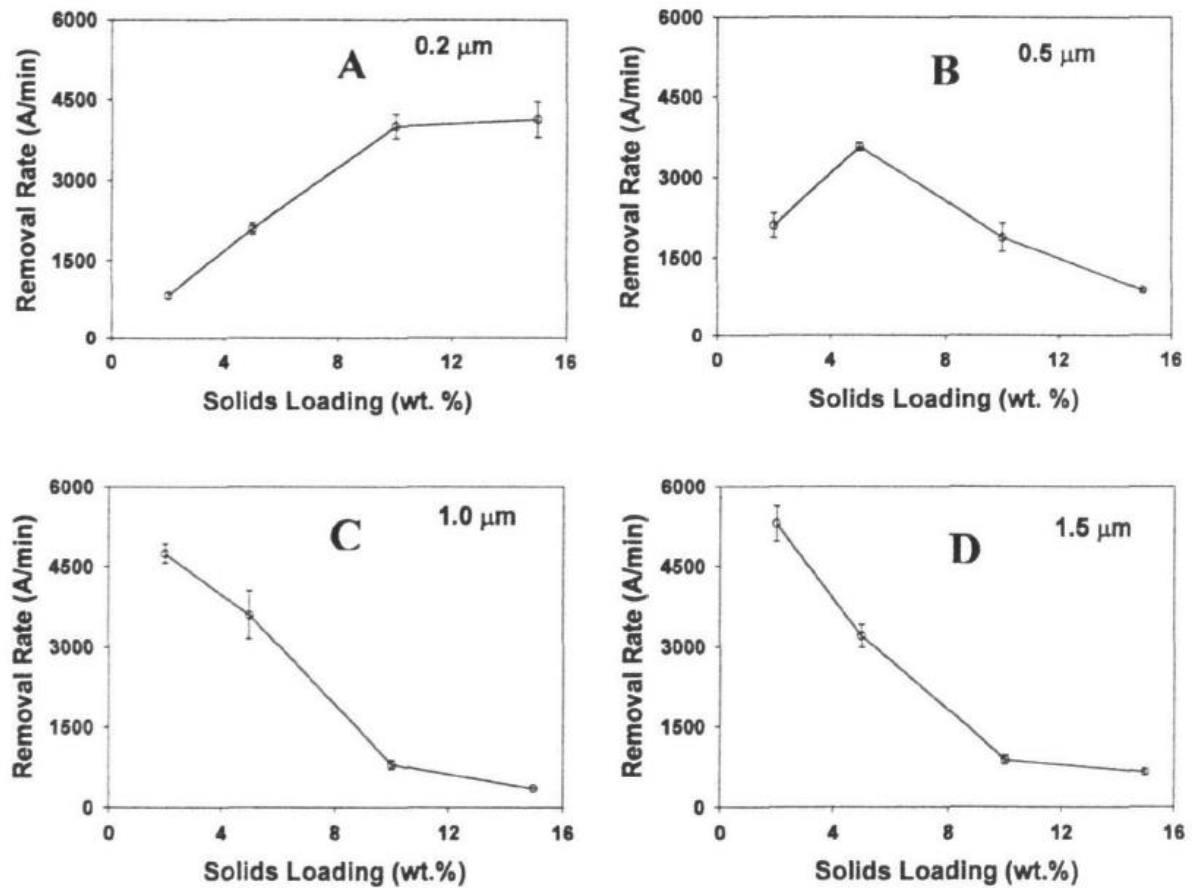
Figure 7.2 Effect of concentration of abrasives of differing size on measured MRR during CMP of silicon oxide.[2] The slurry contained no chemicals other than DI water at pH 10.5.

7.2.2 Influence of the size of abrasive particles

Unlike the dependence of MRR during CMP on the concentration of the abrasives, that on the size of the abrasives was significantly varied for both oxide and metal CMP. The MRR during silicon oxide CMP increased, increased and then decreased, or decreased with increasing size of abrasive particles. Very complicated trends of the MRR with the size of abrasives were observed by Armini *et al.*[22] as shown in Figure 7.3. Similarly, the MRR behavior for metal CMP is also complicated. Either increasing or decreasing MRR with the size of abrasives were observed at different pH, as shown in Figure 7.4 and Figure 7.5, respectively, for fairly comparable abrasive concentrations.
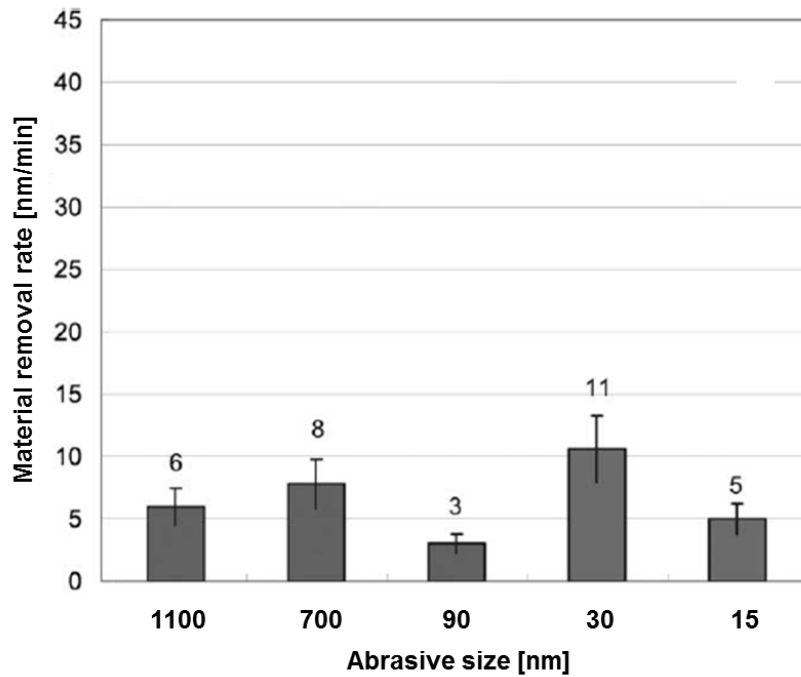
Figure 7.3 Material removal rate of silicon oxide during CMP for slurries at pH 10 with different sizes of colloidal silica abrasives at 5 wt%.[22]
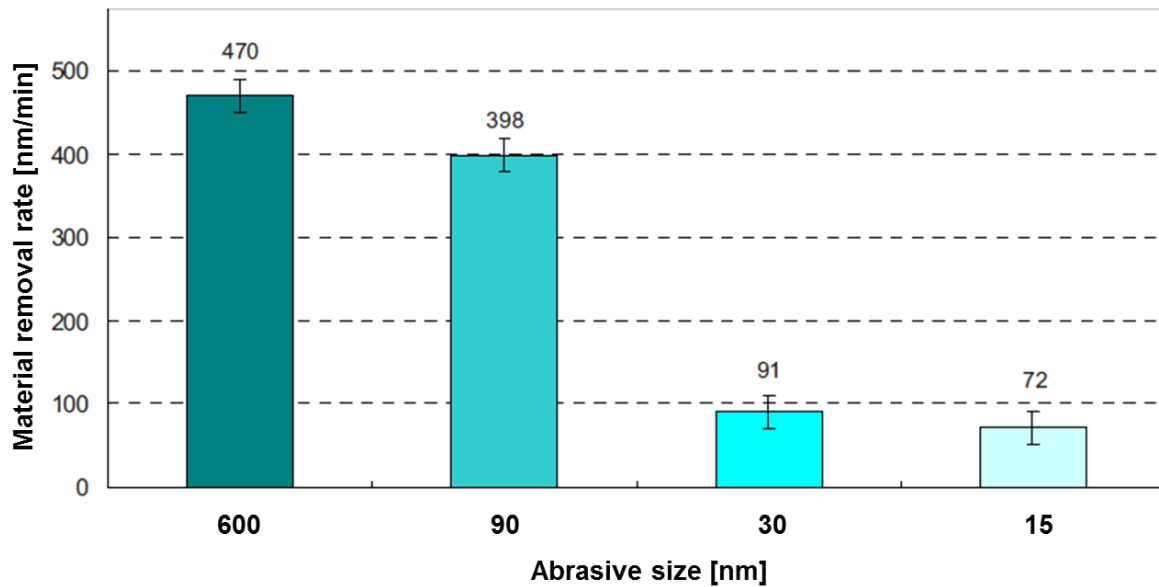
Figure 7.4 Material removal rate of copper during CMP for slurries with different sizes of silica abrasives at 5 wt%.[19] 1 wt% glycine, 0.018 wt% BTA, 0.3 vol% H_2O_2 at pH 6.
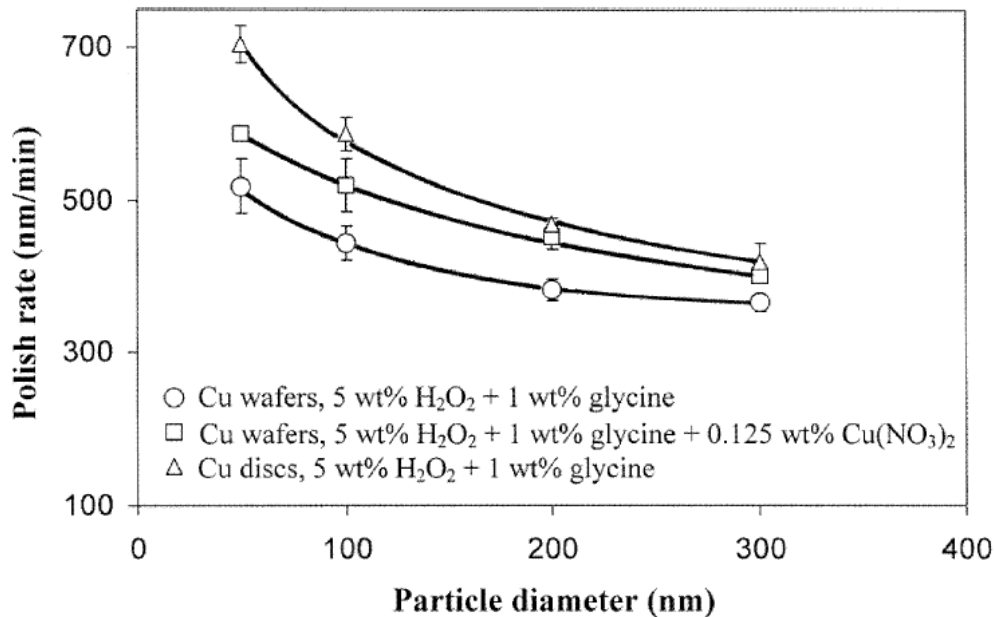
Figure 7.5 MRR during CMP of copper using slurries with varying sizes of silica abrasives at 3 wt%.[21] 5 wt% H_2O_2 and 1 wt% glycine were added to the slurry at pH 4 with or without 0.125 wt% $Cu(NO_3)_2$.

7.3 Proposed mechanisms

The mechanisms proposed for the various dependencies of MRR on the size and the concentration of the abrasives largely fall into two categories: one is a combination of contact area-based and indentation-based mechanisms proposed by Mahajan and Bielmann *et al.*[2,12,23] where the relative dominance of each mechanism depends on the size of the abrasive particles, and the other considers the MRR to depend on the volume of material on the wafer indented by abrasive particles. For the latter, the force applied on an abrasive is a crucial factor that determines the depth, and thereby the volume, of the indentation.

7.3.1 Contact area-based and indentation-based mechanisms
Mahajan and Bielmann *et al.*[2,12,23] proposed two removal mechanisms to explain the dependence of MRR during silicon oxide CMP on the concentration of the abrasive particles, namely contact area-based and indentation-based mechanisms, which dominate for submicron sized and larger abrasive particles, respectively. The contact area-based mechanism was proposed to be due to chemical interaction between abrasives and a wafer, while the indentation-based mechanism dominates when the indented volume of the wafer by the abrasives determines the MRR. For the contact area-based mechanism, the MRR is proportional to the total contact area between abrasives and the wafer, A_{ab}, giving the following expression:

$$MRR \sim A_{ab} \propto c_{wt}^{1/3} r_{ab}^{-1/3} \qquad (7.1)$$

where c_{wt} is the weight concentration of abrasive particles in a slurry and r_{ab} is the average radius of the abrasive particles. For the indentation-based mechanism, the wafer volume indented by the contacting abrasives, V_{ab}, is proportional to the MRR, and thus:

$$MRR \sim V_{ab} \propto c_{wt}^{-1/3} r_{ab}^{4/3} \qquad (7.2)$$

The derivation of these expressions has not been published, to the best of our knowledge. Based on equation (7.1) and (7.2), Mahajan et al. suggested that increasing MRR with increasing concentration of abrasives, as observed for smaller abrasive particles, demonstrated dominance of the contact area mechanism, while the opposite trend of MRR for larger abrasives demonstrated dominance of the indentation-based mechanism.[2]

Although these mechanisms were originally proposed to account for the experimentally observed dependencies of MRR on the concentration of abrasive particles during silicon oxide CMP, they have been widely accepted by other researchers to explain the trends of MRR for other materials, including metals, on the sizes of abrasives for a fixed concentration, and on the concentration of abrasives.[7,19,20,21,22] These mechanisms have also been employed to interpret the MRR behavior when slurries with mixed sizes of abrasive particles were used for silicon oxide[22,23] and for copper[19]. Choi et al. utilized the contact area-based model to explain decreasing MRR during silicon oxide CMP as the abrasive particles increased in size from 48 to 110 nm and their concentration decreased from 30 to 2 wt%.[7] Armini et al. invoked both mechanisms to explain the change of MRR of silicon oxide with the sizes of silica particles in a slurry, ranging from 15 to 1100 nm, but could not explain the observed MRR trends shown in Figure 7.3.[22] Armini et al. also invoked indentation-based mechanisms to explain increasing copper MRR with increasing size of silica abrasive particles, from 15 to 600nm.[19] Lu et al. observed that the MRR for copper CMP decreased as the abrasive size increased from 40 nm to 300 nm, which was explained by the contact area-based mechanism.[21] Zhang et al. applied the contact area-based and indentation-based mechanisms to explain the increasing and then decreasing MRR for silicon oxide film as the size of the silica abrasive particles increased from 40 to 120 nm at 10 wt%.[20] They attributed the initial increase in MRR with increasing particle size for smaller particles to the indentation-based mechanism, and the subsequent decrease in MRR with increasing size for larger particles to the contact area-based mechanism. However, this explanation contradicts the suggestion of Mahajan et al.[2] that the contact area-based dominated for smaller abrasives and the indentation-based mechanism dominated for larger particles.

7.3.1.1 *Limitation of the proposed models*
The proposed models of Mahajan et al.[2] captured the experimentally observed effect of the concentration of abrasives on the MRR. Unfortunately, when the models are applied to the effect of abrasive size on the MRR, they predict that the MRR will decrease with the increasing size of abrasives where the contact area based mechanism is dominant, i.e. smaller abrasives, and increase with the increasing size of abrasives where the indentation-based

mechanism is relevant, i.e. larger abrasives. This predicted behavior has never been observed; the opposite behavior has been observed by several researchers[3,18,20]. In contrary, if the indentation based mechanism and the contact area based mechanism are dominant for smaller and larger abrasives, respectively as Zhang *et al.* [20] proposed, those mechanisms cannot explain the MRR behavior with varying concentration of abrasives: the predicted MRR decrease and then increase with increasing concentration of abrasives, which has never been observed. This clearly points to a significant limitation of the mechanisms.

7.3.1.2 Influence of surface area of abrasives

Several studies emphasized the importance of the specific surface area of non-porous abrasives, which is proportional to the contact area between the abrasives and a wafer, because of a chemical interaction between the particles and a wafer surface. Note that the specific surface area of abrasives decreases linearly with increasing size of abrasives for a given concentration of abrasives. Li *et al.* proposed that the increase in MRR of tantalum and copper with decreasing silica particle sizes in a slurry was due to increasing chemical interaction between silica and tantalum and to higher concentration of ~SiOH groups formed between silica particles and copper with decreasing particle sizes, respectively.[13] However, this observed trend was exactly the opposite of the results by Armini *et al.*[19], who reported that increasing the size of the silica particles increased the copper MRR. Oh *et al.* argued that chemical bonding between ceria abrasives and the silicon oxide substrate explained the increase in MRR with increasing size of abrasives.[17]

7.3.2 Mechanism assuming abrasion of a wafer by abrasive particles

Another major group of proposed models originates from the idea that the MRR during CMP can be predicted if the number of the abrasives and the volume that each abrasive particle removes are known, along with the velocity with which each abrasive particle moves.[18,24,25,26,27,28,29,30,31,32,33,34,35,36] Numerous models have been developed to predict MRR during CMP, based on the indentation of the wafer by abrasive particles held between the wafer and asperities on the pad. They followi the generalized form proposed in Chapter 6:

$$MRR = K_{re} \frac{n_{ab}{}^{*} A_i v}{A_w} \tag{7.3}$$

where K_{re} is a factor accounting for partial removal of the dislodged material of a wafer by the abrasive particles, $n_{ab}{}^{*}$ is the number of the abrasive particles participating in the material removal, A_i is the cross sectional area of a trench on a wafer generated by the indentation of a sliding abrasive, v is the sliding velocity of a wafer over the polishing pad and A_w is the area of the wafer surface. The equation gives the MRR in units of thickness reduction per unit time. In the following discussion, only parameters that are relevant to the size and concentration of abrasives are discussed, to show the dependencies of these parameters on the MRR.

Table 7.2 summarizes the literature that examines MRR during CMP in terms of the sum of the removal rates of individual abrasive particles. Models in the literature are categorized in

terms of the use of the factor K_{re}, how the number of abrasives that contribute to material removal were evaluated, and the deformation mode of a wafer by abrasives during CMP.

7.3.2.1 *Portion of the dislodged material contributing to material removal*

Most researchers have considered the volume indented by abrasive particles to contribute directly to the removal of the material[24,25,26,27,29,30,31,32,33,34], while some have considered only a fraction of the material dislodged by the indentation, represented as a factor K_{re}, to become detached debris contributing to material removal[18,28,35,36]. Che *et al.* argued that the wafer material ahead of moving abrasives is deformed in "shear segmentation mode", where sheared material is displaced along the trench and sticks to the wafer. This piled up material is then detached only when scratched by another abrasive.[33]

Table 7.2 Representation of the parameters in equation (7.3) by various researchers

	$K_{re} < 1$	$K_{re} = 1$
Portion of the dislodged material contributing to material removal (K_{re})	Xie *et al.*[18], Zhao *et al.*[28], Che *et al.*[33], Jiang *et al.*[35], Bozkaya *et al.*[36]	Ahmadi *et al.*[24], Fu *et al.*[25], Luo *et al.*[26,29], Bastawros *et al.*[27], Jeng *et al.*[30], Qin *et al.*[31], Bastaninejad *et al.*[32], Zeng *et al.*[34]
	All abrasives near the wafer	Abrasives with certain sizes
Number of abrasive particles involved in the abrasion (n_{ab}^*)	Ahmadi *et al.*[24], Fu *et al.*[25], Bastawros *et al.*[27], Zhao *et al.*[28], Jeng *et al.*[30], Qin *et al.*[31], Bastaninejad *et al.*[32], Che *et al.*[33]	Xie *et al.*[18], Luo *et al.*[26,29], Zeng *et al.*[34], Jiang *et al.*[35], Bozkaya *et al.*[36]
	Plastic deformation	Elastic deformation
Deformation mode of a wafer by the indention of squeezed abrasives	Xie *et al.*[18], Fu *et al.*[25], Luo *et al.*[26,29], Bastawros *et al.*[27], Zhao *et al.*[28], Jeng *et al.*[30], Qin *et al.*[31], Bastaninejad *et al.*[32], Che *et al.*[33], Zeng *et al.*[34], Jiang *et al.*[35], Bozkaya *et al.*[36]	Ahmadi *et al.*[24] (JKR theory)

7.3.2.2 *Number of trapped abrasives*

The number of abrasive particles near the interface of a pad asperity and the wafer, or a fraction of them (discussed below) has been estimated to be the number of abrasive particles that are trapped between the asperity and the wafer, n_{ab}. Its representation by different researchers is tabulated in Table 7.3. Only the dependences on the bulk weight concentration of abrasive particles in a slurry, c_{wt}, and on the average radius of abrasive particles assuming spherical abrasives, r_{ab}, are considered in this work. Other parameters, such as the density of a slurry and abrasives, and the average area of contacts between a pad asperity and a wafer, can be regarded as fixed parameters for a given experimental condition. All of the previous models reviewed in this work assumed that the local concentration of abrasives near the surface of a wafer is equal to that in the bulk. The number concentration of the abrasives in

the bulk slurry with units of particles/cm^3 can be written as:

$$c_{ab} = \frac{3c_{wt}\rho_{slurry}}{4\pi r_{ab}^{3}\rho_{ab}}$$

(7.4)

where ρ_{slurry} and ρ_{ab} is the density of slurry and abrasives, respectively.

Table 7.3 Expressions for the number of abrasive particles trapped between a pad asperity and a wafer by various researchers

Description	Number of trapped abrasives, n_{ab}	References
Conversion of volumetric concentration to areal concentration	$\dfrac{c_{wt}^{2/3}}{r_{ab}^{2}}$	Zhao et al.[28,37], Jiang et al.[35], Choi et al.[38]
Abrasives within a slurry film thickness of r_{ab}	$\dfrac{c_{wt}}{r_{ab}^{2}}$	Ahmadi et al.[24**], Fu et al.[25], Bastawros et al.[27], Qin et al.[31], Bastaninejad et al.[32††], Che et al.[33], Zeng et al.[34††], Brown et al.[39**]
Abrasives within a certain thickness of the slurry film independent of r_{ab}	$\dfrac{c_{wt}}{r_{ab}^{3}}$	Luo et al.[26,29], Jeng et al.[30], Bastaninejad et al.[32]
Modification of Stokes equation	$\dfrac{c_{wt}}{r_{ab}^{1.7}}$	Xie et al.[18]

One group of researchers estimated the number of trapped abrasive particles by directly converting the volumetric concentration of abrasives to an areal concentration by taking the power of 2/3.[28,35,37,38] Then, n_{ab} is proportional to the 2/3 power of the weight concentration of abrasives and inversely proportional to the square of the diameter of the abrasive particles. The resulting number of abrasive particles can be understood as the number of particles lying on a plane through the slurry.

Other researchers used the number of abrasive particles adjacent to the surface of a wafer and within a specified thickness of a slurry film as an estimate of the number of particles trapped between pad asperities and a wafer, as shown in Figure 7.6. n_{ab} is determined by assessing the number of abrasives in the slurry film as:

$$n_{ab} = c_{ab}V_{film}$$

(7.5)

where V_{film} is the volume of the slurry film. The thickness of the slurry film was assumed to be the average diameter of abrasives[25,27,31,33] (Figure 7.6a) or the maximum size of the abrasive particles, which is taken as $d_{ab}+3\sigma_{ab}$ where d_{ab} is the average diameter of abrasives and σ_{ab} is the standard deviation of the abrasive sizes (Figure 7.6b).[32,34] Some researchers

---

** Fill factor, χ
†† Slurry film thickness of $d_{ab}+3\sigma_{ab}$

107

used a fill factor, χ, which is the areal coverage of the surface of a wafer by abrasives, instead of the weight or volumetric concentration.[24,39] The areal coverage of the surface by particles can be interpreted as the volumetric concentration of abrasives in a slurry film with a thickness of d_{ab} at the wafer surface. In this case, n_{ab} is proportional to c_{wt} and roughly inversely proportional to the square of r_{ab}.

It has also been argued that trapped abrasives originate from a slurry film on a wafer with a thickness that is independent of the size of the abrasive particles. Luo and Dornfeld argued that the number of trapped particles is equivalent to the number of abrasives in a slurry film with a thickness of the average height of the pad asperities, h_{ab} (Figure 7.6c).[26,29] Jeng *et al.* used a similar concept but took the thickness of the slurry film to be the change of the heights of the tallest asperities before and after deformation, h_{max}-d, as illustrated in Figure 7.6d[30]. Here h_{max} is the maximum height of the asperities and d is the distance between the surface of a wafer and the mean plane of asperities after the pad asperities have been deformed. Note that the number of trapped abrasives given by cases c and d in Figure 7.6 is much larger than that obtained from cases a and b in Figure 7.6 because of the significant difference in the length scale of the abrasives and the asperities. Thus researchers adopting the cases depicted in Figure 7.6c and Figure 7.6d used a concept of "active abrasives", which are the abrasives within a specific range of sizes, in order to scale down the number of trapped abrasives and thereby the predicted MRR values.[26,29,30] This is further discussed later in this chapter. Bastaninejad *et al.* determined n_{ab} by assuming that only a fraction of the abrasives in the recessed regions on a pad are involved in the abrasion.[32] For those cases, n_{ab} is inversely proportional to the cube of r_{ab} and proportional to c_{wt}, which is consistent with equation (7.4). Researchers who used the concept of "active abrasives" regarded the number of active abrasives to be the number of trapped particles that are involved in abrasion of the wafer material, n_{ab}^{*}, whereas other researchers considered all trapped particles to participate in abrasion. Also, the dependencies of n_{ab} presented in Table 7.3 are equal to those of n_{ab}^{*} because the filtering functions for active abrasives are independent of the size or concentration of abrasives, as discussed below.

Xie *et al.* regarded the number of abrasive particles that have settled onto the surface of pad asperities to be the number actually involved in abrasion.[18] To calculate the settling velocity, they modified Stokes equation through settling experiments using small particles (0.12 − 3 μm diameter) and determined that n_{ab} and n_{ab}^{*} are proportional to c_{wt} and inversely proportional to $r_{ab}^{1.7}$.
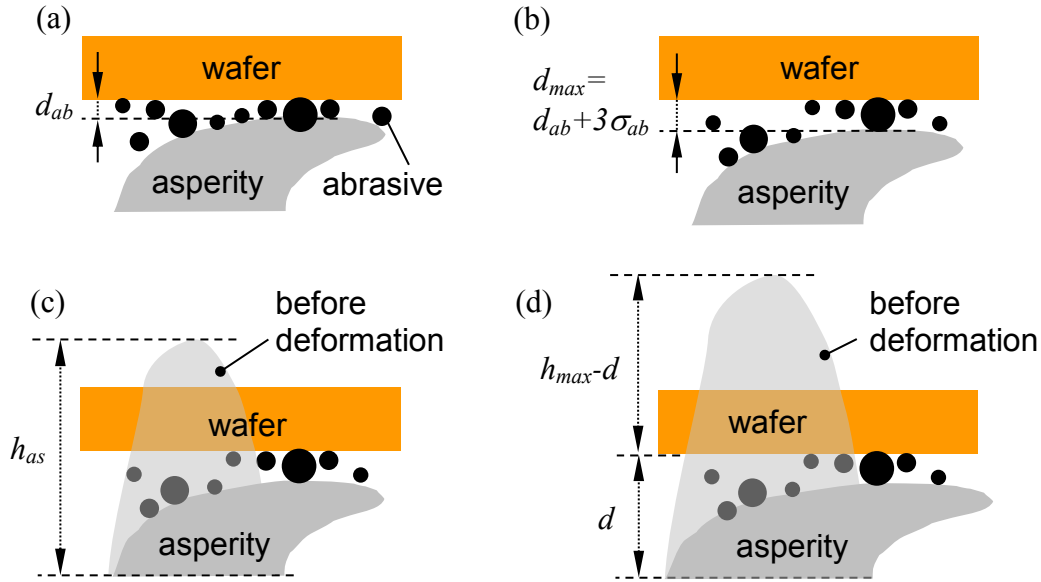
Figure 7.6 Thickness of a slurry film near a wafer used to evaluate the number of abrasive particles that are trapped between a wafer and pad asperities: (a) average diameter of the abrasives, (b) maximum diameter of the abrasives, (c) average height of the asperities, and (d) change in the heights of an asperity of the maximum height before and after deformation.

7.3.2.3 *Active abrasives concept*

Some researchers argued that only a fraction of the trapped abrasives n_{ab} contribute to the removal of a material by abrasion. Xie *et al.* qualitatively explained that a fraction of the abrasives in the vicinity of the wafer surface become trapped between the pad asperities and the wafer, contributing to material removal.[18] Luo and Dornfeld proposed that only abrasives within a certain range of sizes become active or contribute to material removal.[26,29] Assuming a Gaussian distribution of particle sizes, the suggested size limit was between $d_{ab}+3\sigma_{ab}-(h_w+h_{as})$ and $d_{ab}+3\sigma_{ab}$ where h_w and h_{as} are the indentation depth by an abrasive into a wafer and an asperity, respectively. This limit implies that only large enough particles can be squeezed between asperities and a wafer such that they contribute to material removal. Similarly, the criteria adopted by Jiang *et al.*[35] and Bozkaya *et al.*[36] were that the abrasives must be larger than $d_{ab}+3\sigma_{ab}$ and larger than $d_{ab}-h_{as}$, respectively. Zeng *et al.*[34] considered the roughness of the wafer surface, r_a, giving a size limit between $d_{ab}-(h_w+h_{as})+r_a$ and $d_{ab}+3\sigma_{ab}+r_a$. Note that those filtering functions decreased the resultant MRR by reducing the number of abrasives involved in the abrasion. When a Gaussian distribution of the sizes of the abrasives was assumed Jiang, *et al.*'s [35] filtering function indicated that only 0.3% of the trapped abrasives are involved in the material removal. Note that the role of this filtering function is comparable to the factor K_{re}, that is used to account for the partial removal of material dislodged from a wafer by abrasive particles, in that it scales down the MRR. The fltering functions are insensitive to the size of the abrasive particles; instead, they are related to the distribution function of the sizes. Therefore, the dependences of the size and the concentration of the abrasives on the number of the active abrasives can be regarded as

equivalent to the dependences on the number of the trapped particles given in Table 7.3.

7.3.2.4 *Deformation mode of a wafer by squeezed abrasives*

The cross sectional area of a trench on a wafer generated by a squeezed abrasive can be generally expressed as:

$$A_i \propto h_w w_{ab} \qquad (7.6)$$

where h_w is the indentation depth into a wafer of a squeezed abrasive and w_{ab} is the width of such a contact. Indentation by trapped abrasives has usually been analyzed by assuming plastic deformation of the wafer[18,25,26,29,30,32,33,34] or of a chemically modified surface layer on the wafer[27,28,31,35] using the hardness or the yield strength of the material. The adhesion between abrasive particles and the wafer has been considered by some researchers[32] to add a force component to the indentation force. In contrast, Ahmadi *et al.* evaluated the indentation depth using the JKR model (after Johnson, Kendall and Roberts), which is an elastic contact model that considers adhesive forces between the abrasives and the wafer.[24] They also considered the adhesive wear of the wafer material by abrasives during rolling of the abrasives. When a material is deformed elastically, it recovers its shape once the indenting load has been removed, hence this deformation mode cannot induce removal of the material. Therefore, elastic deformation of a wafer is not discussed in this work. The width and the depth of the indentation by a squeezed abrasive has been generalized in the literature as follows. Assuming spherical abrasives and a small penetration depth into a wafer, the width of the indented area can be approximated as:

$$w_{ab} = 2\sqrt{2 r_{ab} h_w} \qquad (7.7)$$

When a wafer is plastically deformed, the depth of the indentation h_w can be expressed as:

$$h_w = \frac{f_{ab}}{\pi r_{ab} H_w} \qquad (7.8)$$

where f_{ab} is the force exerted by a trapped abrasive particle on the wafer and H_w is the hardness of a wafer. For the case where a chemically modified surface layer is indented, the hardness of this layer replaces H_w. The cross sectional area, A_i, of a trench created by a sliding spherical abrasive particle can be expressed as:

$$A_i \propto h_w w_{ab} \propto \frac{f_{ab}^{3/2}}{r_{ab}} \qquad (7.9)$$

110

Then, using equations (7.3) and (7.9), the MRR during CMP can be seen to be proportional to $n_{ab}f_{ab}^{3/2}/r_{ab}$.

7.3.2.5 *Applied force on an abrasive*

The force applied by a squeezed abrasive particle was estimated for different configurations of local contacts between a pad asperity and the wafer between which abrasive particles are embedded, as illustrated in Table 7.4.[24,25,26,27,33,34] The amount of deflection of a pad asperity by the abrasives was determined using the nominal applied pressure on the wafer[27], the compliance of the pad[24,25,26,27,33,34] and the concentration of abrasives[24,25,27,33,34]. In general, smaller sizes and lower concentrations of abrasives, and softer pad materials allow elatively large local deflection of a pad asperity, leading to full contact between the deflected asperity and the wafer (Table 7.4c), whereas larger sizes and higher concentrations of abrasives, and harder pad materials prevent contact between the wafer and pad asperities (Table 7.4a). For intermediate cases, only a part of the deflected asperity contacts the surface of a wafer (Table 7.4b). Some researchers postulated all three of the configurations shown in the figures in Table 7.4a-c[24,27,33,34] while others argued that only one or two of these simulated the real CMP processes[25,26]. The upper bound of the estimated force applied on a squeezed abrasive is when the force exerted on a pad asperity is transmitted only to the squeezed abrasives and the pad asperity is not deflected enough to contact the surface of a wafer (Table 7.4a). This upper bound of the estimated force on an abrasive, f_{ab-ub}, is estimated as:

$$f_{ab-ub} = f_{as}/n_{ab} \qquad (7.10)$$

where f_{as} is the average force transmitted through a single pad asperity.

The lower bound of the estimated force, f_{ab-lb}, is given when a pad asperity is deformed enough to encapsulate the squeezed abrasive particles and to contact the surface of the wafer; so that the force exerted on the asperity is evenly distributed throughout the abrasives and the deformed asperity contacting the wafer (Table 7.4c). Then the force on an abrasive is independent of the number of embedded abrasives as follows:
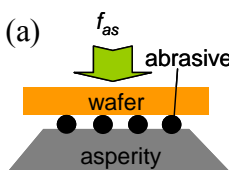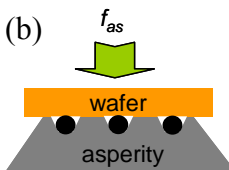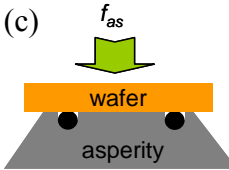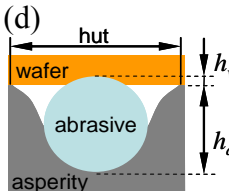
$$f_{ab-lb} = \pi r_{ab}^{2}(f_{as}/a_{as}) \qquad (7.11)$$

where a_{as} is the average area of contact between pad asperities and a wafer.

If the pad asperities are deflected to partly contact the surface of the wafer but do not completely encapsulate the squeezed abrasive (Table 7.4b), the force applied on an abrasive particle will be intermediate between the upper and lower bounds and will inversely be proportional to the area of the contact between the deflected asperity and the wafer. Fu *et al.*[25] modeled the deflection of a pad asperity supported by embedded abrasives using beam theory and evaluated the force applied on an abrasive as:

$$f_{ab} \propto \frac{r_{ab}^{1/4}}{\sqrt{n_{ab}}} \qquad (7.12)$$

Table 7.4 Local contact between a pad asperity and the wafer during CMP: (a) an asperity is not deflected enough to contact the wafer, (b) an asperity is deflected to partly contact the surface of the wafer, (c) an asperity is deformed enough to encapsulate the abrasives and to contact the wafer and (d) a geometric relation between the size of the abrasives and the indentation depth on the wafer and on an asperity.

Local contact mode between an asperity and a wafer	Expressions for f_{ab}	Dependencies of *MRR* on r_{ab} and c_{wt} when n_{ab} has the following proportionalities			
		$n_{ab} \propto \dfrac{c_{wt}^{2/3}}{r_{ab}^2}$	$n_{ab} \propto \dfrac{c_{wt}}{r_{ab}^2}$	$n_{ab} \propto \dfrac{c_{wt}}{r_{ab}^3}$	$n_{ab} \propto \dfrac{c_{wt}}{r_{ab}^{1.7}}$
(a)	$f_{ab} = f_{as}/n_{ab}$	$\dfrac{1}{c_{wt}^{1/3}}$	$\dfrac{1}{c_{wt}^{1/2}}$ [25,27,34] $\dfrac{r_{ab}}{c_{wt}^{3/2}}$ [33‡‡]	$\dfrac{r_{ab}^{1/2}}{c_{wt}^{1/2}}$	$\dfrac{1}{r_{ab}^{0.15}c_{wt}^{1/2}}$
(b)	$f_{ab} \propto \dfrac{r_{ab}^{1/4}}{\sqrt{n_{ab}}}$ [25] (beam theory)	$\dfrac{c_{wt}^{1/6}}{r_{ab}^{9/8}}$	$\dfrac{c_{wt}^{1/4}}{r_{ab}^{9/8}}$ [25,34] $\dfrac{1}{r_{ab}^{7/8}c_{wt}^{1/4}}$ [33‡‡]	$\dfrac{c_{wt}^{1/4}}{r_{ab}^{11/8}}$	$\dfrac{c_{wt}^{1/4}}{r_{ab}^{1.05}}$
	$f_{ab} \propto r_{ab}^2$ [33] (FEM)	$c_{wt}^{2/3}$	$\dfrac{c_{wt}}{r_{ab}c_{wt}}$ [27][33‡‡]	$\dfrac{c_{wt}}{r_{ab}}$	$c_{wt}r_{ab}^{0.3}$
(c)	$f_{ab} = \pi r_{ab}^2(f_{as}/a_{as})$	$c_{wt}^{2/3}$	$\dfrac{c_{wt}}{r_{ab}c_{wt}}$ [27,31,34][33‡‡]	$\dfrac{c_{wt}}{r_{ab}}$ [26,29,32]	$c_{wt}r_{ab}^{0.3}$
(d)	$h_w \propto r_{ab}$	$c_{wt}^{2/3}$ [28,35]	c_{wt}	$\dfrac{c_{wt}}{r_{ab}}$ [30]	$c_{wt}r_{ab}^{0.3}$ [18]

Che *et al.* modeled the contacts between embedded abrasives and a pad asperity using the finite element method (FEM) and argued that the pressure over the deflected region of the asperity around a squeezed abrasive, which is called a hut (see the figure in Table 7.4d) , was concentrated on the abrasive.[33] Since the radius of the hut is proportional to the radius of the abrasive, the force applied on an abrasive is proportional to the square of the radius of the abrasive:

---

‡‡ A term f_{ab}/r_{ab} (=h_w) was multiplied

$$f_{ab} \propto r_{ab}^2 \tag{7.13}$$

The concentration of abrasives increases as the configuration of the interface of a wafer and the pad asperity changes from the figure in Table 7.4c to that in Table 7.4a.

Instead of invoking the force applied on an abrasive, some researchers determined the depth of indentation from the geometric relation between the amount of deflection of the wafer and an asperity and the size of the abrasive. The sum of the indented depth into the pad asperity and into the wafer was assumed to be equal to the diameter of the abrasive assuming encapsulation of the abrasive by the deflected asperity[28,30,35] or to be the diameter of the abrasive less a distance between the tip of the deformed pad asperity and the wafer where deformation was not large enough[18] (Table 7.4d). For those cases the depth of indentation was proportional to the radius of the abrasive:

$$h_w \propto r_{ab} \tag{7.14}$$

This led to the indented cross-sectional area being proportional to r_{ab}^2. Thus, the MRR in this case was proportional to $n_{ab}r_{ab}^2$.

7.3.2.6 *Evaluated dependence of MRR*

The dependencies of material removal rate on the size and the concentration of abrasives are summarized in Table 7.4 for the different configurations of the local pad and a wafer contacts and for various representations of the number of trapped abrasive particles. References for each expression are also given in the table; expressions with no reference indicate those were not found in the literature. Note that Che *et al.* argued the removal of a material only where two scratches by abrasives were intersected.[33] Since the volume of the pile-up material that is removed is proportional to $A_i h_w \omega$, where ω is the angular velocity of the wafer, the final expression for the MRR differs from that of other models by the term h_w which is equal to f_{ab}/r_{ab}. Also note that Fu *et al.* neglected the influence of the size of abrasives on the number of active particles[25]; thus the corrected relationships that consider this influence are shown in Table 7.4.

7.3.2.7 *Limitation of the proposed models*

Since the case (d) in Table 7.4 cannot explain the varying dependencies of MRR on r_{ab} and c_{wt}, only cases (a), (b) and (c) are discussed to compare the predictions with the experimental observations. As the concentration and the size of the abrasives increase, the configuration of the local contacts between asperities and the wafer changes from that of figure (c) to figure (a) in Table 7.4. Figure 7.7 shows the predicted MRR as a function of the concentration of abrasives. Regardless of the precise expression chosen for the number of trapped abrasives, the predicted MRR qualitatively agrees with experimental observations for silicon oxide CMP. For small abrasive particles the local contact mode is represented as shown in figure

(c) in Table 7.4, where the predicted MRR increases with increasing concentration of abrasives, agreeing well with the experimental results shown in Figure 7.2. For intermediate sizes and larger sizes of abrasives, the prediction given in Figure 7.7 also agreed well with the results in Figure 7.2. This implies that the various relationships between MRR and the concentration of abrasives are related to the change of the local contact mode between asperities and the wafer, as illustrated in Table 7.4. However, any of the references cited in this work fully explained all three of the MRR behaviors exhibited using the different contact modes; the researchers examined conditions where only some of the contact modes were at play. Only a part of the MRR behaviors was explained by Fu et al.[25], Bastawros et al.[27] and Che et al.[33]. The ascending portion of the curves in Figure 7.7 also well described the behavior of MRR during metal CMP, provided that the contact mode between the asperities and the wafer follows figure (b) or (c) in Table 7.4. However, there is no experimental finding that the contact mode during metal CMP is as depicted in figure (b) or (c) in Table 7.4.
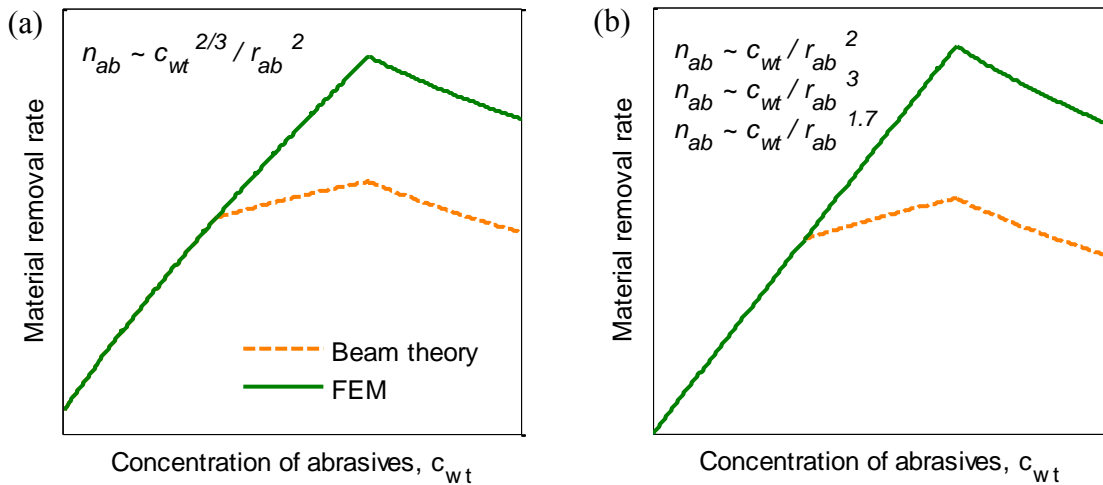
Figure 7.7 Predicted MRR during CMP as a function of the concentration of abrasives when the number of trapped abrasives is proportional to (a) $c_{wt}^{2/3}/r_{ab}^2$ and (b) c_{wt}/r_{ab}^2, c_{wt}/r_{ab}^3 and $c_{wt}/r_{ab}^{1.7}$. Intermediate size of abrasives are assumed giving the configuration in the figure (b) in Table 7.4.

Figure 7.8 shows the predicted MRR as a function of the size of the abrasive particles. The local contact mode between a wafer and a pad asperity changes from the figure (c) to (b) and (a) in Table 7.4 as the size of abrasives increases. Since the predicted effect of abrasive particle size on MRR is indenpendent of the concentration of abrasives or inconsistent with the experimental observations presented in Figure 7.3, Figure 7.4 and Figure 7.5, the models assuming abrasion of a wafer by abrasive particles are unsuccessful explaining the influence of the size of abrasives on the MRR. It is evident from the contrasting experimental observations in Figure 7.4 and Figure 7.5 which used similar concentrations of abrasives with similar sizes that the dependence of MRR on the size of abrasives is not solely determined by the local contact mode between asperities and the wafer. Considering that different slurries containing different chemical additives at different pHs were used to generate the data shown

114

in Figure 7.4 and Figure 7.5, the chemical additives and/or the pH of the slurry are most likely responsible for the contrasting observations. This is discussed further in Chapter 8.
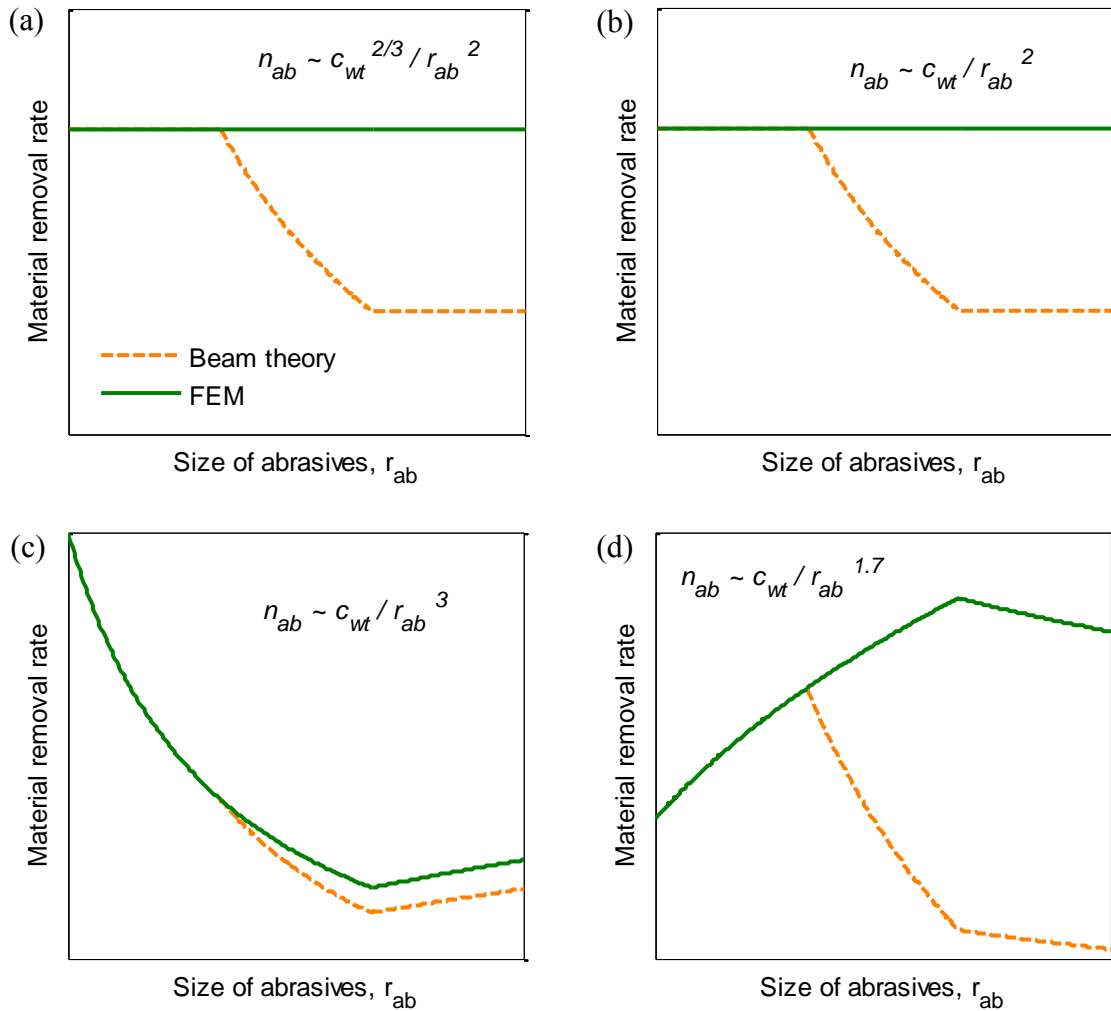
Figure 7.8 Predicted MRR during CMP as a function of the size of the abrasive particles when the number of trapped abrasives is proportional to (a) $c_{wt}^{2/3}/r_{ab}^{2}$, (b) c_{wt}/r_{ab}^{2}, (c) c_{wt}/r_{ab}^{3} and (d) $c_{wt}/r_{ab}^{1.7}$

It is interesting to note that the dependencies of MRR on r_{ab} and c_{wt} in the equations in Table 7.4 are qualitatively similar to those predicted by the contact area- and indentation-based mechanisms proposed by Bielmann et al.[12] in which the concentration of the trapped abrasives is expressed as being proportional to $\dfrac{c_{wt}}{d_{ab}^{3}}$. Both the proposed models assuming abrasion of a wafer by abrasive particlesand the model proposed by Bielmann et al.[12] were unsuccessful in explaining the various trends of MRR with the size of abrasives although both models well explained the MRR behavior with the concentration of abrasives.

115

7.3.3 Other proposed mechanisms

A model by Che et al.[33] described increasing MRR with increasing sizes of abrasives for all the local contact modes in Table 7.4. This model cannot explain the decrease in MRR with increasing size of abrasives unless the force relationship in equation (7.12) is used for the force applied on an abrasive. However, equation (7.12) was derived assuming beam theory for the deflection of the pad; the validity of this assumption is questionable because of the different dimensions of the two dimensional beam and the three dimensional polishing pad. In addition, the argument that material was only removed during CMP at the piled up region formed by a sliding abrasive particle, and the corresponding expression for the volume removed by an abrasive, was based on a scratching experiment using a micro-scale indenter[40]. However, the detachment of piled up material at the nano-scale where abrasive particles and the wafer contact[41] may be very different from that at the macro- or micro-scales, which calls for further verification at the nano-scale.

There have also been efforts to account for the presence of the optimal size of the abrasive particle where the MRR is maximized, as illustrated in Figure 7.2b. Zhou et al. observed a maximal MRR during SiO$_2$ CMP at a certain size of abrasives for silica abrasive particles 10 to 140 nm in size, under various down pressures and sliding velocities. They suggested that only particles of a certain size range can be entrained between pad asperities and the wafer because the thickness of the slurry film between the asperities and the wafer changes with the down pressure and the sliding velocity.[3] It was implicitly assumed by Zhou et al. that the number of abrasives trapped between asperities and the wafer is proportional to the material removal rate during the process, regardless of the particle size. Zeng et al. considered the evolution of the surface roughness of a wafer with time to estimate the thickness of the gap between the wafer and pad asperities.[34] The material removal rate was obtained by considering the total volume on a wafer that is indented by squeezed or active abrasives. Note that the MRR they obtained was actually the material removal rate at the contact regions between pad asperities and a wafer, not for the entire wafer. Cooper et al. argued that the material removal rate for silicon oxide with silica abrasives is determined by the collisions of the abrasive particles to the surface. The increasing MRR with increasing concentration was due to the decreased mean particle separation, which was a power of 1/3 of the weight concentration of abrasives.[4] Apparently, those models described only a part of the experimentally observed MRR behaviors.

7.4 Summary

In summary, the models proposed to account for the dependencies of MRR during CMP on the size and the concentration of abrasives can largely be divided into two categories: one was the model of Bielmann et al. where the relevance of a specific mechanism, either contact area-based or indentation-based mechanism, was determined by the size of abrasive particles, and the other is the models that predicted the material removal rate during CMP as a sum of the amount of material abraded by particles trapped between the wafer and pad asperities. The latter models postulated three different modes of local contact between pad asperities and the wafer between which abrasive particles are trapped. The deflection of the pad asperity was varied by the size and the concentration of the abrasives so that the deflected

asperity may or may not contact the surface of a wafer. Both of those models successfully analyzed the MRR behavior for varying concentration of the abrasives, especially for oxide CMP. However, none of those models could capture the various MRR behaviors observed for different sizes of abrasives. Therefore, the current models are inadequate at explaining various MRR trends with the size of the abrasive particles. A novel approach to addressing this will be discussed in Chapter 8.

References

[1] R. Jairath, M. Desai, M. Stell, R. Tolles and D. Scherber-Brewer, *Mat. Res. Soc. Symp. Proc.*, **337**, 121 (1994).

[2] U. Mahajan, M. Bielmann and R. K. Singh, *Mat. Res. Soc. Symp. Proc.*, **566**, 27 (2000).

[3] C. Zhou, L. Shan, J. R. Hight and S. Danyluk, *Tribol. Trans.*, **45**, 232 (2002).

[4] K. Cooper, J. Cooper, J. Groschopf, J. Flake, Y. Solomentsev and J. Farkas, *Electrochem. Solid-State Lett.*, **5**, G109 (2002).

[5] A. Philipossian and S. Olsen, *Mat. Res. Soc. Symp. Proc.*, **767**, F2.8.1 (2003).

[6] W. Choi, J. Abiade, S.-M. Lee and R. K. Singh, *J. Electrochem. Soc.*, **151**, G512 (2004).

[7] W. Choi and R. K. Singh, *Jpn. J. Appl. Phys.*, **44**, 8383 (2005).

[8] B. Park, H. Lee, Y. Kim, H. Kim and H. Jeong, *Jpn. J. Appl. Phys.*, **47**, 8771 (2008).

[9] B. Park, S. Jeong, H. Lee, H. Kim, H. Jeong and D. A. Dornfeld, *Jpn. J. Appl. Phys.*, **48**, 116505 (2009).

[10] Z. Zhang, W. Liu and Z. Song, *Microelectron. Eng.*, **87**, 2168 (2010).

[11] Q. Luo, S. Ramarajan and S. V. Babu, *Thin Solid Films*, **335**, 160 (1998).

[12] M. Bielmann, U. Mahajan and R. K. Singh, *Electrochem. Solid-State Lett.*, **2**, 401 (1999).

[13] Y. Li, M. Hariharaputhiran and S. V. Babu, *J. Mater. Res.*, **16**, 1066 (2001).

[14] L. Guo and R. S. Subramanian, *J. Electrochem. Soc.*, **151**, G104 (2004).

[15] H. Lee, S. Joo and H. Jeong, *J. Mater. Process. Technol.*, **209**, 6134 (2009).

[16] K. Yoshida, *J. Sol-Gel Sci. Technol.*, **43**, 9 (2007).

[17] M.-H. Oh, R. K. Singh, S. Gupta and S.-B. Cho, *Microelectron. Eng.*, **87**, 2633 (2010).

[18] Y. Xie and B. Bhushan, *Wear*, **200**, 281 (1996).

[19] S. Armini, C. M. Whelan, M. Moinpour and K. Maex, *J. Electrochem. Soc.*, **156**, H18 (2009).

[20] Z. Zhang, W. Liu and Z. Song, *Appl. Opt.*, **49**, 5480 (2010).

[21] Z. Lu, S.-H. Lee, S. V. Babu and E. Matijevic, *J. Colloid Interface Sci.*, **261**, 55 (2003).

[22] S. Armini, C. M. Whelan and K. Maex, *Electrochem. Solid-State Lett.*, **11**, H280 (2008).

[23] G. B. Basim, J. J. Adler, U. Mahajan, R. K. Singh and B. M. Moudgil, *J. Electrochem. Soc.*, **147**, 3523 (2000).

[24] G. Ahmadi and X. Xia, *J. Electrochem. Soc.*, **148**, G99 (2001).

[25] G. Fu, A. Chandra, S. Guha and G. Subhash, *IEEE Trans. Semicond. Manuf.*, **14**, 406 (2001).

[26] J. Luo and D. A. Dornfeld, *IEEE Trans. Semicond. Manuf.*, **14**, 112 (2001).

[27] A. Bastawros, A. Chandra, Y. Guo and B. Yan, *J. Electron. Mater.*, **31**, 1022 (2002).

[28] Y. Zhao and L. Chang, *Wear*, **252**, 220 (2002).

[29] J. Luo and D. A. Dornfeld, *IEEE Trans. Semicond. Manuf.*, **16**, 469 (2003).

[30] Y.-R. Jeng and P.-Y. Huang, *Electrochem. Solid-State Lett.*, **7**, G40 (2004).

[31] K. Qin, B. Moudgil and C.-W. Park, *Thin Solid Films*, **446**, 277 (2004).

[32] M. Bastaninejad and G. Ahmadi, *J. Electrochem. Soc.*, **152**, G720 (2005).

[33] W. Che, Y. Guo, A. Chandra and A. Bastawros, *J. Manuf. Sci. Eng.*, **127**, 545 (2005).

[34] T. Zeng and T. Sun, *IEEE Trans. Semicond. Manuf.*, **18**, 655 (2005).

[35] J.-Z. Jiang, Y.-W. Zhao, Y.-G. Wang and J.-B. Luo, *Wear*, **265**, 992 (2008).

[36] D. Bozkaya and S. Muftu, *J. Electrochem. Soc.*, **156**, H890 (2009).

[37] Y. Zhao, L. Chang and S. H. Kim, *Wear*, **254**, 332 (2003).

[38] W. Choi, S.-M. Lee, J. Abiade and R. K. Singh, *J. Electrochem. Soc.*, **151**, G368 (2004).

[39] N. J. Brown, P. C. Baker and R. T. Maney, *Proc. SPIE,* **306**, 42 (1981).

[40] W. Che, Y. Guo, A. Chandra and A.-F. Bastawros, *ASME J. Manuf. Sci. Eng.*, **125**, 731 (2003).

[41] S. Choi, F. M. Doyle and D. Dornfeld, *Procedia Eng.*, **19**, 73 (2011).

Chapter 8
Explanation of the Dependencies of MRR during CMP on the Size and the Concentration of Abrasives by Considering the Deposition of Abrasives on the Surface of a Wafer

8.1 Introduction

Chemical Mechanical Planarization (CMP) is an enabling technology for multilevel metallization during semiconductor manufacturing processes. The uneven topography resulting from the deposition processes is planarized during CMP, enabling subsequent deposition or lithography processes. It is believed that the chemical and mechanical actions interact synergistically during CMP to remove material from protruding areas of the wafer surface while protecting the recessed areas, allowing planarization of the surface. The chemical composition of the slurry varies according to the application, but slurries usually contain abrasive particles with a diameter on the order of 10 to 100 nm, as well as chemical additives such as oxidizing agents (for metal CMP), complexing agents, inhibitors and surfactants. The effect of each chemical additive and the abrasive particles on material removal has been extensively studied. Among others, the influence of the abrasive particles on the performance of the CMP process has attracted significant interest, as reviewed in Chapter 7. The effect of increasing weight concentration of abrasives in a slurry on the material removal rate (MRR) during CMP of various materials has been investigated by a number of researchers, as summarized in Table 8.1. For CMP of silicon oxide, the measured MRR increased[1,2,3,4,5,6,7,8,9], peaked[2,5,6] or decreased[2] with increasing weight concentration of the abrasives. For silicon CMP an increasing[10] or increasing and then decreasing[11] MRR was observed. However for CMP of metals such as tungsten[1,12], copper[4,13,14,15,16] and tantalum[13] the observed MRR only increased with increasing weight concentration of the abrasives and no decreasing trend was observed. The influence of the size of the abrasives in the slurry on the MRR during CMP has also been studied. The MRR during CMP of silicon oxide the MRR increased[6,17], increased and then decreased[3,18] or decreased[6,7] with the increase in the size of the abrasives. Similar trends were observed for metal CMP in that the MRR increased[19,20], increased and then decreased[18] or decreased[12,14,21]. Those experimental observations were theoretically explained by a model that predicts MRR using the volume of a wafer indented by the abrasives particles.[22,23,24,25,26,27,28,29] Also, Bielmann *et al.* proposed two competing mechanisms, namely a contact area-based or an indentation-based

mechanism, where the dominant mechanism is determined by the size of the abrasive particles.[2,12, 30] They argued that the contact area-based mechanism dominates material removal for small abrasive particles, whereas the indentation-based mechanism prevails for larger abrasives. The proposed models, especially that of Mahajan *et al.*[2], described the effect of the weight concentration of the abrasive on the MRR well. However, none of these models could capture the various effects of abrasive particle size on the MRR. The model of Bielmann *et al.*[12] predicted that the MRR will decrease and then rise with increasing size of the abrasives - but this prediction is the exact opposite of the experimental observation of Zhang *et al.*[18]. The models based on the volume of the wafer indented by the abrasives predicted that the MRR will be independent of the size of the abrasives, or will decrease and then increase with increasing abrasive size if the number of abrasive particles participating in the abrasion is inversely proportional to the square or cube of the size of the abrasives, respectively. Therefore, the current models are inadequate at explaining various MRR trends with the size of the abrasive particles. Considering that the proposed models described the effect of abrasive concentration on MRR well, the proposed mechanism of material removal, in which three different local contact modes between an asperity and a wafer are envisaged and the removal of the plastically deformed material by abrasives is assumed, seemed to be valid, although some modification of the removal of the plastically deformed material is needed as described in Chapter 6. The reason for the inadequacy of the models for describing the MRR behavior for the different sizes of abrasives is largely attributed to the poor estimation of the number of abrasive particles that are involved in the material removal. This has usually been estimated based on the bulk concentration of abrasives. However, the transportation of colloidal particles in a suspension is size dependent, so it would not be surprising if transportation affects the number of attached particles. Also, it is well known that the attachment of colloidal particles onto a substrate like a wafer is strongly influenced by the surface potentials of the particles and substrate. Therefore, the transportation mechanisms and the zeta potential of the particles and the wafer must be taken into account to accurately describe the number of abrasives participating in abrasion of a material.

The zeta potentials of the abrasive particles and the wafer have been considered to affect the MRR during CMP.[31,32,33,34,35,36,37] The zeta potential of the abrasive particles determines the size of the agglomerates[38,39,40], and it has also been shown that attractive interactions between the abrasive particles and the wafer surface increase the MRR while repulsive interactions reduce the MRR.[31,32,33,34] Lu *et al.*[34] and Abiade *et al.*[35] argued that this change of the MRR is due to a change in the number of abrasive particles deposited on the surface of the wafer, but they did not explore this quantitatively. The ionic strength of the slurry has also been suggested to influence the MRR by affecting the magnitude and range of the electrostatic interactions between the wafer and the abrasives.[32,36] Again, however, no quantitative analysis was conducted in these studies.

Table 8.1 Effect of the size or weight concentration of abrasive particles in a slurry on the experimentally observed material removal rates during CMP of various materials.

	Effect of increasing concentration or size on MRR	Silicon Oxide or Silicon CMP
Weight concentration	Increasing	Jairath *et al.*[1], Mahajan *et al.*[2], Zhou *et al.*[3], Cooper *et al.*[4], Philipossian *et al.*[5], Choi *et al.*[6,7], Park *et al.*[8,10§§], Zhang *et al.*[9]
	Increasing then decreasing	Mahajan *et al.*[2], Philipossian *et al.*[5], Choi *et al.*[6], Yoshida *et al.*[11§§]
	Decreasing	Mahajan *et al.*[2]
Size	Increasing	Choi *et al.*[6], Oh *et al.*[17]
	Increasing then decreasing	Zhou *et al.*[3], Zhang *et al.*[18]
	Decreasing	Choi *et al.*[6,7]

The work reported in this chapter relates these two areas of interest, namely the mechanical removal of the material by abrasive particles and the influence of slurry chemistry on the deposition of the abrasives on the surface of a wafer, to quantitatively explain the dependencies of the MRR on the size or the weight concentration of abrasives in a slurry during CMP. In addition, theories of colloid science were adopted to delve into the poorly understood interactions between the abrasive particles in a slurry and the surface of a wafer.

8.2 Interaction of the abrasive particles with the surface of a wafer

The flux of abrasive particles that contact the surface of a wafer during planarization was estimated by considering the rate of such contacts in the laminar flow developed by the relative motion of the wafer with regard to the pad while slurry is present between them. The flow of the slurry between the pad and the wafer during CMP remains laminar because of the low Reynold's number, 0.1 to 50, calculated from the slurry film thickness at the troughs of the pad asperities[41,42,43]. A contact is highly dependent on the surface forces between the abrasive particles and the wafer, such as the London van der Waals force and the electrical double layer interaction force. The overall electrostatic interaction between the abrasive particle and the wafer surface is described by the DLVO (Derjaguin-Landell-Verway-Overbeek) theory. For opposite signs of the charges of the particle and the wafer surface or no surface charges (favorable condition), the interaction between them is attractive so that the contact of particles with the surface is controlled by the transport of the abrasive particles toward the surface. The electrostatic interaction between the surface and the particle attracts the particle toward the surface and the particle adheres to the surface at the primary minimum of the interaction potential because of the dispersion interaction between them.

In contrast, when the particles and the surface have the same charge (with a repulsive electrostatic force), the DLVO theory predicts the presence of an energy barrier that the

---

§§ Silicon

particles must overcome to collide with the surface (Figure 8.1a). The extent of the energy barrier depends upon the ionic strength; for typical CMP slurries it is of the order of a few nanometers from the surface. The magnitude of the barrier increases with the surface potential and the size of the particle by DLVO theory.[44] The rate of deposition with electrostatic repulsion, j, is related to that with electrostatic attraction, j_0, by the particle collision efficiency, α as follows:[45,46]

$$j = \alpha j_0 \qquad (8.1)$$
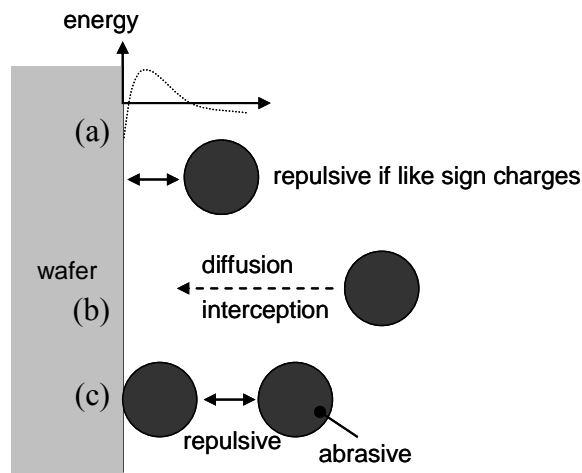
Figure 8.1 Deposition of abrasive particles on the surface of a wafer. (a) An energy barrier is present when the charges on the wafer and the particle have the same signs. (b) Transport of the abrasives toward the surface is dominated by diffusion or interception, depending on the size of the abrasives. (c) Repulsive interaction exists between deposited abrasives and the incoming ones.

While current theories predict well the rate of the deposition of particles under favorable conditions (with electrostatic attraction), they do not predict well the rate of deposition[47,48] under unfavorable conditions (with electrostatic repulsion), predicting much lower particle attachment rates than experimental observations[49,50,51,52]. The discrepancy has been attributed to the heterogeneous charge distribution on the surface[44,48,49,53,54], hydrodynamic particleparticle and particle-surface interactions (although these contributions are small)[52], the dynamics of interaction[55], deposition in a secondary minimum (which is not likely to occur)[48,56,57,58,59,60,61], surface roughness[44,49,56,62,63,64,65,66,67], and the presence of other deposited particles[68].

The DLVO theory predicts an energy barrier that is higher for larger particles[44], but experimentally, the particle collision efficiency (defined as the ratio of the number of particles deposited on the surface in the presence of the barrier to that in absence of the barrier) is independent of the size of the particles.[44,48] It was shown that the range of the electrostatic interaction, characterized as the Debye length κ, is much more important than the strength of the interaction in favorable condition.[69,70]

Although fewer particles are deposited on the surface under unfavorable conditions than

under favorable conditions, the efficiency, α, is independent of the size and concentration of the abrasives. Thus the following discussion focuses on the number of abrasive particles deposited on the surface of a wafer under favorable conditions, and estimates the number under unfavorable conditions using the particle collision efficiency. The influence of the gravity on the transportation of the abrasive particles was not considered because the size of the abrasives lies within the colloidal size range, which is usually considered in between 1 nm and 1 μm.[71]

Figure 8.2 shows schematically the interface between a wafer and a CMP pad during copper CMP. The pad asperities contact the surface of the wafer as they are deformed by the applied down pressure and slide across the surface of the wafer. Between the asperities and the wafer are abrasive particles that have been deposited on the surface from the bulk slurry. The trapped abrasives are involved in the abrasion of the surface of the wafer that removes protective surface layer or the wafer material. Such an interaction between an asperity and a wafer at a point on the wafer occurs every t_{as-as}, which is determined from the characteristics of the contact area between the pad and the wafer and the sliding velocity of the wafer over the pad as follows:

$$t_{as-as} = \frac{\pi d_{as}}{4 v r_{contact}} \qquad (8.2)$$

where v is the sliding velocity of the wafer over the CMP pad, $r_{contact}$ the fraction of real area of contact between a CMP pad and a wafer and d_{as} is the average diameter of the circular contact areas between asperities and wafer. During CMP abrasive particles can only be deposited on the surface of a wafer during t_{as-as}, which is of the order of 1 -10 ms.[72] The deposited abrasives are periodically contacted by the pad asperities with this time interval.
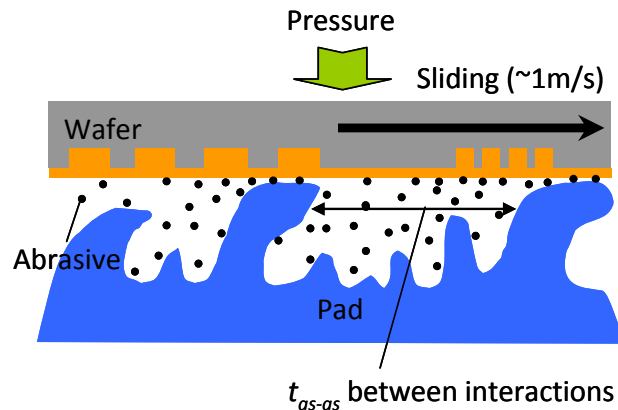
Figure 8.2 Interface of a wafer and a CMP pad during copper CMP. Asperities contact a point on the wafer every t_{as-as}.

The number of abrasive particles that participate in the removal of the material can be estimated using the number of abrasive particles deposited during t_{as-as}. It was assumed that only a fraction f_{ra} of the deposited abrasives adhere to the pad asperity while trapped between the wafer and the asperity and move away from the original deposition site, leaving some fraction f_{rw}, smaller than 1-f_{ra}, of the deposited abrasives remaining on the surface of the wafer after such an interaction. Some other fractin of the abrasives is detached from the surface of the wafer during the interaction with the pad asperities. Then the number of abrasive particles, n_{ab}^*, participating in abrasion when the next asperity slides across the same point on

the surface can be determined by adding the number of abrasive particles remaining on the surface of the wafer and on the tip of the asperity and the newly deposited abrasives during t_{as-as}, n_{dep}. The number of the abrasives participating in abrasion by the next asperity can be determined as:

$$n_{ab}^* = f_{rw}n_{ab}^* + f_{ra}n_{ab}^* + n_{dep} \tag{8.3}$$

It is assumed that the number of the abrasive particles involved in the abrasion is at a steady state, constant value for each interaction by the asperities. Also, any abrasive particles depositing on the surface of the asperity tip from the bulk slurry during t_{as-as} were considered to leave again, and not become trapped between the asperity and the wafer when they next approached each other. These assumptions allow equation (8.3) to be simplified as:

$$n_{ab}^* = \frac{n_{dep}}{1 - f_{rw} - f_{ra}} \tag{8.4}$$

Assuming that the sum of the fractions f_{rw} and f_{ra} are independent of the size and the weight concentration of the abrasives, the dependencies of the number of abrasives involved in the abrasion n_{ab}^* on the size and the weight concentration of the abrasives are equal to those of the number of the deposited abrasives n_{dep} following equation (8.4). Therefore, the number of abrasive particles deposited on the surface of a wafer was investigated to evaluate the dependencies of the number of abrasives participating in the abrasion and thereby the MRR on the size and the weight concentration of the abrasives.

8.2.1 Deposition of abrasives dominated by transportation

The influence of electrostatic interaction is negligible until the distance between the abrasive particles and the surface of the wafer becomes comparable to the distance of the secondary minima of the interaction potentials. Transport of the abrasive particles up to this distance can be described as the convective diffusion in a laminar flow. However, analytically solving the convective diffusion equation is challenging and requires numerical calculation.[73] The rotating wafer during CMP can be modeled as a rotating disk. The Peclet number Pe that describes the ratio of the hydrodynamic and diffusion effects for particles moving near a rotating disk can be written as[74]

$$\text{Pe} = \frac{1.02\omega^{3/2}r_{ab}^3}{v_k^{1/2}D_\infty} \tag{8.5}$$

where ω is the rate of rotation of the wafer, r_{ab} is the average radius of the abrasives, v_k is the kinematic viscosity of the slurry and D_∞ is the Brownian diffusion coefficient of the particles, which can be expressed as:

$$D_\infty = kT / 6\pi\eta_v r_{ab} \tag{8.6}$$

where k is the Boltzman constant, T is the temperature and η_v is the viscosity of the slurry for spherical particles given by the Stokes-Einstein equation. The Peclet number during CMP where the wafer is rotating at 60 rpm and the viscosity of water is used instead of the slurry viscosity ranges from 7.3×10^{-10} to 7.3×10^{-6} for average abrasive radius of 10 -100 nm. These small values imply that the transport of abrasive particles during CMP is dominated by the diffusion of the particles rather than the hydrodynamic flow of the slurry. Thus, instead of solving the complex convective diffusion equation, a simple diffusion equation was used to evaluate the concentration of the abrasive particles during CMP.

Since the surface of the wafer is equally accessible everywhere by the abrasive particles, the diffusion of abrasive particles can be described by one dimensional diffusion equation:

$$\frac{\partial C_{ab}}{\partial t} = D_\infty \frac{\partial^2 C_{ab}}{\partial h^2} \tag{8.7}$$

where C_{ab} is the number concentration of the abrasives per unit volume and h is the distance from the surface of a wafer. When an abrasive particle diffuses closely enough, i.e. the distance of the primary minimum of the interaction energy, to the surface of the wafer the particle is deposited on the surface and does not move from the location where it is deposited. Using this "perfect sink"[75] assumption the boundary condition of the diffusion equation can be simplified to $C_{ab}(0, t)=0$. Also the initial condition can be described as $C_{ab}(h, 0)=C_\infty$ assuming that the abrasive particles are uniformly dispersed throughout the slurry. The number concentration of the abrasives in the bulk C_∞ can be expressed using the weight concentration and the average radius of the abrasives as:

$$C_\infty = \frac{3c_{wt}\rho_{slurry}}{4\pi r_{ab}^3 \rho_{ab}} \tag{8.8}$$

where ρ_{slurry} and ρ_{ab} is the density of slurry and abrasives, respectively. The solution of the diffusion equation, then, is:

$$C_{ab}(h,t) = C_\infty erf\left(\frac{h}{\sqrt{4D_\infty t}}\right) \tag{8.9}$$

The flux of the abrasives per unit area toward the surface of the wafer by diffusion $(j_{ab})_d$ can be obtained as:

$$(j_{ab})_d = D_\infty \frac{\partial C_{ab}}{\partial h}\bigg|_{h=0} = C_\infty \sqrt{\frac{D_\infty}{\pi t}} \tag{8.10}$$

Assuming that all the abrasive particles that diffuse toward the wafer are deposited on the surface, the number of particles deposited per unit area during consecutive asperity and wafer interactions t_{as-as} is obtained using equation (8.6), (8.8) and (8.10) as:

$$N_{ab} = \int_0^{t_{as-as}} j_{ab}dt = 2C_\infty \sqrt{\frac{D_\infty t_{as-as}}{\pi}} = \frac{3\rho_{slurry}}{2\pi^2 \rho_{ab}} \sqrt{\frac{kT t_{as-as}}{6\eta_v}} \frac{c_{wt}}{r_{ab}^{7/2}} \tag{8.11}$$

Further assuming that the abrasive particles are irreversibly deposited only on the surface of a wafer, not onto particles already deposited on the surface (for which there would be electrostatic repulsion unless the particles were uncharged), the fraction of the wafer surface, θ_{ab}, covered by particles can be calculated as:

$$\theta_{ab} = \pi r_{ab}^2 N_{ab} = \frac{3\rho_{slurry}}{2\pi\rho_{ab}} \sqrt{\frac{kT t_{as-as}}{6\eta_v}} \frac{c_{wt}}{r_{ab}^{3/2}} \tag{8.12}$$

It shows that the fraction covered by the abrasives linearly increases with the weight concentration of the abrasives and inversely proportional to the 3/2 power of the radius of the abrasives. This means that for a given t_{as-as} the fraction of the surface covered by abrasives deposited by diffusion decreases as the abrasive size increases.

Unlike the transport of abrasive particles by diffusion (equation (8.10)), the transport of abrasive particles by interception increases with increasing particle size for a given number concentration of the abrasives, which is pronounced for particles larger than 500 nm, which have alarge Peclet number.[45,46,69,70,76] Interception dominates for larger particles because of the increased contribution of the convective flowof the slurry relative to diffusion for larger particles. The rotation of a wafer during CMP causes the slurry to flow perpendicular to the surface of the wafer as well as tangentially. Due to this perpendicular component of the slurry flow abrasives particles with significant size move toward the surface and are deposited on the surface. For a rotating disk substrate such as a wafer during CMP, the interception flux $(j_{ab})_i$ is expressed using the slurry flow in the perpendicular direction as[69,77,78]

$$(j_{ab})_i = 0.51 \frac{\omega^{3/2}}{v_k^{1/2}} f^2 r_{ab}^2 C_\infty \tag{8.13}$$

where f is the ratio of the effective interaction radius of a particle to the radius of the particle

defined as $f = 1 + \frac{\xi}{\kappa r_{ab}} - \frac{2}{\kappa r_{ab}} \ln(1 + \frac{\xi}{\kappa r_{ab}})$ and $\xi = \ln \frac{2\varepsilon \kappa r_{ab}^2 |\zeta_{ab}\zeta_w|}{\mathrm{Pe}kT}$, ζ_{ab} and ζ_w are the zeta

potentials of the abrasives and the wafer, respectively. Equation (8.13) can be rewritten using equation (8.8) as

$$(j_{ab})_i = 0.12 \frac{c_{wt}\rho_{slurry}\omega^{3/2}f^2}{\rho_{ab}v_k^{1/2}r_{ab}} \tag{8.14}$$

Assuming steady state flux and irreversible deposition of all the transported particles on the surface, the number of abrasive particles deposited per unit area between consecutive asperity and wafer interactions t_{as-as} is

$$N_{ab} = 0.12 \frac{\rho_{slurry}\omega^{3/2}f^2 t_{as-as}}{\rho_{ab}v_k^{1/2}} \frac{c_{wt}}{r_{ab}} \tag{8.15}$$

Then the fraction of the surface covered becomes proportional to the size of the abrasive particles as follows:

$$\theta_{ab} = 0.38 \frac{\rho_{slurry}\omega^{3/2}f^2 t_{as-as}}{\rho_{ab}v_k^{1/2}} c_{wt} r_{ab} \tag{8.16}$$

Unlike the deposition of abrasives by diffusion, the fractional coverage due to interception increases with the size of the abrasives along with the weight concentration.

8.2.2 Jamming of the surface of a wafer with the deposited abrasives

As the fraction of the surface covered by abrasive particles increases, the deposition of additional particles becomes harder because the surface is increasingly occupied by other particles. Although some of the surface may be unoccupied by other abrasive particles, an approaching particle can be deposited only when it approaches a vacant site, which becomes increasingly improbable as the surface saturates. A particle approaching an occupied site will be repelled and move in the slury in a Brownian manner. This type of behavior is well described by a random sequential adsorption (RSA) model.[69,79,80,81] In the RSA model, particles are irreversibly deposited on a surface within the first monolayer and block and reject the deposition of additional particles onto that monolayer. Lateral diffusion of

deposited particles is not considered. The rejected particles behave like other particles in the slurry. The maximum attainable fractional surface coverage, the jamming limit θ_{jam}, using the RSA model is 0.547 for monodispersed hard spheres where the interaction between particles is not considered.[82,83,84] Note that this limit is lower than the maximum coverage by monodispersed particles, 0.91, which can only be achieved if the particles are able to diffuse along the surface. When repulsive interparticle interactions are considered, the RSA model with hard spheres is inappropriate; instead an effective hard particle approximation can be used.[85] In this approach colloid particles are treated as hard spheres whose radius is extended by the effective interaction range of the electrostatic interactions, h^* (Figure 8.3). Then the equivalent hard sphere radius r_{ab}^* is given by:

$$r_{ab}^* = r_{ab} + h^*$$

(8.17)

The area in which the center of other particles cannot be deposited is indicated in Figure 8.3 as the geometrically excluded area S_e.
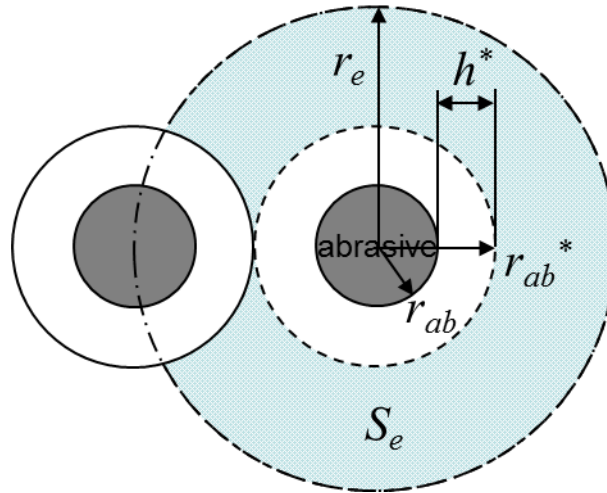
Figure 8.3 Interaction of two deposited abrasive particles. The effective hard sphere is shown as the circle with a dashed line and the geometrically excluded area S_e for RSA is indicated as the shaded area. The solid circle is an abrasive particle.

Adamczyk et al. showed that the dimensionless effective interaction range ($H^*=h^*/r_{ab}$) is linearly proportional to $1/\kappa r_{ab}$, i.e. the effective interaction range h^* is linearly proportional to the Debye length κ^{-1}, for a broad range of κr_{ab} and obtained the proportionality constant by comparing the interaction energy of a pair of spherical particles with a characteristic energy to determine the equivalent hard sphere radius[85]. Russel et al. analytically obtained the equivalent hard sphere radius by comparing the interaction energy with the thermal energy[86] as

$$r_{ab}^* = \frac{\ln(A/\ln A)}{2\kappa}$$

(8.18)

where $A = \dfrac{\lambda Z^2 \kappa L_B \exp(2\kappa r_{ab})}{1 + \kappa r_{ab}}$ for monodispersed spherical particles, λ is an appropriate constant, Z is the effective charge of a particle and L_B is the Bjerrum length, which is about 0.72 nm in water. Semmler et al. showed that the equivalent hard sphere radius given by equation (8.18) agreed well with the results of Adamczyk et al.[87] when $\lambda=2.8$. They used a

saturated effective charge, which is determined by[88,89]

$$Z = \frac{r_{ab}(4\kappa r_{ab} + 6)}{L_B}$$

(8.19)

The maximum fractional surface coverage by abrasive particles at the jamming state is expressed using the equivalent hard sphere radius as:

$$\theta_{max} = \theta_{jam}(r_{ab}/r_{ab}^{*})^2$$

(8.20)

and is shown as a function of κr_{ab} in Figure 8.4 for various κ and r_{ab} values. The Debye parameter κ is proportional to the square root of the ionic strength of the slurry. Figure 8.4 shows that the maximum surface coverage increases with increasing particle size for a given Debye parameter. This is due to the relative magnitude of the effective interaction range and the size of the abrasives, i.e. H^{*}, decreases as the size of the abrasive increases (Figure 8.5). This clearly shows that the area occupied by smaller abrasive particles (Figure 8.5 a) is much smaller than that by larger particles (Figure 8.5 b). Figure 8.4 also shows that the trends of the maximum surface coverage with κr_{ab} for various κ or r_{ab} are nearly invariant. It was also shown that this trend is fairly insensitive to the deposition methods[87], validating the use of these analytic equations to describe the behavior of abrasives during CMP.
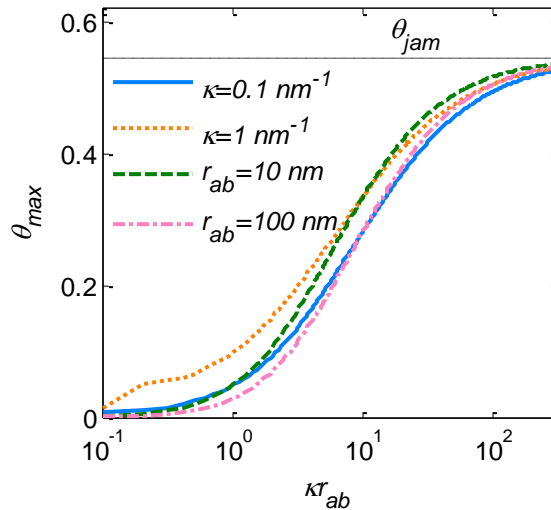
Figure 8.4 Maximum fractional surface coverage by deposited abrasives on the surface of a wafer with varying Debye parameter κ and abrasive particle radius, r_{ab}. Jamming limit for a hard sphere θ_{jam} is indicated as a horizontal line.
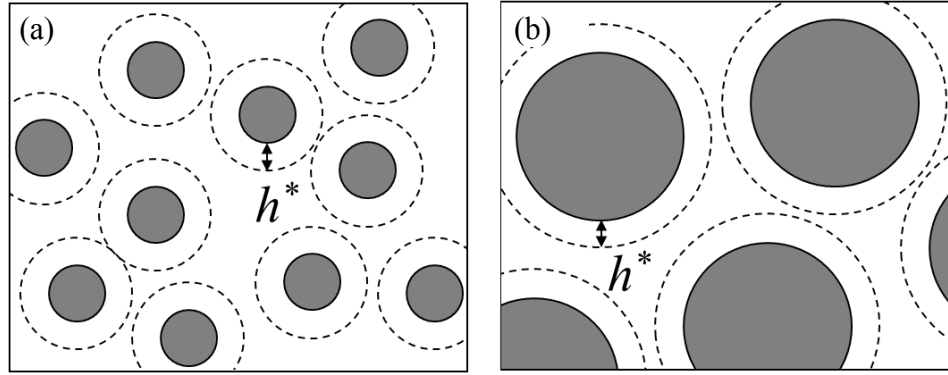
Figure 8.5 Equivalent hard spheres for (a) small and (b) large abrasive particles for the same effective interaction range h^*. The circles with dashed and solid line shows the equivalent hard sphere radius and the abrasive radius, respectively.

This approximation of the maximum surface coverage ratio agreed well with experimental measurements for κr_{ab} larger than 5 when the substrate and the particle were oppositely charged.[89] Even for smaller κr_{ab} values, the trend of the fractional coverage with κr_{ab} was maintained. The number of abrasive particles per unit area on the surface at the jamming state for a given slurry is evaluated from equation (8.20) as:

$$N_{ab} = \frac{\theta_{jam}}{\pi r_{ab}^{*2}}$$ (8.21)

Note that N_{ab} and θ_{max} are independent of the weight concentration of the abrasives in the slurry, as particles cannot be deposited further on the surface once the surface is saturated with the abrasive particles, regardless of the c_{wt}. For both diffusion and interception mechanisms the surface coverage ratio is proportional to the weight concentration of the abrasives as shown in equation (8.12) and (8.16). The number of abrasive particles that are trapped between a wafer and a pad asperity can be determined by multiplying N_{ab} and the average area of the contact between a wafer and an asperity a_{as}:

$$n_{ab} = N_{ab} a_{as}$$ (8.22)

The number of particles deposited per unit area and the fractional surface coverage for the two different transport mechanisms, namely diffusion and interception, and at the jamming state are summarized in Table 8.2. The variables are rearranged to show the dependencies of the parameters on the weight concentration and the size of the abrasives. It is seen that the fractional surface coverage differs for the two transport mechanisms with increasing size of the abrasives: increasing coverage ratio for interception and decreasing trend for diffusion.

Table 8.2 Number of deposited abrasives per area and the fractional surface coverage for two transportation mechanisms, namely diffusion and interception, and at the jamming state.

	Jamming State	Diffusion	Interception ($r_{ab} > 500$ nm)
Number of deposited abrasives per unit area N_{ab} [cm^{-2}]	$\dfrac{\theta_{jam}}{\pi r_{ab}^{*2}}$	$\dfrac{3\rho_{slurry}}{2\pi^2\rho_{ab}}\sqrt{\dfrac{kTt_{as-as}}{6\eta_v}}\,\dfrac{c_{wt}}{r_{ab}^{7/2}}$	$0.12\dfrac{\rho_{slurry}\omega^{3/2}f^2 t_{as-as}}{\rho_{ab}v_k^{1/2}}\dfrac{c_{wt}}{r_{ab}}$
Coverage ratio θ_{ab}	$\theta_{jam}(r_{ab}/r_{ab}^{*})^2$	$\dfrac{3\rho_{slurry}}{2\pi\rho_{ab}}\sqrt{\dfrac{kTt_{as-as}}{6\eta_v}}\,\dfrac{c_{wt}}{r_{ab}^{3/2}}$	$0.38\dfrac{\rho_{slurry}\omega^{3/2}f^2 t_{as-as}}{\rho_{ab}v_k^{1/2}}c_{wt}r_{ab}$

8.3 Surface coverage ratio by abrasives during CMP

Considering abrasive particles transported by diffusion the fractional coverage as a function of time is shown in Figure 8.6 a. Zero time is the moment when a pad asperity disturbs a given location on the surface of a wafer to completely remove all the deposited abrasives. Again, it was assumed that the all the transported abrasives attach to the surface. The interception mechanism was not considered in the figure because the radii of the abrasives were smaller than 500 nm. The figure shows that the surface coverage ratios increase following equation (8.12) until they saturate at values given by equation (8.20). A slurry containing silica abrasives was postulated in the calculation. These fractional coverage values allow modeling of the surface coverages that would be present for different periods between successive asperity interactions with a given point on the surface. Figure 8.6 b shows these for three different times, indicated by vertical dotted lines on Figure 8.6 a, and the resulting MRR values. Note that the three different hypothetical values with large differences of t_{as-as} were chosen to clearly show their influence on the resulting MRR. This shows various trends of the surface coverage, depending on the time interval between consecutive asperity-wafer interactions, t_{as-as}. The coverage reaches a maximum for $t_{as-as(2)}$ and $t_{as-as(3)}$ at abrasive sizes of 20 nm and 50 nm respectively and decreases with increasing abrasive size for $t_{as-as(1)}$. For slurries with abrasives below a certain size, the coverage is its maximum, saturation value. This is because the flux of abrasive particles to the surface is high because of the number of particles in the slurry is inversely proportional to the cube of the size of the abrasives for a fixed weight concentration. As the size of the particles increases, the flux of the abrasives to the surface decreases, leading to the number of particles deposited during t_{as-as} being too few to saturate the surface. In this case, diffusion determines the number of deposited abrasives. Thus the surface coverage decreases with increasing size of the abrasives. Note that t_{as-as}, which is the time during which abrasives in the slurry can be deposited on the surface, determines what limits the number of abrasive particles. As indicated in equation (8.2) this parameter is dependent on the sliding velocity of the wafer over the pad and the contact area between the pad and the wafer. Thus the choice of the pad and the conditioning specification, and the sliding velocity influence the limiting step of the deposition of the abrasives and thereby the dependence of MRR on the size of the abrasives during CMP.
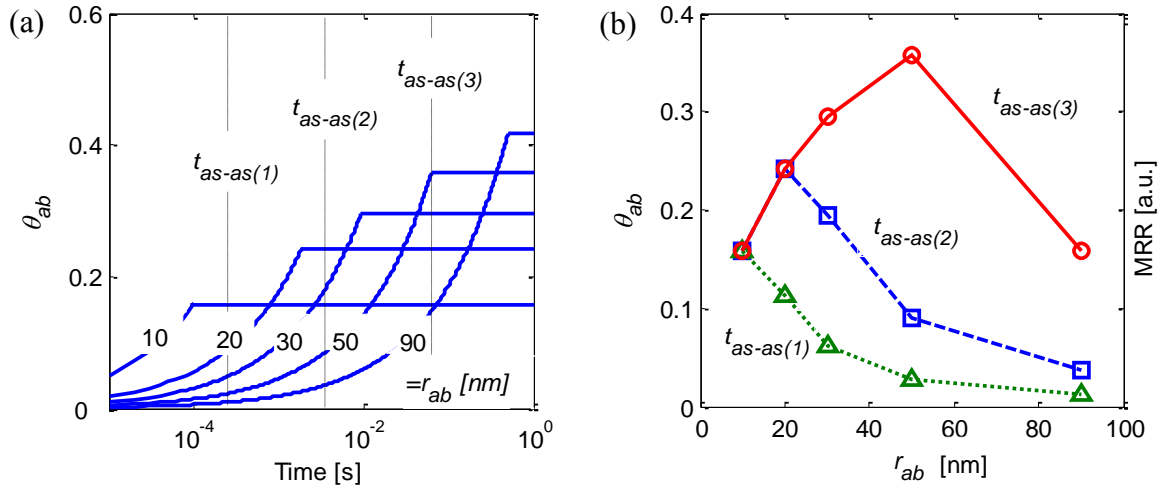
Figure 8.6 (a) Fractional surface coverage by abrasive particles from 10 to 90 nm in radius, as a function of time since complete removal of previously deposited abrasives by a pad asperity. c_w=0.1 (10 wt%), ρ_{ab}=2.65 g/cm^3, η=0.001002 Pa·s, κ=0.3 nm^{-1}. Three hypothetical values of the duration between consecutive asperity and wafer interactions is indicated as dotted vertical lines.. (b) The fractional surface coverage and MRR for various particle radii at $t_{as\text{-}as(1)}$, $t_{as\text{-}as(2)}$ and $t_{as\text{-}as(3)}$.

Also note that the surface coverage by abrasives can be higher than that estimated from the number of particles deposited between successive interactions of a given point on the wafer surface with asperities because these interactions would not necessarily remove all particles, as allowed for in equation (8.4). If the actual surface coverage is higher than the estimation, the surface would saturate at a lower flux of abrasive particles than shown in Figure 8.6 a, which would shift the size of the abrasive particles that maximize the surface coverage to a larger value, e.g. from the curve for $t_{as\text{-}as(1)}$ to that for $t_{as\text{-}as(3)}$ in Figure 8.6b.

In contrast, the repulsive interactions between the surface of a wafer and the abrasives under unfavorable conditions would greatly reduce the number of abrasives deposited by a factor of the particle collision efficiency α. However, any roughness on the surface of the wafer during CMP could enhance the deposition of the abrasives in the unfavorable condition even when the scale of the surface roughness is two orders of magnitude lower than the scale of the particles[90]. This is especially true for CMP processes where surface roughness is of the order of 0.1 to 1 nm and the particle size is of the order of 10 to 100 nm. Valleys formed by the roughness can be a preferential region for particle deposition.[64] It has been shown that under unfavorable conditions colloidal particles only adsorb at preferential sites where the energy barrier is low due to heterogeneity of the substrate surface.[91] Since a roughened surface at the abrasive scale is continuously formed across the wafer by the sliding of the abrasives and the chemical additives in the slurry during CMP, continuous deposition of the abrasives would be expected. Thus the constant material removal rate during CMP is attained while the surface of the wafer is continuously abraded.

8.4 Estimation of the MRR

131

Assuming that all the deposited abrasives that are trapped between a wafer and pad asperities and plastically deform a wafer as they slide on the surface and the plastically deformed amount is regarded as the removed material, the material removal rate during the process is determined as the volume of the removed amount by an abrasive multiplied by the number of the trapped abrasives as discussed in Chapter 6:

$$MRR \propto \frac{n_{ab}{}^* A_i V}{A_w} \tag{8.23}$$

where A_i is the cross sectional area of the trench on the wafer formed by the indentation of the sliding abrasive and A_w is the area of the wafer surface. The equation gives the MRR in units of thickness reduction per unit processing time. Assuming the wafer is plastically deformed by trapped abrasive particles that are hard spheres, the cross sectional area of a trench on the wafer generated by a trapped abrasive can be expressed as

$$A_i \propto h_w w_{ab} \propto \frac{f_{ab}{}^{3/2}}{r_{ab}} \tag{8.24}$$

where f_{ab} is the force exerted by a trapped abrasive particle on the wafer, the depth of the indentation $h_w = \frac{f_{ab}}{\pi r_{ab} H_w}$ and the width of the trench $w_{ab} = 2\sqrt{2 r_{ab} h_w}$. Then the MRR during CMP can be expressed using equation (8.23) and (8.24) as
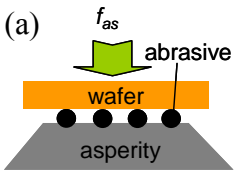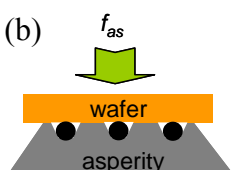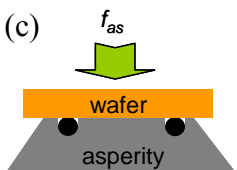
$$MRR \propto \frac{n_{ab}{}^* f_{ab}{}^{3/2} V}{r_{ab} A_w} \tag{8.25}$$

The dependencies of the material removal rate during CMP on the size and the weight concentration of abrasives are expressed using equation (8.25) in Table 8.3. This shows the dependencies for various configurations of the local contact between a wafer and an asperity when the deposition of the abrasives is dominated by diffusion or interception, or limited by jamming state of the abrasives. Note that the number of the deposited abrasives n_{ab} is shown in the table because it is proportional to the number of the abrasive particles that participate in the abrasion of the wafer $n_{ab}{}^*$ by equation (8.4). As the weight concentration of the abrasives decreases the deflection of the asperity by the trapped abrasive particles increases as shown in the figures in the table from (a) to (c). The resultant force applied to a single abrasive particle is summarized for each configuration. This shows that the MRR decreases with ncreasing size of the abrasives when the number of trapped particles is small (Table 8.3c), while it increases when the number is large (Table 8.3a) when the number of the trapped abrasives is limited by the diffusion of the particles. For large particles (> 500 nm) where the interception mechanism determines the number of the trapped abrasives, the MRR increases with increasingparticle size when the number of the trapped abrasives is small (Table 8.3c). At larger number of trapped abrasives (Table 8.3a) the MRR decreases with the increasing size of the abrasives where the interception mechanism is dominant. The dependencies of the MRR on the weight concentration of the abrasives are identical for both transportation mechanisms: the MRR increases with increasing weight concentration of the abrasives for low numbers of trapped particles, but decreases with increasing weight concentration when the number of the trapped abrasives is large. Also shown are the dependencies when the surface of the wafer is jammed with the deposited abrasives. The dependencies of MRR on the size of the abrasives are included in Table 8.3 and the effect of particle size on MRR for jammed surfaces is illustrated in Figure 8.7. Note that the relative

magnitude of the MRRs for each configuration in Figure 8.7 is not represented in the figure; only the trends were shown. The MRR increases with increasing size of the abrasives when the number of the trapped abrasives is small but decreases when the number is large.

Table 8.3 Dependencies of the material removal rate during CMP on the size and the weight concentration of the abrasives for various configurations of the interface between a wafer and a pad asperity: (a) an asperity is not deformed enough to contact the wafer, (b) an asperity is deflected to partly contact the surface of a wafer, and (c) an asperity is deformed enough to encapsulate the abrasives and to contact the wafer.

Local contact mode between an asperity and the wafer	Expressions for f_{ab}	Dependencies of *MRR* on r_{ab} and c_{wt} when n_{ab} is determined by one of the three following mechanisms		
		Diffusion $n_{ab} \propto \dfrac{c_{wt}}{r_{ab}^{7/2}}$	Interception $n_{ab} \propto \dfrac{c_{wt}}{r_{ab}}$	At the jamming state
(a)	$f_{ab} = f_{as}/n_{ab}$	$\dfrac{r_{ab}^{3/4}}{c_{wt}^{1/2}}$	$\dfrac{1}{r_{ab}^{1/2}c_{wt}^{1/2}}$	$\dfrac{r_{ab}^{*}}{r_{ab}}$
(b)	$f_{ab} \propto r_{ab}^{2}$ (FEM)	$\dfrac{c_{wt}}{r_{ab}^{3/2}}$	$c_{wt}r_{ab}$	$\left(\dfrac{r_{ab}}{r_{ab}^{*}}\right)^{2}$
(c)	$f_{ab} = \pi r_{ab}^{2}(f_{as}/a_{as})$	$\dfrac{c_{wt}}{r_{ab}^{3/2}}$	$c_{wt}r_{ab}$	$\left(\dfrac{r_{ab}}{r_{ab}^{*}}\right)^{2}$

Note that all of the above analysis was based on the assumption that the local contact mode of an asperity with the wafer during CMP changes dramatically, as illustrated in the figures in Table 8.3. For very small abrasive particles the maximum surface coverage at the jamming state can be very low, especially when the ionic strength of the slurry is low, giving significant repulsive interparticle interaction. In this case, the contact mode shown in Table 8.3a is implausible, due to the large spacing between the particles, resulting in the configurations of Table 8.3b or c. Comparison of cases b and c in Table 8.3 reveals the same effect of abrasive size and the weight concentration on MRR as on the surface coverage ratio (Table 8.2). Therefore, the trends for the fractional surface coverage in Figure 8.6b would be expected to represent the trends of the MRR during CMP. This predicts that the MRR increases with increasing size of the abrasives when the number of the trapped particles is limited by the jamming of the surface, whereas the MRR would be expected to decrease with

increasing size when the number of deposited abrasives is under transport control. The finding that the MRR predicted from the volume of the wafer indented by the abrasives has the same dependence on the size or the weight concentration of the abrasives as the surface coverage ratio, which is proportional to the number and the squre of the size of the abrasives, suggests that material removal mechanisms such as "chemical tooth" model[92] where the MRR is related to the surface area of the abrasives, which is also proportional to the number and the square of the size of abrasives, will also result in the same dependencies on those parameters. Thus the dependences of MRR on the size and the weight concentration of abrasives were discussed in this work without the consideration of the exact removal mechanism.
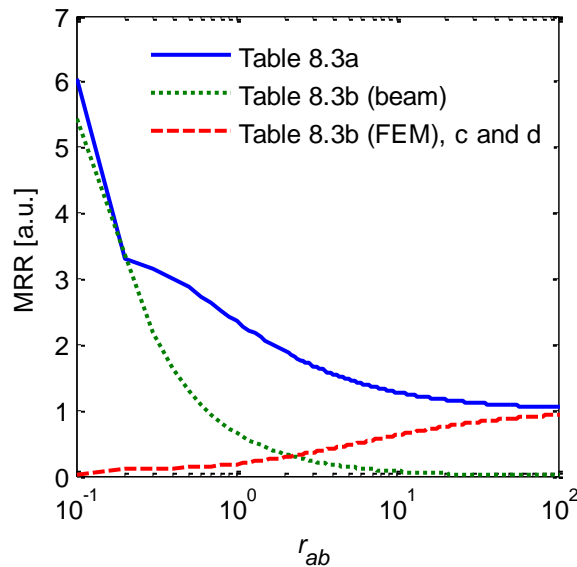

Figure 8.7 Material removal rate during CMP as a function of size of the abrasive particles when the number of abrasive particles that are involved in the material removal is determined for a wafer surface jammed with abrasive particles. Constant weight concentration of the abrasives. The relative magnitude of the curves is not represented

8.5 Comparison with experimental results

The effect of abrasive size and weight concentration on the MRR was predicted assuming different limiting processes for the surface concentration of abrasive particles on the wafer, namely transport of the abrasive particles by diffusion or interception, and the saturation limit of particles on the surface. , The experimental observations from the literature tabulated in Table 8.1 were analyzed to test the validity of these predictions. Since the surface charge of the wafer surface is highly dependent on the chemical additives in the slurry and the precise species present (for example, dielectric, or passivating species present on copper), which are not readily available in the literature, only experimental results for oxide CMP are examined here. Also, the focus is on the effect of the size of the abrasive particles on MRR, because on the effect of the weight concentration was discussed by Mahajan *et al.*[2]. Figure 8.8 to Figure

8.11 compare fitted trend lines with experimental data. Diffusion was considered for small particles, interception for large ones. The lines follow the relevant trends outlined in Table 8.3.

Choi et al.[6] measured the MRR during silicon oxide CMP using slurries containing 0.5-30 wt% of silicon oxide abrasives 0.2, 0.5, 1.0 and 1.5 μm in diameter and deionized water. pH was adjusted to 10.5. At lower abrasive concentrations, 0.5-2 wt%, the MRR increased with increasing size of the abrasives, while at higher concentrations, 15-30 wt%, the MRR decreased with increasing size of the abrasives as illustrated in Figure 8.8. This can be explained considering the transportation of the abrasives by interception as the limiting step for deposition of the abrasives. Diffusion and the jamming state were not considered because of the large sizes of the abrasives and the sensitiveness of the observed MRR on concentration of abrasives. At lower abrasive concentrations, the mode of local contact between the pad asperities and the wafer can be depicted as the figure in Table 8.3b or c, where the deflected asperities only partly or completely contact the surface of the wafer. This is because the distance between the deposited particles is large, making the deflection of the asperity large. Then the interception mechanism predicts that the MRR will be proportional to the size and the weight concentration of the abrasives, which is observed in the experimental results for 0.5-2 wt% of abrasives in Figure 8.8a and for 0.2 μm in Figure 8.8b. As the concentration of the abrasives increases to 5 wt% the MRR increases with the size of the abrasives up to 0.5 μm and then begin to decrease. The trends of the increasing MRR can again be explained by postulating the local contact mode as shown in the figure in Table 8.3b or c and the interception mechanism. The decreasing MRR with increasing size of the abrasives can be understood if the local contact mode between the asperity and the wafer is as in Table 8.3a. The change in the local contact mode is plausible because the distance between the asperity and the wafer separated by the larger abrasives is larger than when smaller abrasives are trapped, making it difficult for the deflected asperity to contact the wafer. Then the interception mechanism predicts that the MRR decreases with increasing size of the abrasives (inverse square root of the size). This is indicated by the solid lines in Figure 8.8a for 5, 15 and 30 wt% of abrasives, agreeing well with the experimental observations. The interception mechanism predicts that the MRR decreases with the square root of the weight concentration of the abrasives, as shown in Figure 8.8b for 0.5, 1 and 1.5 μm cases. The fitted trend lines describe reasonably well the experimental observations. Note that both the abrasives and the wafer surface have negative charges, which will exert a repulsive force between them. Thus the energy barrier on the surface of the wafer makes saturation of the wafer surface implausible, especially for low number concentration of the abrasives.
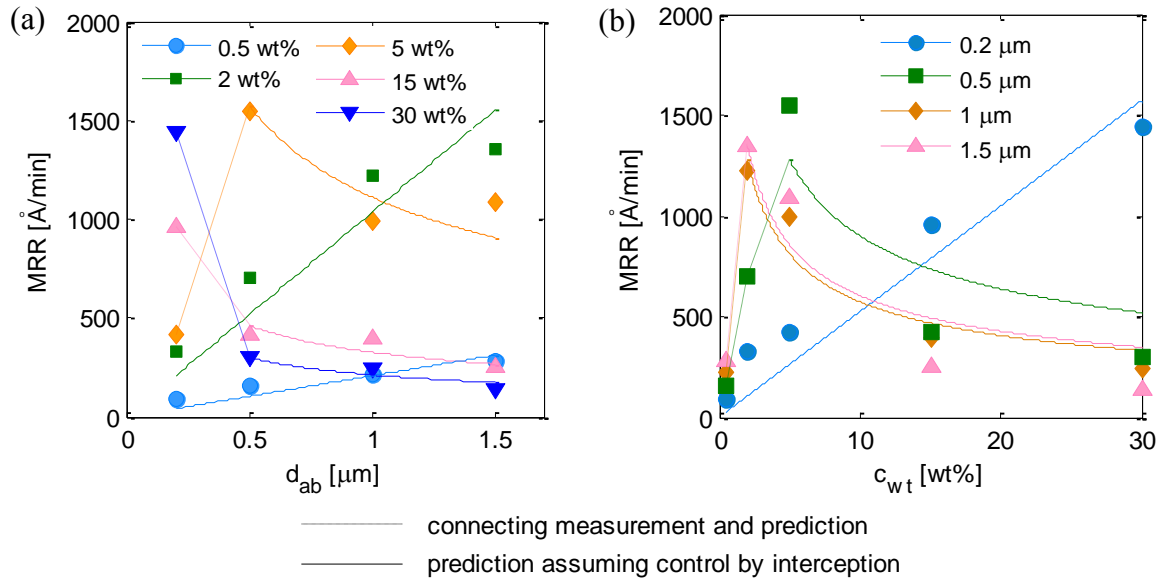
Figure 8.8 (a) Effect of silica abrasive particle size on material removal rates for silicon oxide CMP using a pH 10.5 slurry containing different concentration of the silicon oxide abrasives, as reported by Choi _et al._[6] (b) Effect of abrasive concentration on material removal rates for the same experiment. Diameters of the abrasives are indicated. Measured MRRs are shown as data points. The solid lines are the MRRs predicted assuming control by interception. Dotted lines connect measured values and the prediction.

Choi _et al._[7] also performed CMP on silicon oxide wafers using commercial slurry at pH 10.5 containing smaller silicon oxide abrasives, 48-110 nm in diameter, and observed that the MRR decreased with increasing size of the abrasives, as shown in Figure 8.9a. The MRR increased with increasing weight concentration of the abrasives, from 2-30 wt% as shown in Figure 8.9b. The results suggest that the deposition of the abrasives may be limited by the diffusion of the abrasives toward the surface of the wafer while the local contact mode between the asperities and the wafer is either as in the figure in Table 8.3b or c (low concentrations of abrasives). The prediction by the diffusion mechanism approximates the measurements at lower abrasive concentrations reasonably well, butdeviates significantly from the measurements at high concentration (Figure 8.9a). This suggests that the material removal at high abrasive concentration was largely affected by the undisclosed chemical constituents of the commercial slurry, enhancing the MRRs at the condition.
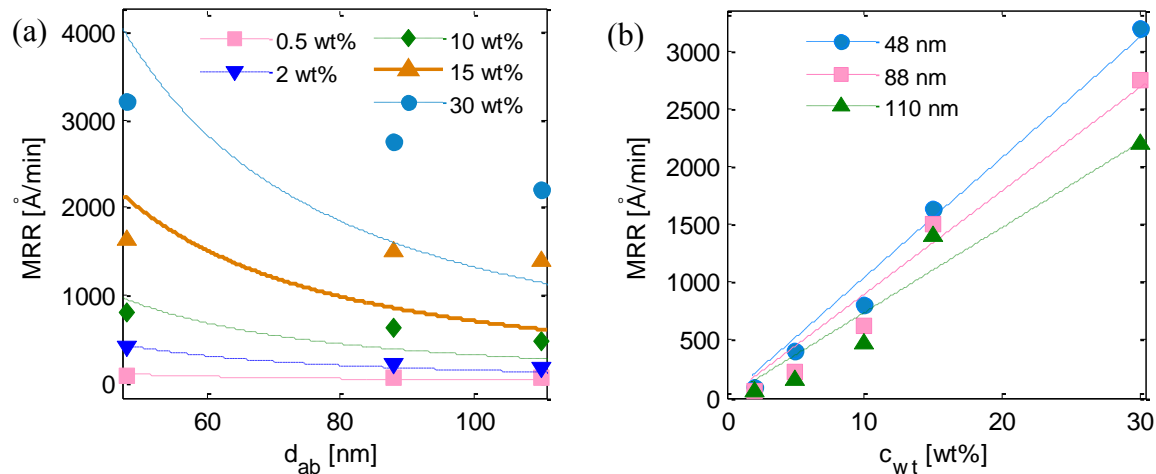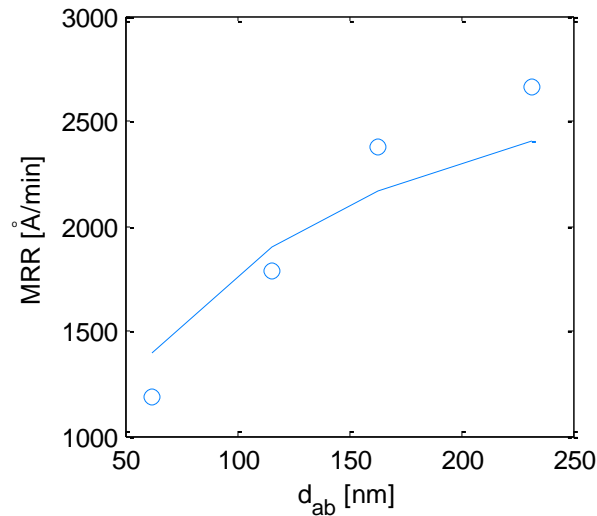
Figure 8.9 (a) Material removal rates of silicon oxide during CMP using slurry at pH 10.5 containing different weight concentration of the silicon oxide abrasives with different sizes by Choi et al.[7] (b) Material removal rates at the same experiment with the weight concentration of the abrasives. Diameters of the abrasives were indicated. Measured MRRs are shown as markers. The lines are the prediction of the MRRs using the diffusion mechanism.

Zhou *et al.* observed that the MRR of silicon oxide increases and then decreases with increasing diameter of silica abrasives from 10 nm to 140 nm at 30 wt% at various down pressures and sliding velocities, as shown in Figure 8.10a.[3] The pH of the slurry was adjusted to11 and the abrasives were dispersed in deionized water containing no other chemicals. The increasing MRR with increasing diameter up to 80 nm is attributed to the maximum surface coverage ratio being limited by repulsive interactions between the deposited abrasives. The surface of the wafer can saturate with abrasives because the number concentration of abrasives is very high for such a high weight concentration of the small size. The prediction by this mechanism is indicated in Figure 8.10a as a dashed line, showing excellent agreement with the experimental observations. The maximum surface coverage for each size of the abrasives was scaled to approximate the experimental values, by a factor determined by averaging the ratios of the measurement to the evaluated maximum surface coverage for all conditions. Note that the predictions at each down pressure and sliding velocity were well scaled with each other using Preston's equation, e.g. measured MRR at 32 kPa and 0.6 m/s is (32/18)*(0.6/0.4) times larger than that at 18 kPa and 0.4 m/s. As the size of the abrasives increases, the number concentration of the abrasives decreases, leading to insufficient abrasive particles to saturate the surface of the wafer. Then the number of deposited abrasives becomes controlled by the transport of the abrasives, i.e. diffusion. The MRRs predicted by the diffusion mechanism are also shown in Figure 8.10a as solid lines. Similar trends were also observed by Zhang *et al.,* as shown in Figure 8.10b where glass was polished using commercial slurry at pH 10 containing 10 wt% of silica abrasives.[18] In this case the same argument is applicable because of the high number concentration of the abrasives.
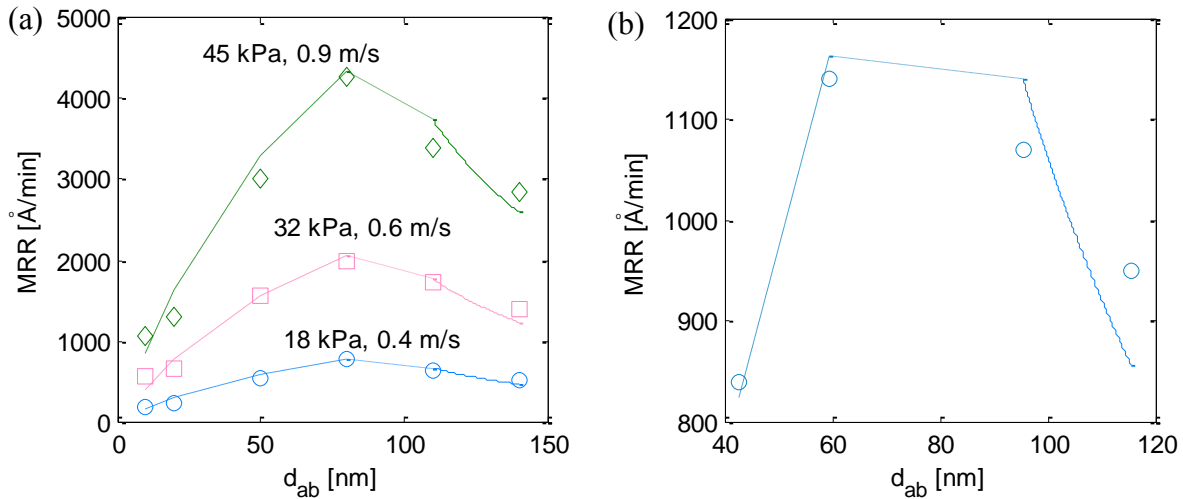
Figure 8.10 (a) Material removal rates of silicon oxide during CMP for various diameters of the abrasives, as reported by Zhou *et al.*[3] 30 wt% of abrasives were contained in the slurry at pH 11. Three different down pressures and sliding velocities were used as indicated. (b) MRR of glass during CMP with various abrasive sizes. 10 wt% of abrasives were contained in the slurry at pH 10, as reported by Zhang *et al.*[18] The experimental measurements, prediction from saturated surface coverage by deposited abrasives, and from the diffusion mechanism are indicated by data points, dashed lines and solid lines, respectively. The dotted lines connect between the predictions from the two mechanisms.

Oh *et al.* observed increasing MRR of silicon oxide with increasing abrasive particle size when polished using slurry at pH 6.5-6.7 containing 2 wt % of ceria abrasives, as shown in Figure 8.11.[17] The diameters of the abrasives ranged from 62 to 232 nm and 0.04 wt% of polyacrylic acid (PAA) was used as a dispersant. This trend can be explained by the maximum surface coverage being dependent on the size of the abrasives, as predicted by the solid line in Figure 8.11. The surface of the wafer could be jammed at such a low weight concentration of abrasives because the zeta potential of the ceria abrasives at this pH was positive[93] whereas the silicon oxide was negative, giving attractive interactions between them. Unlike the other experimental data discussed above, there was no energy barrier in the boundary layer adjace to the surface of the wafer. Thus the deposition of the abrasives was uninhibited, leading to higher concentrations of the deposited abrasives. The local contact mode between the asperities and the wafer can be regarded as in Table 8.3b or c because the low ionic strength of the slurry makes the surface coverage by the deposited abrasives low even at the jamming state.

Figure 8.11 Material removal rates of silicon oxide during CMP using slurry containing 2 wt% of ceria abrasives at pH 6.5-6.7 with various abrasive sizes, as reported by Oh *et al.*[17] The experimental measurements and prediction from the maximum surface coverage by deposited abrasives are indicated by data points and solid lines, respectively.

8.6 Conclusion

The proposed mechanisms successfully explained the various dependencies of the MRR during CMP on the size and the weight concentration of the abrasives. It was shown that during CMP the surface of a wafer can be saturated with abrasives when there are attractive interactions between the surface and the abrasives and the number concentration of the abrasives in the slurry is very high. If the flux is insufficient the deposition of the abrasives is limited by the transport of the abrasives: diffusion or interception is dominant when the size of the abrasives is smaller or larger than 500 nm, respectively.

In addition, the proposed mechanisms recognized the influence of slurry chemistry on the deposition of the abrasives on the surface of the wafer, which has attracted little attention in the CMP area except for some qualitative mention in previous work. The ionic strength of the slurry influences the range of the electrostatic double layer interactions between the abrasives and the wafer as well as those between the abrasives. Especially when the surface of the wafer is saturated with deposited abrasives, the repulsive interparticle interactions determine the maximum attainable surface coverage ratio by the abrasives. Also, the ionic strength along with the pH of the slurry determine the magnitude of the energy barrier on the surface of the wafer when the charges on the wafer and the abrasives are of the same sign. The energy barrier interferes with the deposition of the abrasives on the surface. It was also shown that the sliding velocity of the wafer, the type of the CMP pad or the conditioning specification may affect the limiting step of the deposition by influencing the time between consecutive asperity and wafer interactions, which determines the allowed time for the

deposition of the abrasives. If the interval between consecutive asperity and wafer interaction is large, the abrasives will have more time to be deposited on the surface of the wafer, leading to more deposited abrasives and vice versa. The influence of the type of the pad on the MRR behavior with the size of the abrasives was shown in Xie et al.[19]'s experimental data.

The proposed mechanism also has some implication in the case where two different types of abrasives are used in a slurry to enhance the MRR and the planarization efficiency during the process[20,94,95,96]. The increase in the MRR can either be attributed to the increase in the surface coverage ratio, because smaller abrasives can sit between the larger abrasives where the larger abrasives cannot be deposited provided that the pad asperities can reach the smaller abrasives, or to the coating by the smaller abrasives that might have the opposite charge to the surface of the wafer, allowing the coated abrasives to be attracted by the wafer.

References

[1] R. Jairath, M. Desai, M. Stell, R. Tolles and D. Scherber-Brewer, *Mat. Res. Soc. Symp. Proc.*, **337**, 121 (1994).

[2] U. Mahajan, M. Bielmann and R. K. Singh, *Mat. Res. Soc. Symp. Proc.*, **566**, 27 (2000).

[3] C. Zhou, L. Shan, J. R. Hight, S. Danyluk, S. H. Ng and A. J. Paszkowski, *Tribol. Trans.*, **45**(2), 232 (2002).

[4] K. Cooper, J. Cooper, J. Groschopf, J. Flake, Y. Solomentsev and J. Farkas, *Electrochem. Solid-State Lett.*, **5**(12), G109 (2002).

[5] A. Philipossian and S. Olsen, *Mat. Res. Soc. Symp. Proc.*, **767**, F2.8.1 (2003).

[6] W. Choi, J. Abiade, S.-M. Lee and R. K. Singh, *J. Electrochem. Soc.*, **151**(8), G512 (2004).

[7] W. Choi and R. K. Singh, *Jpn. J. Appl. Phys.*, **44**(12), 8383 (2005).

[8] B. Park, H. Lee, Y. Kim, H. Kim and H. Jeong, *Jpn. J. Appl. Phys.*, **47**(12), 8771 (2008).

[9] Z. Zhang, W. Liu and Z. Song, *Microelectron. Eng.*, **87**(11), 2168 (2010).

[10] B. Park, S. Jeong, H. Lee, H. Kim, H. Jeong and D. A. Dornfeld, *Jpn. J. Appl. Phys.*, **48**, 116505 (2009).

[11] K. Yoshida, *J. Sol-Gel Sci. Technol.*, **43**(1), 9 (2007).

[12] M. Bielmann, U. Mahajan and R. K. Singh, *Electrochem. Solid-State Lett.*, **2**(8), 401 (1999).

[13] Q. Luo, S. Ramarajan and S. V. Babu, *Thin Solid Films*, **335**, 160 (1998).

[14] Y. Li, M. Hariharaputhiran and S. V. Babu, *J. Mater. Res.*, **16**(4), 1066 (2001).

[15] L. Guo and R. S. Subramanian, *J. Electrochem. Soc.*, **151**(2), G104 (2004).

[16] H. Lee, S. Joo and H. Jeong, *J. Mater. Process. Technol.*, **209**(20), 6134 (2009).

[17] M.-H. Oh, R. K. Singh, S. Gupta and S.-B. Cho, *Microelectron. Eng.*, **87**(12), 2633 (2010).

[18] Z. Zhang, W. Liu and Z. Song, *Appl. Opt.*, **49**(28), 5480 (2010).

[19] Y. Xie and B. Bhushan, *Wear*, **200**, 281 (1996).

[20] S. Armini, C. M. Whelan, M. Moinpour and K. Maex, *J. Electrochem. Soc.*, **156**(1), H18 (2009).

[21] Z. Lu, S.-H. Lee, S. V. Babu and E. Matijević, *J. Colloid Interface Sci.*, **261**(1), 55 (2003).

[22] G. Fu, A. Chandra, S. Guha and G. Subhash, *IEEE Trans. Semicond. Manuf.*, **14**(4), 406 (2001).

[23] A. Bastawros, A. Chandra, Y. Guo and B. Yan, *J. Electron. Mater.*, **31**(10), 1022 (2002).

[24] T. Zeng and T. Sun, *IEEE Trans. Semicond. Manuf.*, **18**(4), 655 (2005).

[25] W. Che, Y. Guo, A. Chandra and A. Bastawros, *J. Manuf. Sci. Eng.*, **127**(3), 545 (2005).

[26] K. Qin, B. Moudgil and C.-W. Park, *Thin Solid Films*, **446**(2), 277 (2004).

[27] J. Luo and D. A. Dornfeld, *IEEE Trans. Semicond. Manuf.*, **14**(2), 112 (2001).

[28] J. Luo and D. A. Dornfeld, *IEEE Trans. Semicond. Manuf.*, **16**(3), 469 (2003).

[29] M. Bastaninejad and G. Ahmadi, *J. Electrochem. Soc.*, **152**(9), G720 (2005).

[30] G. B. Basim, J. J. Adler, U. Mahajan, R. K. Singh and B. M. Moudgil, *J. Electrochem. Soc.*, **147**(9), 3523 (2000).

[31] W.-C. Chen, S.-C. Lin, B.-T. Dai and M.-S. Tsai, *J. Electrochem. Sci.*, **146**(8), 3004 (1999).

[32] S. Ramarajan, Y. Li, M. Hariharaputhiran, Y.-S. Her and S. V. Babu, *Electrochem. Solid-State Lett.*, **3**(5), 232 (2000).

[33] S. Hegde and S. V. Babu, *Electrochem. Solid-State Lett.*, **7**(12), G316 (2004).

[34] Z. Lu, N. P. Ryde, S. V. Babu and E. Matijević, *Langmuir*, **21**(22), 9866 (2005).

[35] J. T. Abiade, W. Choi and R. K. Singh, *J. Mater. Res.*, **20**(5), 1139 (2005).

[36] S.-Y. Chiu, Y.-L. Wang, C.-P. Liu, S.-C. Chang, G.-J. Hwang, M.-S. Feng and C.-F. Chen, *Thin Solid Films*, **498**, 60 (2006).

[37] N. K. Penta, P. R. D. Veera and S. V. Babu, *Langmuir*, **27**(7), 3502 (2011).

[38] A. Nennemann, M. Voetz, G. Hey, L. Puppe and S. Kirchmeyer, *Progr. Colloid. Polym. Sci.*, **133**, 159 (2006).

[39] Q. Luo, D. R. Campbell and S. V. Babu, *Lanmuir*, **12**(15), 3563 (1996).

[40] R. Ihnfeldt and J. B. Talbot, *J. Electrochem. Soc.*, **153**(11), G948 (2006).

[41] R.S. Subramanian, L. Zhang and S.V. Babu, *J. Electrochem. Soc.*, **146**(11), 4263 (1999).

[42] D.G. Thakurta, C.L. Borst, D.W. Schwendeman, R.J. Gutmann and W.N. Gill, *Thin Solid Films*, **366**, 181 (2000).

[43] A. Philipossian and S. Olsen, *Jpn. J. Appl. Phys.*, **42**, 6371 (2003).

[44] H. Reerink and J. Th. G. Overbeek, *Discuss. Faraday Soc.*, **18**, 74 (1954).

[45] K. M. Yao, M. T. Habibian and C. R. O'Melia, *Environ. Sci. Technol.*, **5**(11), 1105 (1971).

[46] N. Tufenkji and M. Elimelech, *Environ. Sci. Technol.*, **38**(2), 529 (2004).

[47] J. N. Ryan and M. Elimelech, *Colloid Surf. A,* **107**, 1 (1996).

[48] M. Elimelech and Ch. R.O'Melia, *Langmuir*, **6**(6), 1153 (1990).

[49] M. Hull and J. A. Kitchener, *Trans. Faraday Soc.*, **65**, 3093 (1969).

[50] J. Gregory and A. Wishart, *J. Colloids Surf.*, **1**, 313 (1980).

[51] J. E. Tobiason, *Colloids Surf.*, **39**(1), 53 (1989).

[52] S. Lin and M. R. Wiesner, *Langmuir*, **28**(30), 11032 (2012).

[53] J. Sjollema and H. J. Busscher, *Colloids Surf.*, **47**(C), 323 (1990).

[54] M. L. Grant and D. A. Saville, *J. Colloid Interface Sci.*, **171**(1), 35 (1995).

[55] M. W. Hahn and C. R. O'Melia, *Environ. Sci. Technol.*, **38**(1), 210 (2004).

[56] C. Shen, F. Wang, B. Li, Y. Jin, L.-P. Wang and Y. Huang, *Langmuir*, **28**(41), 14681 (2012).

[57] N. H. G. Penners and L. K. Koopal, *Colloids Surf.*, **28**(c), 67 (1987).

[58] G. R. Wiese and T. W. Healy, *Trans. Faraday Soc.*, **66**, 490 (1970).

[59] R. Hogg and K. C. Yang, *J. Colloid Interface Sci.*, **56**(3), 573 (1976).

[60] A. Marmur, *J. Colloid Interface Sci.*, **72**(1), 41 (1979).

[61] Y. Liu, D. Janjaroen, M. S. Kuhlenschmidt, T. B. Kuhlenschmidt and T. H. Nguyen,

Langmuir, **25**(3), 1594 (2009).

[62] E. M. V. Hoek and G. K. Agarwal, *J. Colloid Interface Sci.*, **298**(1), 50 (2006).

[63] G. K. Darbha, C. Fischer, A. Michler, J. Luetzenkirchen, T. Schäfer, F. Heberling and D. Schild, *Langmuir*, **28**(16), 6606 (2012).

[64] E. M. V. Hoek, S. Bhattacharjee and M. Elimelech, *Langmuir*, **19**(11), 4836 (2003).

[65] E. Martines, L. Csaderova, H. Morgan, A. S. G. Curtis and M. O. Riehle, *Colloids Surf., A*, **318**, 45 (2008).

[66] S. Bhattacharjee, C.-H. Ko, and M. Elimelech, *Langmuir*, **14**(12), 3365 (1998).

[67] X. F. Huang, S. Bhattacharjee and E. M. V. Hoek, *Langmuir* **26**(4), 2528 (2010).

[68] P. K. Das and S. Bhattacharjee, *Langmuir*, **21**(10), 4755 (2005).

[69] Z. Adamczyk, B. Siwek, M. Zembala and P. Belouschek, *Adv. Colloid Interface Sci.*, **48**(15), 151 (1994).

[70] M. Elimelech, *J. Colloid Interface Sci.*, **164**, 190 (1994).

[71] C.-J. Chin, S. Yiacoumi and C. Tsouris, *J. Colloid Interface Sci.*, **206**(2), 532 (1998).

[72] S. Tripathi, S. Choi, F. M. Doyle and D. A. Dornfeld, *Mater. Res. Soc. Symp. Proc.*, **1157,** E02-03 (2009).

[73] Z. Adamczyk, T. Dabros´, J. Czarnecki and T. G. M. Van De Ven, *Adv. Colloid Interface Sci.*, **19**(3), 183 (1983).

[74] V. G. Levich, *Physicochemical Hydrodynamics*, Prentice-Hall, NJ (1962).

[75] M. Smoluchowski, *Phys. Z.*, **17**, 585 (1916).

[76] J. Zhuang, J. Qi and Y. Jin, *Environ. Sci. Technol.*, **39**(20), 7853 (2005).

[77] Z. Adamczyk, B. Siwek, M. Zembala and P. Warszyński, *J. Colloid Interface Sci.*, **130**(2), 578 (1989).

[78] Z. Adamczyk, L. Szyk and P. Warszyński, *Colloids Surf., A*, **75**(C), 185 (1993).

[79] P. J. Flory, *J. Am. Chem. Soc.*, **61**, 1518 (1939).

[80] B. Widom, *J. Chem. Phys.*, **44**, 3888 (1966).

[81] M.R. Oberholzer, J.M. Stankovich, S.L. Carnie, D.Y.C. Chan and A.M. Lenhoff, *J. Colloid Interface Sci.*, **194**(1), 138 (1997).

[82] J. Feder, *J. Theor. Biol.*, **87**(2), 237 (1980).

[83] J. Feder and I. Giaever, *J. Colloid Interface Sci.*, **78**(1), 144 (1980).

[84] E. L. Hinrichsen, J. Feder and T. Jøssang, *J. Stat. Phys.*, **44**, 793 (1986).

[85] Z. Adamczyk and P. Warszyński, *Adv. Colloid Interface Sci.*, **63**, 41 (1996).

[86] W. B. Russel, D. A. Saville and W. R. Schowalter, *Colloidal Dispersions*, p.525, Cambridge University, Cambridge (1989).

[87] M. Semmler, E. K. Mann, J. Rička and M. Borkovec, *Langmuir*, **14**(18), 5127 (1998).

[88] W. C. Chen and P. N. Sen, *J. Chem. Phys.*, **77**(9), 2042 (1982).

[89] M. Semmler, J. Rička and M. Borkovec, *Colloids Surf., A*, **165**, 79 (2000).

[90] W. R. Bowen and T. A. Doneva, *J. Colloid Interface Sci.*, **229**(2), 544 (2000).

[91] Y. Lüthi, J. Rička and M. Borkovec, *J. Colloid Interface Sci.*, **206**(1), 314 (1998).

[92] L. M. Cook, *Journal of Non-crystalline Solids*, **120**, 152 (1990).

[93] M. Nabavi, O. Spalla and B. Cabane, *J. Colloid Interface Sci.*, **160**(2), 459 (1993).

[94] S. Armini, C. M. Whelan and K. Maex, *Electrochem. Solid-State Lett.*, **11**(10), H280 (2008).

[95] Z. Lu, S.-H. Lee, V. R. K. Gorantla, S. V. Babu and E. Matijevic, *J. Mater. Res.*, **18**(10), 2323

(2003).

[96] A. Jindal, S. Hegde and S. V. Babu, *Electrochem. Solid-State Lett.*, **5**(7), G48 (2002).

Chapter 9
Conclusion

9.1 Material removal mechanisms

A quantitative and physicochemical model of copper CMP that predicts MRR was proposed focusing on the interplay of consumables and copper and the synergisms between chemical and mechanical aspects of the process. Two synergistic mechanisms of the material removal during copper CMP were suggested: chemically dominant and mechanically dominant mechanisms. The total MRR during copper CMP was determined by summing those two contributions. Material removal by each mechanism is summarized as follows.

The surface of copper reacts with the chemical additives in the slurry to form a protective material on the surface. This protective material is essential for copper CMP because it protects recessed regions on the wafer from active chemical dissolution, contributing to dissimilar MRRs at protruded and recessed regions and thus to planarization of the wafer. The protective material is repetitively interrupted by sliding pad asperities and abrasive particles squeezed between the asperity and the wafer. The interval between consecutive interruptions by pad asperities is of the order of one millisecond, which is insufficient to grow a complete monolayer of the protective material. Thus the grown protective material occupies only a fraction of the surface of a wafer. During this interruption by an asperity the protective material is removed where the squeezed abrasive particles slide. The ratio of the reduced surface coverage by the protective material to the total surface coverage before the abrasion is termed as the removal efficiency. As the number of the squeezed abrasives on an asperity increases the removal efficiency also increases, but it will saturate at unity if successive abrasions do not remove any more material. The interval between consecutive abrasive-wafer interactions is of the order of one microsecond; thus any electrochemical changes during this short time were neglected. The growth and the removal of the protective material are balanced during CMP. Then the surface of a wafer during copper CMP can be regarded as being occupied by the protective material by a certain coverage ratio. It was assumed that the dissolution occurs both at occupied regions (by the protective material) and non-occupied regions with different rates. Since the chemical dissolution occurs at the surface of copper by the oxidizing agents in the slurry, the overall dissolution rates for the entire copper wafer is maintained constant. Also, the rate of the formation of the protective material, which is balanced with the removal of this material, is also maintained constant. Therefore, the chemically dominant MRR can be measured from the summation of the constant dissolution rate and the rate of the formation of the protective material.

The surface of copper also contains some deposited abrasive particles because of the electrostatic attraction between the copper and the abrasives. The number of the deposited abrasives is limited by the time allowed for the deposition. Again, the time interval between

consecutive asperity and copper interactions determine this time. During this short time, the deposition can be very rapid resulting in saturation of the surface with the deposited abrasives or the deposition can still be limited by the transportation of abrasives toward the substrate. The deposited abrasives participate in the abrasion of the copper as well as the abrasion of the protective material if squeezed between asperities and the wafer. The force applied on a squeezed abrasive is determined by considering the relative deflection of an asperity by the supporting abrasives.

The shear stress induced in copper by the force applied on an abrasive is usually lower than the ideal shear strength of copper, which is the relevant property for plasticity at this length scale. However, the crystallographic defects in the copper crystal may reduce the hardness of the material. Especially the roughness of the surface induced by chemical additives in the slurry greatly reduces the resistance to plastic deformation of copper. Because of the random and localized spatial distribution of those crystallographic defects the plastic deformation occurs only locally. Also, only a part of the plastically deformed material will be detached from the surface by preferential oxidization at highly defect regions or by a process similar to cutting, contributing to the MRR. The mechanically dominant MRR is determined by the removal of the material by this mechanism, which is determined by the number of the squeezed abrasives that really induces plastic deformation of copper and the fraction of the plastically deformed copper that is removed from the surface.


9.2 Modeling to Explain Pattern Dependent Variability

Utilizing the proposed physicochemical model of copper CMP, a modeling framework for the pattern dependent variability is proposed as shown in Figure 9.1. The success of this approach is dependent on the evaluation of the input parameters of the proposed MRR model for copper CMP. The consumable, workpiece and processing parameters determine the adsorption kinetics of a protective material and the number of abrasives deposited on the surface on the surface of copper. The chemistry of a slurry, the type workpiece materials, conditioning and type of the CMP pad and the down pressure and sliding velocity determine adsorption kinetics of the protective material. Along with the parameters of the type and size of the abrasives those parameters also determine the zeta potential and Debye length of the abrasives, copper, barrier and dielectric materials. Also the size of the abrasives, the slurry chemistry and the time interval between consecutive asperity and wafer interactions, which is determined by the type and the conditioning of the pad, down pressure and the sliding velocity, determine the limiting mechanism of the deposition of abrasives on the surface of a wafer and thus the number of the squeezed abrasives that will participate in the abrasion of the wafer materials. The evaluated number of the deposited abrasives influences the local removal response of the protective material and the copper.
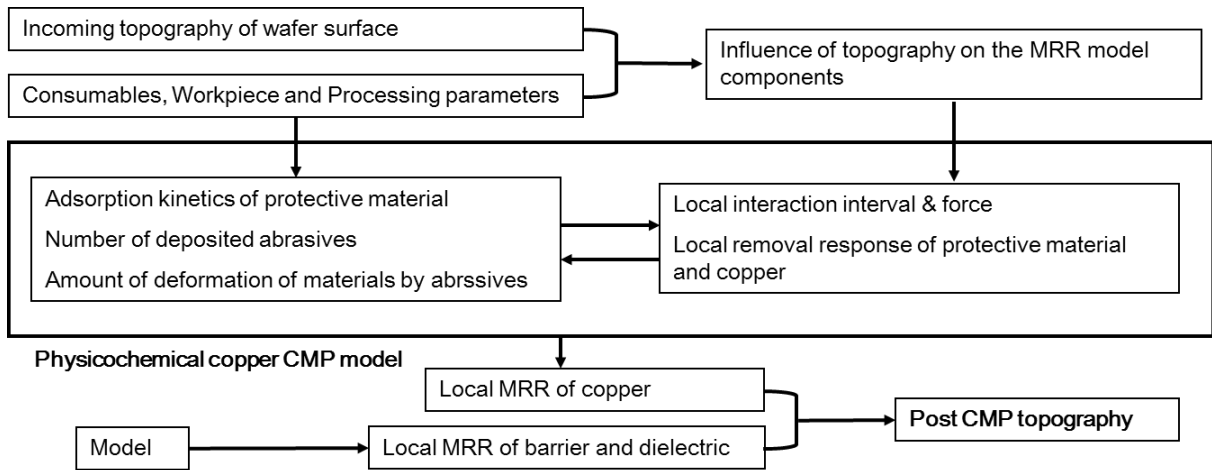
Figure 9.1 Modeling framework for pattern dependent variability during copper CMP

The influence of the wafer topography on the input parameters was qualitatively investigated. Assuming that the length and size of the pad asperities follow a probability distribution function (such as Gaussian distribution), only asperities smaller and longer than the size of a trench can reach the bottom of the trench. In addition, large asperities can deform to reach the bottom of a smaller trench. Both of those mechanisms are illustrated in Figure 9.2. These two mechanisms affect the number and size of the asperity and copper contact, ultimately influencing the time between consecutive asperity/copper interactions, the removal efficiency and the mechanically dominant removal of copper. As the metal line width increases, the number of asperities that can reach inside of the metal line increases, resulting in decreased time interval between consecutive copper/asperity interactions. The frequent interactions remove more protective material on the copper surface, allowing more copper to be dissolved. Also, more copper will be deformed and subsequently oxidized by the frequent abrasion by abrasives trapped by the asperities. The expected output is more dishing for wider metal lines as experimentally confirmed[1]. Also, the fact that the grain size of copper is smaller at narrow features on the wafer than at the wider features[2] as shown in Figure 9.3 suggests that copper at narrow lines will be more susceptible to mechanically dominant removal, resulting in dishing. Once the input parameters of the proposed MRR model are evaluated by considering these effects, the local MRR and thus eventually the post CMP topography can be determined if the MRR of dielectrics and barrier materials are predicted by a robust CMP model. The various proposed mechanisms in this work can also be adopted to the modeling of the material removal mechanisms of dielectric and barrier materials.
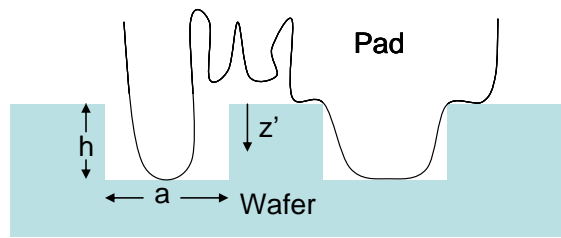
Figure 9.2 Two mechanisms whereby an asperity contacts a trench.
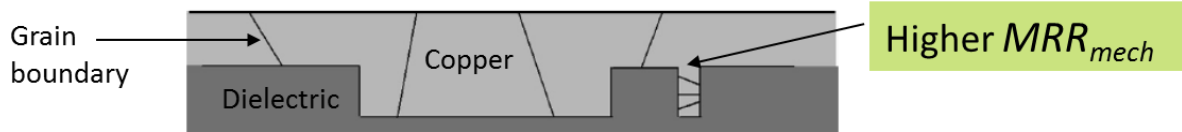
Figure 9.3 Influence of very narrow copper lines on MRR$_{mech}$.

References

[1]T. Park, T. Tugbawa and D. Boning , *Proc. CMP-MIC* 2000: 196-205, Santa Clara, CA.
[2] V. Carreau, S. Maitrejean, M. Verdier, Y. Brechet, A. Roule, A. Toffoli and V. Delaye, *Microelectron. Eng.* **84**, 2723 (2007).